INAUGURAL-DISSERTATION
zur
Erlangung der Doktorwürde
der
Gesamtfakultät für Mathematik,
Ingenieur- und Naturwissenschaften
der
Ruprecht–Karls–Universität
Heidelberg

vorgelegt von
M.Sc. Sahra Greve

Tag der mündlichen Prüfung: 24-10-2025

From River to Reef: Developing Coral $\delta^{234}U$ as a Proxy for Freshwater Influence in the Caribbean and Beyond

Gutachter:

Prof. Dr. Norbert Frank

Prof. Dr. Oliver Friedrich

Abstract

Freshwater input plays a critical role in shaping marine environments and regional hydroclimate, yet reliable marine archives for reconstructing past freshwater variability remain limited. Traditional proxies often conflate temperature, salinity, upwelling, and/or biological effects, making it difficult to isolate freshwater contributions. This thesis explores the potential of uranium isotopes in corals, specifically $\delta^{234}U$, as a proxy for freshwater flux, with a focus on applications in the Caribbean region.

The research assesses the precision and reliability of coral $\delta^{234}U$ measurements, identifying methodological constraints and best practices for sampling tropical corals. A baseline value for the Caribbean basin is then established, confirming that the region shares the open-ocean $\delta^{234}U$ signature. Building on this foundation, site-specific studies reveal the sensitivity of coral $\delta^{234}U$ to local hydrological influences. A Cuban coral record demonstrates a stable baseline with variability linked to local precipitation, while enhanced variability at the end of the Little Ice Age points to increased Mississippi River influence or change in Cuban land use. Along the Yucatán Peninsula, $\delta^{234}U$ variability is dominated by submarine groundwater discharge, which in turn is modulated by relative sea-level changes. A comparative study in Tahiti further illustrates the proxy's potential, showing distinct $\delta^{234}U$ signatures in seawater, river water, and groundwater, as well as a sea-level dependence of groundwater discharge that may allow for the reconstruction of ENSO variability.

A synthesis of all available Caribbean coral records indicates that no coherent basin-wide freshwater signal emerges. Instead, local hydrological processes dominate coral $\delta^{234}U$, and the strong Atlantic throughflow effectively dilutes freshwater inputs, rendering the Caribbean basin similar to the open ocean on average. In contrast, marginal basins with restricted circulation, such as the Mediterranean or the East China Sea, exhibit clearer freshwater signals.

Overall, this thesis demonstrates the potential of coral $\delta^{234}U$ as a freshwater proxy. While it also captures valuable information about local hydrology and land-ocean interactions, its application in regions with high oceanic exchange requires careful interpretation. These findings expand the methodological toolkit of paleoclimate research and provide new insights into the hydroclimatic dynamics of the Caribbean and beyond.

Zusammenfassung

Der Süßwassereintrag ist ein Schlüsselfaktor für die Gestaltung mariner Ökosysteme und die regionale Hydroklimatik. Dennoch stehen bislang nur wenige zuverlässige marine Archive zur Rekonstruktion vergangener Süßwasservariabilität zur Verfügung. Herkömmliche Proxies vermischen häufig Temperatur-, Salzgehalts-, Auftriebs- und/oder biologische Signale, wodurch sich Süßwassereinträge nur schwer eindeutig abgrenzen lassen. Diese Dissertation untersucht das Potenzial von Uranisotopen in Korallen, insbesondere $\delta^{234}U$, als Proxy für Süßwasserflüsse, mit besonderem Fokus auf Anwendungen in der Karibik.

Zunächst werden die Präzision und Reproduzierbarkeit von $\delta^{234}U$-Messungen an Korallen geprüft. Dabei werden methodische Einschränkungen diskutiert und Vorgehensweisen für die Probenahme tropischer Korallen vorgestellt. Anschließend wird ein Referenzwert für das Karibische Becken etabliert, der bestätigt, dass die Region den $\delta^{234}U$-Signaturen des offenen Ozeans entspricht. Darauf aufbauend verdeutlichen standortspezifische Fallstudien die Sensitivität von Korallen-$\delta^{234}U$ gegenüber lokalen hydrologischen Einflüssen. Ein kubanisches Korallenarchiv zeigt, dass die erhöhte Variabilität am Ende der Kleinen Eiszeit auf einen verstärkten Einfluss des Mississippi zurückzuführen ist. Entlang der Halbinsel Yucatán wird die $\delta^{234}U$-Variabilität maßgeblich durch submarinen Grundwasserabfluss gesteuert, wobei relative Meeresspiegelschwankungen eine entscheidende Rolle spielen. Eine Vergleichsstudie auf Tahiti erweitert den geographischen Rahmen: Analysen von Korallen, Meerwasser, Flusswasser und Grundwasser belegen deutliche $\delta^{234}U$-Endglieder sowie eine Meeresspiegelabhängigkeit des submarinen Grundwasserabflusses, die Rückschlüsse auf ENSO-Variabilität ermöglicht.

Eine Synthese aller karibischen Korallenarchive zeigt hingegen, dass kein kohärentes regionales Signal erkennbar ist. Vielmehr dominieren lokale hydrologische Prozesse die $\delta^{234}U$-Signaturen, während der starke Atlantik-Durchfluss Süßwassereinflüsse verdünnt und das Karibische Becken im Mittel den offenen Ozean widerspiegelt. Im Gegensatz dazu weisen marginale Meeresbecken mit eingeschränkter Zirkulation, wie das Mittelmeer oder das Ostchinesische Meer, deutlichere Süßwassersignale auf. Insgesamt demonstriert diese Arbeit das Potenzial von Korallen-$\delta^{234}U$ als Proxy für Süßwassereinträge. Während wertvolle Informationen über lokale Hydrologie und Land-Ozean-Interaktionen gewonnen werden, erfordert die Anwendung in Regionen mit starkem ozeanischen Austausch eine besonders sorgfältige Interpretation. Die Ergebnisse erweitern die Methoden der Paläoklimaforschung und liefern neue Einblicke in die hydroklimatische Dynamik der Karibik und darüber hinaus.

Contents

List of Abbreviation

AMOC	Atlantic Meridional Overturning Circulation
AMV	Atlantic Multidecadal Variability
AWP	Atlantic Warm Pool
CT	Computer Tomography
$\delta^{18}O_{sw}$	$\delta^{18}O$ of the sea water
$\delta^{234}U_{sw}$	$\delta^{234}U$ of the sea water
DIC	Dissolved Inorganic Carbon
DOC	Dissolved Organic Carbon
ECS	East China Sea
ENSO	El-Niño Southern Oscillation
HT	High Tide
HU-1	Harwell Uraninite 1
ICP-OES	Inductively Coupled Plasma - Optical Emission Spectrometry
ITCZ	Inter Tropical Converges Zone
KED	Kinetic Energy Discrimination
LGM	Last Glacial Maximum
LIA	Little Ica Age
LT	Low Tide
MC-ICP-MS	Multi Collector - Inductively Coupled Plasma - Mass Spectrometer
PCA	Principle Component Analyses
SGD	Submarine Groundwater Discharge
SLP	Sea Level Pressure
SOI	Southern Oscillation Index
SSS	Sea Surface Salinity
SST	Sea Surface Temperature
Sv	Sverdrup (1 Sv = 10^6 m^3/s)
VPDB	Vienna Pee Dee Belemnite
yr	Year

1 Motivation

Understanding past variations in freshwater input to marine systems is fundamental for reconstructing hydroclimate dynamics and their influence on ecosystems and societies. Freshwater discharge into the coastal ocean directly affects salinity, circulation, and biogeochemical processes, and thus plays a critical role in shaping both marine and terrestrial environments (Drinkwater, 1986). In tropical regions such as the Caribbean, where human communities and ecosystems are highly sensitive to freshwater variability, robust proxies of past river discharge are urgently needed. Yet, despite decades of paleoclimate research, reliable marine archives of past freshwater flux remain scarce. Traditional approaches, such as stable oxygen isotopes in foraminifera or trace-element ratios in corals, often conflate signals of temperature, salinity, upwelling and/or biological effects, making it difficult to disentangle the freshwater contribution (Leder et al., 1996; Watanabe et al., 2002; Ourbak et al., 2006; LaVigne et al., 2016; Stevenson et al., 2018; Yamazaki et al., 2021). This limitation hampers our ability to place modern hydroclimatic changes into the context of long-term variability.

Recent studies suggest that uranium-series isotopes, particularly $\delta^{234}U$, hold promise as a novel proxy for freshwater input (Li et al., 2018; Li et al., 2023; Greve et al., 2025). The rationale lies in the contrasting uranium isotopic signatures of riverine and marine waters: rivers often display higher variability in $\delta^{234}U$ values compared to seawater (Andersen et al., 2007; Andersen et al., 2010; Kipp et al., 2022), such that variations in river discharge may be imprinted in the coralline aragonite of coastal settings. However, the use of coral $\delta^{234}U$ as a freshwater proxy has not been systematically tested, and its application to tropical settings such as the Caribbean remains underexplored. Establishing and validating this approach is therefore of high scientific significance.

The Caribbean region provides a compelling case study for developing and applying coral $\delta^{234}U$ as a freshwater proxy. Positioned at the confluence of Atlantic climate dynamics, Caribbean hydroclimate is strongly influenced by the Intertropical Convergence Zone (ITCZ), Atlantic Multidecadal Variability (AMV), and El-Niño Southern Oscillation (ENSO) teleconnections (Alexander et al., 2002; Wang et al., 2010; Alexander et al., 2014; Wang, 2019). Freshwater fluxes from both regional precipitation and riverine discharge exert profound impacts on coral reef ecosystems, fisheries, and coastal livelihoods. Furthermore, the region is projected to face intensified droughts and floods under future climate scenarios (Antuña-Marrero et al., 2016; Jones et al., 2016), yet the observational record remains too short to capture

the full range of natural variability. High-resolution reconstructions extending beyond the instrumental period are therefore essential to improve our understanding of long-term hydroclimatic dynamics and to constrain the sensitivity of the Caribbean hydrological cycle to external forcing.

My doctoral research addresses this gap by systematically exploring the potential of coral $\delta^{234}U$ as a proxy for freshwater input. By analysing modern coral specimens from sites across the Caribbean and comparing them with instrumental records of river discharge and precipitation, I assess the degree to which freshwater flux is recorded in coral uranium isotopic composition. In addition, I investigate the historical variability of freshwater input and its possible links to regional climate drivers. This dual approach, combining modern calibration with paleoclimate reconstruction, provides both methodological innovation and new insights into Caribbean hydroclimate.

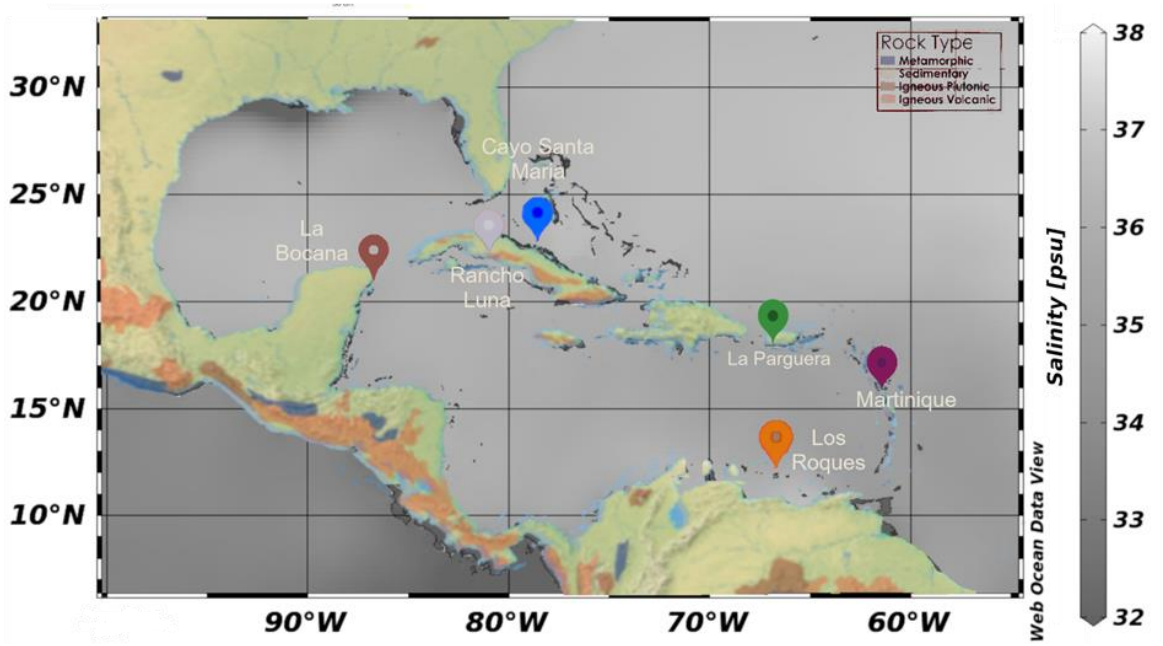

Figure 1.1 Location of coral sampling sites in the Caribbean the map is showing sea surface salinity distribution (psu) and sampling locations.

By addressing these questions, this thesis develops a new application of uranium isotopes in corals and situates the findings within the broader context of tropical hydroclimate research. The structure of the thesis reflects a progression from methodological development to regional synthesis.

Chapter 4 focuses on testing the precision of coral $\delta^{234}U$ measurements and establishing methodological constraints. In doing so, it identifies potential sources of uncertainty and provides guidance on best practices for sampling tropical corals, laying the foundation for reliable application of this proxy.

Building on this, **Chapter 5** establishes a baseline for the Caribbean by confirming that the open-ocean $\delta^{234}U$ value is valid for the Caribbean basin. This result provides a crucial reference point against which site-specific coral records can be evaluated.
The subsequent chapters present detailed case studies.
Chapter 6 examines a Cuban coral archive, revealing a stable baseline with superimposed variability that reflects local precipitation patterns over Cuba. Importantly, the record shows that at the end of the Little Ice Age $\delta^{234}U$ variability increases markedly, which suggests a stronger influence of Mississippi River discharge at that time.
Chapter 7 then turns to the Yucatán Peninsula, where a coral record demonstrates that submarine groundwater discharge exerts a strong control on $\delta^{234}U$, with its variability linked to relative sea-level changes. This study underscores the sensitivity of $\delta^{234}U$ to hydrological processes occurring at the land-ocean boundary.
Chapter 8 extends the investigation beyond the Caribbean to Tahiti in the Pacific Ocean. Here, in addition to coral material, seawater, river water, and groundwater were analysed, revealing distinct $\delta^{234}U$ endmembers for the island's different reservoirs. The findings demonstrate a sea-level dependence of groundwater discharge, which in turn suggests that coral $\delta^{234}U$ can provide a means of reconstructing ENSO-related variability.
Finally, **Chapter 9** synthesizes all available Caribbean coral records. The comparison shows that no coherent basin-wide signal emerges; instead, local hydrological influences dominate coral $\delta^{234}U$. When contrasted with marginal basins such as the Mediterranean or the East China Sea, the Caribbean appears distinct, as its high-throughflow Atlantic exchange dilutes freshwater inputs and causes the basin to approximate open-ocean $\delta^{234}U$ conditions on average.
Together, these chapters advance understanding of coral $\delta^{234}U$ as a freshwater proxy, clarifying its potential and limitations while highlighting the conditions under which it reflects local or regional hydroclimatic variability.

2 Fundamentals

2.1 Freshwater

Freshwater input into marine systems plays a pivotal role in shaping oceanic dynamics, including currents, water column stratification, nutrient availability, and pollution dispersal. The inflow of freshwater reduces seawater density, altering buoyancy-driven circulation patterns and creating vertical stratification, which can affect the vertical transport of nutrients and heat. Furthermore, freshwater input delivers substantial amounts of terrestrial nutrients and anthropogenic pollutants into marine ecosystems, which can significantly influence biogeochemical cycles and coastal water quality (Drinkwater, 1986).

Since 2004, the Global Runoff Data Centre (GRDC) has provided the dataset Freshwater Fluxes into the World's Oceans, which includes annual runoff values for 1901–2016, resolved by 5° and 10° latitude bands and UNEP GIWA regions. These data estimate a total freshwater input of 40,181 km^3 per year (1.277 Sv) to the global ocean between 90°N and 60°S. In addition to riverine runoff, submarine groundwater discharge (SGD) directly supplies groundwater to coastal seas, contributing an estimated 460 km^3 per year, or about 10% of the total flux (Kuang et al., 2024). Global freshwater inputs vary interannually by roughly 10–20%, while large uncertainties remain regarding the magnitude and spatial distribution of SGD.

Human activity and climate change have measurably altered these fluxes and their chemical composition, particularly through dam construction, groundwater extraction, and land-use change. Although modern monitoring provides increasingly detailed records, reconstructing natural variability in groundwater fluxes prior to the instrumental period remains a major challenge (Kuang et al., 2024). Semi-enclosed basins are especially sensitive to freshwater input, as restricted circulation enhances the influence of both river runoff and SGD. Examples include the Andaman Sea, Arctic Ocean, Mediterranean Sea, East China Sea, and, most relevant here, the Caribbean Sea and Gulf of Mexico.

The Caribbean Sea and Gulf of Mexico receives about 3120 km^3/a of freshwater from major rivers and shows an annual variance of 17% (Figure 2.1) (GRDC, 2025). The groundwater fluxes remain largely unquantified, but the Yucatan peninsula lacks major rivers and groundwater essentially moves via SGD towards the Caribbean Sea (Bauer-Gottwein et al., 2011). Therefore, this ocean basin is of particular interest when establishing novel tools to study the natural freshwater flux variance and its possible implication on the larger scale ocean circulation and nutrient supply. Consequently, in this work we focus on the Caribbean Sea and Gulf of Mexico to

investigate its variability of traceable freshwater contributions, using corals and geochemical proxies.

In the western tropical Atlantic, freshwater primarily enters the system from three major rivers: the Mississippi, Orinoco, and Amazon. The Mississippi River, which drains the largest watershed (40%) in the United States, discharging an estimated 0.0168 Sv of freshwater annually into the Gulf of Mexico (Dai & Trenberth, 2002). This input has profound effects on the Gulf's stratification and salinity, which are particularly important when examining on the strength of the Gulf stream (Enfield et al., 2001). The Orinoco River, located at the eastern edge of the Caribbean, contributes freshwater at a higher rate, discharging approximately 0.0376 Sv (Dai & Trenberth, 2002). Its proximity to the Caribbean Sea means that its freshwater directly influences the salinity, nutrient content, and water dynamics at the entrance to the basin (Chérubin & Richardson, 2007). The Amazon River is the largest freshwater contributor, with a discharge of approximately 0.17 Sv (Figure 2.1). Although the Amazon does not flow directly into the Caribbean, its waters are transported into the basin via the Guiana and Brazil Currents (Chérubin & Richardson, 2007). These currents carry vast amounts of low-salinity water, as well as nutrients and sediment from the Amazon Basin, into the western tropical Atlantic, significantly affecting salinity and nutrient distributions over a large area (Kilbourne et al., 2007; Paterne et al., 2023). Smaller rivers in the region also contribute freshwater, although their influence is largely localized to coastal areas and does not extend to the main throughflow currents (Beier et al., 2017). However, the geological evolution of these riverine freshwater fluxes, and their long-term impact on uranium and nutrient cycling within the Caribbean basin, remain poorly constrained. While modern studies document the influence of large rivers such as the Orinoco and Amazon on salinity, sediment supply, and nutrient delivery (Chérubin & Richardson, 2007; Wesselingh & Hoorn, 2011; Aguiar et al., 2022), it is less clear how these fluxes have varied over geological timescales or during periods of climatic reorganization. Changes in drainage patterns, sediment routing, and sea-level–controlled river mouths likely altered the magnitude and composition of freshwater inputs, yet their cumulative effect on basin-wide biogeochemistry is not well understood (Stallard, 1985; Wesselingh & Hoorn, 2011). As a result, the role of riverine fluxes in shaping both the chemical framework of the Caribbean and its connectivity with the open Atlantic remains an open question.

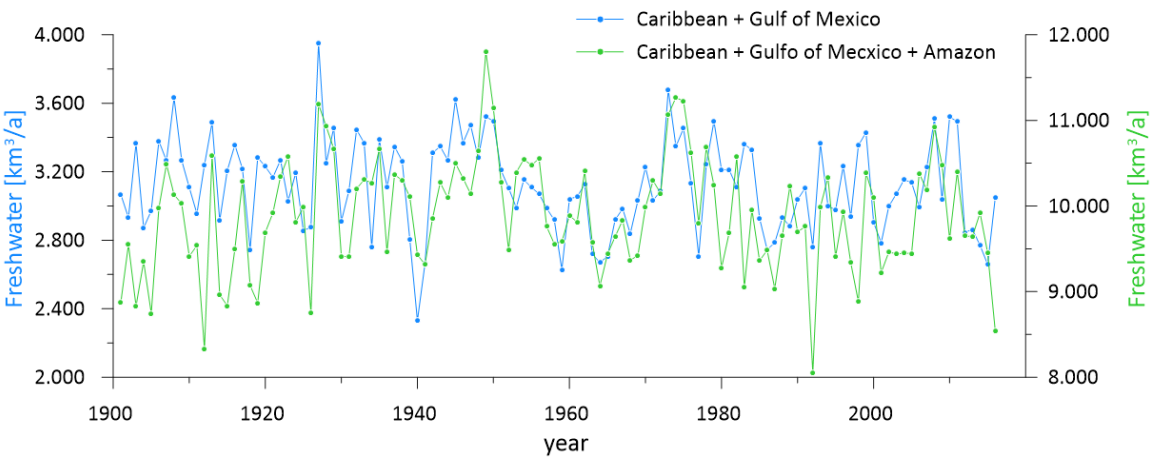

Figure 2.1 Freshwater flux into the Caribbean Sea, and Gulf of Mexico with and without the contribution of the Amazon. The Caribbean receives about 8% of the global freshwater. When adding the flux of freshwater from the Amazon river it receives 25% of the global freshwater. The annual variance is on the order of 15% and the flux of SGD is largely unknown but likely important. (Data from GRDC, 2025).

In areas underlain by karstic geology, SGD becomes an important additional source of freshwater. SGD is particularly significant in karstic regions due to the high permeability of the underlying substrate, allowing large volumes of groundwater to flow directly into the ocean (Bauer-Gottwein et al., 2011). Moreover, SGD is a crucial yet often underestimated contributor to global freshwater budgets, nutrient cycling, ecological health, and coastal water chemistry. While rivers account for the majority (90–99%) of freshwater input into coastal regions (Church, 1996), the remaining 1–10% comes from aquifers, which discharge fresh SGD directly into coastal wetlands, beaches, and continental shelves (Burnett et al., 2003). In addition to fresh SGD from terrestrial sources, saline groundwater also flows through the seabed at significant rates (Kwon et al., 2014). Estimates suggests that tropical coastlines, such as in the Caribbean Sea, account for over 56% of global fresh SGD, whereas arid regions in midlatitude areas contribute likely only 10% (Zhou et al., 2019). These contributions can locally affect salinity, nutrient levels, and pollution distribution in coastal zones as well as element and isotope concentrations of trace element such as uranium (Null et al., 2014). Because SGD enters the coastal ocean in close proximity to reef environments, its influence on corals is more immediate and pronounced than that of larger, more distal freshwater sources (Xu et al., 2024).

Between the diverse riverine inflows originating from contrasting geological and weathering regimes and the widespread inputs of SGD, the Caribbean Sea experiences a mosaic of localized effects. Each source carries its own chemical fingerprint, shaped by the lithology, hydrology, and climate of its catchment, and these inputs can alter salinity, nutrient supply, and carbonate chemistry on regional to reef scales. As a result, the Caribbean Basin is characterized not by a single uniform freshwater signal,

but by a patchwork of local influences that interact with the broader circulation to produce high spatial variability in environmental conditions.
Importantly, the flow of freshwater and groundwater into the Caribbean Sea and Gulf of Mexico and its mixing with seawater along the path strongly depends on the topography of the ocean basins and the hydroclimate stimulating changes in the water cycle.

2.1.1 Caribbean Basin

The Caribbean Sea and Gulf of Mexico are dynamic marine environments influenced by various natural processes, including the complex interactions between ocean currents, freshwater inputs, and geological features.
The western tropical Atlantic comprises these two distinct basins semi-enclosed systems, bordered by the North, Central, and South American continents to the north, west, and south. To the east, the Caribbean Sea is partially enclosed by an arc of islands collectively known as the Lesser and Greater Antilles, which form a natural boundary between the Caribbean Sea and the Atlantic Ocean (Uchupi, 1975). The basins have evolved over tens of millions of years due to the complex movements and interactions of tectonic plates, including the North American, South American, and Caribbean plates. Geologically, the Caribbean region is dominated by marine limestone, which forms much of the underlying bedrock and has been deposited over geological timescales in shallow, warm marine environments. In addition to limestone, igneous rocks are also present, albeit in smaller quantities. These igneous formations are primarily associated with the tectonic activity of the region, such as subduction zones and volcanic arcs, which have played a critical role in shaping the region's unique geological features (Fox & Heezen, 1975).
Due to the tectonically active status of the Caribbean island arc, frequent earthquakes and associated processes continuously reshape the seafloor. Submarine landslides, sediment resuspension, and shifts in seafloor morphology create a dynamic margin where depositional environments can evolve rapidly in both space and time (Dorel, 1981; Feuillet et al., 2011). In addition, the interaction of multiple tectonic plates drives volcanism, active faulting, and cycles of uplift and subsidence, all of which contribute to a constantly evolving coastal and marine landscape. These processes also influence geochemical conditions: fracturing of the crust enhances fluid circulation, submarine volcanic activity releases magmatic gases and hydrothermal fluids, and disturbed sediments can alter oxygen availability and redox conditions (Martin et al., 1996). Together, these factors create a margin where both the physical

and chemical environment are in flux, shaping the framework within which biological, hydrological, and oceanographic processes operate.

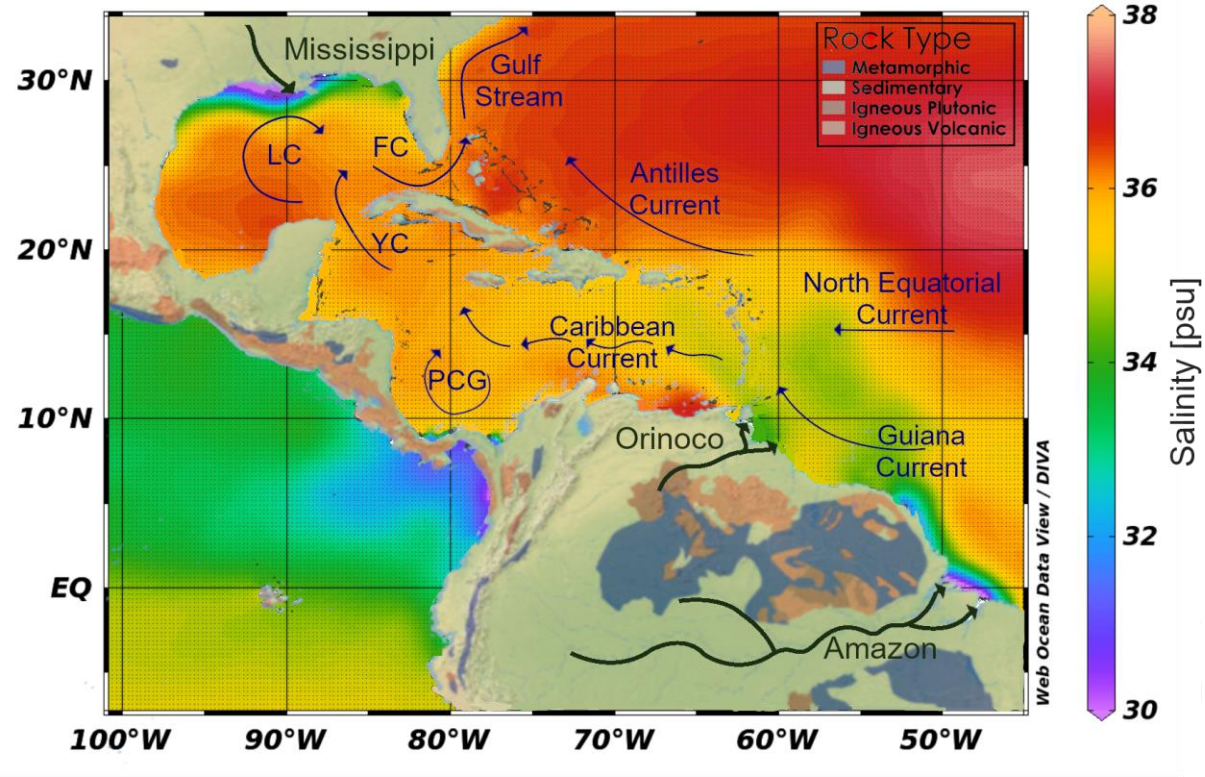

Figure 2.2 Surface ocean circulation and annual salinity distribution in the western tropical Atlantic, Caribbean Sea, and Gulf of Mexico. The map illustrates major ocean currents (blue arrows) and riverine freshwater inputs (black arrows) from the Amazon, Orinoco, and Mississippi Rivers. The background colour scale represents surface salinity levels (PSU), ranging from lower salinity (green/blue) in regions influenced by freshwater discharge to higher salinity (orange/red) in open ocean waters. Rock types are indicated in the upper legend, highlighting the geological diversity of the region. Abbreviation: LC – Loop Current, FC – Florida Current, YC – Yucatán Current, PCG – Panama-Colombia Gyre.

2.1.2 Currents

The semi-enclosed nature of the Caribbean and Gulf of Mexico basins governs the predominant direction of water flow through these regions. Oceanic water enters the Caribbean Sea from the South and Central Atlantic via two major currents: the Guiana Current and the North Equatorial Current. These currents flow westward and pass into the Caribbean primarily through the passages within the Lesser Antilles, forming the Caribbean Current. This current continues to flow west and northward, giving rise to the Yucatán Current as it enters the Gulf of Mexico. From there, the flow transitions into the Florida Current, which exits the Gulf through the Florida Strait and forms the Gulf Stream, a major component of the Atlantic Meridional Overturning Circulation (AMOC), traveling north-eastward in the open Atlantic Ocean (Centurioni & Niiler, 2003). This circulation system is an integral part of the global thermohaline

circulation, drives northward advection of saline and warm waters from the tropics followed by deep water formation in the Nordic Seas of the North Atlantic. The circulation through the basins is part of the subtropical gyre circulation, which is stimulated by the average clockwise wind pattern of the tropical easterly trade winds and the mid-latitude westerlies. The total inflow into the Caribbean is approximately 28 Sverdrups (Sv), which is partitioned between water entering through the Lesser Antilles (18 Sv) and the Greater Antilles (10 Sv). The combined outflow through the Florida Strait is estimated to balance the total inflow as evaporative water loss is compensated by river runoff (Johns et al., 2002). The water movement within the basins is further influenced by numerous eddies, gyres, and the Loop Current in the Gulf of Mexico, which serve to redistribute water away from the primary flow pathways and cause strong mixing (Centurioni & Niiler, 2003). These mesoscale features are generated by the interaction of the North Brazil Current, the Caribbean Current, and the inflow through the island passages with topography, leading to a circulation that is highly variable in both space and time. Anticyclonic and cyclonic eddies are common throughout the Caribbean Sea, where they trap and transport water masses, nutrients, and heat over large distances (Murphy et al., 1999; Beier et al., 2017). In the Gulf of Mexico, the Loop Current and its associated eddies play a key role in modulating the exchange between the Caribbean and the subtropical North Atlantic, while within the Caribbean Sea itself, gyres and recirculation zones contribute to a complex hydrographic structure that shapes salinity patterns, vertical mixing, and residence times of water masses (Androulidakis et al., 2020).

On a finer scale, variations in flow rates are controlled by relative sea-level differences among the interconnected basins. Even small gradients in sea-surface height can generate pressure-driven currents through the narrow island passages, enhancing or restricting exchange between basins. These differences act as a key driver of regional circulation patterns, influencing how water masses are distributed within the Caribbean and how they ultimately connect to the Gulf of Mexico and the Atlantic Ocean (Ezer, 2022).

2.1.3 Caribbean Climate

The northern Caribbean is part of the Atlantic Warm Pool (AWP), which is defined by the sea surface temperature (SST) isotherm exceeding 28.5°C. This warm pool develops each year during early summer (June) and gradually expands into the Gulf of Mexico and the western tropical North Atlantic as summer progresses (July–October) (Wang & Enfield, 2001; Wang et al., 2008). Its seasonal growth represents one of the most significant thermal features of the tropical Atlantic, as the AWP reaches its maximum extent during boreal autumn. In this region, strong evaporation

leads to increasing sea surface salinity (SSS), while tropical warming and high solar irradiance drive elevated SSTs, together forming the seasonal development of the AWP (Wang et al., 2008). The presence and extent of the AWP play a critical role in regulating regional climate, influencing the strength of atmospheric convection, moisture availability, and the potential for hurricane intensification. Most importantly the seasonal migration of the Intertropical Convergence Zone (ITCZ) further exerts a strong control on Caribbean climate, particularly in the south. As the ITCZ shifts northward during boreal spring and summer, it brings increased rainfall to the southern Caribbean, resulting in a distinct wet season that lasts from April to October (Martinez et al., 2019). The strong tropical surface ocean heating further supplies the energy to atmospheric storm, which can evolve into hurricanes often moving north westward in the late summer and fall (Terry & Kim, 2015). The combined influence of the AWP and ITCZ thus creates a pronounced seasonal rhythm, marked by warm, saline waters and heightened storm activity in the north, and abundant precipitation and freshwater input in the south.

In addition to these seasonal drivers, the Caribbean climate is modulated by longer-term oceanic and atmospheric variability. On interannual timescales, the El Niño–Southern Oscillation (ENSO) exerts a strong influence, with El Niño events typically associated with warmer SSTs and suppressed rainfall across much of the basin, and La Niña phases enhancing precipitation and storm activity. The North Atlantic Oscillation (NAO) modulates the strength of the trade winds and evaporation rates, thereby influencing both regional salinity and the delivery of moisture into the Caribbean. On multi-decadal scales, the Atlantic Multidecadal Variability (AMV) has been linked to shifts in rainfall patterns, the frequency of droughts, and hurricane activity, while changes in monsoonal regimes alter moisture transport from South America (Wang & Enfield, 2001; Wang, 2002; Wanner et al., 2011; Cai et al., 2019).

In the tropical Americas, future climate scenarios predict increased warming also in the lower latitudes (Taylor et al., 2018). Over the latter half of the last century to the present, there has been a mean warming the tropics in both air and SST of more than 0.5°C (Glenn et al., 2015; Antuña-Marrero et al., 2016; Jones et al., 2016). With greater summer SSTs, higher tropical storm energies, and hence, the appearance of more frequent, and/or more intense Hurricanes is likely (Bender et al., 2010; Patricola & Wehner, 2018).

Variance in river runoff and SGD into the Caribbean Sea and Gulf of Mexico is shaped by climate-driven shifts in the ITCZ, multi-annual to decadal ocean–atmosphere dynamics, and occasionally by volcanism. While many of these parameters are well monitored today, little is known about their development since the Little Ice Age (LIA) or in earlier centuries. Tracers are therefore required to capture changes in

hydroclimate and ocean dynamics across timescales from months to millennia. Recent work has shown that the isotopic composition of uranium in seawater can reflect global freshwater fluxes and circulation changes (Border, 2020; Shang et al., 2021; Li et al., 2023). In this thesis, we assess the potential of this proxy to reconstruct the past two centuries of climate and circulation variability in the Caribbean Sea and Gulf of Mexico.

2.2 The Marine Uranium Cycle

Uranium is a naturally occurring salt like element in seawater that provides an important geochronological toolbox for the precise dating of marine carbonates and more recently was used in paleoceanographic reconstructions due to its redox sensitivity. Its isotopic composition and concentration provide valuable insights into past ocean chemistry, weathering inputs, and carbonate.

Uranium is found in varying concentrations across most rock types but is particularly enriched in acidic rocks, granites and gneiss with concentrations of up to 10 µg/g. In contrast sedimentary rocks may contain hundreds of µg/g uranium when those form in reducing environments. Particular high concentrations of up to 350 µg/g are found in Black Shales and phosphate sedimentary rocks. Those rocks from reducing environments point to the major sink of U in the marine cycle (Dunk et al., 2002)

Due to the ionic similarity of ca, Sr, Ba, and U the latter is also incorporated in marine carbonates shells, with aragonite reflecting the mineral with the highest U concentrations of up to 10 µg/g. Through the process of weathering and leaching, uranium is mobilized from continental rocks and transferred into the hydrological systems, where it is carried by both groundwater and rivers to the oceans (Bourdon et al., 2003; Choppin et al., 2013). Groundwater contributes approximately 42.0 ± 14.5 Mmol/yr of uranium, while rivers transport around 9.3 ± 8.7 Mmol/yr of uranium to the oceanic reservoir. Once in solution, uranium predominantly exists in the highly soluble hexavalent state (U(VI)) under oxic conditions, leading to a high complex potential and solubility. These inputs, derived from rivers and SGD, sustain the oceanic uranium reservoir in balance, which is estimated to contain 19,000,000 ± 1,200,000 Mmol of uranium (Dunk et al., 2002). Due to its residence time in seawater of 200–400 thousand years, the uranium concentration in the ocean is considered stable over recent geological eras such as the glacial cycles, with minor fluctuations (Ku et al., 1977; Dunk et al., 2002). The removal of uranium from the ocean occurs primarily under suboxic to anoxic conditions, where uranium transitions to the less soluble tetravalent state (U(IV)), leading to its precipitation in sediments. This process results in a removal rate of approximately 11.6 ± 6.0 Mmol/yr in suboxic environments and 15.3 ± 10.6 Mmol/yr in anoxic settings (Dunk et al., 2002). Such

conditions strongly affect uranium concentrations in river estruaries, as illustrated by the Amazon system. In the Amazon delta, the development of anoxic and reducing porewaters drives the reduction of soluble U(VI) to insoluble U(IV), leading to uranium precipitation and burial in the sediments. This process effectively removes uranium from the dissolved load (Border, 2020). Weather this process in the Amazon delta is seasonally active or was active in the past is not known.

Another important sink are biogenic carbonates, such as corals, which incorporate around 13.3 ± 5.6 Mmol/yr of uranium into their structures contributing to long-term sequestration in marine carbonates. Smaller quantities of uranium are also removed from the ocean through incorporation into altered basalt during hydrothermal processes, hydrogenous phases, and biogenic silica, although these pathways represent trace amounts compared to the primary mechanisms of removal (Dunk et al., 2002). The amout of Uranium being transported from the groundwater into the Oceanic reservoir is not well constrained, but studies indicate that this the amount is stubstation at least in the semi constrained setting of the Mediterrainean (Border, 2020).

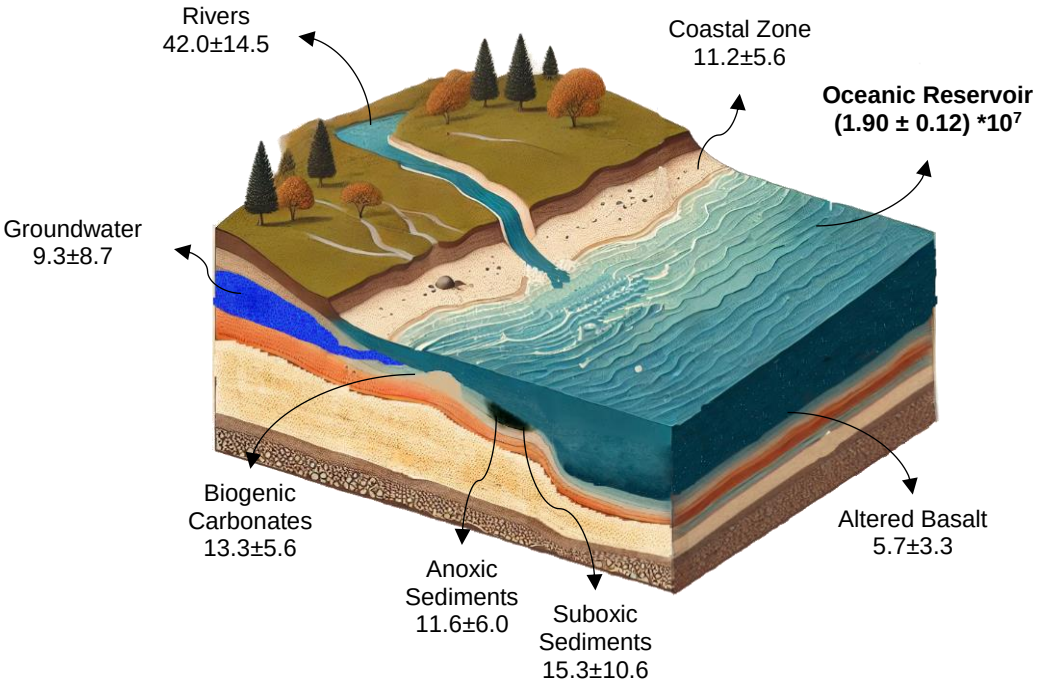

Figure 2.3 Conceptual model of uranium cycling between terrestrial and marine reservoirs. Major uranium fluxes (Mmol/year) calculated by Dunk et al. (2002), are shown for key pathways, including riverine (42.0 ± 14.5 Mmol/yr) and groundwater (9.3 ± 8.7 Mmol/yr) inputs, as well as removals through anoxic (11.6 ± 6.0 Mmol/yr) and suboxic (15.3 ± 10.6 Mmol/yr) sedimentation, biogenic carbonate incorporation (13.3 ± 5.6 Mmol/yr), and altered basalt uptake (5.7 ± 3.3 Mmol/yr). The oceanic uranium reservoir is estimated at 19,000,000 ± 1,200,000 Mmol.

2.2.1 Uranium Isotope Composition ($\delta^{234}U$)

Three isotopes of uranium are naturally occurring: ^{238}U, ^{235}U, and ^{234}U, with relative abundances of approximately 99.275%, 0.720%, and 0.005%, respectively (Choppin et al., 2013). Among these, ^{238}U and ^{234}U are part of the same decay chain. ^{238}U undergoes alpha decay to form ^{234}Th, which subsequently decays to ^{234}Pa and then to ^{234}U. The chain continues with ^{234}U decaying to ^{230}Th, eventually ending with the formation of stable ^{206}Pb. The intermediate isotopes ^{234}Th and ^{234}Pa have very short half-lives and are therefore not considered in long-term geochemical processes. Nevertheless, those can have a great influence on the environmental distribution of ^{234}U via chemical fractionation of ^{234}Th and ^{234}U.

^{238}U and ^{234}U have half-lives of 4.46 billion years and 245.6 thousand years, respectively (Jaffey et al., 1971; Ivanovich & Harmon, 1992; Cheng et al., 2013). This makes them relatively stable isotopes that persist over geological timescales and are central to uranium cycling in natural systems. During the alpha decay of ^{238}U, an alpha particle is emitted, causing the daughter isotope (^{234}Th) to experience a recoil effect that displaces it by up to 30 nanometres. When this decay occurs at the sediment-water interface, the recoil can eject ^{234}Th atoms from the solid phase into the liquid phase. As a result, ^{234}U, which is generated from the rapid decay of ^{234}Th accumulates in the water relative to ^{238}U, creating a disequilibrium between the two isotopes (Kigoshi, 1971; Chabaux et al., 2008). Note, this preferential ^{234}U emission process can also be reversed, when the solution contains higher ^{238}U than the solids and the excess ^{234}U production is eliminated when the host rocks readily dissolve completely. The disequilibrium is quantified using the activity ratio of $^{234}U/^{238}U$ expressed typically as the permille deviation from equilibrium $\delta^{234}U$, which is calculated as follows, where $\left(^{234}U/_{238}U\right)_{Standard}$ is in secular equilibrium:

$$\delta^{234}U\ (‰) = \left(\frac{\left(^{234}U/_{238}U\right)_{Probe}}{\left(^{234}U/_{238}U\right)_{Standard}} - 1 \right) * 1000$$

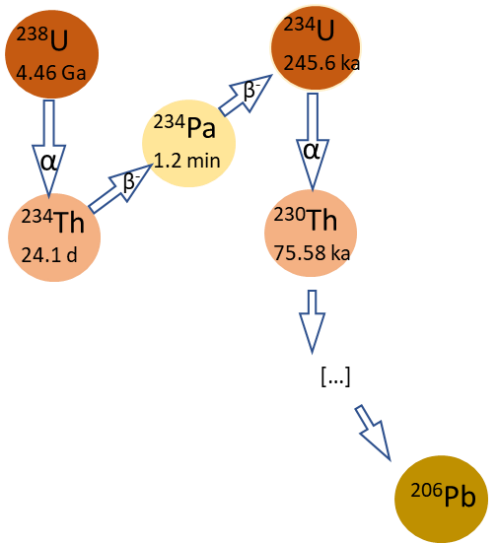

Figure 2.4 The simplified decay chain of ^{238}U to ^{206}Pb, highlighting key intermediate radionuclides and their half-lives. ^{238}U, with a half-life of 4.46 billion years, undergoes alpha decay to form ^{234}Th, which further decays with a short half-life of 24.1 days. The chain continues through ^{234}Pa with a very short half-life before forming ^{234}U, which has a much longer half-life of 245.6 thousand years. Subsequent decay leads to ^{230}Th, an important isotope for dating marine carbonates due to its 75.58-thousand-year half-life. The series continues with further alpha and beta decays, ultimately reaching stable ^{206}Pb.

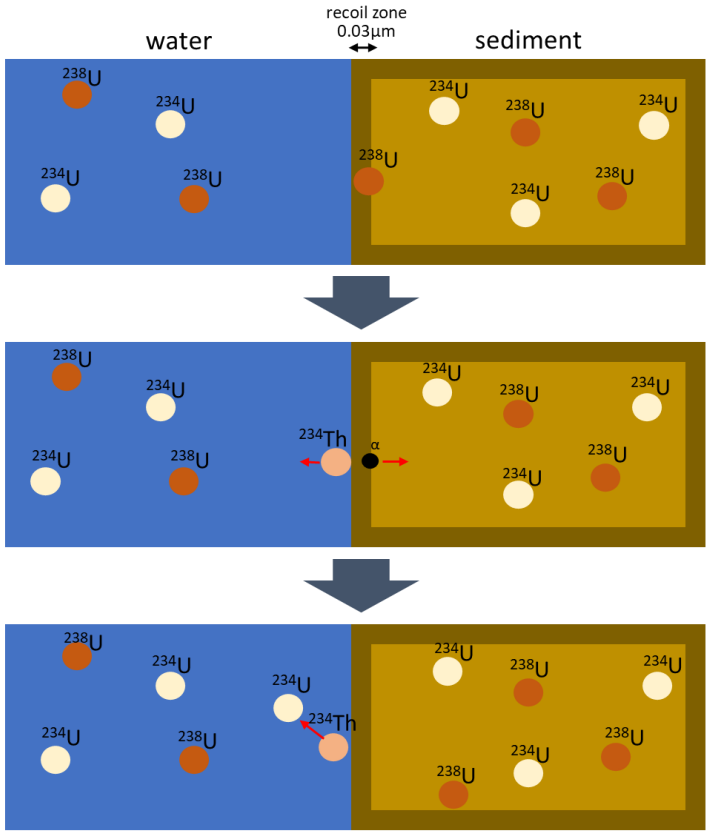

Figure 2.5 Schematic representation of the alpha recoil effect during the radioactive decay of ^{238}U and its influence on ^{234}U mobility. In the initial state (top panel), ^{238}U and ^{234}U are distributed between a solid-phase mineral (yellow) and surrounding fluid (blue). Upon the decay of ^{238}U to ^{234}Th (middle panel), alpha recoil ejects the newly formed ^{234}Th nucleus, potentially displacing it from the solid phase into the surrounding fluid. As ^{234}Th decays to ^{234}U (bottom panel), the uranium isotope distribution in the fluid is altered, leading to an excess of ^{234}U relative to secular equilibrium.

The mean $\delta^{234}U$ value of modern seawater is approximately 145.5‰, and due to the long residence time of uranium in the ocean (200–400 thousand years), it is nearly homogeneously distributed throughout the global oceans (Kipp et al., 2022). Knowledge of the initial $\delta^{234}U$ is essential in U-series dating of carbonates, because the initial $\delta^{234}U$ ratio is often used as a quality control parameter of U series open system behaviour. Deviations from the true initial value, and in particular correlated deviation measured the activity ratio of ($^{230}Th/^{238}U$) and $\delta^{234}U$ are a clear indication of carbonate U series open system behaviour and U exchange with the environment (Thompson et al., 2003; Villemant & Feuillet, 2003; Scholz et al., 2004; Frank et al., 2006).

The $\delta^{234}U$ values of river waters exhibit considerable variability, ranging from 70‰ to over 1000‰ (Dunk et al., 2002). This variation is primarily driven by differences in uranium concentrations in the host rocks, the residence time of water within the watershed, and the intensity of weathering processes (Palmer & Edmond, 1993). Rivers serve as a major source of uranium to the ocean, and their $\delta^{234}U$ signatures contribute to the overall uranium isotope composition and ^{234}U excess of seawater. Once introduced into the ocean, these riverine uranium inputs leave a distinct isotopic imprint on seawater (Ku et al., 1977; Chen et al., 1986; Delanghe et al., 2002; Robinson et al., 2004a; Andersen et al., 2010; Andersen et al., 2015; Kipp et al., 2022). Thus, in coastal environments, localized processes can lead to deviations from the average open ocean value. Inputs such as terrestrial runoff (Palmer & Edmond, 1993; Chabaux et al., 2008), SGD (Border, 2020), and glacial meltwater (Andersen et al., 2007; Chen et al., 2016; Li et al., 2023) can introduce uranium with different $\delta^{234}U$ signatures, leading to spatial and temporal variations in local and regional seawater composition, particularly in nearshore regions. On glacial-interglacial timescales, seawater $\delta^{234}U$ has undergone moderate but measurable changes in response to variations in global ice volume, the groundwater hydrology and weathering processes. During the Last Glacial Maximum (LGM), seawater $\delta^{234}U$ was about 5–7‰ depleted compared to present-day values, likely due to a reduction in meltwater input from ice sheets and glaciers, in particular into the Arctic Ocean and North Atlantic (Chen et al., 2016). The decreased input of uranium, combined with potentially lower chemical weathering rates in a colder polar environments, sea-level changes, and drier tropical climate, and mangrove forest reorganisation, caused this global shift in the oceanic uranium isotope balance (Esat & Yokoyama, 2006, 2010; Chutcharavan et al., 2018). A sensitivity of oceanographic $\delta^{234}U$ values to freshwater input would not only imply the possibility to investigate ocean circulation, but also reconstruct freshwater pathways. Because no significant sinks affect the isotopic composition of uranium in the ocean, any influx of excess ^{234}U can only be balanced by its long-term radioactive

decay. Variability in the flux of uranium and its isotopes from continental sources therefore drives the observed global to regional changes. Owing to its long residence time, uranium is relatively enriched in seawater, with average concentrations of ~3.3 µg/L. In contrast, rivers and groundwaters typically carry much lower concentrations (~1 µg/L), which reduces the relative sensitivity of the coastal ocean to changes in isotope and uranium fluxes (Dunk et al., 2002; Andersen et al., 2010).

Because natural variations in $\delta^{234}U$ are typically only on the order of a few tens of per mil, detecting meaningful environmental signals requires very high analytical precision. To distinguish genuine changes in sea water from analytical noise, reproducibility better than ±1‰ is required. Due to the high seawater uranium concentration only very small deviations are caused by freshwater inputs, changes in weathering regimes, and/or groundwater contributions. In practice, $\delta^{234}U$ is determined by high-precision isotope ratio mass spectrometry and results are calibrated against internationally recognized uranium standards to ensure accuracy and comparability across laboratories. Recent laboratory assessments by Kipp et al. (2022) and Chutcharavan et al. (2018) have highlighted both the achievable reproducibility of <1‰ and the importance of rigorous calibration, underlining that the reliability of $\delta^{234}U$ as a tracer rests directly on maintaining such analytical standards.

To trace such minor changes in either the global ocean over millennial time scales or near freshwater inputs over decades to centuries, archives are needed that store the seawater U isotope composition without fractionation. Such an archive are tropical corals with aragonite skeletons.

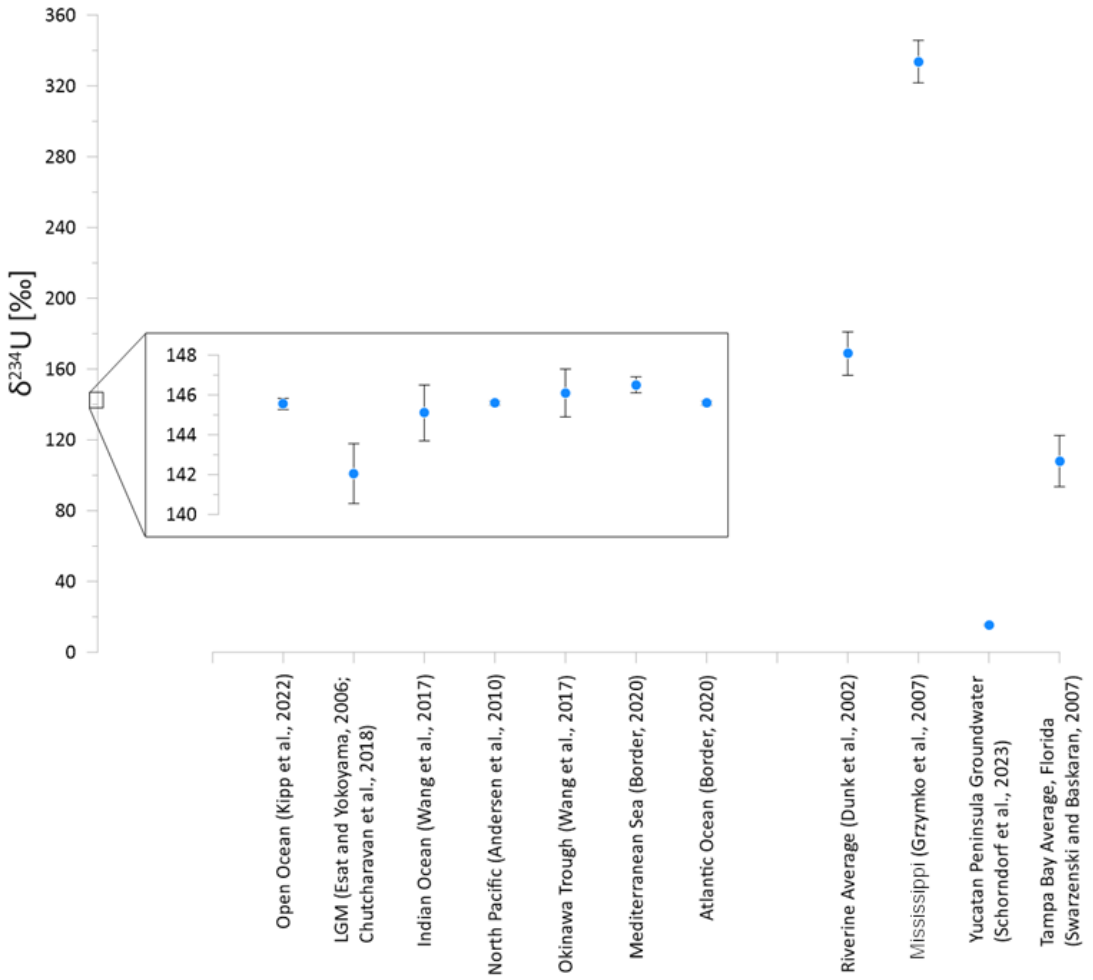

Figure 2.6 Global and regional $\delta^{234}U$ values compiled from modern marine, riverine, and groundwater sources. Marine values include open ocean (Kipp et al., 2022), LGM reconstructions (Esat & Yokoyama, 2006; Chutcharavan et al., 2018), and specific basins (e.g., Indian Ocean, Mediterranean Sea) (Andersen et al., 2010; Wang et al., 2017; Border, 2020), showing $\delta^{234}U$ generally between ~142‰ and 147‰. Riverine and groundwater sources display broader variability (Dunk et al., 2002; Grzymko et al., 2007; Swarzenski & Baskaran, 2007; Schorndorf et al., 2023). A close-up inset highlights the narrow range of marine $\delta^{234}U$ values relevant for comparison with proxy records.

2.3 Tropical Corals

Surface dwelling corals are marine organisms that thrive in tropical to subtropical regions, primarily in the shallow surface ocean (Figure 2.7) where conditions such as temperature, light availability, and water chemistry support their growth in symbiosis with algae. They comprise a diverse range of species, yet only certain groups, especially massive reef-building scleractinian corals such as *Porites*, *Diploria*, *Siderastrea* and *Orbicella*, are suitable for geochemical studies for climate reconstruction, as their dense aragonitic skeletons can be preserved over centuries and millennia. In the Caribbean the *Siderastrea* and *Orbicella* (formally *Montastrea*) are most common for annual to seasonal climate reconstruction, due to their clear skeletal structures and massive coral colonies (Watanabe et al., 2003; Giry et al., 2010; DeLong et al., 2011; DeLong et al., 2016). Some coral species can live for up to 250

years, providing long-lived archives of past oceanographic and climatic conditions (Veron, 1995).

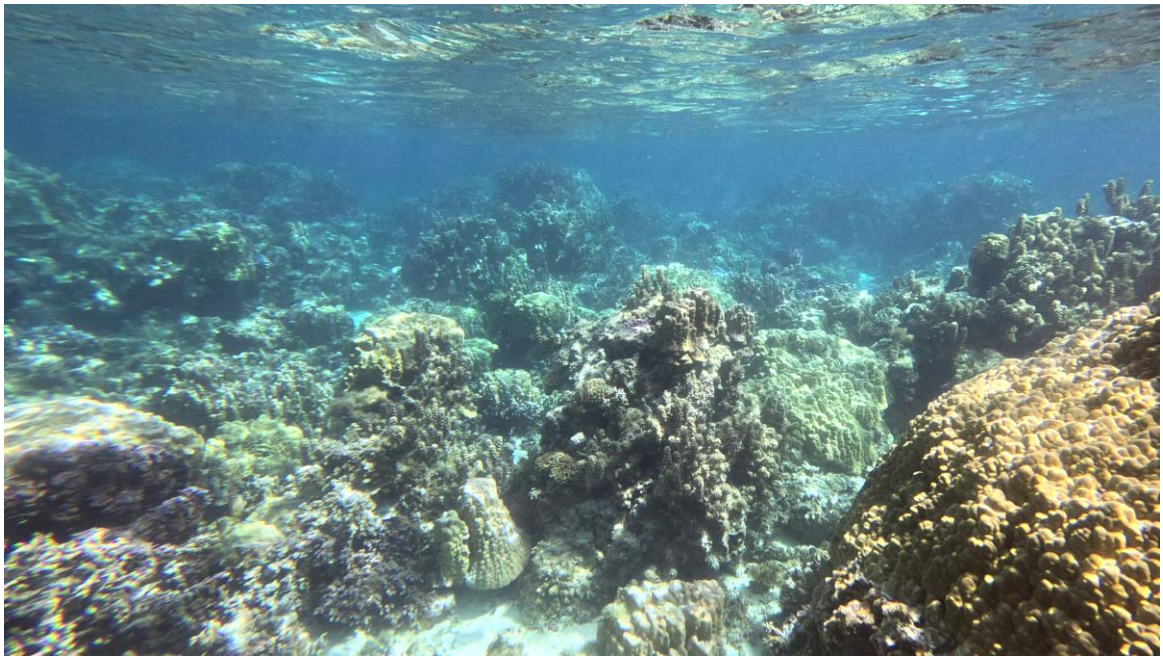

Figure 2.7 Healthy coral reef in Tahiti (French Polynesia) illustrating the diversity of growth forms, including massive boulder corals, finger corals, and branching corals.

The coral colony is comprised of a large number of coral polyps which together build a large sometimes several meter sized aragonite skeletons. The Ca^{2+} and bicarbonate (HCO_3^-) to build the skeleton is taken from the seawater, together with a large number of other ions. The organisms regulate the internal PH to generate supersaturation of CO_3^{2-} which causes the formation of the solid carbonate fabric, often in various textures.

$$Ca^{2+}_{(aq)} + CO^{2-}_{3\,(aq)} \rightarrow CaCO_{3\,(aragonite)}$$

During their growth, aragonitic carbonate skeletons develop distinct density bands that often change seasonally. These density variations allow for precise dating of coral growth layers by layer counting, similar to tree rings, enabling sub-annual chronological reconstructions (Barnes & Devereux, 1988). Coral sclerochronology, based on counting annual density bands, provides a widely used approach for establishing age models. Small offsets of a few years (1–2yrs) are within the typical uncertainty of this method, arising from band-counting precision, surface preparation, and sampling resolution (Buddemeier et al., 1974). In addition to density band counting, $^{230}Th/U$ dating can be applied due to the high uranium concentration in coral skeletons, providing absolute age constraints even for corals of solely a few ages (Shen et al., 2008; Frank & Hemsing, 2021). When coral skeletons remain well preserved and are not exposed to meteoric water, their geochemical composition can be used for paleoenvironmental studies. Depending on the species, corals incorporate

trace elements from seawater into their skeletons. Several trace element proxies are particularly important for climate reconstructions. For example, the Sr/Ca ratio is widely used to estimate past sea surface temperatures (SST) (Beck et al., 1992; McCulloch et al., 1994; Marshall & McCulloch, 2002), while $\delta^{18}O$ provides insights into both temperature and hydrological changes (Epstein et al., 1953; Fairbanks & Dodge, 1979). Additionally, the Ba/Ca ratio serves as an indicator of terrestrial runoff or variations in nutrient availability, offering further constraints on past environmental conditions (Lea et al., 1989; McCulloch et al., 2003). Depending on the species, growth rates, and the position within the reef some trace elements or isotope ratios can be influenced by these environments (de Villiers et al., 1995; Giry et al., 2010; Fowell et al., 2016).

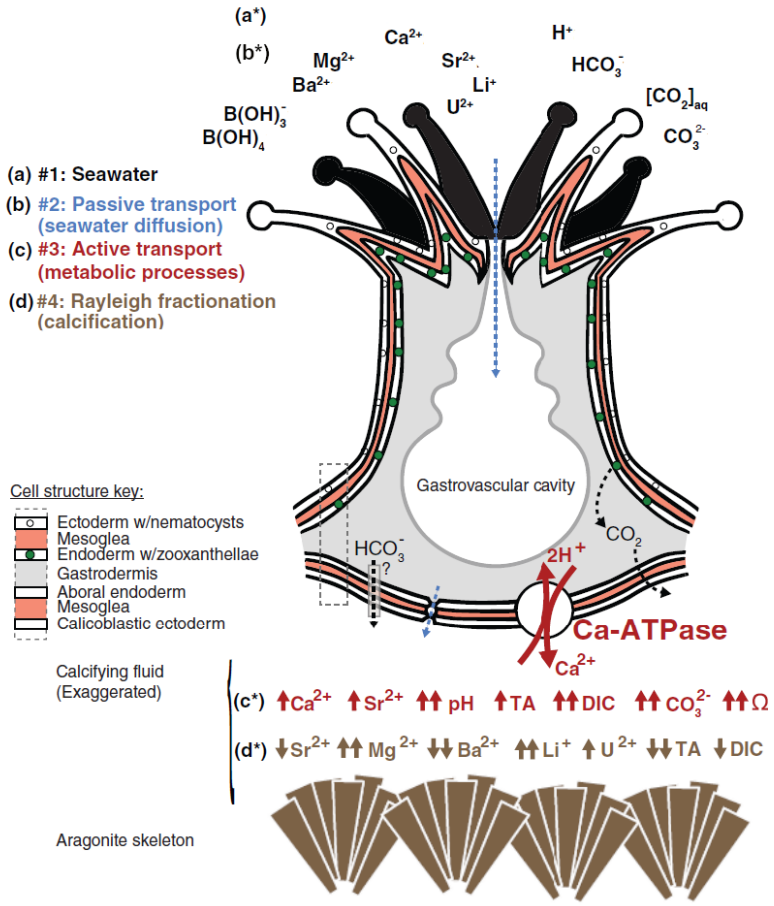

Figure 2.8 Schematic representation of coral biomineralization and elemental incorporation into the aragonite skeleton. Seawater-derived ions (a) enter the coral through passive diffusion (b) and active transport processes (c), facilitated by metabolic mechanisms such as Ca-ATPase, which regulates calcium uptake for skeleton formation. The calcifying fluid is enriched in Ca^{2+}, Sr^{2+}, pH, and dissolved inorganic carbon (DIC), promoting aragonite precipitation. Rayleigh fractionation (d) during calcification influences the incorporation of trace elements such as Sr, Mg, Ba, Li, and U into the coral skeleton, which serve as proxies for past environmental conditions. Modified after Thompson (2021).

2.3.1 Uranium in Corals

The skeletons contain uranium as a substitute of Ca, which is incorporated from seawater without measurable isotopic fractionation (Robinson et al., 2004b; Robinson et al., 2006). The uranium-to-calcium (U/Ca) ratio in aragonite corals has been utilized to infer past variations in SST (Shen & Dunbar, 1995; Ourbak et al., 2006; Felis et al., 2009), salinity (Ourbak et al., 2006), seawater pH (Inoue et al., 2011), and carbonate chemistry (Shen & Dunbar, 1995; DeCarlo et al., 2016), providing insights into ocean acidification and climate change.

Overall, the uranium concentration varies by 20 to 30% influenced by those physico-chemical properties with a median of aragonitic skeletons of 2.75±0.55 µg/g (Chutcharavan et al., 2018). In most species is the incorporated uranium concentration unaffected by metabolic processes, as uranium uptake occurs passively from seawater rather than through biologically mediated pathways (Thompson, 2021). However, during the precipitation of aragonite, uranium can undergo Rayleigh fractionation, reflecting progressive partitioning between the calcifying fluid and the growing skeleton. In this process, uranium is fractionated according to its partition coefficient between aragonite and seawater, leading to systematic variations in U/Ca ratios as calcification proceeds (DeCarlo et al., 2015). Although these effects do not alter the bulk availability of uranium, they can impart subtle but measurable signatures on coral geochemistry, which must be considered when interpreting uranium-based proxies. Thus, the Sr-U proxy serves as an alternative SST proxy, further reducing the biological mediated or "vital" effects that influence the traditional Sr/Ca thermometer (DeCarlo et al., 2016). Isotopic fractionation of uranium during coral calcification has not been demonstrated, and several studies have reported that $\delta^{234}U$ values measured in both tropical and cold-water corals are indistinguishable from those of ambient seawater (Wang et al., 2017; Kipp et al., 2022; Li et al., 2023). Thus, beyond seawater chemistry reconstructions, uranium in corals has been widely used in paleoceanographic studies. Coral $\delta^{234}U$ has been extensively applied to reconstruct past sea-level changes, using the $^{230}Th/U$ dating and the corals position relative to the modern sea level. As fossil corals from different periods preserve the uranium isotopic composition of seawater at the time of their growth, such records have provided constraints on the timing and magnitude of glacial–interglacial sea-level and global ice-volume fluctuations. Thus, capturing not only the major rise at the Last Deglaciation but also abrupt meltwater pulses and smaller-scale oscillations in sea level during the late Quaternary. Since variations in continental weathering regimes impact the seawater $\delta^{234}U$ ratio, the delivery of glacial meltwater, and shifts in freshwater routing can modify the $\delta^{234}U$ composition of seawater,

thereby leaving a measurable imprint of this process on fossil corals. (Esat & Yokoyama, 2006, 2010; Hibbert et al., 2016; Chutcharavan et al., 2018). More recently, novel applications of $\delta^{234}U$ have expanded to include tracing large-scale coastal ocean or semi-closed ocean basin circulation patterns, since spatial differences in uranium isotopic composition can reflect variations in water-mass mixing (Border, 2020; Shang et al., 2021). In addition, distinct $\delta^{234}U$ signatures from freshwater and glacial melt have been used to track the dispersal of meltwater plumes, providing insights into the role of ice-sheet dynamics in ocean–climate interactions (Li et al., 2023).

When using corals to reconstruct past seawater $\delta^{234}U$ skeleton diagenesis and U series system opening can massively alter the original uranium signature in corals (Henderson et al., 1993; Thompson et al., 2003; Villemant & Feuillet, 2003; Scholz et al., 2004), strongly impacting its usability as pale-circulation and freshwater proxies. Early diagenetic processes, such as marine cementation and aragonite dissolution-reprecipitation, can modify U/Ca ratios and α-recoil of ^{234}Th and ^{230}Th can modulate the corals $\delta^{234}U$ values in absence of chemical alteration, leading to post-depositional uranium exchange with seawater or sediment porewaters. Subaerial diagenesis, including meteoric alteration and secondary calcite formation, can further overprint primary uranium signals, necessitating careful screening of samples to ensure robust geochemical reconstructions (Thompson & Goldstein, 2005; Frank et al., 2006).

While thousands of $^{230}Th/U$ dated tropical corals have been compiled in a recent database systematic $\delta^{234}U$ variability has not been observed. In fact, for the past 200 years large variabilities of ±10‰ were found surrounding the mean value of 145.5‰ in the Eastern Indian Ocean (Sumatra) (N=17), the South China Sea (Pacific) (N=64) and the Great Barrier Reef (Western South Pacific) (N=261) (Figure 2.9) (Hibbert et al., 2016; Chutcharavan et al., 2018).

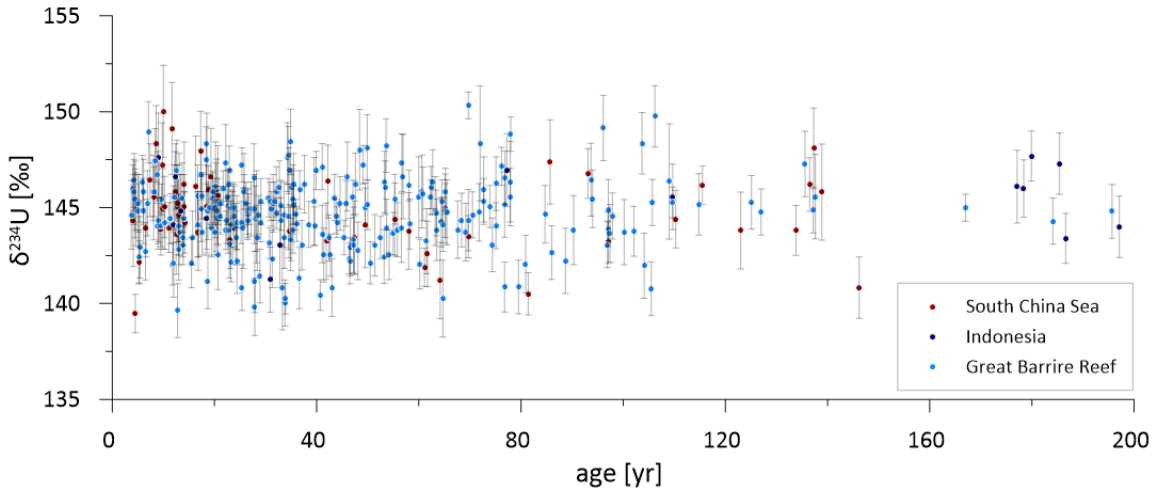

Figure 2.9 Three areas with >15 measurements over the past 200 years and analytical precision <2.5‰. Whether these observations include direct impacts of local freshwater fluxes or SGD is unknown. Data from Chutcharavan et al. (2018).

Thus, no systematic study to date has explored $\delta^{234}U$ values in annual banded tropical corals with the aim of testing whether the variability is driven by regional freshwater fluxes and ocean circulation. Nor has the potential differences between coral species and skeletal structures been investigated. While previous studies and compilations confirmed that coral $\delta^{234}U$ broadly reflects ambient seawater values, these were typically based on a limited number of bulk samples or single colonies, providing little insight into short-term variability (Wang et al., 2017; Kipp et al., 2022; Li et al., 2023). As a result, it remains unclear whether intra-annual changes in $\delta^{234}U$ occur during calcification, whether different coral growth forms or taxa incorporate uranium isotopes in systematically different ways, and how such factors might affect the use of $\delta^{234}U$ as a freshwater proxy.

3 Material and Methods

3.1 Samples

The corals analysed in this thesis originated from a range of sites across the Caribbean, encompassing different hydrographic and climatic settings. This spatial diversity provides an opportunity to evaluate both regional commonalities and site-specific influences on coral geochemistry (Figure 3.1). Additionally, a separate study was concluded on ground- and river water as well as a coral from Tahiti (Figure 3.7).

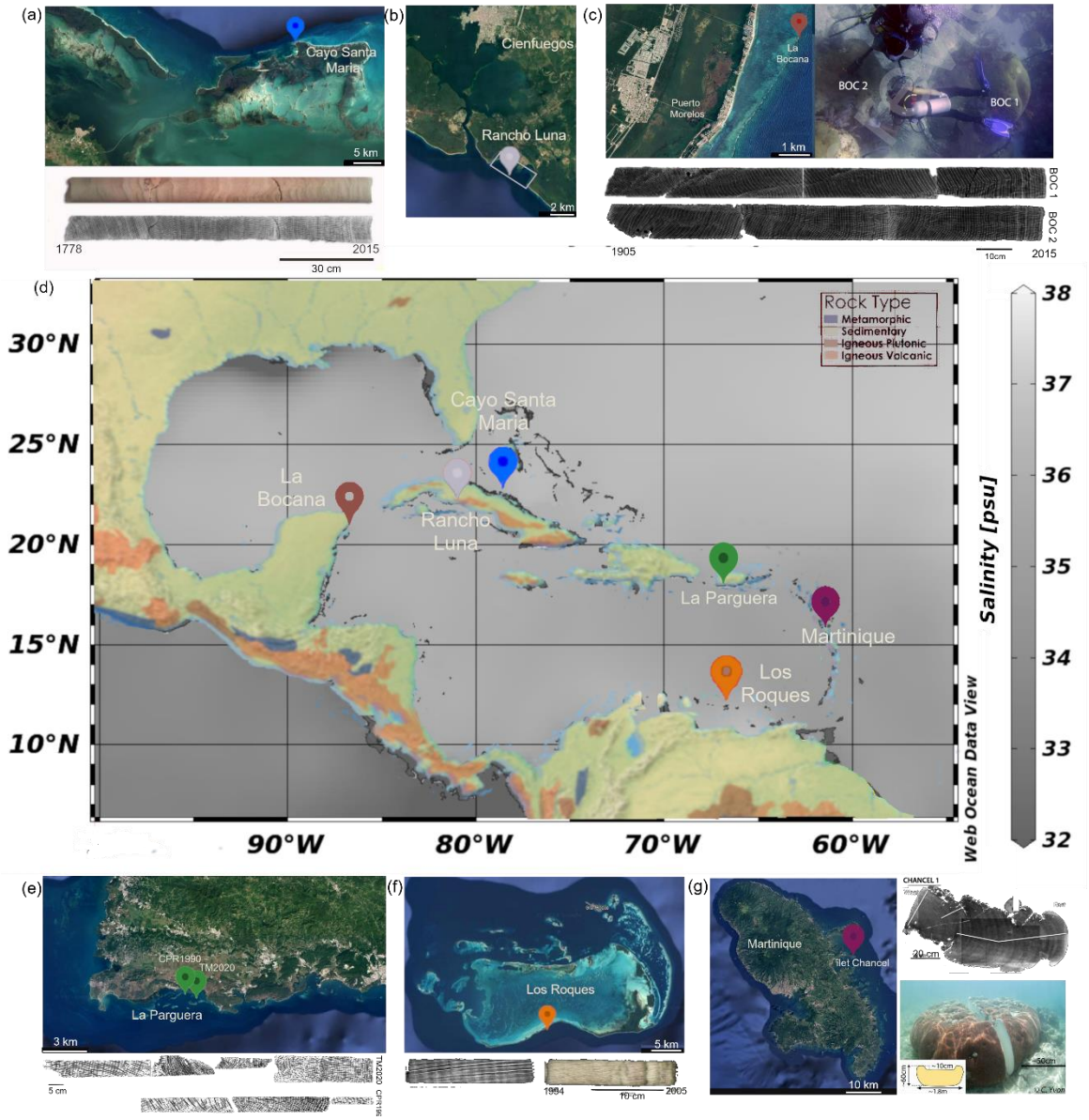

Figure 3.1 Location of coral sampling sites in the Caribbean. (a) Satellite view of Cayo Santa María, Cuba, with associated coral core photograph and X-ray image; (b) Rancho Luna lagoon, Cuba, where 15 coral species were collected; (c) La Bocana reef, Mexico, with aerial image of the reef and a picture showing proximity of two sampled coral colonies and their respective X-ray images; (d) Caribbean map showing sea surface salinity distribution (psu) and sampling locations; (e) Sampling site in La Parguera Puerto Rico with X-ray images of the two collected corals; (f) Los Roques, Venezuela, located ~140 km offshore, with coral core photograph and X-ray image; (g) Sampling site in Martinique with a X-ray image as well as a photo of the living microatoll.

3.1.1 Cuba Timescale

The oldest coral used in this thesis is a 97 cm-long coral core collected in March 2016 from the Sabana Camaguey Archipelago, Cayo Santa María, Cuba (79.10 W, 22.66 N) approximately 20 km from the main island (Figure 3.2), at approximately 10 m depth (Alonso-Hernández et al., 2022). The core was obtained from a scleractinian coral colony of the genus *Orbicella faveolata* and dated via sclerochronology on the basis of radiographic density images, revealing a maximum age of 237 years, ranging from 1778 to 2015 (Alonso-Hernández et al., 2022); which led to an average growth rate of 4.08 ± 0.12 mm yr^{-1}. Additionally, the coral exhibited green growth bands with high Mg contents, possibly due to the incorporation of relatively high levels of organic material into the coral skeleton (Alonso-Hernández et al., 2022). This coral was used to assess the influence of the Ca matrix on the measurement routine (Chapter 4), as well as establishing the longest timescale of coral uranium isotopes ($\delta^{234}U$) and examine its temporal change in the context of climate change and anthropogenic influence (Chapter 6).

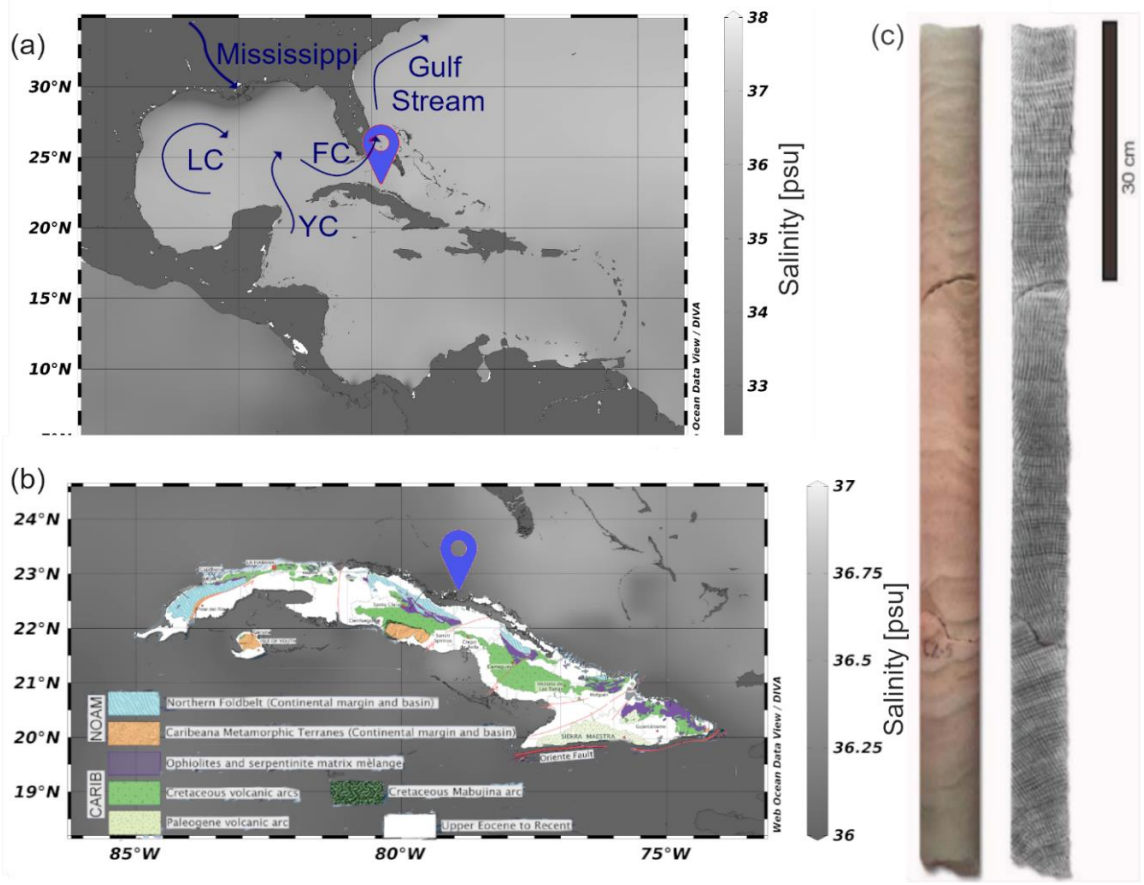

Figure 3.2 (a) Caribbean annual sea surface salinity with the location of the selected coral core the on the northern shore of Cuba, directly influenced by the Florida Current (FC) travelling eastwards from Yucatán Current (YC) and the Gulf of Mexico forming the Gulf Stream. The Loop Current (LC) carries the less saline Mississippi water towards the core location; (b) Annual sea surface salinity off the coast of Cuba, showing less saline waters (darker) at the core location due to terrestrial runoff; (c) X-ray image of the slab used in the optical densitometry analysis and photograph of the analysed core (CSM1) with visible green banding (Alonso-Hernández et al., 2022).

The climate of the region is influenced by the southwestern edge of the high-pressure system over the Atlantic (North American Subtropical High). The summer and fall seasons (June to October) correspond to the rainy season (250 mm per month) with occasional extreme events, such as hurricanes. Hurricanes from off the west coast of Africa typically follow a westward and poleward track, with landfall on the southeast coast of Cuba once every 20 years (Limia et al., 2003; Terry & Kim, 2015). During the winter season (November to May), the hydroclimate tends to be dry, with precipitation rates decreasing from 250 mm per month in summer to as low as 25 mm per month in winter (Vose et al., 1992).

The location of the sample core lies within the Florida Strait (Figure 3.2), serving as the outflow path for water masses from the Gulf of Mexico, with an estimated flow rate of 28 Sv (Leaman et al., 1995). As a result, the coral is influenced primarily by waters originating from the Caribbean and Gulf of Mexico, as well as very local continental runoff from the northern part of Cuba and eutrophic waters from mangroves bordering the southern key. An additional major yet distant source of freshwater, the Mississippi River, is located approximately 2,500 km away, but its flood plumes can extend hundreds of kilometres into the Atlantic (Hitchcock et al., 1997). This large North American river has an annual discharge rate of 0.015 Sv, which can increase fivefold during major flood events. In addition, the Mississippi carries large volumes of sediment particles, which have halved during the past century due to the creation of dams (Folwell, 1921; Carroll, 1990). The mean $\delta^{234}U$ value of the Mississippi waters was assessed to be 335‰, including strong seasonal variability (± 110‰) (Grzymko et al., 2007).

3.1.2 Cuba Species

To assess species variability under similar environmental conditions (Chapter 4), 11 coral colonies representing 10 species were collected from Rancho Luna, Cuba. These included: *Siderastrea siderea, Mycetophyllia lamarckiana, Acropora palmata, Agaricia agaricites, Meandrina meandites, Acropora cervicornis, Colpophyllia natans* (two specimens)*, Diploria labyrinthiformis, Montastrea cavernosa,* and *Orbicella faveolata.* All of the colonies were sampled within an 800 m^2 area at water depths of 3–8 m. The upper skeletal portions were sampled in 2015 and cleaned mechanically using a Dremel tool.

3.1.3 Venezuela

A *Pseudodiploria strigosa* colony from Los Roques, Venezuela (2 m water depth; 140 km offshore), was sampled at biannual to seasonal resolution (Chapter 4). The age model was established by counting annual growth bands visible in X-ray images,

anchoring the chronology to the collection date (2005), and aligning the $\delta^{18}O$ values with a previously dated nearby coral from Hetzinger et al. (2008). This 167 mm-long core represents approximately 10 years of growth (1995–2004), resulting in an average linear extension rate of ~14 mm yr^{-1}. Biannual resolution was achieved by taking one sample per density band, while seasonal resolution was achieved by subdividing each band and sampling the upper and lower halves.

3.1.4 Puerto Rico

Two *Orbicella annularis* coral cores (CPR1990-09-25 and TM2020-12-04) were collected by Amos Winter in September 1990 and December 2020, respectively, from reef systems located off the coast of La Parguera in southwest Puerto Rico (17.97°N, 67.05°W). The CPR1990 core was extracted from Pinnacles Reef, which is situated within a sheltered lagoonal environment characterized by low hydrodynamic energy, reduced turbidity, and relatively stable salinity levels. In contrast, the TM2020 core was obtained from the adjacent Turromote Reef, which occupies a more exposed position within the La Parguera Lagoon and is subject to increased water column mixing, higher turbidity, and intermittent terrestrial inputs (Appeldoorn & Bejarano, 2013).

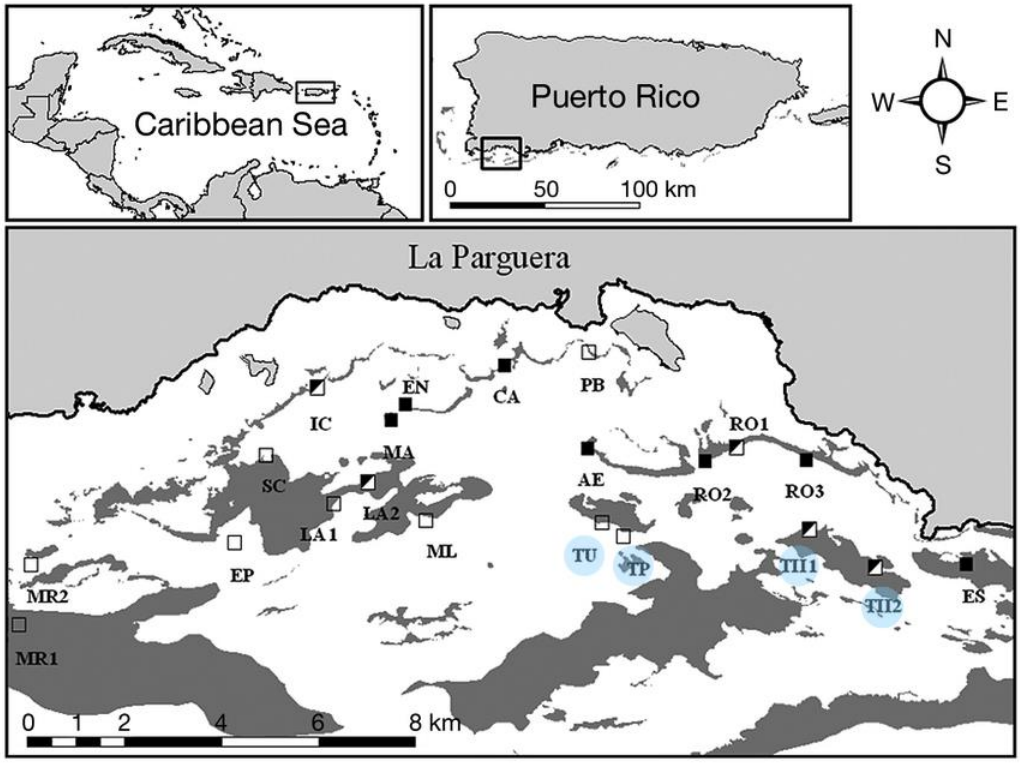

Figure 3.3 Site location: Coral reefs near La Parguera, Puerto Rico (Appeldoorn & Bejarano, 2013). Coral reef areas are shaded in dark gray, the markers indicate turbidity as measured by Appeldoorn and Bejarano (2013), with increasing turbidity from clear over half/half to filled squares. CPR1990-09-25 originates from Pinnacles (TP) reef and TM2020-12-04 from Turrumote I or II (TU or TII), marked in blue.

Although the lagoon system does not receive direct freshwater discharge from local rivers, episodic runoff events from the surrounding karstic and forested landscapes can introduce pulses of organic matter, sediments, and nutrients, particularly during periods of intense rainfall. Moreover, the region is periodically influenced by the distal effects of the Amazon River plume, which has been shown to extend across the Caribbean basin under prevailing current conditions (Chérubin & Richardson, 2007). This plume can lower ambient salinity levels and deliver dissolved organic carbon and trace elements.

The CPR1990 core is 60 cm in length with a diameter of 5 cm and consists of three sequential segments (1a, 1b, and 1c) (Figure 3.4). The TM2020 core is 90 cm long with a diameter of 8 cm and comprises four segments (1, 3B top, 3B bottom, and 4A) (Figure B.1). Notably, TM2020 segment 3B exhibits multiple post-depositional modification such as boreholes from microorganisms, along with ingrown mussels and sediment infiltration. Core drilling and bisection were performed along the primary growth axis for CPR1990 segments 1a and 1b, whereas other segments were cut obliquely.

Chapter 4 presents analyses of intra-colony replication of $\delta^{234}U$ signals across density bands. Further in Chapter 5 a study investigating several proxies for freshwater runoff was concluded and a Caribbean $\delta^{234}U$ baseline was established.

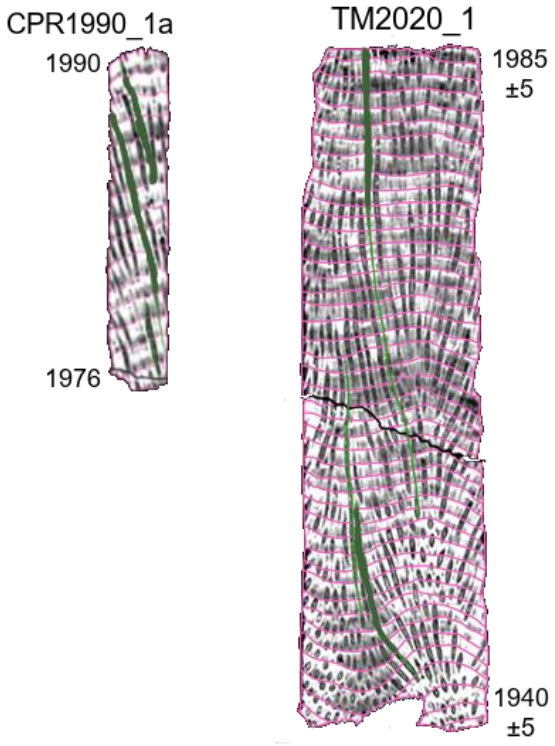

Figure 3.4 High-resolution CT scans of *Orbicella annularis* coral cores CPR1990-09-25 (left) and TM2020-12-04 (right). Annual density banding patterns are highlighted in red, delineating successive years of skeletal growth. The green lines indicate the micro-sampling transects used for trace element and stable isotope analysis along the primary growth axis for the analysed years of 1980s and 1940s.

3.1.5 Mexico

The coral cores BOC1 (9 cm in diameter, 1.5 m long) and BOC2 (9 cm in diameter, 1.2 m long) were collected in summer 2016 from two *Orbicella faveolata* colonies at 7 m water depth in La Bocana (20° 52.490´ N, 86° 51.044´ W) growing only 1 m apart from each other within the National Park Puerto Morelos Reef, Mexican Caribbean (Figure 3.5). SCUBA divers extracted the cores along the coral's main growth axis using a Tech 2000© hydraulic drill with a 9-cm-diameter, 85-cm-long diamond-bit core barrel. A 1 cm-thick slab was taken from the core's centre, and radiographs were captured using a General Electric Medical X-ray system at the Radiological Center of Cancun. The age model of the BOC1 inferred from these x-radiographs indicates the coral's maximum age is ~100 years, with an average extension rate of 0.89 ± 0.16 cm yr^{-1} and a density of 0.76 ± 0.12 g cm^{-3} (Rico-Esenaro et al., 2019).

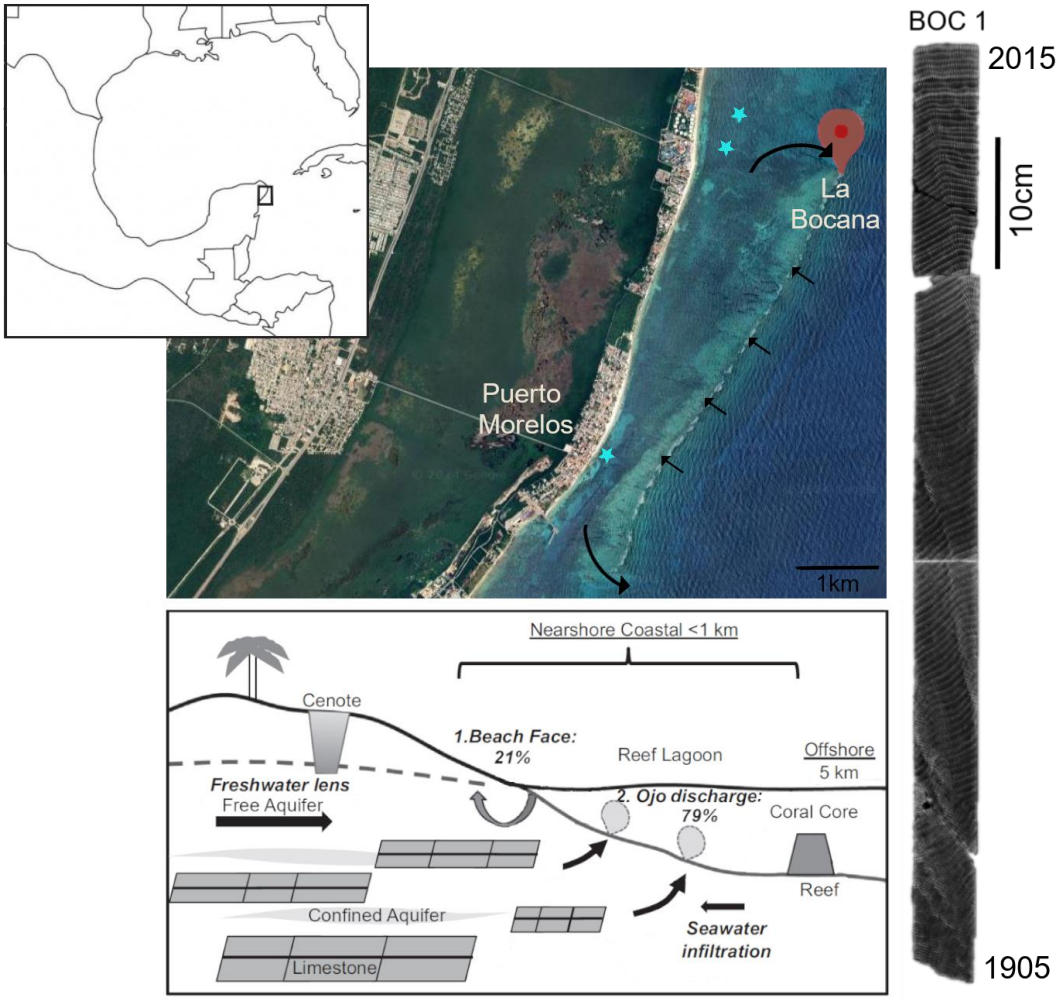

Figure 3.5 Study area near Puerto Morelos, Mexican Caribbean, showing the sampling location at La Bocana (red marker) and other freshwater discharge sites (blue stars). The inset at the bottom illustrates the coastal groundwater system, highlighting freshwater discharge through "ojos" (submarine springs) and seawater infiltration in the porous limestone aquifer. The coral core sampling site is located offshore near the reef, where groundwater influence is expected (modified after Null et al. (2014)). On the right, an X-ray image of the sampled coral core reveals its internal growth structures (Rico-Esenaro et al., 2022).

The Puerto Morelos Reef is part of the Mesoamerican Reef System, located in the northeastern Yucatán Peninsula. A ~4 km-long coral barrier lies ~1 km offshore, forming a reef lagoon rich in seagrass populations. The lagoon, with an average water depth of 3–4 m, connects to the open sea through two channels: La Bocana to the north (maximum water depth: 8 m), and the Navigation Channel to the south (maximum water depth: 10 m). Seawater primarily flows over the reef crest, with deeper water masses exiting through these channels (Coronado et al., 2007). Puerto Morelos has a rainy season from June to October, a dry season from March to May, and northern winds from November to February (Instituto Nacional de Ecología, 2006). The Puerto Morelos Reef does not receive terrestrial surface runoff due to high infiltration rates of the region's karstic environment (Bauer-Gottwein et al., 2011). Instead, freshwater is transported to the reef through submarine groundwater discharge (SGD). The lagoon's bed is dotted by ~10 to 15 point-source discharges, some of which form visible surface bulge during the low tides (Parra et al., 2016). Approximately 79% of SGD in Puerto Morelos originates from point-source springs, while 21% is discharge through the beach interface of brackish water (Figure 3.5) (Null et al., 2014). The discharge at point-source springs is driven by a hydraulic gradient (water level slope) between the aquifer and sea, ranging from 5 mm km^{-1} to 100 mm km^{-1} (Beddows, 2004). At Puerto Morelos, a discharge rate of 0.29 m^3 s^{-1} per kilometre of coastline has been recorded from the local aquifer. However, the offshore springs are likely fed by a larger regional aquifer extending across Quintana Roo (González-Herrera et al., 2022).

To analyse the isotopic composition of coastal waters along the Mexican coast, two water samples were collected in proximity to the La Bocana. One sample was taken while snorkelling inside the lagoon, in a location sheltered by the barrier reef (20°52'48.0"N 86°51'54.0"W), while the second sample was collected outside the reef during a SCUBA dive in open marine conditions (20°49'27.0''N 86°43'19.0''W).

To assess the spatial variability of $\delta^{234}U$ values within a single coral species across a reef, both cores were analysed. Further, both powdered and bulk samples were collected along the main growth axis at annual resolution using a handheld Dremel drilling device to compare $\delta^{234}U$ values by sample preparation type (Chapter 4). In addition, a study investigated a timeseries of BOC1 showing SGD influencing the $\delta^{234}U$ values (Chapter 7).

3.1.6 Martinique

Martinique is a volcanic island of ~1,000 km^2 in the Lesser Antilles, eastern Caribbean (Figure 3.1). Situated near the subduction zone of the Lesser Antilles trench, it forms

part of the active volcanic arc and hosts Mont Pelée. The island's eastern Atlantic coast features a well-developed carbonate platform, underlain by the volcanic arc (Leclerc et al., 2015).

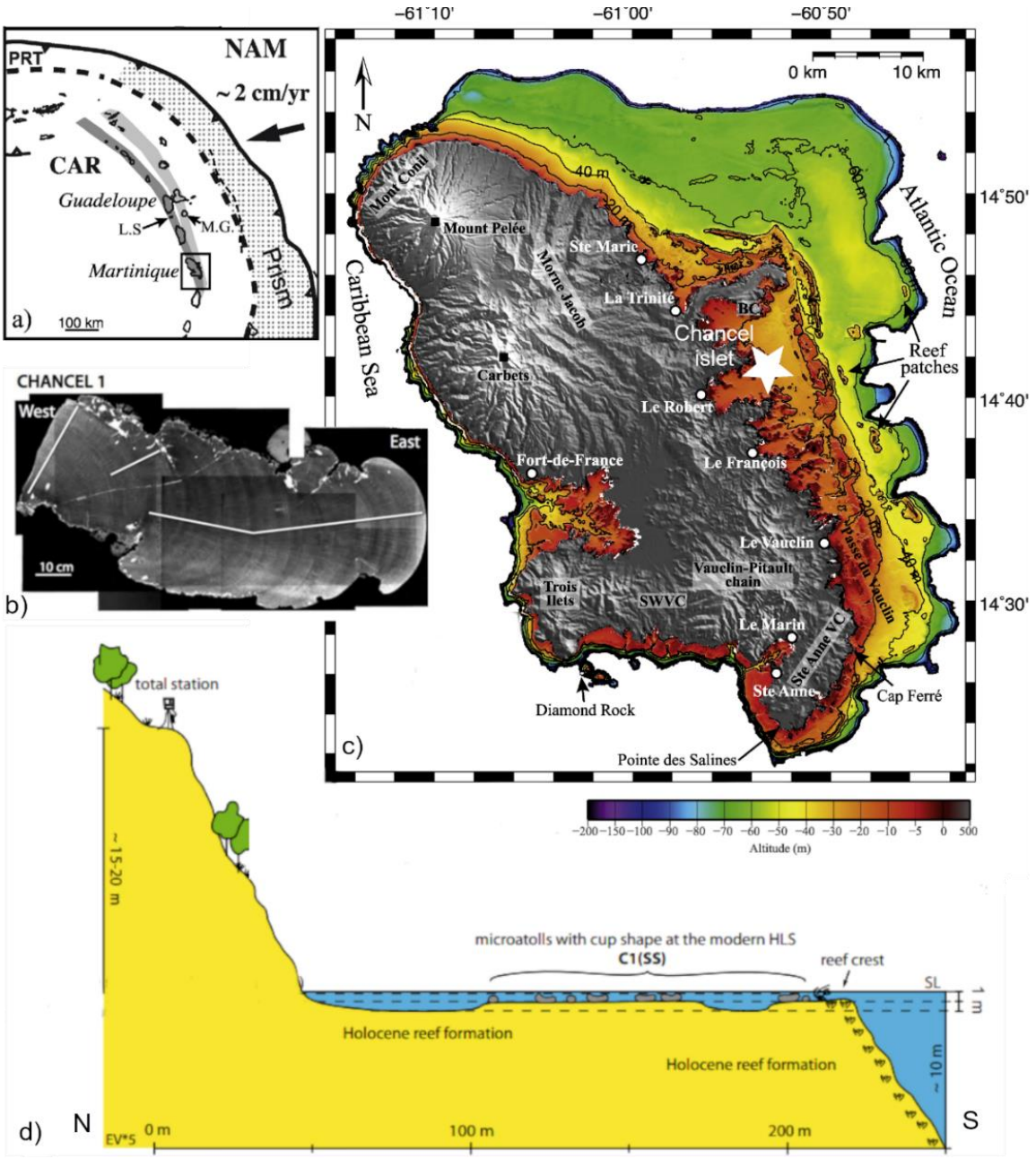

Figure 3.6 (a) Tectonic setting of Martinique within the Lesser Antilles arc, located in a tectonically active zone where the North American Plate converges toward the Caribbean Plate at ~2 cm yr^{-1}, forming an accretionary prism east of the island (Leclerc et al., 2015). (b) X-ray image of the sampled *Siderastrea siderea* microatoll (specimen CHANCEL 1) from Chancel Islet, showing white lines indicating sampling paths (Paterne et al., 2023). (c) Topographic map of Martinique and surrounding bathymetry, with colourful shallow areas representing the carbonate platform and grey tones depicting volcanic structures; the coral sampling site is marked with a white star (Leclerc et al., 2015). (d) North–south cross-section of the lagoonal setting at Chancel Islet, showing a wide (~170 m) but shallow (~1 m deep) lagoon, bounded by a steep coastline and reef crest, with Holocene reef formations and the position of microatolls with cup-shaped morphologies at the modern highest living surface (HLS) (Weil-Accardo et al., 2016).

The coral studied here, "Chancel 1," is a massive *Siderastrea siderea* colony sampled alive in January 2008. It formed part of a microatoll (Weil-Accardo et al., 2016) and grew at a depth of 1.5 m on the Atlantic coast near Îlet Chancel (14°70′ N, 60°90′ W; Figure 3.6). The location is characterised by a shallow lagoon with microatolls extending ~210 m from the steep coast (15-20 m elevation). The chronology of the coral is based on $^{230}Th/^{238}U$ dating and annual density band counting from X-radiographs (Paterne et al., 2018). Growth interruptions occurred at (1884 ± 4), (1896 ± 4), (1931 ± 3), (1948 ± 2), and (1989 ± 1) (Figure B.12). These are interpreted as the result of abrupt relative sea-level changes, likely caused by episodes of tectonic subsidence, and are supported by independent evidence of widespread earthquakes and large landslides during some of these events (Aubaud et al., 2013; Weil-Accardo et al., 2016).

Samples were taken along three growth axes (Paterne et al., 2023), but only the longest axis was analysed here. The powdered coral samples, prepared at annual resolution, were provided by Dr. Martine Paterne and Dr. Eric Douville. For this study, only material from selected intervals between 1887 and 1982 was analysed, and provided insights on the Caribbean $\delta^{234}U$ baseline (Chapter 5).

3.1.7 Pacific

To assess the effect of sample mass on measurement precision (Chapter 4), subsamples were prepared from a beached *Porites sp*. colony collected at Moruroa Atoll in the Pacific Ocean. The sample was extracted using a Dremel hand held saw fitted with a diamond blade. A 1 g sample was ultrasonically cleaned and dissolved in 7 N HNO_3. This solution was subdivided into aliquots containing 20, 30, 35, 40, 40, 45, 50, 55, 60, 70, 80, 100, 120, and 150 mg coral material. Each subsample was processed following the procedure described in Chapter 3.2.

As part of a mobility scholarship from the SPP2299 a fieldtrip to Tahiti, French Polynesia was organised in 2024 to collect water from SGD. Tahiti, the largest island in French Polynesia, is located in the central South Pacific and consists of two volcanic massifs: Tahiti Nui in the northwest and the smaller Tahiti Iti in the southeast (Figure 3.7). Formed by hotspot volcanism between approximately 1.5 and 0.45 million years ago, the island is composed predominantly of basaltic rocks formed during four distinct volcanic phases (Hildenbrand et al., 2004). The island experiences high annual precipitation, particularly on the windward (north-eastern) slopes, with rainfall exceeding 4,000 mm yr^{-1} in some catchments (Benoit & Sichoix, 2023). The steep topography, permeable volcanic substrate, and high annual rainfall, particularly on the windward (north-eastern) side, create favourable conditions for groundwater recharge and rapid subsurface flow (Hildenbrand et al., 2005). SGD sources occurs

along the island's coastal margins, particularly where fractured basaltic aquifers intersect the coastline (Haßler et al., 2019). In some areas, carbonate platforms are present below the barrier reef, though these are often overlain by volcanic material and are typically characterized by anoxic conditions at depth (Rougerie et al., 2004). The island's dynamic hydrology and variable aquifer structures make Tahiti an ideal natural laboratory for studying SGD processes in a volcanic island setting.

Figure 3.7 Map of Tahiti showing sampling locations of different water sources and coral cores. Submarine groundwater discharge (SGD) sites are marked in dark blue, seawater sampling sites in light blue, river water sites in green, and coral sampling sites in pink. The main study area in the southwest lagoon near Maraa is highlighted by the red box and shown in greater detail in the inset. Locations include modern coral core Maraa-7 and nearby SGD and seawater monitoring points used to assess freshwater influence on the reef environment.

During the field campaign, seven SGD sites were sampled, six located on the southwestern coast of Tahiti Nui and one on the northern shore of Tahiti Iti (Figure 3.7). An additional sample was collected at the mouth of the Papenoo River on the northern coast of Tahiti Nui. Furthermore, six seawater samples were collected in 2018 and 2019 by Dr. Martin Kölling (MARUM, University of Bremen).

The approximate locations of the SGD sites were known from previous studies (Haßler et al., 2019) and were further confirmed visually by the presence of transparent filaments or streaks in the coastal seawater, often associated with the discharge of cooler freshwater. Groundwater was sampled directly at the discharge source using a funnel placed over the spring to isolate the freshwater from surrounding seawater. A second sample was taken approximately 1 m downstream by collecting surface water (~0.5 m water depth) with a clean bottle. Most sites were

sampled under both high tide and low tide conditions to assess tidal influences (Chapter 8).

A coral core, used for the analysis of temporal $\delta^{234}U$ variability, was provided by Dr. Thomas Felis (MARUM, University of Bremen) (Chapter 8). The core was collected in 2009 from a *Porites sp*. colony growing on the inshore side of the barrier reef near the settlement of Maraa, in southern Tahiti Nui. The age of this core was also determined by sclerochronology using x-radiographs and seasonal $\delta^{18}O$ variability (Knebel et al., 2024).

3.2 Sample Treatment

To minimize contamination, coral samples underwent a rigorous cleaning process to remove organic material, detritus, and residual sawing dust embedded in pore spaces. Coral slices were sonicated in Milli-Q water at full intensity using a SONOREX ultrasonic bath.

Sampling for the measurement of uranium isotopes ($\delta^{234}U$) and radiocarbon (^{14}C) mainly consisted of extracting coral pieces from a single annual growth band using a Dremel hand held saw fitted with a diamond blade. In most corals, the outermost band (typically representing the most recent months) was not sampled, as this layer is enriched in organic material and surface alteration products that can compromise geochemical analyses. The sampled coral pieces were cleaned ultrasonically again to remove contamination from saw dust.

The separation of uranium from the sample carbonate matrix followed the protocol established by Wefing et al. (2017), with modifications outlined by Kerber et al. (2023). For each analysis, approximately 50–100 mg of skeletal aragonite was dissolved in 7 N HNO_3. For water samples, a range of 40–100 mL was measured, depending on the uranium concentration of the water. To serve as a concentration reference, 100 µL of TriSpike, a mixture containing the synthetic isotopes ^{233}U, ^{236}U and ^{229}Th, was added. Next, uranium was purified by ion-exchange chromatography using U/TEVA resin. To remove Ca and other matrix elements, 300 µL U/TEVA chromatographic ion exchange columns were rinsed three times with 7 N HNO_3. Uranium was then eluted with 3 N and 1 N HCl (Horwitz et al., 1992). The sample was dried and redissolved, and the column purification was repeated until the Ca concentration of the final solution was <10 ppm. For MC-ICP-MS measurements, the final uranium fraction was evaporated and redissolved in 1.2 mL of 1% HNO_3 and 0.05% HF, and any particulates were removed by centrifugation.

To assess potential matrix effects from residual calcium, an experiment was conducted using the certified reference material NBS-CRM-112A spiked with known

calcium concentrations (0, 6.25, 12.5, 25, 50, and 100 ppm). Calcium was added using certified element standards (Inorganic Ventures).
The Puerto Rican coral was further sampled for trace element and stable isotope measurement. Therefore, six samples per annual growth band were micromilled with a handheld Dremel tool along individual corallite pathways wherever possible, ensuring continuity across the sampled decade.

3.3 Sample Analyses

3.3.1 Uranium Isotopes

Uranium isotopes were measured at the Institute of Environmental Physics, Heidelberg, using a Thermo Fisher Neptune Plus multi-collector inductively coupled plasma mass spectrometer (MC-ICP-MS), coupled to an ARIDUS II desolvating system and an ESI SC-2DX autosampler. The cup configuration and corresponding resistors used are shown in Table 3.1.

Table 3.1 Cup configuration with the corresponding resitor settings used in the MC-ICP-MS to meassure uranium isotopes.

Cup	L1	C	H1	H2	H3
Mass number	233	234	235	236	238
Resistor Ω	10^{11}	10^{13}	10^{11}	10^{11}	10^{10}

Each sample was measured over 60 cycles, with an integration time of 4.097 seconds per cycle. A standard-sample bracketing technique was applied using the Harwell Uraninite 1 (HU-1) standard to correct for instrumental drift and ensure long-term stability. Between each measurement, the system was rinsed for several minutes with 1% HNO_3 + 0.05% HF. Blank levels were confirmed through chemical blank runs conducted prior to each sample and standard data evaluation was performed using a custom Python script developed by the Institute of Environmental Physics for U-Th dating analysis (Kerber et al., 2025). This script encompasses instrumental background corrections, identification and correction of signal outliers, adjustment for mass bias, accounting for hydride formation, and addressing tailing of ^{238}U (Kerber et al., 2023). All measurements were normalized to the HU-1 standard, assuming secular equilibrium. The $\delta^{234}U$ value is reported in per mil (‰) and calculated from the activity ratio using the following formula:

$$\delta^{234}\mathrm{U}\ (‰) = \left(\frac{\mathrm{A}_{^{234}\mathrm{U}}}{\mathrm{A}_{^{238}\mathrm{U}}} - 1\right) * 1000$$

with decay constants of λ_{238} = $1.55125 \cdot 10^{-10}$ (Jaffey et al., 1971) and λ_{234} = $2.82206 \cdot 10^{-6}$ (Cheng et al., 2013). Internal errors were determined as 2σ from each measurement, whereas external errors were determined through repeated measurements of the NBS-CRM-112A (CRM112A) standard and an in-house seawater standard. Interlaboratory comparison of the $\delta^{234}U$ values was achieved via continuous measurements of the CRM112A standard and HU-1 as a presumed secular equilibrium standard. Owing to the observed offset towards the certificate value of CRM-112A and its relative value to HU-1, renormalization was necessary, which involved applying the offset of CRM-112A from its certificate value of -1.20 ‰ (Cheng et al., 2013) to the $\delta^{234}U$ (HU-1) normalized data (Figure 4.1). All the results are provided for consistency with other works normalized to HU1 ≠ 0, as suggested by Chutcharavan et al. (2018) and Kipp et al. (2022).

3.3.2 Ca and U Concentrations

Prior to uranium isotope analysis on the MC-ICP-MS, a pre-screening routine was conducted to determine calcium and uranium concentrations using a Thermo Fisher iCAP Q ICP-MS. For this purpose, 50 µL aliquots of each sample solution were diluted 1:10 with 0.5 N HNO_3 and measured in standard mode. Results were corrected for instrumental drift and blank levels. Samples with calcium concentrations below 10 ppm were deemed sufficiently low to minimize matrix effects and were selected for further uranium isotope analysis on the MC-ICP-MS Uranium concentrations were also quantified to ensure compatibility with the bracketing standard (HU-1) used in MC-ICP-MS measurements. If necessary, samples were diluted to match the target uranium concentration of approximately 50 ppb.

Ba/Ca ratios were measured on the Q ICP-MS as well. Samples were introduced as 10 ppm Ca aliquots via an apex sample introduction system and analysed in kinetic energy discrimination (KED) mode with a collision gas flow rate of 5.02 mL min^{-1}. The standard deviation across 10 main runs was <0.77%. Inter-laboratory comparability was ensured through measurement of NIST RM 8301 coral standard as well as Ishi-B SPP2299 (E. Hathorne, pers. Comm.). Drift corrections were applied using an in-house coral standard and assessed via Allan variance analysis.

3.3.3 Radiocarbon

Radiocarbon (^{14}C) measurements were conducted by Marika Hiemisch's Master thesis on coral carbonate samples to track temporal variability in surface ocean radiocarbon and to evaluate the influence of water mass dynamics on coral geochemistry. Carbon extraction and measurements were performed at the Institute of Environmental Physics, Heidelberg University and at the Curt-Engelhorn-Centre

for Achaeometry, Mannheim, respectively, following the protocol detailed by Beisel et al. (2025), with results expressed as $\Delta^{14}C$ relative to the post-1950 standard.
The coral $\Delta^{14}C$ was used in the interpretation of site-specific influences, including localized variations in ocean circulation (Chapter 5).

3.3.4 Computed Tomography (CT)

To establish the age model and determine the optimal sampling path of both Puerto Rican coral cores, the samples were scanned using a Philips Spectral CT 7500 at Heidelberg University Hospital under the supervision of medical physicist Dr. sc. hum. Wolfram Stiller. The scanning parameters were set to 120 kVp and 300 mAs. Computed tomography (CT) imaging was employed to examine the three-dimensional growth axis prior to slab preparation and to determine density growth bands. This approach facilitates the selection of optimal sampling transects by avoiding growth troughs and off-axis corallites (Reed et al., 2021).

3.3.5 Trace Elements

Sr/Ca and Mg/Ca ratios were measured at the MARUM (University of Bremen) from 40 ppm Ca aliquots of samples dissolved in 2% HNO_3. Analyses were conducted using an Agilent 720 series simultaneous axial inductively coupled plasma optical emission spectrometer (ICP-OES) equipped with a Twister spray chamber and a concentric nebulizer. Each sample was measured in triplicate, and Sr, Mg, and Ca concentrations were averaged. The standard deviation for Sr/Ca and Mg/Ca ratios across replicates was typically <0.3%. Instrumental drift was corrected by measuring an in-house coral standard before and after every sample run, assuming stable Sr/Ca and Mg/Ca ratios. Inter-laboratory comparability was ensured through regular measurement of the JCp-1 standard (at least every 50 samples). The Ishi-B SPP2299 and RM 8301 standards were included as informational standards, although community consensus on reference values for Ishi-B SPP2299 remains unresolved.

3.3.6 Stable Oxygen and Carbon Isotopes

Approximately 30–90 µg of powdered coral was weighed with high precision using a Sartorius balances. Stable oxygen ($\delta^{18}O$) and carbon ($\delta^{13}C$) isotope compositions were analysed using a ThermoFinnigan MAT253 Plus gas source mass spectrometer equipped with a Thermo Fisher Scientific Kiel IV carbonate device at the Institute of Earth Sciences, Heidelberg University. Since $\delta^{18}O$ and $\delta^{13}C$ values are reported relative to Vienna Pee Dee Belemnite (VPDB), an in-house standard (powdered Solnhofen limestone) was analysed alongside the samples for normalization. The in-house standard was calibrated against the IAEA-603 reference material (calcite) and

repeat measurements yielded an external precision of better than 0.03‰ for $\delta^{13}C$ and 0.06‰ for $\delta^{18}O$ (Schorndorf et al., 2023). Stable isotope values were normalized to VPDB using single-point normalization following Paul et al. (2007):

$$\delta\mathrm{VPDB}_{sample} = \left[\frac{(\delta\mathrm{M}_{sample} + 1000)(\delta\mathrm{M}_{standard} + 1000)}{(\delta\mathrm{M}_{standard} + 1000)}\right] - 1000$$

The method of Ren et al. (2003) was used to establish the $\delta^{18}O$ of the seawater ($\delta^{18}O_{sw}$) by separating the influence of sea surface Temperature (SST) on $\delta^{18}O$ of the coral ($\delta^{18}O_c$) using Sr/Ca-reconstructed SST ($SST_{Sr/Ca}$) and a previously described SST dependence of $\delta^{18}O$. For *Porites,* this value lies between -0.18 and -0.24‰/°C (Epstein et al., 1953; Fairbanks & Dodge, 1979; Shen et al., 1992), and an average of -0.21‰/°C is used here.

$$\delta^{18}O_{SW} = 0.21 * SST_{Sr/Ca} + \delta^{18}O_c$$

4 Precision Measurement of $\delta^{234}U$ in Annually Banded Tropical Corals

The fine-scale chronological control provided by tropical coral annual density banding in corals offers a unique opportunity to resolve past seawater $\delta^{234}U$ variability at sub-annual to annual resolution (Greve et al., 2025). This capability enables the construction of detailed $\delta^{234}U$ time series, capturing short-term fluctuations that are critical for interpreting rapid environmental changes and transient hydrological events. Similarly large statistical relevant data sets allow to identify rapid fresh water release events, even in the open ocean as has been demonstrated in the Southern Ocean using deep sea corals (Li et al., 2023). Tropical coral reefs host remarkable biodiversity, and multiple coral genera like massive *Porites sp., Acropora sp., Siderastrea sp., Montastrea sp.*, and *Orbicella sp.* are commonly used in geochemical proxy records. Each genus exhibits distinctive skeletal architectures and growth morphologies, which pose varying analytically challenges due to differences in skeletal densities, porosities, and growth rates (de Villiers et al., 1995; Sadler et al., 2014; Ross et al., 2019). Moreover, the skeletal architecture can vary not only between genera but also within individual colonies, both at micro- and macroscales, affecting both primary geochemical signals and potential diagenetic alteration pathways (Perrin, 2003; DeLong et al., 2016; Reed et al., 2021).

To ensure that $\delta^{234}U$ values measured in coral skeletons accurately reflect the $\delta^{234}U$ composition of ambient seawater, this chapter presents a series of methodological tests on various coral genera and conduct a quality assessment of isotopic measurements and $\delta^{234}U$ reconstructions. These include evaluation of potential calcium matrix effects on measurement precision and accuracy, assessments of analytical reproducibility via repeated measurements, procedural replicates of chemical preparation steps, and skeletal structure replicates sampled from different regions within the same coral colony. In addition, comparative analyses were conducted across different coral genera and among individuals of the same species collected from the same reef. Together, these tests form a robust validation framework, providing critical confidence that coral-based $\delta^{234}U$ records can be reliably used to reconstruct the local and past seawater uranium isotope compositions at high temporal resolution.

4.1 $\delta^{234}U$ Measurements

External analytical uncertainty was assessed through repeated measurements of the NBS-CRM-112A standard within each measurement batch. Across 66 analyses, the mean value for NBS-CRM-112A was -38.12‰ with a standard deviation of ±0.38‰ (Figure 4.1). These results are consistent with previously reported values for NBS-CRM-112A relative to the secular equilibrium standard HU-1 (Robinson et al., 2002; Shen et al., 2002; Deschamps et al., 2003; Andersen et al., 2004a; Fietzke et al., 2005; Andersen et al., 2010). Based on the known offset of +1.2‰ between NBS-CRM-112A and HU-1 (Cheng et al., 2013) and the fact that some laboratories report data normalized to the certified NBS-CRM-112A value, the data were renormalized here to $\delta^{234}U$ (HU-1) = -1.2‰ to ensure inter-comparability with other studies. To further test reproducibility in the range typical for coral $\delta^{234}U$ values, an in-house seawater standard was measured 12 times. It yielded a mean values $\delta^{234}U$ values of 145.75‰ with a standard deviation of ±0.33‰, thus comparable to the NBS-CRM-112A results (Figure 4.2).

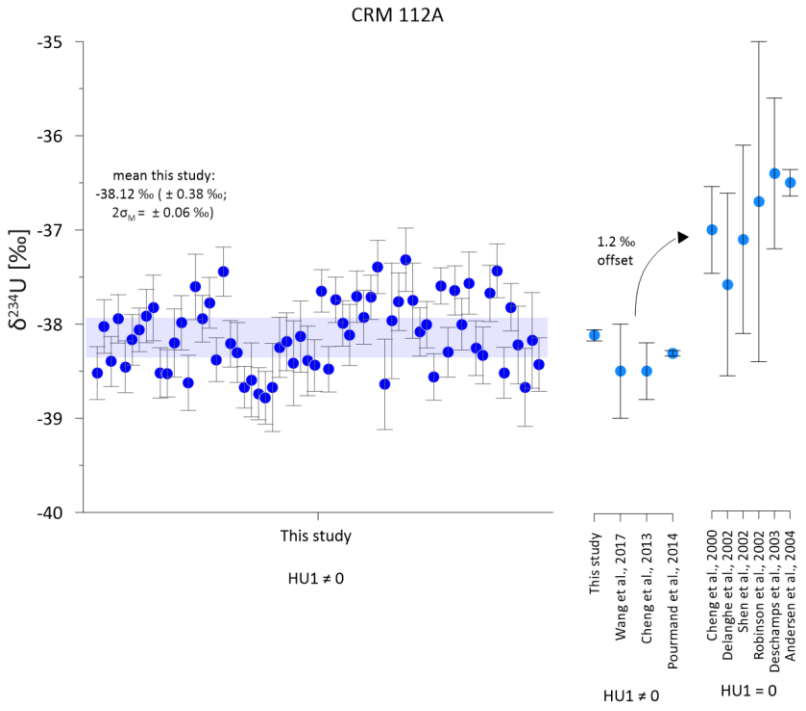

Figure 4.1 66 measurements of the external CRM 112A standard in this study yield a mean $\delta^{234}U$ of –38.12‰ ± 0.38‰ (2σ, n = 66), with a $2\sigma_M$ of ± 0.06‰, indicating high analytical precision. Results are shown relative to literature values corrected for different HU-1 normalization (HU-1 ≠ 0 and HU-1 = 0), highlighting a ~1.2‰ offset.

The accuracy of $\delta^{234}U$ measurements in this study is supported by these 66 analyses of the reference material NBS-CRM-112A. These results fall well within the range reported by previous studies, which have documented $\delta^{234}U$ values for NBS-CRM-112A between -38.3‰ ± 1‰ to -37.6‰ ± 0.8‰ (Cheng et al., 2000; Delanghe et al.,

2002; Robinson et al., 2002; Shen et al., 2002; Deschamps et al., 2003; Andersen et al., 2004b; Cheng et al., 2013; Pourmand et al., 2014; Wang et al., 2017) (Figure 4.1). The higher analytical precision reported in this study reflects recent improvements in data processing, including refined outlier detection, hydride correction, and mass bias adjustments (Kerber et al., 2023; Kerber et al., 2025).

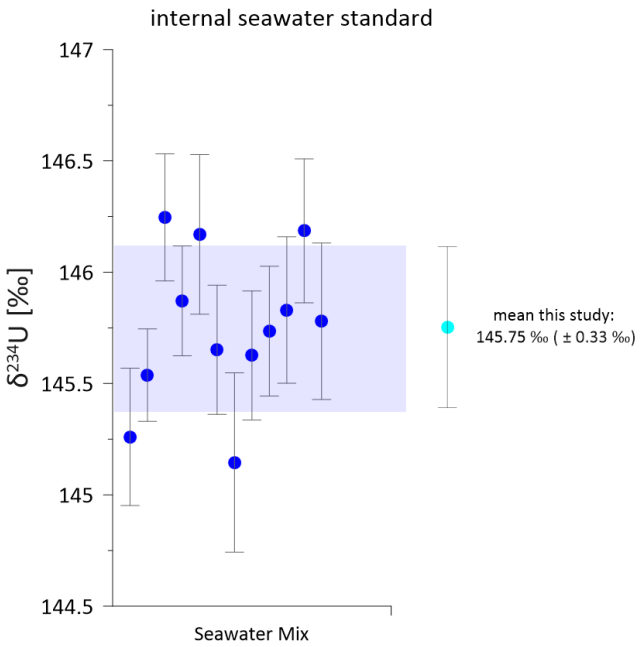

Figure 4.2 Measurements of the internal seawater U standard yield a mean $\delta^{234}U$ of 145.75‰ ± 0.33‰ (2σ, n = 18), consistent with expected marine values.

A total of 21 replicate $\delta^{234}U$ measurements were performed, yielding values that ranged from 144.4‰ to 146.1‰. The overall standard deviation across all samples was 0.3‰, indicating high internal consistency. However, the maximum deviation between individual replicates reached up to 1‰, leading to an estimated uncertainty of ±0.5‰ for measurements, which is moderately higher than the statistical uncertainty (Figure 4.3). Figure 5 exhibits nine replicate $\delta^{234}U$ measurements performed on the TM2020 *Orbicella annularis* coral from Puerto Rico. Two subsamples were taken from the same growth band but from different spatial positions within the skeletal structure. These measurements ranged from 144.5‰ to 147.1‰, with a resulting standard deviation of ±0.65‰ (n=9) (±0.33‰; n=6) (Figure 4.4), which is used here as the upper bound of procedural uncertainty, this represents excellent reproducibility for carbonate-based uranium isotope analysis. Procedural blank measurements were conducted between each sample and standard measurement. These blanks revealed an average ^{234}U background of 6 counts per

second, consistent with Kerber et al. (2025). All measured chemical blanks remained below this threshold (n = 20).

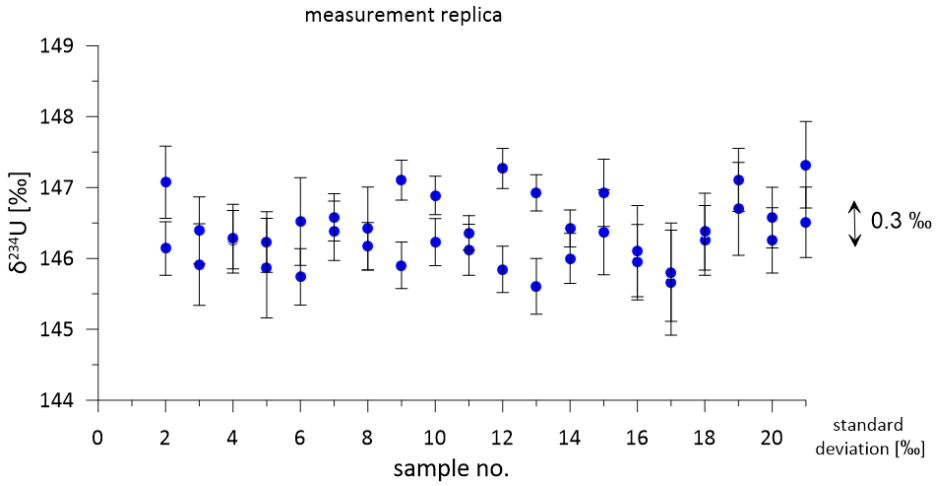

Figure 4.3 21 replicate measurements of $\delta^{234}U$, with values ranging from 144.4‰ to 146.1‰, the standard deviation across all samples is 0.3‰. highest deviation between replicas reach up to 1‰, resulting in error an of these individual points of 0.5‰.

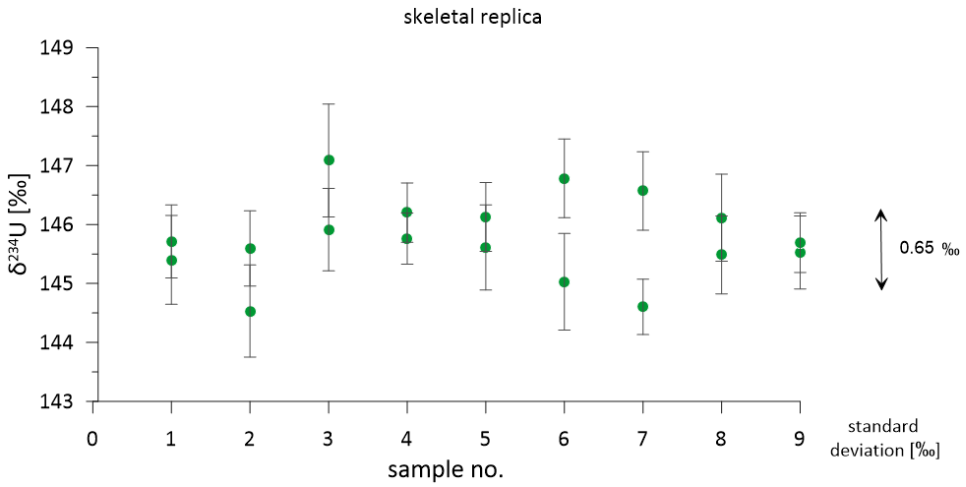

Figure 4.4 nine chemical replica samples, collected from the same growth band of the coral from Puerto Rico, exhibiting $\delta^{234}U$ values ranging from 144.5‰ to 147.1‰, with a standard deviation between these replicates of 0.65‰.

The high level of precision achieved in this study allows for the resolution of subtle variations in seawater $\delta^{234}U_{sw}$. For example, recent work has reported modern variability in $\delta^{234}U_{sw}$ on the order of 1.3‰ (Kipp et al., 2022). Even small differences of this magnitude can be resolved with confidence in annually banded corals using the methodology presented here. For example, during past climatic shifts such as the Last Glacial Maximum, characterized by low sea level and extensive global ice volume, with enhanced weathering rates, the $\delta^{234}U_{sw}$ values decreased by approximately 6‰ ± 2‰ (Henderson, 2002; Esat & Yokoyama, 2006; Chutcharavan et al., 2018). These shifts highlight the sensitivity of the $\delta^{234}U$ signal to changes in global continental

weathering and hydrological balance, reinforcing its value as a paleoenvironmental tracer. An additional experiment assessed the impact of uranium concentration on measurement precision. Fourteen samples of varying uranium concentration were analysed, revealing an exponential decrease in analytical error with increasing U concentration (Figure 4.5). At concentrations >20 ppb, the analytical error decreased from 1.7‰ to 0.6‰, and plateaued at 0.3‰ for U concentrations >40 ppb, up to the maximum measured concentration of 174.4 ppb.

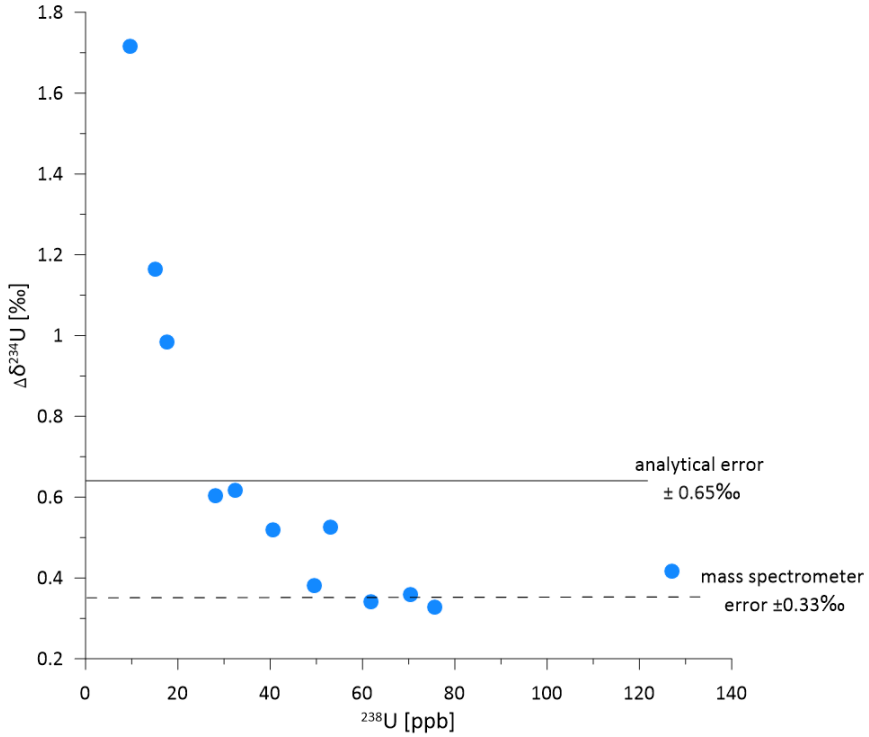

Figure 4.5 individual errors of 14 $\delta^{234}U$ measurement against their ^{238}U concentrations. The error drops from 1.7‰ to 0.6‰ with >20 ppb Uranium in solution, at >40 ppb Uranium the error plateaus at 0.3‰ until the maximum Uranium concentration of 174.40 ppb.

4.2 Matrix Effect

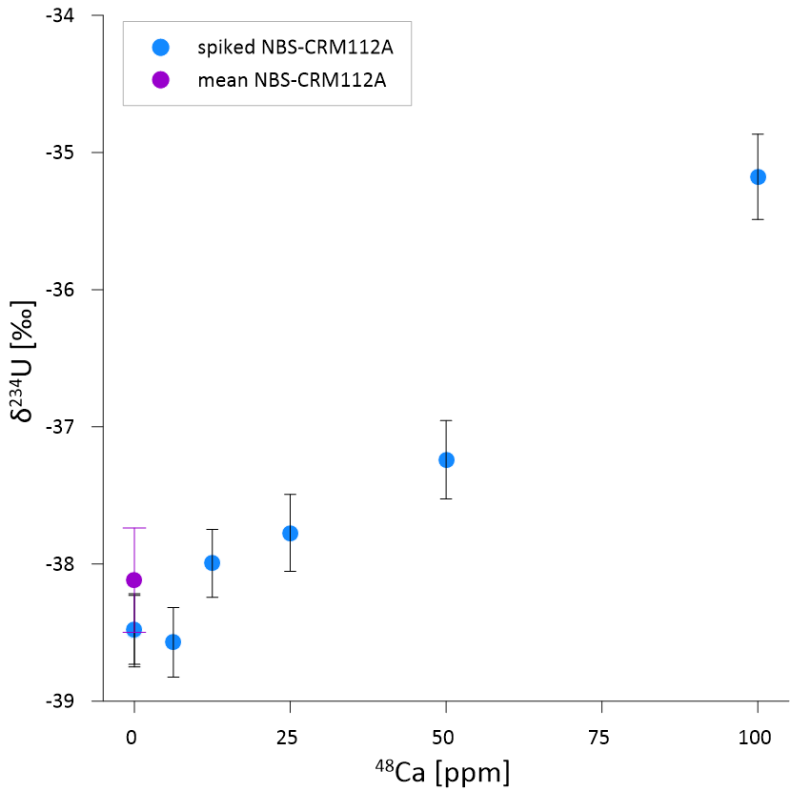

Figure 4.6 $\delta^{234}U$ values of Ca-spiked CRM-112A samples, above a Calcium concentration of 10 ppm the $\delta^{234}U$ significantly deviates

Matrix effects are a well-documented challenge in MC-ICP-MS analysis and are known to enhance instrumental mass bias (Douville et al., 2010). In this study calcium-spiked NBS-CRM-112A samples (Figure 4.6) reveal a clear matrix effect, with $\delta^{234}U$ values showing significant deviations from established reference values when calcium concentrations exceed 10 ppm (Robinson et al., 2002; Shen et al., 2002; Deschamps et al., 2003; Andersen et al., 2004a; Fietzke et al., 2005; Andersen et al., 2010). A positive linear correlation was observed between $\delta^{234}U$ values and increasing calcium concentrations above 10 ppm, indicating that excess calcium interferes with accurate isotope ratio determination. To mitigate these matrix effects, all treated carbonate samples were screened for calcium concentration using a Thermo iCAP Q ICP-MS. If calcium concentrations exceeded 10 ppm, the column chemistry procedure was repeated a third time to ensure sufficient removal of matrix elements prior to final $\delta^{234}U$ measurement. While Douville et al. (2010) reported reduced $\delta^{234}U$ signal intensity at similar calcium levels, they observed no significant isotopic bias when using ICPQMS reflecting the order of magnitude lower measurement precision of 3–4‰, archived with such instruments. In contrast, the higher reproducibility achieved in this study (±0.65‰) makes such bias detectable, which must originate from scattering calcium ions reaching mass 234 given the perfectly linear dependence to

the calcium concentration. The recent discovery of a Ghost signal related to the scattering of ^{238}U on masses of 229 and 230 shows that such scattering ions effects cause significant impacts on isotope ratios of isotope systems with low abundance ratios such as $^{234}U/^{238}U$ (Kerber et al., 2023). This trend confirms that calcium matrix effects may introduce systematic positive biases in $\delta^{234}U$ values when not adequately testing and removing calcium during chemical sample preparation. If analytical precision further increases, this test has to be repeated and the scattering effect of calcium ions need to be better quantified.

Thus, under controlled conditions, a linear correction may be applied if the sample Ca concentration is precisely known. However, for maximum accuracy, matrix removal through repeated column chemistry remains the preferred approach when Ca concentrations exceed 10 ppm. Also note, here only calcium was tested, but other elements may cause matrix effects when studying U isotopes in different minerals.

4.3 Sampling Strategy

Numerous studies have explored the spatial variability of trace element concentrations and isotopic compositions within coral skeletons, often identifying differences among microstructural components such as the theca, septa, and dissepiments (Perrin, 2003; DeLong et al., 2016; Reed et al., 2021). Additionally, variations in coral growth rates under different environmental conditions have been shown to influence geochemical signatures (Felis et al., 2003). In the present study, the relatively large material demand for uranium isotope analysis of 50 mg necessitated the integration of multiple skeletal components into single "bulk" samples.

Despite this approach, replicate $\delta^{234}U$ measurements taken along the same growth band, each incorporating different proportions of skeletal microstructures, revealed no statistically significant differences in $\delta^{234}U$ values (Figure 4.4). This suggests that, at the resolution applied here, intra-band heterogeneity in $\delta^{234}U$ is minimal or remains within analytical uncertainty. While some degree of microstructural variability likely exists, its influence on bulk $\delta^{234}U$ signal appears negligible regarding the precision, reproducibility and accuracy obtained here. The results support the validity of using integrated skeletal material for high-resolution isotope analysis when sample quantity is limited.

Additional tests comparing sampling methods (bulk vs. milled powder) on two neighbouring *Orbicella faveolata* colonies from the Mesoamerican Reef system off Puerto Morelos, Mexico revealed further insights. For bulk sampling, solid sections were cut from annual density bands using a handheld Dremel tool fitted with a diamond saw blade. And for powdered sampling, material was milled along the

growth axis to collect finely powdered samples from the same bands. Correlation coefficients between these sampling approaches are summarized in Table 4.1.

Table 4.1 Pearson correlation coefficients (r) between $\delta^{234}U$ records obtained from bulk and pulverised samples of two coral colonies (BOC1 and BOC2) at La Bocana, Mexico. All correlations are based on overlapping time intervals. Bold values indicate statistically significant correlations ($p < 0.05$).

	BOC1 bulk	BOC1 pulv	BOC2 pulv	BOC2 bulk
BOC1 bulk				
BOC1 pulv	**0.705**			
BOC2 pulv	0.285	0.475		
BOC2 bulk	**0.695**	**0.536**	0.411	

In the first coral (BOC1), $\delta^{234}U$ values from bulk and powdered samples were identical, suggesting homogeneity in internal skeletal composition or minimal structural influence on uranium incorporation. This consistency implies that either sampling approach is reliable when structural heterogeneity is low. In contrast, the second coral (BOC2), located only one meter away, exhibited measurable difference between the adjacent first sample (Table 4.1). In addition, significant but punctuated deviations are visible between bulk and pulverised samples. These discrepancies illustrate a variable degree of microscale heterogeneity between coral colonies. It is interesting to note that both corals reveal a 0.8 to 1‰ difference over almost two decades, when suddenly the variability of $\delta^{234}U$ increases, but absolute values merge. In absence of further mineralogical and geochemical studies of both corals, the origin of small but systematic deviations and intra-skeletal heterogeneity in U isotopes remains unknown. These findings highlight the importance of skeletal structure and sampling scale in $\delta^{234}U$ analysis and underscore the need for consistency in sampling methods when comparing records across colonies. Note that the temporal pattern is preserved even if small systematic biases exist between individual corals or over several decades of growth. Since such differences do not exceed the analytical reproducibility by more than a factor of two, we can safely interpret isotope variability larger than 1‰ as originating in seawater.

The temporal resolution achievable in $\delta^{234}U$ analyses is largely constrained by the amount of available coral material. Therefore, $\delta^{234}U$ values from the Venezuelan *Pseudodiploria strigosa* coral core were measured at both biannual and seasonal resolution are presented in Figure 4.7. Biannual $\delta^{234}U$ values ranged from approximately 143‰ to 148‰ over the period 1996–2002. Seasonal measurements

exhibit a similar range, from ~142‰ to 148‰, but capture finer intra-annual variability that is not evident in the lower-resolution dataset.

To assess the effect of sampling resolution, a relative deviation was calculated between each annual biannual sample and the mean of its corresponding seasonal samples. These deviations are also plotted in Figure 4.7 and generally fall within ±2‰ with the largest excursion occurring around the year 2000. Nonetheless, for most of the record, deviations remain minimal and centred near zero, indicating strong consistency between the two resolution approaches.

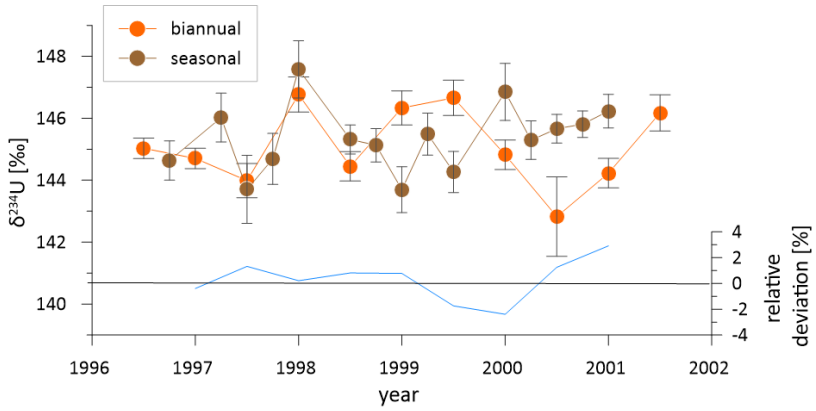

Figure 4.7 Comparison of seasonal (brown) and biannual (orange) $\delta^{234}U$ values measured in coral samples from Los Roques, Venezuela, between 1996 and 2002. Error bars represent analytical uncertainty (2σ). The blue line shows the relative deviation (%) between the two records. While overall trends are similar, notable divergence occurs around 2000–2001.

As shown in Figure 4.7, seasonal sampling does not consistently resolve well-defined biannual averages. Moreover, the biannual records are not merely smoothed versions of the seasonal signals, suggesting that averaging does not fully preserve intra-annual variability, likely due to variability of the uranium concentration in individual growth bands. This discrepancy may also result from the sampling process itself. During sawing or subsampling an uneven loss of material may disproportionately affect the averaging of seasonal values, which are better defined when using biannual bulk samples extracted by sawing.

A notable divergence occurs around 2000–2001, when the biannual records exhibits a pronounced minimum of 142.8‰, a feature not apparent in the corresponding seasonal dataset. This absence may be attributed to material loss or uneven sample retention during preparation, leading to incomplete capture of short-term isotopic excursions. Importantly, this anomalously low $\delta^{234}U$ value coincides with an extreme hydrological event: the catastrophic rainfall in late 1999 that triggered widespread landslides in Venezuela (Lyon, 2003). Such intense precipitation likely generated rapid surface runoff with minimal water-rock interaction, potentially transporting low $\delta^{234}U$ riverine water over a distance of ~140 km to the coral core site (Li et al.,

2018). Due to its brief duration, this signal may have been inadvertently excluded during material processing.

Achieving high-resolution $\delta^{234}U$ records requires careful sampling techniques, such as micro-drilling or fine-blade sawing; however, micro-drilling may introduce bias if the sampled material does not integrate multiple skeletal components.

4.4 $\delta^{234}U$ Variability Across Coral Genus and Colonies

Species-specific differences in the incorporation of trace elements and isotopes into the coral skeleton are well documented and often attributed to variations in biomineralization strategies, growth rate, morphologies, and ecological preferences (de Villiers et al., 1995; Sadler et al., 2014; Ross et al., 2019). The species analysed in this study are all common throughout the Caribbean (Veron, 1995), yet they represent a broader range of morphotypes, including massive, branching, encrusting and plate corals, than typically used in paleoclimate reconstructions. Among these, genera such as *Siderea, Orbicella* and *Diploria* are frequently used in climate proxy studies and are known to show species-dependent variations in elements such as Sr, Mg, and Li (Giry et al., 2010; DeLong et al., 2011). U/Ca ratios have also been reported to vary by species (de Villiers et al., 1995; Sadler et al., 2014; Ross et al., 2019). In contrast, our results Eleven coral samples representing ten different species from Rancho Luna Bay, Cuba, exhibited $\delta^{234}U$ values ranging from 145.20‰ ± 0.53‰ (Meandrina meandrites) to 145.11‰ ± 0.52‰ (Colpophyllia natans), indicating no significant species-specific fractionation in $\delta^{234}U$ (Figure 4.8). The mean value across all 11 samples was 145.55‰ with a standard deviation of ±0.33‰, consistent with open ocean baselines (Kipp et al., 2022). To test whether species dependent isotope fractionation occurs, mass fractionation needs to be measured on the MC-ICP-MS independent of the $^{235}U/^{238}U$ ratio (Kipp et al., 2022). Since we assume this ratio constant any fractionation would be corrected as mass bias (Kerber et al., 2023). However, the consistency of seawater and coral isotope composition implies no measurable fractionation takes place at the given analytical precision. This consistency supports the robustness of $\delta^{234}U$ as a geochemical proxy, largely unaffected by biological or ecological variability during uranium incorporation.

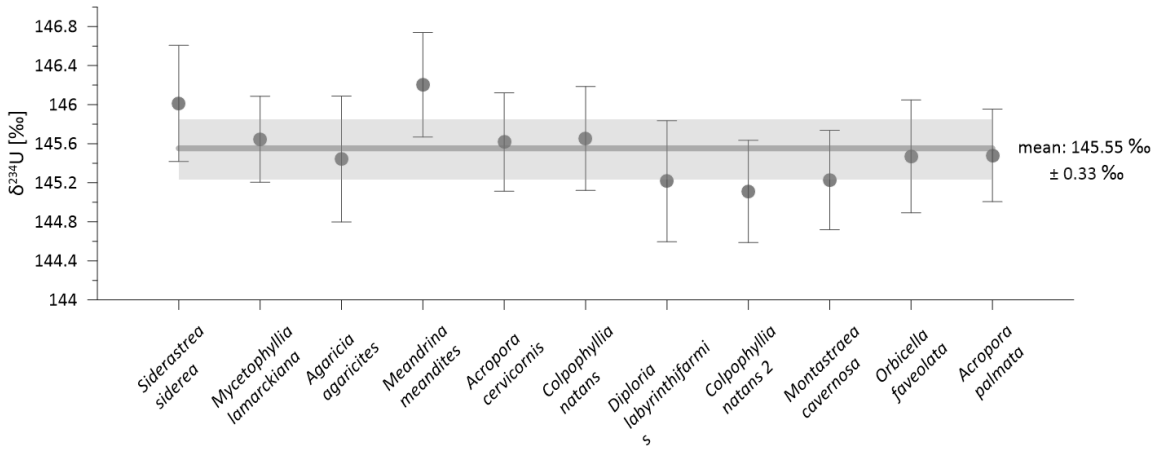

Figure 4.8 $\delta^{234}U$ values measured in 10 different coral species collected from the Rancho Luna reef in Cuba in 2015. The species include massive, branching and encrusting growth forms. Despite biological and morphological differences, all specimens exhibit consistent $\delta^{234}U$ values within analytical uncertainty (mean = 145.55‰ ± 0.33‰, shaded band)

To investigate spatial variability in $\delta^{234}U$ over time within the same reef environment, two colonies of *Orbicella faveolata* (BOC1 and BOC2) growing approximately 1 meter apart were analysed over a 10-year period (Figure 4.9). BOC1 exhibited slightly lower $\delta^{234}U$ values, with a mean of 144.3‰ ± 0.6‰ ($2\sigma_M$), compared to BOC2 with a mean of 145.1‰ ± 0.4‰. Statistically both values are identical within two sigma uncertainty, but the offset in absolute values of 0.8‰ is just moderately larger than expected from the reproducibility of the analytical method applied here (0.65‰). Nevertheless, both records display similar temporal trends, with a strong positive correlation ($r = 0.70$, $p < 0.001$) across the decade-long time series.

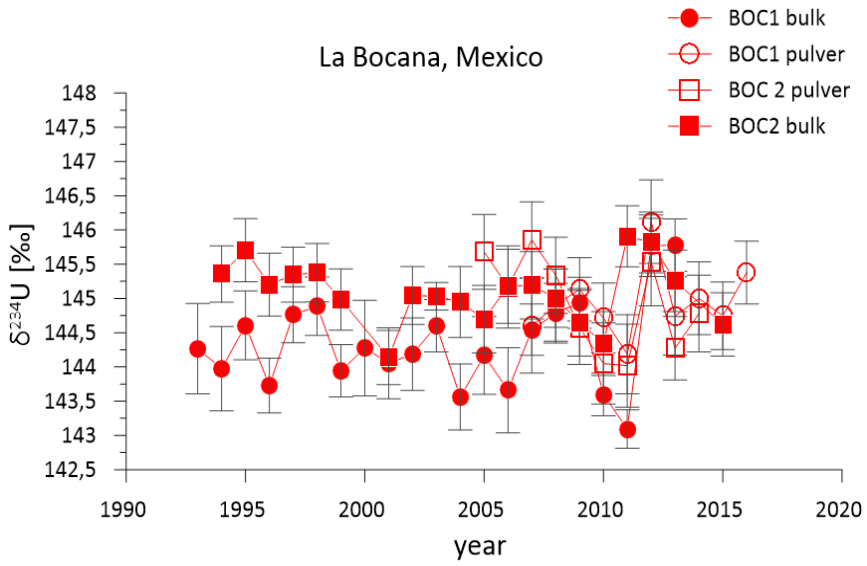

Figure 4.9 Temporal $\delta^{234}U$ records from two neighbouring coral colonies (BOC1 and BOC2) collected at La Bocana, Mexico. Both bulk (solid symbols) and pulverized (open symbols) samples are shown. Despite spatial heterogeneity in absolute $\delta^{234}U$ values, particularly between colonies, the temporal trends are strongly correlated ($r = 0.7$, $p < 0.001$).

This notable spatial heterogeneity in $\delta^{234}U$ values has previously been observed in a similar manner for Sr/Ca ratios and $\delta^{18}O$ within single reef systems (Alpert et al., 2016; Sayani et al., 2019). In this region, submarine groundwater discharge (SGD) is a prominent feature, with numerous point sources contributing freshwater inputs across the reef (Null et al., 2014). Groundwater on the Yucatán peninsula exhibits $\delta^{234}U$ values lower than those of open-ocean seawater (Schorndorf et al., 2023), aligning with the lower $\delta^{234}U$ values recorded in the BOC1 coral. This suggests that BOC1 compared to BOC2 may experience greater exposure to SGD, between 1992 and 1998, while beyond both corals reveal an identical pattern within uncertainty. Previous hydrodynamic studies indicate that seawater inflow occurs primarily above the reef crest, while groundwater and deeper water outflow is restricted to two main channels, one at the southern reef edge and one near La Bocana, the core site (Coronado et al., 2007) (Figure 3.5). Although detailed microcurrent mapping at this reef is lacking, research from comparable systems indicates that water flow is strongly modulated by reef topography and benthic structure (Monismith, 2007; Pomeroy et al., 2023). Such localized dynamics likely contribute to the observed differences in $\delta^{234}U$ values between the two colonies. Indeed, Hernández-Terrones et al. (2021) demonstrated differing degrees of mixing across SGD point sources in this reef, further supporting the role of spatial hydrological variability in shaping the observed coral $\delta^{234}U$ signals. Despite this offset, the temporal $\delta^{234}U$ trends in both corals remain highly correlated ($r = 0.7$, $p < 0.001$), indicating a common response to external drivers over decadal time periods.

4.5 Conclusion

This study demonstrates that high-precision $\delta^{234}U$ measurements in tropical coral skeletons are achievable through methodological advances in mass spectrometry, data processing and calibration, particular using the reference materials such as NBS-CRM 112A. Our analytical procedure demonstrates a full sample replicate precision ($2\sigma_M$, N=66) of ±0.65‰ when considering all aspects contributing uncertainty, such as mass spectrometric matrix effects, total procedural blanks, sample weight constraints, sample micro-heterogeneity on seasonal scale, local reef microcurrents, potential species differences, and frequent sample replication. The pure mass spectrometric analytical uncertainty can be reduced to ±0.3‰ when opting to measure > 50 ppb pure calcium free (<1 ppm) Uranium solutions.

These improvements allow for the detection of subtle $\delta^{234}U$ variations <1‰ associated with changes in seawater composition, including those linked to climatic events. Matrix effects, notably the residual calcium concentration of a sample was shown to introduce measurable linear dependence with $\delta^{234}U$ values at a rate of

±0.04‰ per ppm Ca. Thus, when measuring samples of <10 ppm calcium the impact is within the analytical precision achieved here. While these effects can be better quantified and potentially corrected, complete matrix removal of any contaminating element remains the preferred strategy for ensuring data integrity.

Sampling strategy and intra-skeletal heterogeneity were found to introduce small systematic differences and decreases reproducibility of seawater $\delta^{234}U$ reconstructions. Although the integration of multiple skeletal structures helped minimize variability, certain colonies exhibited microstructural heterogeneity that affected results at finer spatial scales (<1‰).

The temporal resolution was limited by sample availability, with discrepancies between seasonal and biannual values highlighting the sensitivity of $\delta^{234}U$ records to preparation techniques and the risk of missing transient environmental events.

Absence of species-dependent isotopic fractionation is determined from excellent agreement to the surrounding seawater and underscores the robustness of $\delta^{234}U$ as a geochemical proxy, supporting its application across diverse coral taxa. However, spatial differences in $\delta^{234}U$ between neighbouring colonies reflect the influence of local hydrodynamics, particularly submarine groundwater discharge. Despite this, strong inter-colony correlations affirm the reliability of $\delta^{234}U$ time series in recording regional-scale environmental variability when local reef conditions are well understood.

5 Coral and Seawater $\delta^{234}U$ without Direct Freshwater Influences in the Caribbean

Freshwater fluxes play a critical role in shaping regional oceanographic conditions, ecosystem dynamics, and biogeochemical cycling (Drinkwater, 1986). In the Caribbean, freshwater variability is of particular importance due to the ecological sensitivity of coral reef systems, the socio-economic reliance on coastal environments, and the region's exposure to climate extremes such as droughts, hurricanes, and riverine flooding (Maul, 1993). Moreover, freshwater input contributes to salinity variability that influences the Atlantic thermohaline circulation (Schmidt et al., 2004), linking Caribbean hydroclimate processes to the wider climate system. Freshwater delivery occurs through river discharge, precipitation, and groundwater flow, regulating salinity, nutrient input, sediment transport, and organic carbon fluxes (Null et al., 2014; Haßler et al., 2019; Starke et al., 2020; Mayfield et al., 2021). These processes are further modulated by large-scale modes such as El-Niño Southern Oscillation (ENSO), Atlantic Multidecadal Variability (AMV), and Atlantic hurricane activity (Liu et al., 2022), underscoring the need for robust reconstructions of freshwater variability in this region.

To address the limited coverage of instrumental records, coral archives have been widely employed to reconstruct freshwater input. Proxies such as Ba/Ca, $\delta^{13}C$, and $\delta^{18}O_{sw}$ have proven useful in capturing aspects of runoff and precipitation, yet each is subject to confounding influences including sediment resuspension, upwelling, photosynthetic variability, and dual sensitivity to both temperature and salinity (Fairbanks & Dodge, 1979; Leder et al., 1996; Watanabe et al., 2002; McCulloch et al., 2003; Ren et al., 2003; Swart & Grottoli, 2003; Benway & Mix, 2004; Ourbak et al., 2006; Moyer, 2008; Felis et al., 2009; Prouty et al., 2010; Moyer & Grottoli, 2011; Sadler et al., 2014; V. Schoepf et al., 2014; LaVigne et al., 2016; Wu et al., 2017; Yamazaki et al., 2021; Shaw et al., 2024). These complexities highlight the need for complementary tracers that can more directly capture freshwater forcing.

In this context, $\delta^{234}U$ represents a novel and promising approach. Because the isotopic composition of uranium in the open ocean is relatively stable (Andersen et al., 2010; Kipp et al., 2022), detectable shifts in coral $\delta^{234}U$ likely reflect terrestrial inputs from river discharge, groundwater flux, or weathering (Dunk et al., 2002; Andersen et al., 2007; Li et al., 2018; Li et al., 2023). Unlike existing proxies, $\delta^{234}U$ provides a geochemically distinct measure of land-ocean connectivity, integrating freshwater input over time. This makes $\delta^{234}U$ especially valuable for semi-enclosed basins like

the Caribbean, which are strongly influenced by large riverine discharges, while the input from the well-constrained and relatively uniform Atlantic (Kipp et al., 2022) is limited by restricted inflow through the Lesser Antilles (Johns et al., 2002).
However, to use $\delta^{234}U$ effectively, it is first necessary to establish the natural baseline for the entire basin. Establishing the regional reference state is essential to confidently attribute small but meaningful deviations in coral $\delta^{234}U$ to freshwater forcing.
Accordingly, this chapter focuses on establishing the $\delta^{234}U$ baseline for the Caribbean basin.

5.1 Location and Corals

The environmental settings and geographic context of the coral cores are described in detail in Chapter 3. Age models for the Puerto Rican corals were developed by Emma Gerlach as part of her bachelor's thesis, combining annual density band counting from high-resolution computed tomography (CT) scans with U-Th dating of non-continuous segments. Two massive *Orbicella faveolata* cores were analysed: CPR1990-09-25 and TM2020-12-04, collectively covering the period 1736–2020, albeit with notable hiatuses. CPR1990 includes two main intervals: 1885–1909 and 1934–1990, separated by a 23 ± 6-year hiatus, marked by a distinct change in growth direction. U-Th dates from three depths were internally consistent. Age accuracy for segments 1a and 1b is ±1 year, based on precise annual band counts, while the older segment 1c has an estimated error of ±6 years due to discontinuity (Figure B.1). The TM2020 core spans three distinct growth periods: 1736–1776, 1832–1881, and 1940–1980. Two major growth gaps of 59 ± 9 years and 54 ± 11 years, interrupt the record with age models constrained by annual band counting and U-Th dating (Figure B.1).
Annual extension rates were measured along individual corallites, following the primary growth axis to reduce sectioning bias. Measurement uncertainty is estimated at approximately 1 mm, limited by the CT scan resolution and minor alignment discrepancies. The mean extension rates were 6.7 ± 1.6 mm yr^{-1} for CPR1990 (Figure B.2) and 5.9 ± 1.7 mm yr^{-1} for TM2020 (Figure B.3). Notably, growth in CPR1990 segment 1c was significantly slower (5.1 ± 1.3 mm yr^{-1}) than in the other segments, consistent with the identified growth hiatus.
The age model for a *Siderastrea Siderea* microatoll of the Martinique coral was developed by Paterne et al. (2018) based on sclerochronology, U-Th dating and seasonal $\delta^{18}O$ alignment (Figure B.10 and Figure B.11).

5.2 Methods

All analytical procedures, including U-Th dating, isotope ratios ($\delta^{13}C$, $\delta^{18}O$, $\delta^{234}U$) and trace element (Sr/Ca, Ba/Ca) analysis are detailed in Chapter 3. Radiocarbon (^{14}C) measurements were conducted by Marika Hiemisch during her master's thesis, using samples from the CPR1990 core. In that study, a harmonic oscillator model was developed to simulate the corals expected $\Delta^{14}C$ response to atmospheric nuclear weapon testing, commonly known as the bomb $\Delta^{14}C$ peak. This model accounted for atmospheric input and ocean uptake, providing a theoretical curve for interpreting radiocarbon incorporation.

In the present work, the attention is focused on the residuals, or deviations from the modelled bomb $\Delta^{14}C$ curve. These residuals are interpreted to reflect non-atmospheric influences on radiocarbon variability, such as ocean circulation anomalies, upwelling of ^{14}C-depleted subsurface waters, or advection of older water masses with distinct radiocarbon signatures. Comparing measured $\Delta^{14}C$ values against the expected bomb-peak trajectory, enables a broader environmental interpretation of the coral $\Delta^{14}C$ record during the atmospheric nuclear bomb testing, beyond its conventional use as a chronological marker.

5.3 Puerto Rican Coral

5.3.1 Seasonal Variability

The seasonal records from the CPR1990 and TM2020 coral cores reveal distinct patterns in proxy behaviour, shaped by differences in local hydrology and reef setting (Figure 5.1). While both cores record clear seasonal cycles in $\delta^{13}C$ values and Ba/Ca ratios, $\delta^{18}O_{sw}$ values are only available for CPR1990. In that core, $\delta^{18}O_{sw}$ values show coherent seasonal variability, consistent with short-term salinity changes and freshwater influence. The range exceeds that observed in direct seawater measurements from the region (Watanabe et al., 2002), although the mean values agree. This suggests influences from episodic freshwater events or evaporation, which may not be captured by limited seawater sampling campaigns. Additional complexity arises from the contribution of multiple water sources to coral $\delta^{18}O$ values, as highlighted by Smith et al. (2006). At La Parguera, the coral core shows the highest $\delta^{18}O$ values, indicative of strong evaporative enrichment (Stevenson et al., 2018), a plausible result given its shallow, lagoonal environment (Figure B.7). Although skeletal extension rates can influence incorporation of stable oxygen isotopes, the similar $\delta^{18}O$ ranges in both cores, despite differing growth rates, suggest that growth rate alone does not explain the observed patterns (Leder et al., 1996; Smith et al., 2006).

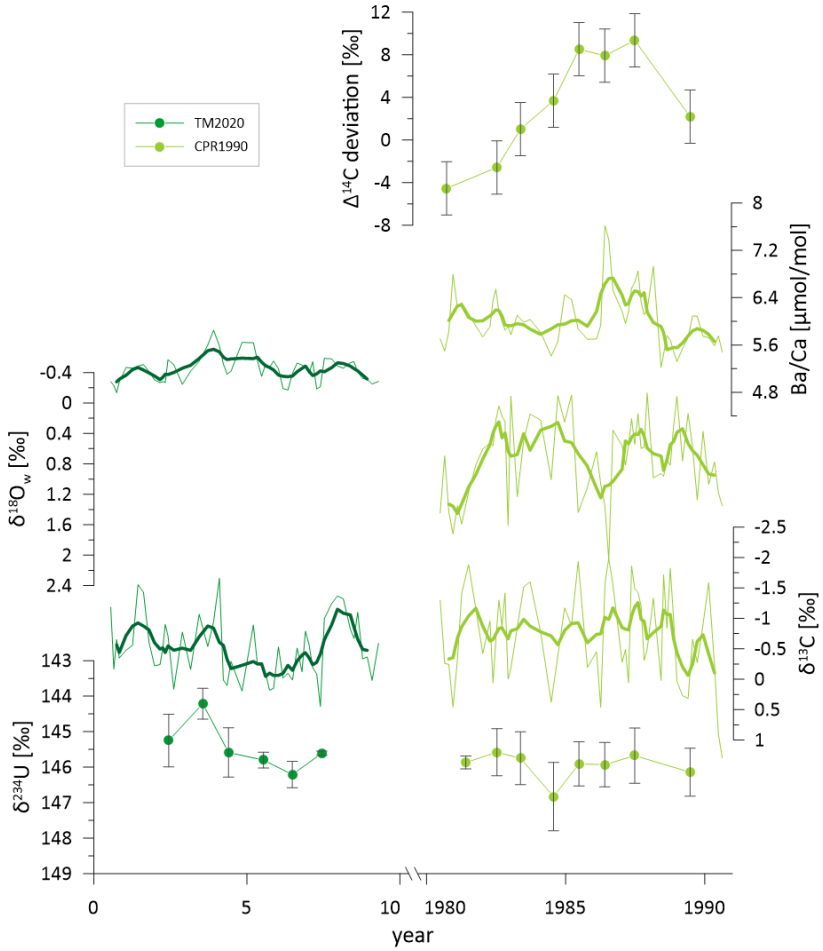

Figure 5.1 Seasonal and annual variability of freshwater-sensitive proxies in coral cores TM2020 (dark green) and CPR1990 (light green). Due to the age uncertainty in the TM coral only relative ages are plotted, but refer to the 1940s. The panels show proxy records for $\Delta^{14}C$ deviation, $\delta^{18}O_{sw}$, $\delta^{234}U$, Ba/Ca, and $\delta^{13}C$. Thin lines represent seasonal-resolution measurements; thick lines represent smoothed annual trends derived from moving averages. $\Delta^{14}C$ and $\delta^{18}O_{sw}$ are only available for CPR1990. $\delta^{234}U$ and $\Delta^{14}C$ are plotted as annual means with error bars. Notably, 1984–1985 shows anomalies in multiple proxies, coinciding with a major precipitation event.

In contrast, $\delta^{13}C$ values (shown in Figure 5.1) display a seasonal variability of ~2.6‰, comparable to values reported by Moyer and Grottoli (2011). At their study site, seasonal $\delta^{13}C$ variability was linked to riverine input of isotopically lighter DIC. Watanabe et al. (2002) also observed $\delta^{13}C$ variability in *Orbicella* corals from La Parguera, but attributed the changes primarily to photosynthetic fractionation under variable cloud cover, rather than to freshwater input.

Ba/Ca records show pronounced seasonal structure in both cores, with strong cycles in TM2020, but generally higher Ba/Ca ratios in CPR, supporting a local difference within the lagoon. The CPR coral was collected at a reef further inside the protected lagoon, where reduced oceanic flushing likely increases the delivery of terrestrial particulates. However, Ba/Ca can also be influenced by nutrient rich upwelled water (Ourbak et al., 2006; LaVigne et al., 2016), though upwelling is not typically reported near the study sites (Rueda-Roa & Muller-Karger, 2013). Additionally, recent work

suggests that Ba incorporation into the coral skeleton may also be dependent on light availability (Yamazaki et al., 2021), offering a possible explanation for the observed seasonal variability due to cloud coverage (Watanabe et al., 2002), especially in the absence of direct fluvial runoff at the core sites.

The TM2020 core, dated to the 1940s, provides a high-quality seasonal record for this period. While it cannot be directly compared to the 1980s CPR1990 record, their contrasting settings and time periods offer valuable insight into the stability of seasonal proxy signals across decades. The upper section of the TM2020 coral was excluded due to signs of diagenetic alteration, particularly elevated Mg/Ca values (Figure B.4) (Allison et al., 2007; Hendy et al., 2007; Nothdurft & Webb, 2008).

At annual scales, the bold lines in Figure 5.1 highlight broader hydroclimatic trends. Notably, $\Delta^{14}C$ deviations exhibit a rising trend through the early to mid-1980s, peaking around 1985–1987 before declining, reflecting the uptake of atmospheric bomb-^{14}C. Atmospheric ^{14}C levels rapidly decrease and since the downward mixing propagates the bomb-peak to depth the values decrease moderately in the late 1990s. In addition, to these external drivers, the radiocarbon decrease in 1990 may reflect changes in cross thermocline exchange, similar to other records, that have been interpreted as shifts in water masses driven by trade wind-modulated Ekman transport (Kilbourne et al., 2007; Paterne et al., 2018; Toggweiler et al., 2019; Paterne et al., 2023). In contrast, Ba/Ca ratios and $\delta^{13}C$ values show no coherent long-term trend across either core, supporting their interpretation as being more sensitive to short-term (seasonal) variability or localized events.

$\delta^{234}U$ values remain stable within analytical uncertainty over the observed period, except for a marked decrease in the third year of the TM coral record. Since this lowered value in the TM coral cannot be dated precisely at present, a comparison to a local or regional event is not feasible. In contrast, a moderately elevated $\delta^{234}U$ value in 1984 in the CPR coral may coincide with Hurricane Klaus, during which intense mountain runoff was reported (Lawrence & Clark, 1985), suggesting a pulse of terrestrial freshwater input that may have temporarily altered the island's weathering regime.

The overall stability of $\delta^{234}U$, together with consistently stable annual mean values of further freshwater proxies Ba/Ca, $\delta^{13}C$, and $\delta^{18}O_{sw}$, indicates that these corals are minimally influenced by episodic freshwater input. This supports the interpretation that the Puerto Rico cores reflect well-mixed open-ocean conditions, allowing their $\delta^{234}U$ signatures to serve as a reliable baseline reference for the Caribbean seawater uranium isotopic composition. Additionally, Puerto Rico's historically dry climate over the past 70 years (Kilbourne et al., 2008; Vieten et al., 2024) supports the general absence of strong freshwater signals in the annual proxy records. Further, the La

Parguera lagoon lacks direct riverine input; the nearest major river, Río Loco, discharges approximately 15 km up current and delivers an estimated 26 ft^3 sec^{-1} (~0.7 m^3 sec^{-1}) (Survey, 2012), limiting the direct influence of river discharge on the coral sites.

In summary, when neglecting the one lowered $\delta^{234}U$ value in the TM coral the 13 remaining measurements yield a mean $\delta^{234}U$ value for the Caribbean Sea of 145.87‰ ± 0.20‰ ($2\sigma_M$), which matches the global ocean mean within uncertainty (Kipp et al., 2022).

5.4 Martinique Coral Record

The analysed coral core from Martinique spans the period of one century from 1887 to 1982 and provides a $\delta^{234}U$ time series based on 30 individual samples, which resolve the long-term mean as well as annual variance (Figure 5.2). The mean $\delta^{234}U$ value across the record is 145.13 ± 0.21‰ (1σ, n = 30), matching the modern open ocean signature (Kipp et al., 2022). This suggests that, on average, the uranium isotope composition at this site reflects well-mixed Equatorial Atlantic seawater with limited freshwater influences.

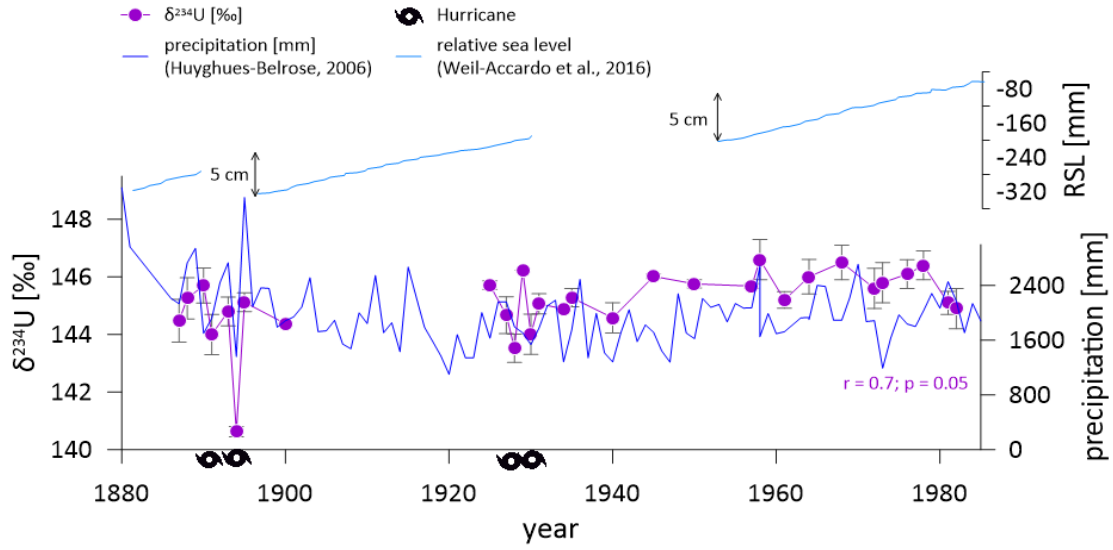

Figure 5.2 Time series of coral $\delta^{234}U$ (‰, purple circles) from Martinique compared with annual precipitation (blue line, right axis; (Huyghues-Belrose, 2006)) and relative sea level (RSL; blue line in upper panels; (Weil-Accardo et al., 2016)) between 1887 and 1982. Hurricane events are indicated by black cyclone symbols. Periods of anomalously high $\delta^{234}U$ values coincide with increased precipitation, suggesting enhanced continental weathering and terrestrial uranium input. The significant positive correlation between $\delta^{234}U$ and precipitation (r = 0.7; p = 0.05) underscores the climatic sensitivity of uranium isotope signatures in nearshore coral archives. Notably, sharp negative $\delta^{234}U$ excursions align with major hurricanes and associated geomorphological disturbances (e.g., landslides), including those near 1894 and 1930. These coincide with coral "die-down" phases and abrupt RSL drops (~5 cm), likely related to tectonic uplift (Weil-Accardo et al., 2016).

As seen in Figure 5.2, the record reveals two several year long periods, with increased variability from the stable mean value, which correspond closely to periods of known climatic and hydrological variability. Notably, elevated $\delta^{234}U$ values in the coral appear to correlate with intervals of increased precipitation, as inferred from historical meteorological records ($r = 0.7$; $p = 0.05$) (Huyghues-Belrose, 2006). This positive correlation suggests that enhanced rainfall amplifies continental weathering processes, leading to increased uranium fluxes from terrestrial sources (Kigoshi, 1971; Li et al., 2018). Martinique, as a volcanic island with steep topography and highly reactive basaltic bedrock, is particularly sensitive to changes in precipitation (Rad et al., 2013; Taïlamé, 2020). As water percolates through these weathered profiles, it results in terrestrial freshwater with most likely elevated $\delta^{234}U$ values. Unfortunately, we have not been able to analyse freshwater from Martinique and thus no further conclusion or mass balance can be established. However, due to the island's small size and limited buffering capacity, this isotopically distinct freshwater is rapidly transported into the surrounding coastal zone during extended wet seasons (Taïlamé, 2020). The coral grew in these nearshore waters, and possibly incorporated this transient freshwater signal into its skeleton, thereby preserving a minor annual average trace of weathering and runoff intensity. Nevertheless, excursions are within the limits of 1‰, which we here consider a significant change compared to the seawater isotope composition. Thus, with the exception of the years 1894 and 1928 the record can be considered a stable reference baseline (145.38‰ ± 0.26‰ ($2\sigma_M$)), driven by Equatorial Atlantic water entering the Caribbean Sea.

The Martinique coral $\delta^{234}U$ record was further compared to the corals $\Delta^{14}C$ data to evaluate the potential influence of upwelled, radiocarbon-depleted water masses and/or Amazon-derived freshwater pulses (Paterne et al., 2018; Paterne et al., 2023). However, no consistent relationship between $\delta^{234}U$ and $\Delta^{14}C$ was observed (Figure B.10). This lack of correlation suggests that the uranium isotope signal in the Martinique coral was not significantly affected by the incursion of older, deeper waters, which would be expected to have lower radiocarbon activity (Andersen et al., 2007). Furthermore, previous work by Paterne et al. (2023) identified distinct pulses of Amazon River water reaching the Lesser Antilles based on $\Delta^{14}C$ anomalies during major discharge events. If these pulses had introduced uranium with a distinct isotopic signature into the Caribbean, a corresponding shift in $\delta^{234}U$ values would be expected even across the Caribbean Sea. However, the absence of such excursions in the Martinique coral supports the conclusion that uranium associated with Amazon discharge was largely diluted or even removed before entering the open Caribbean. This interpretation aligns with the findings of Border (2020) who demonstrated that anoxic conditions in the Amazon delta promote efficient precipitation and retention

of uranium within the estuarine system, thus the Amazon can act both as source and sink of oceanic uranium, however, the net flux of uranium remains unknown. The stability of the $\delta^{234}U$ baseline throughout periods of high discharge, including those discussed by Paterne et al. (2023) indicates that these anoxic processes remained effective in limiting the export of isotopically distinct uranium to downstream coral sites, even under extreme hydrological conditions.

Conversely, sharp negative excursions in $\delta^{234}U$, falling below the expected seawater baseline, coincide with documented hurricane events in 1891, 1894, 1928, and possibly 1930 (Figure 5.2) (Landsea & Franklin, 2013). Notably, these anomalies also align with observed die-down phases in the upper part of the coral skeleton, dated to approximately 1896 ± 4 and 1931 ± 3 (Weil-Accardo et al., 2016). These die-downs are interpreted as periods of physiological stress caused by abrupt exposure of the coral to subaerial conditions, likely triggered by rapid relative sea-level fall. Weil-Accardo et al. (2016) suggest that such sea-level changes may result from tectonic uplift associated with regional seismic activity. Aubaud et al. (2013) identified widespread landslide deposits on Martinique linked to these same time periods. These extreme events, combining heavy rainfall, coastal erosion, and sediment remobilization, likely introduced large volumes of particulate-bound uranium with low $\delta^{234}U$ into the nearshore environment (Swarzenski et al., 2004). The resulting influx of isotopically distinct material would have temporarily overwhelmed the background seawater signature recorded by the coral. Taken together, this evidence suggests that short-lived but intense climatic and tectonic disturbances can leave identifiable, though transient, geochemical fingerprints in coral $\delta^{234}U$ records.

Overall, the Martinique coral record provides a robust baseline for open-ocean seawater $\delta^{234}U$ over the past 100 years, with its long-term average closely matching open-ocean conditions. Significant excursions are limited to periods of extreme disturbance, such as hurricanes, landslides, or tectonic events, which cause annual deviations of <1.5‰ to up to 4‰, after which values rapidly return to baseline due to efficient coastal mixing.

5.5 Conclusion

This chapter examined seasonal to annual-scale coral geochemical records from Puerto Rico and Martinique which are today and in the past century not largely exposed to local freshwater sources. However, large distant freshwater sources such as the Amazon river seem to have no influence on the local water isotope composition. The Puerto Rican coral cores (CPR1990, TM2020) show distinct seasonal cycles in $\delta^{13}C$ and Ba/Ca, with $\delta^{18}O_{sw}$ variability captured at CPR1990. While these proxies reflect local hydrological influences, including evaporation and lagoonal restriction,

their long-term mean values remain stable. Annual averages of Ba/Ca, $\delta^{13}C$, $\delta^{18}O_{sw}$, and $\delta^{234}U$ display minimal variability, supporting the interpretation that the Puerto Rican corals primarily archive well-mixed open-ocean conditions. The stability of $\delta^{234}U$ in particular allows these records to serve as a robust seawater baseline at 145.45‰ ± 1.0‰, with only short-lived anomalies during extreme hydrological events, such as Hurricane Klaus in 1984.

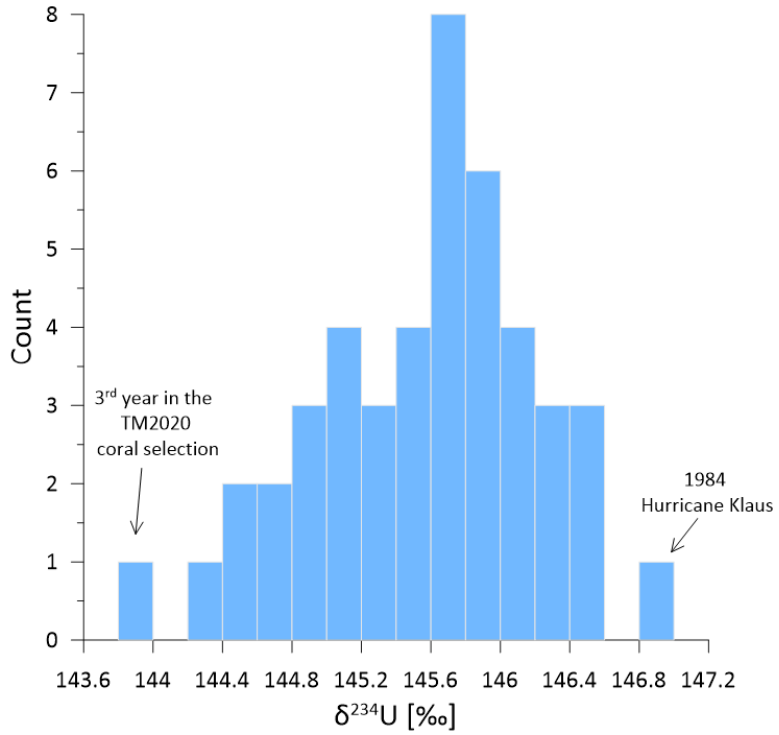

Figure 5.3 Histogram of $\delta^{234}U$ values (‰) from three Caribbean corals (TM2020 (Puerto Rico), CPR1990 (Puerto Rico), and Chancel 1 (Martinique)). The majority of measurements fall within a narrow range around 145–146‰, reflecting a stable regional $\delta^{234}U$ baseline in line with the open ocean value of 145.5‰ (Kipp et al., 2022). Outliers, such as the 3rd year in TM2020 and a value coinciding with Hurricane Klaus in 1984, illustrate occasional short-term deviations but do not affect the overall long-term stability of the baseline.

In contrast, the Martinique coral record (1887–1982) provides a century-long $\delta^{234}U$ baseline that closely matches modern open-ocean values, while capturing distinct excursions during major disturbances including hurricanes, landslides, and possible tectonic uplift events. These transient deviations reflect the island's volcanic terrain and sensitivity to extreme rainfall and geomorphological change, but values consistently return to baseline following such events.

Taken together, the Puerto Rico and Martinique corals demonstrate that $\delta^{234}U$ values in coral skeletons can serve as a reliable tracer of open-ocean seawater composition on decadal to centennial timescales Figure 5.3. Their stability highlights their utility as baselines, while event-driven anomalies provide additional insights into the hydrological and geological processes shaping Caribbean reef environments.

6 Cuban Coral traces Annual Hydrologically driven Variability in $\delta^{234}U$ Values since the End of the Little Ice Age

The content of the following chapter is under review in the journal Paleoceanography and Paleoclimatology ((Greve et al., 2025), https://doi.org/10.22541/au.173990739.96182414 /v1) and has been slightly modified.

Tropical surface-dwelling corals are always situated in shelf environments, with potential influences of U contributions from local river discharge, submarine groundwater releases, or even the distant transport of freshwater from larger river systems.

Consequently, by examining postmodern, well-preserved and annually-resolved corals, the oceanic U isotopic composition can be investigated to identify any potential systematic local or regional disturbances from freshwater fluxes through rivers and submarine groundwater.

To assess the potential impact of shelf water processes on the U isotopic composition of tropical corals and to reveal the potential of U isotopes as freshwater tracers, we selected a long-lived *Orbicella faveolata* coral colony in the western tropical North Atlantic, for which both regional freshwater releases and distant freshwater influences, such as advective transport from the Mississippi River seemed plausible. The tropical Atlantic Ocean is an ideal location for testing potential links between $\delta^{234}U$ and hydrological and oceanographic conditions at the subcentennial scale. The northern Caribbean is part of the Atlantic Warm Pool (AWP), which is defined by the sea surface temperature (SST) isotherm exceeding 28.5°C, which forms each year during early summer (June) and extends into the Gulf of Mexico and the western tropical North Atlantic as summer progresses (July-October) (Wang & Enfield, 2001; Wang et al., 2008). In relation to the AWP and the Intertropical Convergence Zone (ITCZ), the Caribbean hydroclimate is characterized by a wet season from April to October (Martinez et al., 2019), during which hurricanes are also commonly observed (Terry & Kim, 2015). Especially for the Little Ice Age (LIA), which spanned from approximately 1400–1850 (Hodell et al., 2005), substantial changes in the Caribbean SST hydroclimate and potential oceanic circulation have been reconstructed (Haug et al., 2001; Hodell et al., 2005; Richey et al., 2009; Johnson, 2011; Kennett et al., 2012; Fensterer et al., 2013; DeLong et al., 2014; Burn et al., 2016). Consequently, through the study of annual excess ^{234}U variability along a coral core drilled in a colony located

at the north of Cuba, we aimed to qualitatively resolve freshwater fluxes into the Gulf of Mexico since the LIA.

6.1 Seawater $\delta^{234}U$ from Coral Aragonite

Corals incorporate the uranium isotopic ratio of seawater ($\delta^{234}U_{SW}$) into their skeleton without measurable fractionation (Robinson et al., 2004b; Wang et al., 2017; Kipp et al., 2022). However, one known factor that can cause fractionation is the post depositional diagenetic alteration of the coral skeletal material (Delanghe et al., 2002; Robinson et al., 2004b; Wang et al., 2017).

Uranium isotope variations in the Cuban coral are independent of growth parameters (e.g., density) or green banding with high of Mg (Figure 3.1)(Alonso-Hernández et al., 2022). As Mg/Ca is the proxy most sensitive to skeleton diagenesis, such as calcite or secondary aragonite formation (Allison et al., 2007; Hathorne et al., 2011), the absence of correlation between $\delta^{234}U$ and Mg/Ca suggests that diagenesis has not influenced the $\delta^{234}U$ values along the core. Studies have shown that secondary aragonite also has a higher U content than primary skeletal aragonite does (Eggins et al., 2005; Allison et al., 2007; Hathorne et al., 2011), which implies a possible correlation between uranium content and isotopic composition. This correlation was not detected in our results (Figure 6.1). Furthermore, a diagenetic overprint could result in extraordinarily high $\delta^{234}U$ values exceeding 10‰ above those of seawater. According to Chutcharavan et al. (2018), a benchmark of 156‰ is used to indicate diagenetic alteration of fossil coral material. However, in the coral analysed here, no such elevated values were observed.

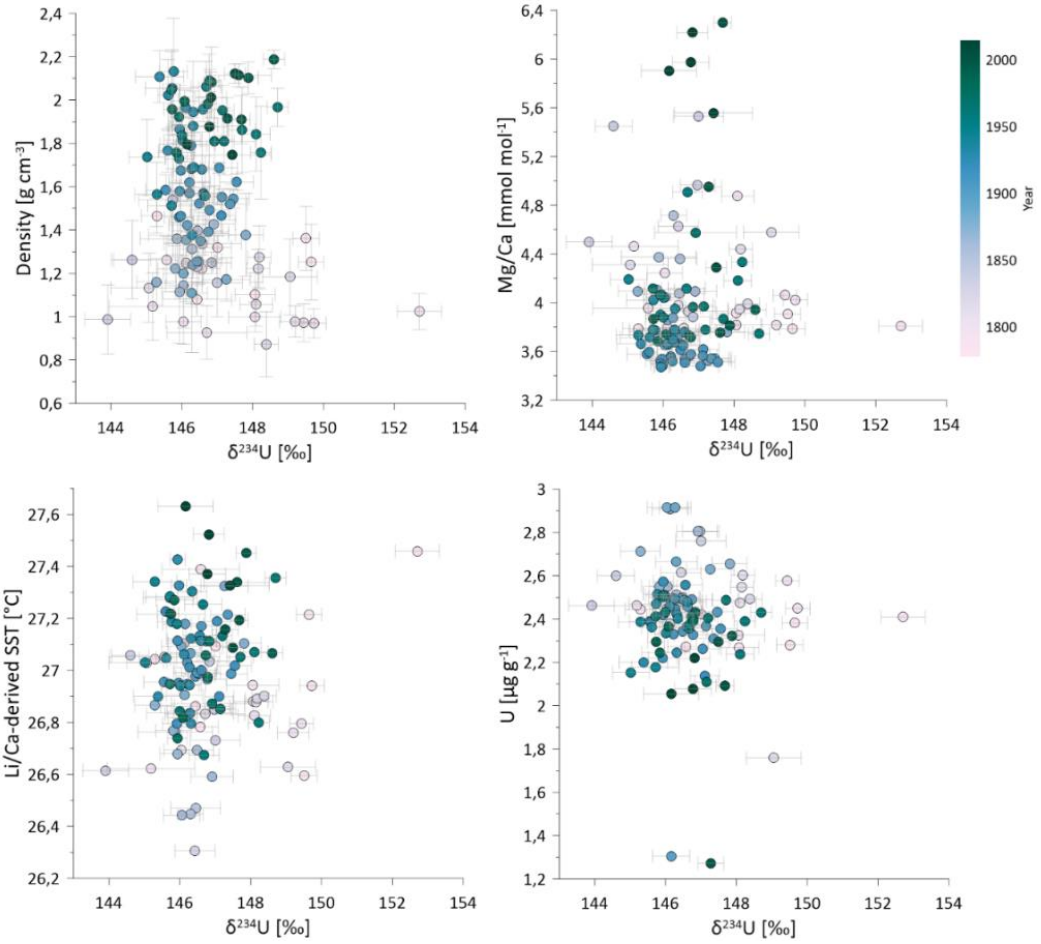

Figure 6.1 no correlation between the coral density, coral Mg/Ca, Li/Ca derived SST (Alonso-Hernández et al., 2022) or U concentration and $\delta^{234}U$ values is visible, implying no $\delta^{234}U$ signal variations due to vital effects or diagenesis. Colour scale denotes sample year.

Figure 6.2 shows a total of 104 samples that were collected from the 237-year record of the coral, with each sample representing an integration of one year. The mean value of all samples comes to a $\delta^{234}U$ value of 145.58‰, with a standard deviation of 1.22‰. The large data ensemble and small variance contribute to an uncertainty in the mean value of ± 0.24‰ ($2\sigma_M$, N = 104). The measured mean $\delta^{234}U$ value of 145.58‰ is identical to that of modern seawater (Kipp et al., 2022). Consequently, the excellent agreement of the mean isotopic compositions of corals with those of with modern seawater, allow for us to conclude that the CSM-1 coral can be used to monitor the U isotopic compositions of local seawater over the past 237 years.

Studies conducted in restricted ocean basins have demonstrated a $\delta^{234}U$ offset towards higher values, a shift attributed to the substantial influence of meltwater or river discharge (Andersen et al., 2007; Zhou et al., 2015; Wang et al., 2017; Arendt et al., 2018). Despite the Caribbean being a semi-enclosed basin, it receives a high inflow rate of Atlantic waters, estimated at 28 Sv, which exit the Caribbean and Gulf of Mexico

near the sample location (Johns et al., 2002). These substantial throughflow rates support the strong control of seawater on the coral mean $\delta^{234}U$ values.

6.2 Coral $\delta^{234}U$ Values as a Proxy for Hydrological Variation

Analysis of the small-scale variability within the last 165 years from 1850–2014 reveals a range of 3.68‰, from 143.82‰ to 147.50‰ (Figure 6.2). This variance is 2.5 times greater than that observed in modern seawater (Kipp et al., 2022). Notably, an even higher variability is observed in earlier years, specifically from 1778–1847, during which the $\delta^{234}U$ values exhibit a total variance of 8.10‰, fluctuating from 143.40‰ to 151.50‰.

With excellent reproducibility and overall high precision, even subtle variability can be resolved. The variability in seawater $\delta^{234}U_{sw}$ was recently reported to be 1.3‰ (Kipp et al., 2022). Under different climate and global weathering conditions, such as during the last sea level low stand and maximum global ice volume, i.e., the Last Glacial Maximum, seawater $\delta^{234}U_{sw}$ decreased systematically worldwide by 6±2‰ (Henderson, 2002; Esat & Yokoyama, 2006; Chutcharavan et al., 2018). The major sources of isotopic variability in the surface ocean are continental runoff and submerged groundwater. Continental freshwater has a very large range of $\delta^{234}U$ values from as low as 70‰ to 1030‰, depending on the continental U cycle driven by erosion and the type of regional weathering (Dunk et al., 2002; Li et al., 2018). In the tropics, chemical weathering prevails, reducing the excess leaching of ^{234}U from the host rock. Moreover, the residence times of freshwater in karstic environments, such as in the Cuban core location, are within days or months to years, resulting in $\delta^{234}U$ values that are at the lower end of the freshwater scale (Dunk et al., 2002; Paces et al., 2002; Gonzalez-De Zayas et al., 2013; Iturralde-Vinent et al., 2016). Thus, changes in the local freshwater contribution to the ocean could cause the $\delta^{234}U_{sw}$ values to shift slightly lower than those of seawater. The annual precipitation from 1960–2008 near the coral location has a mean of 482.9 mm yr^{-1} and varies by approximately 124.5 mm yr^{-1} (Centella-Artola et al., 2023). Thus, the interannual precipitation variability indicates substantial variations of at least ±25% in the local freshwater supply.

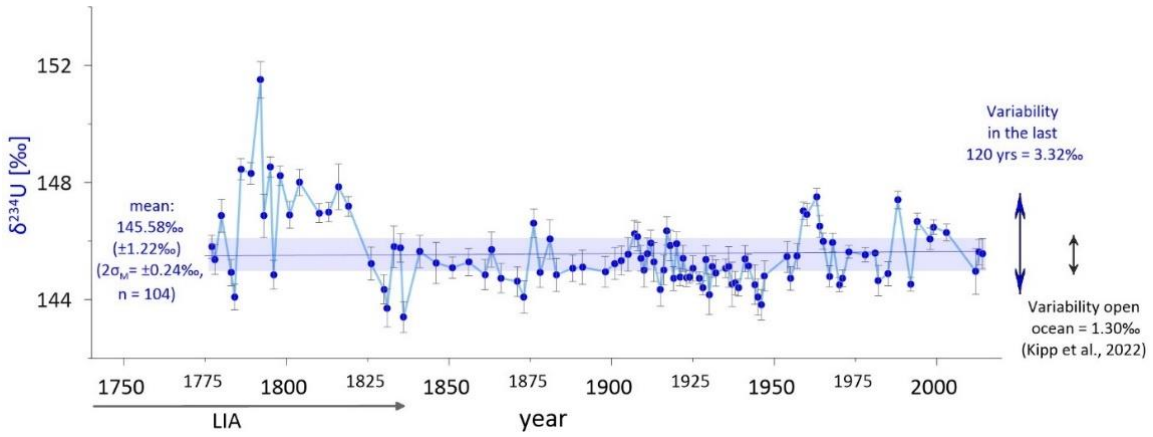

Figure 6.2 Annual $\delta^{234}U$ measurements (n = 104) of a 237-year-old coral. The mean of 145.58 ‰ is identical to the open ocean value of 145.55 ‰ (±0.28 ‰) (Kipp et al., 2022). The largest deviations from 143.40 ‰ to 151.50 ‰ were observed from 1778–1847 at the end of the Little Ice Age (LIA), with the peak value occurring in 1792. The variability in the coral $\delta^{234}U$ over the last 165 years is approximately 2.5 times greater than the variance expected from observations in the open ocean (Kipp et al., 2022).

Over the past 120 years, the coral record has shown considerable variability on decadal timescales, which is approximately 2–3 times greater than that expected in open ocean seawater (Figure 6.2) (Andersen et al., 2010; Kipp et al., 2022). Interestingly, the $\delta^{234}U$ variations have exhibited a negative correlation with the regional precipitation record since 1960 ($r = -0.6$ $p < 0.05$, $N = 21$) (Figure 6.3 and Figure B.13) (Centella-Artola et al., 2023). These subtle variations in $\delta^{234}U$ values are close to the reproducibility limit of the U isotope measurements but are still statistically noteworthy. The local $\delta^{234}U_{SW}$ value is dependent on the input of terrestrial sourced freshwater, such as river runoff and submarine groundwater discharge (SGD). In Cuba, the residence time of precipitated water is relatively short and in the range of days to months due to the karstic terrain (Gonzalez-De Zayas et al., 2013; Iturralde-Vinent et al., 2016). Uranium isotopic compositions in groundwater are influenced by both redox conditions and uranium concentrations. Typically, an inverse relationship exists between groundwater uranium concentration and $\delta^{234}U$; deep, reducing groundwaters with low uranium concentrations tend to show higher $\delta^{234}U$ values than oxic, near-surface waters with higher concentrations (Osmond & Cowart, 1976; Asikainen, 1981). Redox conditions also influence uranium mobility and isotope fractionation, with well-oxidizing groundwaters yielding lower activity ratios (Suksi et al., 2006). Catchment-scale denudation further affects these ratios: a U-shaped relationship has been observed, where both low and high denudation rates correspond to elevated $\delta^{234}U$ values, while intermediate rates yield lower values (Li et al., 2018). Studies from the Yucatán Peninsula and Tampa Bay, Florida, have reported low $\delta^{234}U$ values in groundwater and estuarine waters, which also showed relatively high uranium concentrations

(Osmond & Cowart, 2000; Swarzenski & Baskaran, 2007; Schorndorf et al., 2023). The low $\delta^{234}U$ values in the coral may therefore reflect shallow groundwater runoff influenced by oxidizing conditions and/or moderate denudation rates in riverine waters in the region. Hence, the freshwater runoff coming from the Carbonate Hinterland (Iturralde-Vinent et al., 2008) and related to precipitation may lead to a moderate decrease of $\delta^{234}U$ values in coastal seawater. This process likely explains the anticorrelation of coral $\delta^{234}U$ values, where lower $\delta^{234}U$ values coincided with high annual precipitation over the last 50 years (Figure 6.3). A study of a sediment core situated approximately 100 km east of the analysed coral core revealed a freshwater influence on organic matter by approximately 15% from 1900–1970 (Alonso-Hernández et al., 2022). During this time, the coral exhibited a mean $\delta^{234}U$ value of 145.25‰, at the lower limit of open ocean seawater, possibly reflecting a persistent but minor local freshwater influence. The influence on $\delta^{234}U$ is likely far lower than that observed for organic matter by Alonso-Hernández et al. (2020) because of the lack of high-discharge rivers nearby.

A commonly used proxy for sea surface salinity (SSS) is stable oxygen isotopes in seawater ($\delta^{18}O_{sw}$), as they depend on both freshwater influx and evaporation (Gagan et al., 1998; Gagan et al., 2000; Ren et al., 2003). A comparison with reconstructed $\delta^{18}O_{sw}$ values from tropical corals in proximity to the sample location also revealed similarities at annual time scales (Figure 6.3 and Figure B.13) (Smith et al., 2006; Harbott et al., 2023). The $\delta^{18}O_{sw}$ is calculated from the measured coral $\delta^{18}O$ values (Smith et al., 2006), which are influenced by seawater $\delta^{18}O_{sw}$ and temperature. By subtracting the temperature component derived from the Sr/Ca record of the same coral, the $\delta^{18}O_{sw}$ at the time of coral growth can be calculated (Supplementary Table B.**1**) (Ren et al., 2003). Note that the SST, estimated via the Li/Ca ratio (Alonso-Hernández et al., 2022), is not significant correlated with the coral $\delta^{234}U$ values (Figure 6.1).

For the 19th century, the coral $\delta^{234}U$ values aligned with the $\delta^{18}O$ record of a stalagmite from western Cuba, interpreted as a proxy for rainfall amount (Fensterer et al., 2012). This alignment falls within the uncertainty of the stalagmite age model (Figure 6.3 and Figure B.13). Before 1860, the stalagmite and coral records diverged from one another, suggesting a potential additional source of $\delta^{234}U$ and its variability. Here, we propose that this source is linked to distant freshwater discharge from the North American continent and/or a synchronous reduction in the strength of the Gulf of Mexico current, which is not traced by the hydroclimate record of the stalagmite.

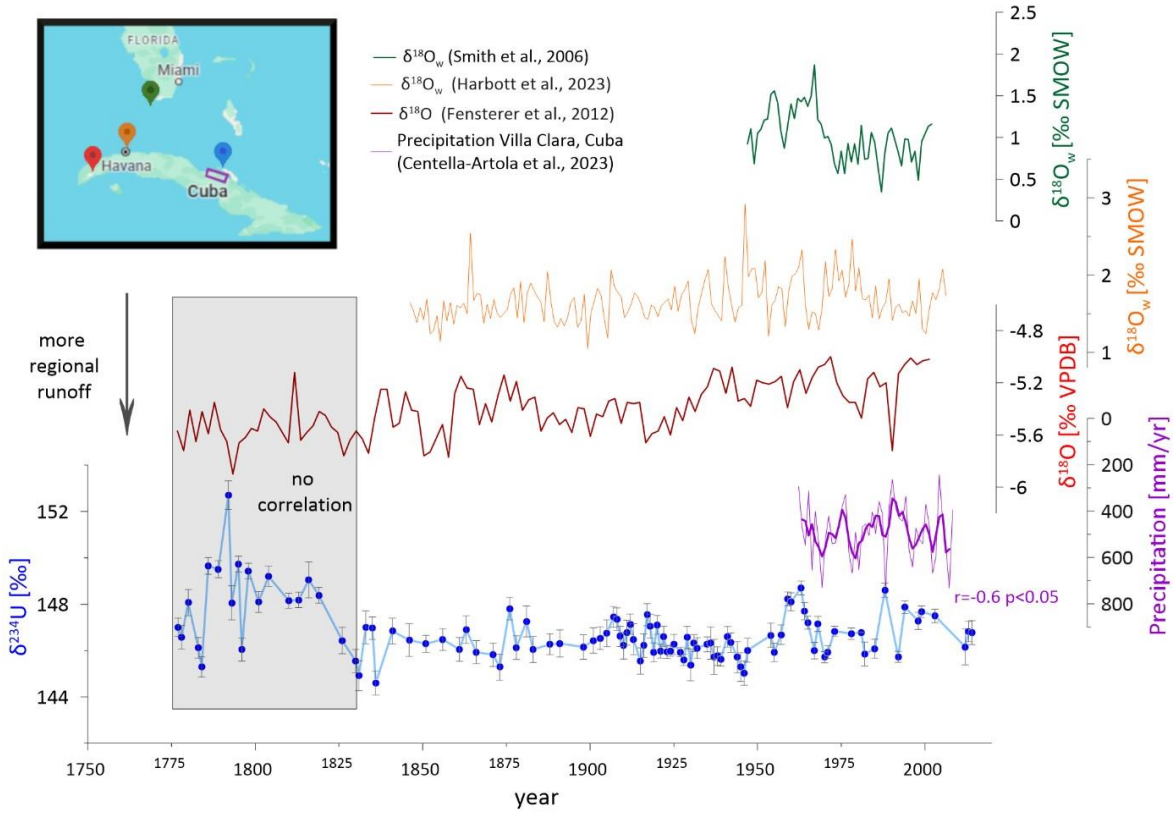

Figure 6.3 The $\delta^{234}U$ values from the analysed coral in central northern Cuba (blue) are negatively correlated (r = -0.60, p<0.05) with a precipitation record from the same region, starting in 1960, with an inverted y-axis (purple) (Centella-Artola et al., 2023). Similar patterns are observed with $\delta^{18}O_{sw}$ values calculated from corals from southern Florida (green) (Smith et al., 2006) and northern Cuba (orange) (Harbott et al., 2023), with high $\delta^{234}U$ values corresponding to high $\delta^{18}O_{sw}$ values. Additionally, since 1860, there has been a similar trend in the $\delta^{18}O$ values from a stalagmite in northwestern Cuba, which are interpreted as a precipitation indicator (red) (Fensterer et al., 2012).

6.3 Variability during the LIA

The highest variability in the coral $\delta^{234}U$ values occurred between 1778 and 1847, with $\delta^{234}U$ values ranging from 143.40‰ to 151.50‰. This time interval of high $\delta^{234}U$ variability coincides with the end of a period of colder SSTs in the Caribbean during the LIA (Winter et al., 2000; Haase-Schramm et al., 2003; Kilbourne et al., 2008).

6.3.1 Fast and High Local Runoff

Some studies infer reduced precipitation during the LIA, including Haug et al. (2001) for the southern Caribbean, Hodell et al. (2005) for the Yucatán Peninsula and Richey et al. (2009) for the Gulf of Mexico. However, other studies have reported highly variable amounts of rainfall in the northern part of the Caribbean and the Gulf of Mexico (Kennett et al., 2012; Fensterer et al., 2013; DeLong et al., 2014; Burn et al., 2016). Historical records in Cuba also documented periods of drought interspersed with several severe hurricanes in the late 1700s (Johnson, 2011) (Figure 6.4). A high

amount of local precipitation with fast discharge rates can explain the low $\delta^{234}U$ values recorded in the coral, as discussed above. The punctuated low values recorded by the coral suggest multiple local extreme precipitation events, particularly from 1778–1847. Wang and Enfield (2001) reported that an extended AWP fuels precipitation and the frequency of more intense tropical storms. Additionally, DeLong et al. (2014) linked fluctuating SSTs in Dry Tortugas and Puerto Rico (Kilbourne et al., 2008) to a variability in the size of the western hemispheric warm pool. The reconstructed SST from the Li/Ca in the analysed coral also exhibited high variability during that time (Alonso-Hernández et al., 2022). Therefore, fluctuating $\delta^{234}U$ values further support times of fast and high local runoff.

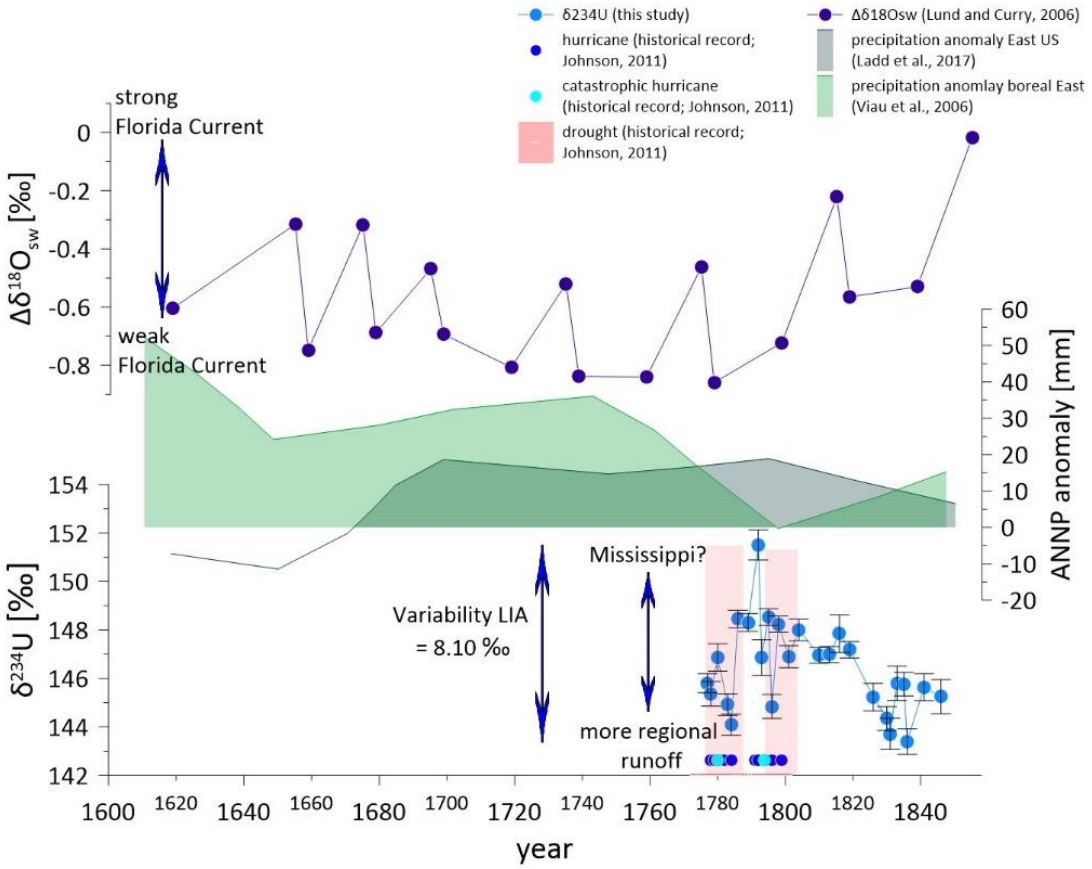

Figure 6.4 $\delta^{234}U$ values (blue) from 1778–1830 plotted together with the timing of hydrological events documented in historical records (Johnson, 2011), indicating times of high hydrological fluctuation with droughts (red), hurricanes (dark blue), and catastrophic hurricanes (light blue). During these times, the $\delta^{234}U$ values exhibited high variability, ranging from 143.40‰ to 151.50‰ in 1792. Florida Current strength is inferred from $\Delta\delta^{18}O_{sw}$ differences between the Gulf of Mexico and the Bahamas Channel (purple;(Lund & Curry, 2006)), where more negative values reflect a weaker current during the LIA. Superimposed precipitation anomalies over eastern North America (dark green; (Ladd et al., 2018)) and the boreal east (light green; (Viau et al., 2006)) show enhanced precipitation during this same interval, consistent with a weakened Florida Current and elevated variability in $\delta^{234}U$ values.

Another possible influence on the $\delta^{234}U$ values is land use change on the Cuban island. Beginning around 1820, widespread deforestation was undertaken to expand sugarcane cultivation (Monzote, 2024). This deforestation likely increased soil

erosion and enhanced continuous runoff into coastal waters (Monzote, 2024), potentially stabilizing $\delta^{234}U$ ratios by maintaining a consistent input of uranium from weathered material.

6.3.2 Possible Mississippi Influence

With a smaller AWP, precipitation over the eastern North American continent has increased due to changes in atmospheric circulation (Wang et al., 2008; Ladd et al., 2018). This enhancement also extended to parts of the Mississippi recharge basin (Ladd et al., 2018), potentially leading to increased runoff. The Mississippi River was found to have elevated $\delta^{234}U$ values averaging approximately 335‰, with strong seasonal variations and values reaching up to 450‰ (Grzymko et al., 2007). During the end of the LIA, the coral $\delta^{234}U$ values are frequently elevated by >3‰ compared with those in the mean ocean and are even more significant than those in locally depleted runoff. Thus, we hypothesize that these elevated $\delta^{234}U$ values resulted from ^{234}U-enriched waters from Mississippi that reached the Gulf of Mexico and induced excess ^{234}U to the coral site. Indeed, analysis of satellite salinity measurements indicates, that Mississippi-sourced waters can extend as far as the Florida Straight (Cummings & Smedstad, 2013). Density cascading in the Straits of Florida may then transport uranium-rich particles from the Florida Current into deeper waters (Robinson et al., 2004b), potentially delivering uranium to the core location and facilitating exchange between surface and intermediate water masses.

Finally, the total U mass fluxes through the Gulf of Mexico depended not only on U runoff but also on the relative amount of water in which this runoff is diluted. A strong Caribbean current would more efficiently dilute any freshwater signal than a reduced Gulf of Mexico throughflow. During the LIA, Lund et al. (2006) as well as a recent study by Forman et al. (2025), reported a decrease in the throughflow rate at the Florida Strait by approximately 10%, predominantly in the wind-driven part of the Florida Current. This reduction, coupled with an increase in precipitation over the eastern part of the North American continent (Lund et al., 2006; Ladd et al., 2018), could reasonably account for a higher total U discharge from the Mississippi River. This scenario likely contributed to the observed punctuated increase in $\delta^{234}U$ values of 2–3‰ during the LIA. Lund and Curry (2006) and Richey et al. (2009) further suggested saltier conditions in the Gulf of Mexico during the LIA, bringing the Caribbean Basin closer to today's conditions of semi-enclosed basins such as the Mediterranean Sea. These basins present elevated $\delta^{234}U$ values due to restricted access from open ocean seawater, high evaporation rates and the input of much freshwater and submerged groundwater from terrestrial sources (Border, 2020). However, changes in

throughflow of up to 10% are small overall compared with possible major changes in U runoff and its isotopic composition.

The discussion above assumes that the $\delta^{234}U$ values in the coral are influenced solely by Mississippi freshwater and seawater, neglecting the potential impact of other sources with different $\delta^{234}U$ ratios. The reduced wind-driven portion of the Florida Current, which originates from the North Atlantic Subtropical Gyre (Lund et al., 2006), results in a greater contribution of South Atlantic sourced water, potentially affecting the coral $\delta^{234}U$ ratios. South Atlantic waters are further influenced by the significant discharge of the Amazon and Orinoco rivers near the entrance of the Caribbean (Vorosmarty et al., 1998; Paterne et al., 2023). The Amazon River has elevated $\delta^{234}U$ values of 204‰ (±4‰) (Swarzenski et al., 2004; Border, 2020). However, a study of uranium concentrations and $\delta^{234}U$ values in the Amazon delta identified a uranium sink due to anaerobic conditions (Border, 2020), suggesting that Amazon-derived uranium does not have a significant large-scale influence on Cuban corals.

6.3.3 Mississippi Mass Calculation

Considering the present-day strong seasonal variability in the U concentration and isotopic composition of the Mississippi River (Grzymko et al., 2007), it cannot be assumed that the uranium concentration and $^{234}U/^{238}U$ activity ratio have behaved conservatively in the Mississippi River over the last 240 years. Binary isotope mixing according to Equation (1) (Roy-Barman et al., 2016) was applied to estimate the potential fraction of the Mississippi River-derived U isotopes in the Gulf of Mexico throughflow.

$$f_r = \frac{\delta_c * C_c - \delta_{sw} * C_{sw}}{\delta_r * C_r - \delta_{sw} * C_{sw}} \quad (1)$$

Here, δ_C is the coral $\delta^{234}U$ ratio and C_C is the coral U concentration converted into the corresponding seawater concentration (assuming 3.5 µg g^{-1} = 3.3 µg L^{-1} at 35.9 PSU). And any other influences on the U concentration, such as temperature and the coral growth rate, on the U concentration are neglected. Similarly, δ_{SW} is the open ocean seawater $\delta^{234}U$ ratio, and C_{SW} is its U concentration (presumed to be constant, $[U]_{Sw} >> [U]_{river}$). Finally, δ_r is the Mississippi $\delta^{234}U$ ratio range, and C_r is the U concentration range. For this two end-member isotope system, the past seawater U concentration remains unknown but is likely to vary within small ranges of a few percent from modern values. To overcome this difficulty, we here used the mean coral U concentration (2.27 µg L^{-1}) as a representative of seawater. Taking these limitations into account, the proportion of Mississippi River freshwater (f_r) reaching the coral site

during the LIA, where the highest $\delta^{234}U$ ratios are recorded, is estimated to vary between 0% and 3.0%.

The seawater U concentration may vary independently of open ocean and freshwater mixing, due to evaporation, for example (Ivanovich & Harmon, 1992). Additionally, U incorporation during coral calcification may vary depending on the growth rate (Inoue et al., 2011), seawater pH (Inoue et al., 2011), carbonate ion concentration, dissolved organic carbon (DeCarlo et al., 2016; Patterson et al., 2021), and temperature (Ourbak et al., 2006; Patterson et al., 2021), causing subtle changes in the coral U concentration independent of the balance between seawater and freshwater. Consequently, any quantitative estimate will remain speculative without monitoring all the above aspects. Nonetheless, the Mississippi freshwater volume contribution to the Gulf of Mexico throughflow is currently less than 0.5‰ in mass balance (Leaman et al., 1995; Grzymko et al., 2007), leading to subtle salt changes and minor changes in oxygen isotopes overprinted by net evaporation. Hence, we must assume that changes in the U concentration of seawater caused by the contribution of the Mississippi are minimal. Consequently, any observed variations in isotopic composition must reflect a major shift in the supply of U and/or an increase in the $\delta^{234}U$ value of river discharge.

In summary, we suggest that the deviation of the Cuban coral $\delta^{234}U$ values from a constant open ocean $\delta^{234}U$ value is most likely driven by two independent excess U sources. First, the local runoff coupled with the variance in precipitation on the island of Cuba likely resulted in minor reductions in the U isotope values compared with the open ocean mean values. The observed correlation between a decrease in isotopic composition and an increase in precipitation accounts for approximately 50% of the variability in the $\delta^{234}U$ time series from 1850–present. At the end of the LIA period (1778–1847), when the climate cooled in the Northern Hemisphere and the tropical climate was unstable, a second process influenced the time variance of the coral $\delta^{234}U$ values. Most likely, the distant influence of the excess ^{234}U contribution from the Mississippi River into a weaker throughflow of the Caribbean current caused a moderate and punctuated strong increase in seawater and thus coral $\delta^{234}U$. Both local precipitation and distant freshwater runoff must influence on the $\delta^{234}U$ time variance and mean of the coral record. Here, these two distinct contributions did not modify the long-term average coral $\delta^{234}U$ value, which is identical to the mean global ocean value. In addition, the variance in $\delta^{234}U$ is less than ±3‰ when the single elevated value in 1792 is excluded. This finding strongly constrains the expected variance in the initial $\delta^{234}U$ values of fossil corals within the Caribbean.

6.4 Conclusion

This study presents a 237-year-long record of seawater $\delta^{234}U$ from the northern part of Cuba, which was obtained via analysis of the uranium isotopic composition of a coral core of *Orbicella faveolata*. Our results confirm that coral $\delta^{234}U$ reliably records the seawater composition ($\delta^{234}U_{SW}$) without significant diagenetic alteration, as evidenced by the lack of correlation between $\delta^{234}U$, density and Mg/Ca ratios. The coral has a mean $\delta^{234}U$ value of 145.53‰ (±0.1‰), which is identical to the open ocean value of 145.55‰ (±0.28‰). Decadal $\delta^{234}U$ variations are approximately 2–3 times greater than those in open ocean seawater and correlate inversely with regional precipitation since 1960 ($r = -0.6$, $p < 0.05$), suggesting an influence of local terrestrial freshwater input, likely from surface runoff and submerged groundwaters. From 1778–1847, coinciding with the end of the Little Ice Age, the $\delta^{234}U$ record exhibited high variability, with values ranging from 143.40‰ to 151.50‰, which suggests substantial hydrological changes characterized by severe droughts and increased hurricane activity. Changes in atmospheric circulation during that time also led to increased precipitation over the eastern North American continent, including the Mississippi drainage basin. Thus, elevated $\delta^{234}U$ values are potentially related to increased freshwater input from the Mississippi River and reduced throughflow in the Florida Strait. Estimates from a binary isotope mixing model indicate that freshwater from the Mississippi may have contributed up to 3% of the total water mass at the coral site during this time. Reduced flow through the Gulf of Mexico, coupled with increased precipitation, likely amplified the uranium isotope signal, causing a 2–3‰ increase in coral $\delta^{234}U$. However, the influence of other far more distant freshwater sources, such as the Amazon River, was likely minimal due to localized uranium sinks.

7 Tracking Coastal Groundwater Flow in the Mexican Caribbean Through a Coral $\delta^{234}U$ Record

Glacial and interglacial sea-level fluctuations have been extensively documented using $\delta^{18}O$ measurements, particularly from benthic foraminifera. These fluctuations are driven by changes in ice sheet volume, reducing or increasing the mass of water in the ocean (Shackleton, 1987; Siddall et al., 2003). Over glacial-interglacial and geological timescales, tectonic activity and isostatic rebound play significant roles in modulating sea level, influencing vertical land movement and basin morphology and altering the sea level on the order of tens to hundreds of meters. Additionally, variable groundwater storage in aquifer and permafrost and the thermal expansion or contraction of ocean water, both driven by climatic changes, contribute to less than 1m of sea-level variability over millennial timescales. On much shorter timescales, such as months to centuries, factors such as storm surges, currents, and groundwater storage induce small (a few cm) and localized sea-level changes (Figure B.14) (Milne et al., 2009; Stammer et al., 2013; Woodworth et al., 2019). Those changes impact coastal dynamics and ecosystems, by changing oceanographic flow paths or weathering dynamics and nutrient input (Passeri et al., 2015).

In particular, regional sea-level variations are further shaped by dynamic oceanic processes. In the Caribbean, the Yucatán Current plays a crucial role in generating and redistributing sea-level anomalies, particularly in relation to eddy activity and Gulf Stream dynamics (Molinari et al., 1978). As one of the strongest currents in the region, the Yucatán Current, is influenced by flow through the passages over the Jamaica Ridge, where two jets occur. Furthermore, the Yucatán Current and its eddy production near Cozumel are linked to eddy vorticity of the Gulf of Mexico (Centurioni & Niiler, 2003), which ultimately influences the strength of the Gulf Stream (Blaha, 1984).

For coastal environments with submarine groundwater discharge (SGD), such as the Yucatán Peninsula, sea-level pressure (SLP) exerts a direct control on freshwater outflow (Null et al., 2014; Parra et al., 2015; Parra et al., 2016; Mayfield et al., 2021). Elevated SLP restricts the groundwater outflow, while reduced SLP enhances the geostrophic gradient, promoting increased freshwater discharge into the ocean (Coronado et al., 2007; Parra et al., 2016). The Yucatán Peninsula is particularly

noteworthy for its high SGD rates and minimal surface runoff, a consequence of its karstic geology, which features both high infiltration and evaporation rates (Bauer-Gottwein et al., 2011).

Here, the relationship between short-term sea-level fluctuations and $\delta^{234}U$ variations in a groundwater-fed system is now examined using a long-lived coral in the influence zone of the submerged groundwater off Mexico. The concept is to provide annual resolution of groundwater driven impacts on the corals $\delta^{234}U$ ratio, which is in first place influenced by the mixing of SDG and seawater, while SDG flux is modulated by sea level and groundwater levels. The unique hydrogeology of the Yucatán Peninsula offers an exceptional opportunity to investigate these dynamics, and their implications for the interconnectedness of sea level changes, SGD, and marine geochemistry. This is because the groundwater system shows a link between $\delta^{234}U$ and sea level on climate time scales (Schorndorf et al., 2023), and because the geochemical interface between seawater underlying the groundwater is well studied (Ritter et al., 2019). Additionally, the sea level influence on the strength of SDG has been demonstrated (Álvera-Azcárate et al., 2009; Yu & Kim, 2011; Torres & Tsimplis, 2013).

Therefore, the detailed analysis of annual $\delta^{234}U$ variability over the past century, allows testing the sea level influence on SDG and $\delta^{234}U$ and diagnose changes prior to instrumental sea level observations. Here we, thus analyse a 100-year-old *Orbicella faveolata* coral that has grown close to an SGD point source recording the ambient sea water $\delta^{234}U$ values of surrounding waters throughout its development (Figure 3.5). In this very first study of SDG, we observe a small but measurable impact of the groundwater $\delta^{234}U$ leading to a reduction of the average local seawater $\delta^{234}U$ of about -0.9‰, but stronger secular depletions, which attest increased fluxes of SDG during periods of reduced local sea level.

7.1 $\delta^{234}U$ over the Past Century

The measured $\delta^{234}U$ values from the BOC1 are shown in Figure 7.1 and exhibit variability around a mean of 144.6‰ ± 0.6‰ (SD, $2\sigma_M$ = 0.1), with individual measurements ranging over 3.25‰ from 143‰ to 146.25‰. Thus, on average the $\delta^{234}U$ the ensemble is 0.85‰ lower than the Caribbean Sea $\delta^{234}U$ average of 145.45‰ and solely 12 out of the studied 74 samples have an isotopic composition, which is identical within analytical precision with the seawater composition. No sample shows a value larger than seawater, but >20 values are more than 1.2‰ lower than the expected seawater value. While the mean difference is within the critical range of <1.2‰ for individual sample variability, we consider the data ensemble to be large

enough, and the number of depleted values to be significant (N>20) to demonstrate a measurable difference from the open ocean expectation value. This, very small mean isotope depletion and the frequently lowered values by up to 2.5‰ suggests a regional influence on the uranium isotope composition originating from a $\delta^{234}U$ depleted source. This observation is attested through the study of an offshore water sample, which revealed a $\delta^{234}U$ value of 145.7‰ ± 0.7‰ ($2\sigma_M$), aligning well with open ocean $\delta^{234}U$ values for the Caribbean. Water circulation in the Puerto Morelos reef system is primarily driven by seawater inflow over the reef crest and outflow of deeper waters through two main channels (Coronado et al., 2007). Since these channels are not in close proximity to the offshore seawater sampling site, the consistency of its $\delta^{234}U$ value with open ocean seawater suggests rapid mixing of uranium from terrestrial and oceanic sources over the reef crest.

Schorndorf et al. (2023) reported low $\delta^{234}U$ values (~16‰) in the Yucatán Peninsula freshwater lens and high U concentrations (~3µg L^{-1}), consistent with other karstic regions (Bonotto & Andrews, 1993). The origin of this Karstic low $\delta^{234}U$ value and high groundwater U concentration lies in the rapid transfer of water from infiltration into the large groundwater system and the effective dissolution of the limestone host rock (Osmond & Cowart, 1976; Asikainen, 1981).

The study by Schorndorf et al. (2023) further demonstrated that the groundwater $\delta^{234}U$ value evolved over the past five millennia from $\delta^{234}U$ values of 25‰ to the present 16‰ synchronous to the terminal rise of sea-level. Hence, the moderately reduced coral $\delta^{234}U$ values imply a regional influence of such $\delta^{234}U$ depleted and U rich groundwater on the uranium isotope composition within the lagoon. Several studies highlight the contribution of freshwater point sources along the Yucatán Peninsula coast to the region's hydrogeochemistry (Bauer-Gottwein et al., 2011; Null et al., 2014; Parra et al., 2016; Mayfield et al., 2021; González-Herrera et al., 2022). Since the coral core was retrieved near SGD sources, it likely records a minor trace of localized $\delta^{234}U$ variability. Since the groundwater has an almost identical U concentration as the seawater isotope mixing can be used to estimate the local groundwater contribution, which amounts to 0.7% on average and up to 2% for the lowest $\delta^{234}U$ values of 143‰. Hence, the selected coral sensitively depicts small but quantifiable groundwater fluxes.

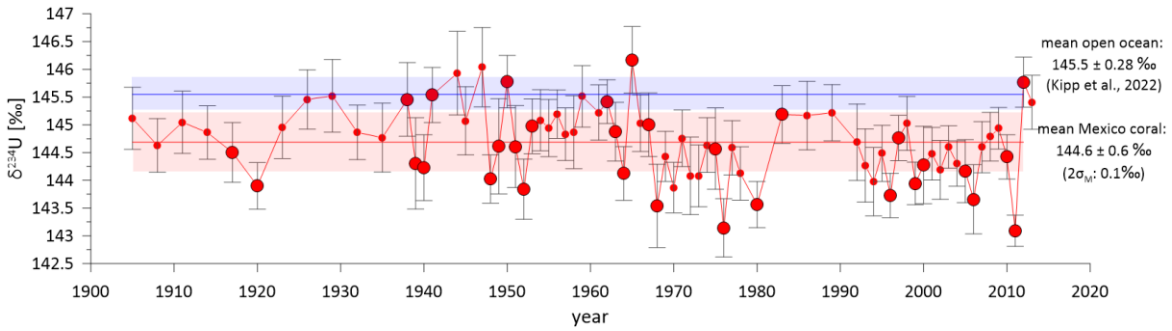

Figure 7.1 Time series of $\delta^{234}U$ measurements from the Mexican BOC-1 coral (red data points) spanning 1900–2020. Error bars represent measurement uncertainty, while the red shaded region indicates the mean $\delta^{234}U$ value for the coral (144.6 ± 0.6‰, $2\sigma_M$: 0.1‰). The mean open ocean $\delta^{234}U$ value (145.5 ± 0.28‰) from (Kipp et al., 2022) is shown as a blue line with a shaded uncertainty band. Large circled data points highlight large fluctuations in $\delta^{234}U$.

7.2 Multidecadal $\delta^{234}U$ Variability and Groundwater Discharge

Out of 71 observations, 22 (~31.4%) depleted values exceed the combined analytical error margin, making them statistically significant (Figure 7.1). The remaining variations mostly fall within the uncertainty range, indicating that the dataset primarily exhibits gradual trends rather than abrupt shifts. The coral $\delta^{234}U$ record shows decadal-scale fluctuations, with notable lower $\delta^{234}U$ excursions occurring around 1920, 1965–1980, and 1990–2010, while $\delta^{234}U$ trends close to open ocean seawater are observed during 1926–1929, 1950–1965, 1983–1989, a recent increase of $\delta^{234}U$ towards open ocean values is in 2012–2013. We here presume that such fluctuations in coral $\delta^{234}U$ values reflect changes in freshwater discharge from these SGD point sources. In Puerto Morelos, two primary sources of SGD have been identified, (1) the beach face, where recycled seawater mixed with shallow freshwater is discharged and (2) the Ojo (submarine spring), where freshwater from a deeper aquifer is released (Figure 3.5). Approximately 21% of SGD occurs at the beach face, while the remaining 79% originates from the Ojo (deep aquifer) (Null et al., 2014). Discharge rates are largely controlled by the pressure gradient between groundwater and the ocean, which is influenced by wind-driven sea-level changes, wave pressure, and the geostrophically balanced Yucatán Current (Coronado et al., 2007; Parra et al., 2016). Lower sea levels reduce oceanic pressure, allowing greater freshwater discharge into the ocean. Conversely, higher sea levels increase oceanic pressure, restricting freshwater flow and promoting seawater intrusion into the coastal aquifer (Beddows, 2004; Bauer-Gottwein et al., 2011; Parra et al., 2016; Canul-Macario et al., 2020). Figure 7.2 (Figure B.15) shows a comparison of short-term coral $\delta^{234}U$ variations with tide gauge data from Puerto Morelos (Caldwell et al., 2015) and Cabo de San Antonio, Cuba (Holgate et al., 2013). These limited in situ sea-level

observations are supplemented by satellite data from the GRACE-FO program, which measures global mass changes and infers groundwater storage and sea level (Landerer et al., 2020). An analysis of data from the grid encompassing Puerto Morelos is in good agreement with the variability of the coral $\delta^{234}U$ record. The large excursion in 2011 is absent in the satellite data, possibly due to the grid resolution (0.25°), as the dip is clearly observed in the local tide gauge data. Over longer timescales, coral $\delta^{234}U$ values exhibit a strong variability with a detrended sea-level reconstruction and thus Yucatán Current speed variations (Figure 7.2 and Figure B.15) (Ezer, 2022). Periods of higher $\delta^{234}U$ values, approaching open ocean values, correspond to positive sea-level anomalies in the Caribbean basin, whereas lower $\delta^{234}U$ values qualitatively coincide with SLP lows. A detrended sea-level reconstruction was used to account for the linear rise in sea level due to thermal expansion. However, this long-term increase also affects groundwater levels on the Yucatán Peninsula, ensuring that the hydrostatic gradient remains unchanged (Canul-Macario et al., 2020). This suggests that coral $\delta^{234}U$ is primarily sensitive to relative sea-level fluctuations rather than long-term, systematic ocean warming trends.

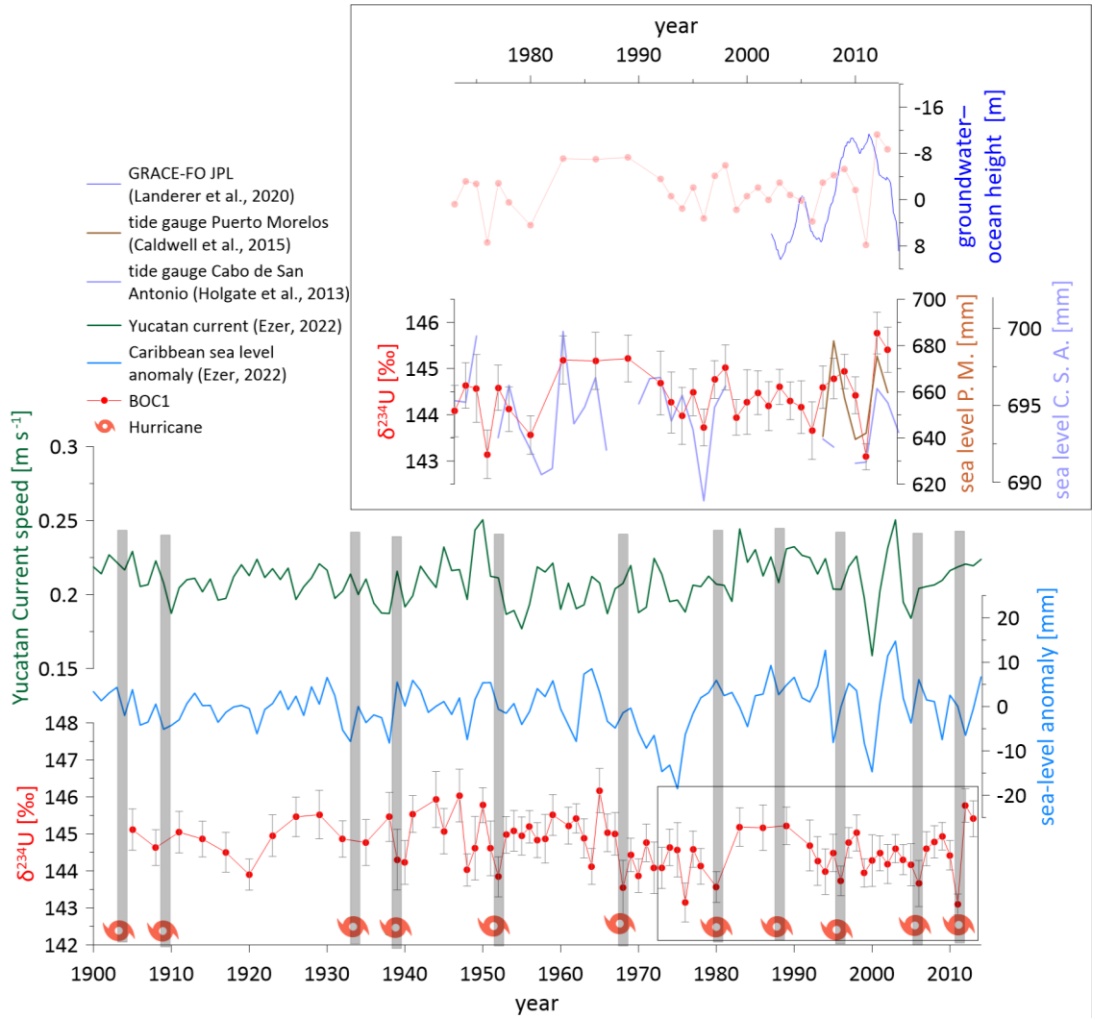

Figure 7.2 Time series comparing coral $\delta^{234}U$ (red data points) with regional oceanographic and hydrological variables from 1900 to 2020. Coral $\delta^{234}U$ values (bottom panel) are shown alongside severe hurricane occurrences (>Cat. 3; red hurricane symbols; (Landsea & Franklin, 2013)). The Caribbean sea-level anomaly (blue) illustrates ocean circulation patterns (Ezer, 2022). The inset (top right) highlights the recent $\delta^{234}U$ variability (red) from 1984–2013 in relation to sea level from tide gauges in Puerto Morelos (brown) (Caldwell et al., 2015) and Cabo de San Antonio (purple) (Holgate et al., 2013), as well as groundwater-ocean height differences from GRACE-FO (dark blue) (Landerer et al., 2020).

At certain intervals (e.g., 1968, 1976, 1980, 2006, and 2011), coral $\delta^{234}U$ values drop more pronounced, suggesting maximal local SGD discharge. Those years coincide with the known occurrence of heavy precipitation events. This pattern aligns with previous studies demonstrating storm-induced SGD intensification (Parra et al., 2016; Coutino et al., 2017). Coutino et al. (2017) documented a hurricane-induced breakdown of stratification in a cenote, where heavy rainfall pushed the freshwater lens downward, forcing greater mixing between fresh and saline groundwater. Reconstructed precipitation amounts during storm events (Lases-Hernández, 2013) often coincide

with periods of low coral $\delta^{234}U$ values, although the correlation is not consistent across all events (Figure 7.3).

In addition to rainfall, atmospheric pressure anomalies of these storm events (Landsea & Franklin, 2013) also offer an explanation: low-pressure systems elevate local sea level via the inverse barometer effect, approximately 1 cm per 1 mbar pressure drop (Pugh & Woodworth, 2014), reducing the hydraulic gradient from land to sea and thus tending to suppress fresh SGD. Consequently, $\delta^{234}U$ reductions during low-pressure events are more likely driven by rainfall-induced aquifer recharge and storm-driven mixing than by the pressure effect itself. Storm surges and wave action during cyclones may also mobilize older, U-depleted groundwater (Coutino et al., 2017), likely lowering lagoon water $\delta^{234}U$ values for a sufficient long time that the corals was able to pick up the post-storm signal. However, not all cyclones produce detectable $\delta^{234}U$ shifts (Figure 7.2 and Figure 7.3), indicating that storm intensity, track, rainfall distribution, and the degree of groundwater-reef connectivity modulate the SGD response.

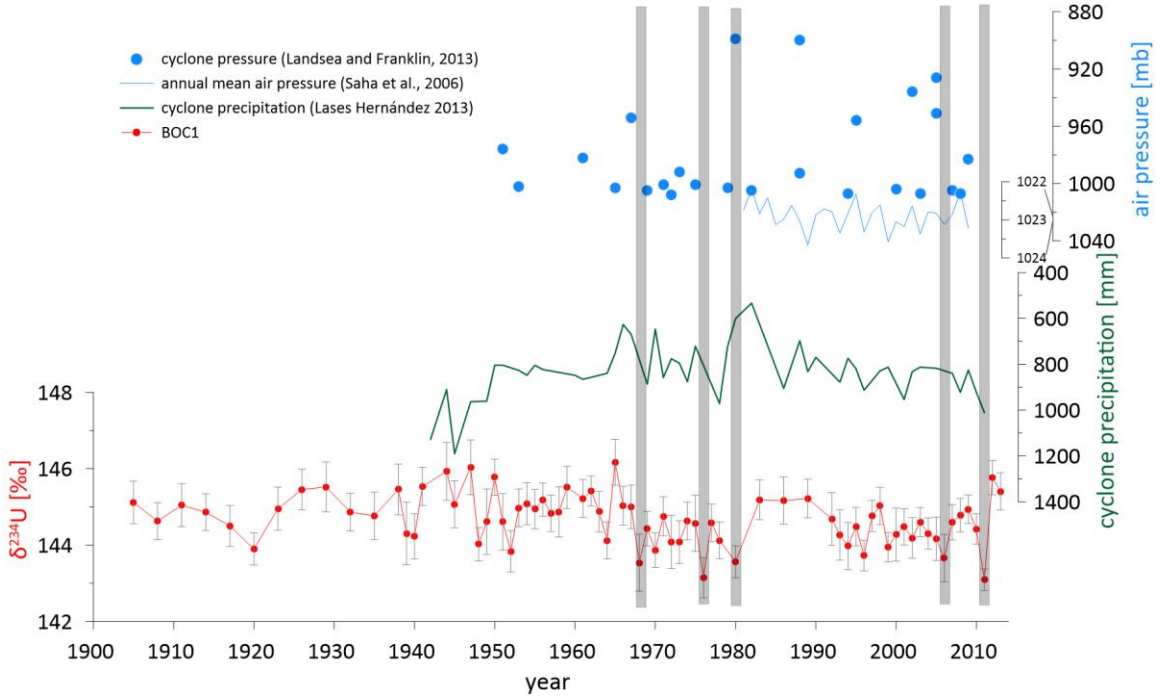

Figure 7.3 Time series of coral $\delta^{234}U$ from BOC1 (red circles) and annual mean air pressure (blue line; inverted axis; (Saha et al., 2006)), air pressure during cyclone events (blue dots; (Landsea & Franklin, 2013); inverted axis), and reconstructed precipitation during cyclone events (green line; (Lases-Hernández, 2013); inverted axis). Several intervals (e.g., 1968, 1976, 1980, 2006, 2011) show notable $\delta^{234}U$ reductions, consistent with storm-induced submarine groundwater discharge (SGD) intensification.

7.3 Periodicities and Climate Modes

Analysis of coral $\delta^{234}U$ values over the past 100 years now provides for the first time a possibility to study changes in the frequency domain to resolve periodicities (Figure 7.4). Two frequencies stand out, most pronounced is the periodicity of 3-years, which is significant above the noise (95%). The second most relevant periodicity is a ~28-year cycle, given that only 71 samples were analysed, the 28-year periodicity must be interpreted cautiously and requires further independent confirmation using other corals ideally spanning longer time windows. These patterns suggest potential links between $\delta^{234}U$ variability and tropical climate modes influencing Caribbean sea level, such as the El Niño-Southern Oscillation (ENSO) (Enfield & Mayer, 1997; Alexander et al., 2002; Álvera-Azcárate et al., 2009; Yu & Kim, 2011; Torres & Tsimplis, 2013).

During El Niño events, regional sea level drops, reducing oceanic pressure and enhancing SGD discharge, which introduces $\delta^{234}U$ depleted groundwater into the lagoon system. Conversely, during La Niña phases, sea level rises, suppressing SGD (Álvera-Azcárate et al., 2009; Yu & Kim, 2011; Torres & Tsimplis, 2013) and therefore increasing the coral $\delta^{234}U$ signature towards the maximum of open ocean isotopy. This correlation may result from reduced trade wind speeds and weakened surface wind pressure (Enfield & Mayer, 1997) or wind curl variations over the Caribbean during El-Niño (Álvera-Azcárate et al., 2009; Torres & Tsimplis, 2013).

The longer period may reflect Atlantic multidecadal variability associated to the Atlantic meridional overturning circulation (AMOC) (Kwon & Frankignoul, 2014; Liu et al., 2022). This large scale ocean transport mechanism is related to regional surface ocean variability such as changes in the strength of the Florida Current transport and the Yucatán Current (Gu et al., 2020; Ezer, 2022). At decadal to multi-decadal scales, AMOC variations correlate with changes in sea level and current strength in the Caribbean. During stronger AMOC phases, Florida and Yucatán Current speeds increase, leading to sea-level suppression (Coronado et al., 2007; Ezer, 2022) and therefore possibly enhanced SGD discharge. Conversely, AMOC weakening has been linked to a decrease in Florida Current strength and accelerated sea-level pressure (Park & Sweet, 2015). The possible 28-year cycle is consistent with AMOC's ~20-year periodicity, driven by interactions between deep equatorward flow and upper ocean gyre circulation (Kwon & Frankignoul, 2014). Variability in surface freshwater fluxes can further enhance density anomalies in the Labrador Sea, lengthening the AMOC oscillation period to 28-years (Liu et al., 2022).

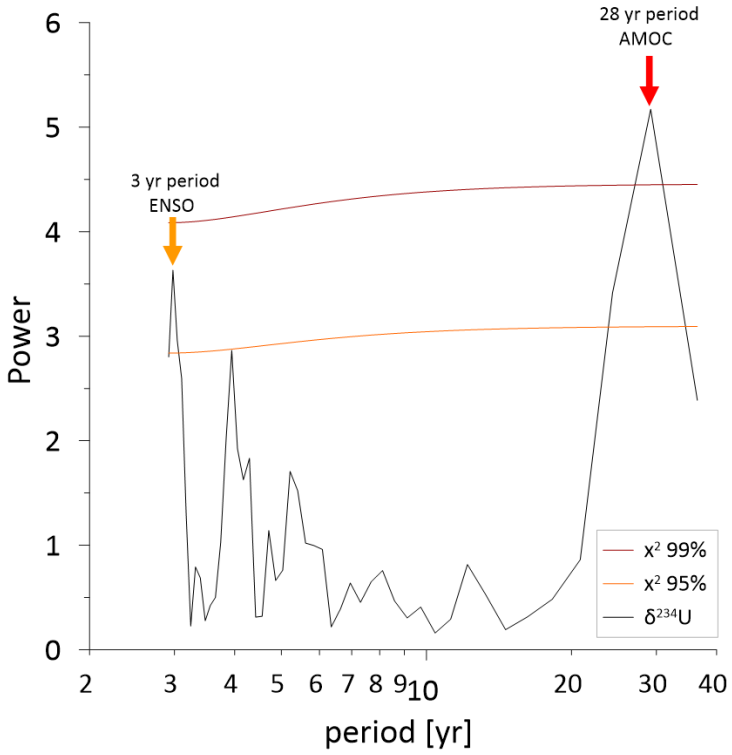

Figure 7.4 Power spectral analysis of coral $\delta^{234}U$ record from BOC_1.

7.4 Other Influences on $\delta^{234}U$

Previous studies suggest that $\delta^{234}U$ values in corals may be influenced by coastal precipitation patterns (Greve et al., 2025). In the Yucatán Peninsula, where the karstic substrate allows rapid infiltration, rainfall directly recharges the extensive aquifer system (Bauer-Gottwein et al., 2011). Here, approximately 14–17% of annual precipitation contributes to groundwater recharge (Lesser, 1976; Back, 1985; Gondwe et al., 2010). However, due to the large size of the groundwater reservoir, seasonal precipitation variations have minimal impact on overall aquifer levels (Gondwe et al., 2010). Beddows (2004) reported only a 5% reduction in SGD between the wet and dry seasons, indicating that seasonal rainfall does not significantly alter the SGD pressure gradient. Furthermore, the absence of major riverine inputs in the region rules out external fluvial influences on coral $\delta^{234}U$ variability. While SGD volume fluctuations seem to primarily drive coral $\delta^{234}U$ variability, temporal changes in groundwater uranium composition are unlikely to contribute. The $\delta^{234}U$ values in groundwater are influenced on longer time scales of centuries to millennia by factors such as surrounding rock uranium content and erosion rates (Schorndorf et al., 2023). Moreover, water residence time within the aquifer plays a role (Li et al., 2018). In coastal lagoons, flow velocities increase and residence times lengthen during the rainy season, nevertheless, on the Yucatán Peninsula, residence times remain short,

typically only a few days (Romero-Sierra et al., 2018). Such a short residence time is insufficient to induce significant changes in weathering and erosion-driven changes in groundwater $\delta^{234}U$ values.

Another potential influence on $\delta^{234}U$ values in the lagoon could be the removal of uranium from infiltrating groundwater and in the sediments under anoxic conditions. Dunk et al. (2002) reported that uranium removal occurs when oxygen penetrates <1 cm into sediments, facilitating U(IV) precipitation. Such processes could alter the concentration of uranium in seawater and groundwater and could thus modulate the relative sensitivity of the isotope mixing.

On the Yucatán Peninsula, lagoon oxygen levels remain above hypoxic thresholds year-round, despite seasonal variations (Romero-Sierra et al., 2018). While short-term seawater intrusion into SGD springs during high sea levels can temporarily lower dissolved oxygen levels, current evidence suggests that it does not reach anoxic conditions sufficient to alter uranium removal rates (Young et al., 2018).

Interestingly, the seawater underlying the groundwater in the Karst system is oxygen and uranium depleted to very low concentration levels, due to the strong density stratification and lack of ventilation of the seawater layer (Perry et al., 2002). Consequently, mixing of ground- and seawater within the aquifer prior to discharge could possibly modulate the mixing balance and thus sensitivity. Nevertheless, so far, we have no evidence of such a modulated uranium concentration, which would be needed to study in the SGD water.

Lastly, early diagenesis of the coral skeletons could alter coral $\delta^{234}U$ values, through removal or uptake of secondary aragonite and thus uranium, which is well attested for fossil tropical corals older than thousands of years. Such a diagenetic overprint does typically result in unusually high $\delta^{234}U$ values and excess ^{230}Th from coincident uptake of α-recoil derived ^{234}U and ^{230}Th (Delanghe et al., 2002; Robinson et al., 2004b; Frank et al., 2006; Wang et al., 2017). In our study, no visible diagenetic features were observed in the analysed coral samples, and the very young age does not provide a strong $\delta^{234}U$ gradient with the environment nor sufficient time needed to promote isotope exchange processes.

7.5 Conclusion

The $\delta^{234}U$ values from BOC_1 coral of the Puerto Morelos reef $\delta^{234}U$ values averaging 144.6‰, which are slightly below the open ocean mean (145.5‰ ± 0.3‰). The small and punctuated up to 3 permille deviation from open ocean $\delta^{234}U$ most likely reflect a persistent influence of $\delta^{234}U$ depleted groundwater source influencing the lagoon water at the coral site.

These $\delta^{234}U$ decreases are interpreted as SGD contribution of uranium to the lagoon water of some less than 2%. The variability of $\delta^{234}U$ and thus the flow of SGD correlates with the local sea-level pressure over the past century.

The periodicity of $\delta^{234}U$ values and thus likely sea-level pressure influences on the SDG reveal a 3- and 28-year duration, which coincides with periods of known tropical climate variability such as ENSO and AMO.

These results indicate that changes in SGD can be detected via the $\delta^{234}U$ ratio of annual growth bands of long-lived coral species. The flux of SGD during the last century seems modulated by local groundwater-seawater interactions modulated by external oceanographic processes that modulate sea-level pressure gradients. Periods of higher sea levels coincide with reduced SGD influence, while lower sea levels enhance the transport of terrestrially derived low- $\delta^{234}U$ groundwater into the reef system.

The coral record also suggests that hurricanes may temporarily intensify SGD, contributing to short-term decreases in $\delta^{234}U$ due to enhanced groundwater mixing.

These findings demonstrate that along the coast of Yucatán, a region with a high uranium concentration in groundwater and a depleted $\delta^{234}U$ of groundwater, coral $\delta^{234}U$ values can potentially serve as quantitative long-term proxy for past groundwater discharge dynamics. Understanding these variations is particularly relevant as climate-driven sea-level changes, shifts in regional water mass transport, and increasing coastal development continue to affect groundwater availability and thus reef ecosystems.

8 From Aquifer to Reef: Uranium Isotopes as Tracers of Submarine Groundwater Discharge in Tahiti

Submarine groundwater discharge (SGD) is increasingly recognized as a vital component of coastal hydrology, with important implications for elemental fluxes, biogeochemical cycling, and marine ecosystem dynamics. While rivers contribute the majority (90–99%) of freshwater entering the coastal ocean, SGD, comprising both fresh and saline groundwater, accounts for an estimated 1–10% of this input (Burnett et al., 2003; Zhou et al., 2019). Despite its relatively small volumetric contribution, SGD can exert a disproportionate influence by transporting nutrients, trace metals, and radionuclides such as uranium (U), radium (Ra), and radon (Rn), and by modulating pCO_2 levels in nearshore waters (Ma & Zhang, 2020; Böttcher et al., 2024; Tomer et al., 2025).

In tropical and tectonically active settings, SGD tends to be especially dynamic due to the combined effects of high rainfall, steep hydraulic gradients, and the permeable nature of volcanic aquifers (Zhou et al., 2019). Volcanic island margins, in particular, are characterized by episodic recharge, complex lithological structures, and significant spatial and temporal variability in SGD (Dişa et al., 2022). Tahiti, a high-relief volcanic island in the South Pacific (Figure 8.1), exemplifies such a setting. Characterized by steep topography, high precipitation rates, and permeable basalt flows (Hildenbrand et al., 2005; Hildenbrand et al., 2008), Tahiti provides an ideal natural laboratory for investigating the hydrogeochemical dynamics of SGD.

Uranium isotopes, in particular $\delta^{234}U$ values, offer a powerful tool for tracing groundwater-seawater interactions (Border, 2020). Due to uranium's conservative behaviour in seawater and sensitivity to water-rock interaction processes within aquifers, this isotope ratio serves as a valuable geochemical tracer (Osmond & Cowart, 2000; Dunk et al., 2002; Henderson, 2002). Recent studies have applied coral $\delta^{234}U$ measurements to a range of settings, including tracing a meltwater plume in the Southern Ocean (Li et al., 2023) and investigating riverine systems to explore the effects of weathering on $\delta^{234}U$ signatures (Li et al., 2018). However, to date, only study by Border (2020) has systematically examined the spatial variability of $\delta^{234}U$ in a SGD setting. Further no study has yet systematically explored its potential as a tracer for SGD. Understanding such variability is crucial as $\delta^{234}U$ values are influenced by

multiple factors, such as flow path length, lithology, residence time, redox conditions, and seawater mixing (Osmond & Cowart, 2000; Dunk et al., 2002; Chabaux et al., 2008), all of which can vary considerably, even over short stretches of coastline and short time periods.

This chapter addresses that knowledge gap presenting a spatially resolved $\delta^{234}U$ dataset from SGD sites around Tahiti, in combination with seawater and coral core analyses (Figure 8.1). It explores how local hydrological, geological, and tidal conditions shape uranium isotope composition of SGD and how these spatial patterns compare to the temporal variability recorded in a coral $\delta^{234}U$ time series from 2000–2008. Additionally, this study attempts to explore the role of regional climate variability as traced by indices such as the Southern Oscillation Index (SOI) and Niño 3.4 on SGD. Assuming a correlation of such indices with SDG, this would infer that large-scale ocean-atmosphere variability, modulates SGD and their geochemical signals.

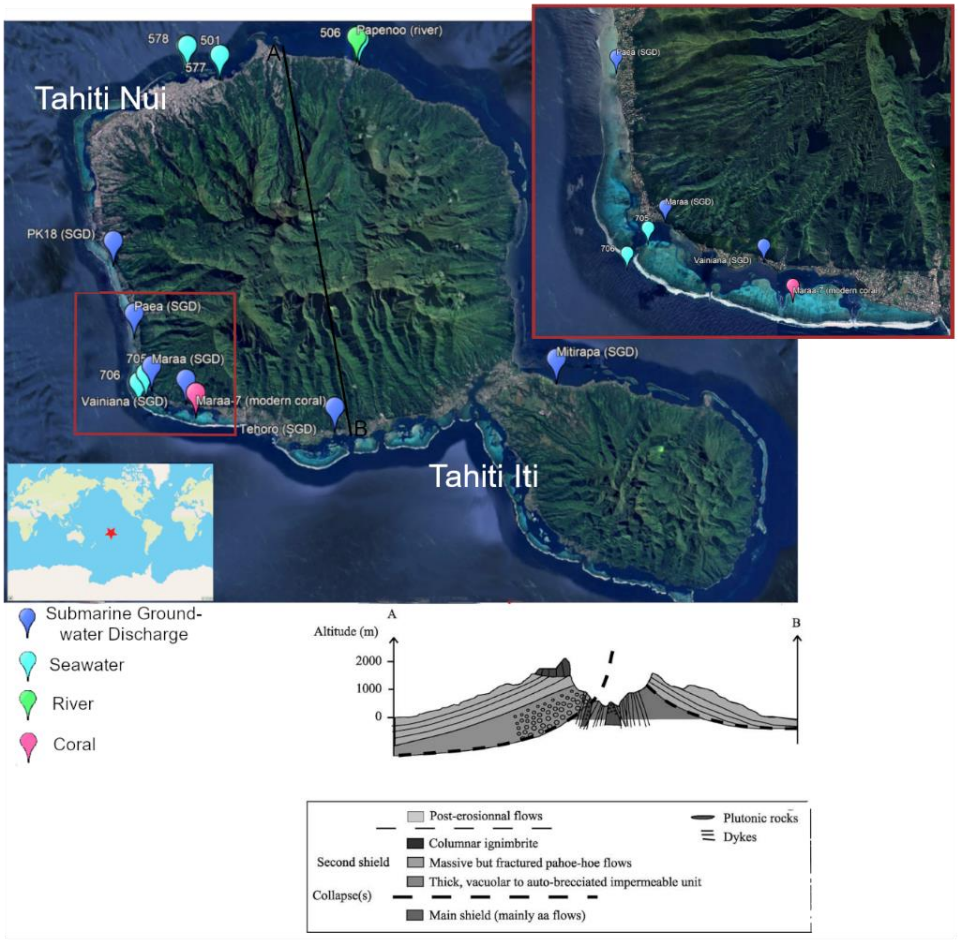

Figure 8.1 Satellite imagery of Tahiti Nui and Tahiti Iti showing sample locations for submarine groundwater discharge (SGD), seawater, river water, and coral. The inset provides a zoomed view of the southwestern coast, highlighting dense SGD sampling around Maraa. The north-south A–B transect corresponds to the geological cross-section below, illustrating the island's volcanic structure with main shield and post-erosional units, collapses, and dykes (Hildenbrand et al., 2004). Groundwater flow paths are inferred along structural discontinuities associated with past collapse events.

8.1 Seawater $\delta^{234}U$: A Homogeneous Baseline

To evaluate the impact of SGD on the uranium isotopic composition ($\delta^{234}U$) of the waters around Tahiti, seawater samples were first collected from multiple coastal locations (N = 7), both within and outside the barrier reef Figure 8.1. All seawater samples, marked by a salinity >34 PSU, exhibited remarkably consistent $\delta^{234}U$ values, with a mean of 145.6‰ ±0.5‰ (Figure 8.2), closely aligning with the global open-ocean average of 145.5‰ ±0.3‰ (Kipp et al., 2022). This isotopic uniformity underscores the conservative behaviour of uranium in well-mixed seawater and supports its use as a stable reference endmember in this system.

Notably, sample 705, obtained from within the back reef, displayed slightly elevated $\delta^{234}U$ values of 146.7‰ ±0.4‰ compared to sample 706, which was collected just beyond the reef crest (145.2‰ ±0.4‰). According to the analytical precision and reproducibility (Greve et al., 2025) this difference of 1.5‰ is, however, statistically relevant.

The absence of substantial local deviations (>1.5‰), and only slightly elevated values within the reef, suggests that, at the spatial scale of this study, coastal mixing processes exert minimal influence on the uranium isotopic composition. Thus, once terrestrially sourced waters cross the reef crest, they equilibrate rapidly with the surrounding open-ocean water, adopting $\delta^{234}U$ values that are indistinguishable from the open-ocean baseline. In contrast, the sample from Paea exhibits salinity levels (34.1 PSU) close to seawater, indicating minimal groundwater input. This interpretation is supported by field observations at Paea, where visible discharge was limited and sampling proved challenging.

These rapid mixing observations are consistent with regional circulation dynamics in the central South Pacific. In reef systems such as those on nearby Moorea, water exchange is primarily driven not by tidal forcing, but by episodic wave-driven and wind-driven circulation (Hench et al., 2008). Leichter et al. (2013) further documented rapid nutrient and dissolved organic matter (DOC) fluxes in Moorea's back reef, associated with a thin boundary layer. Offshore swell and local wind forcing thus promote efficient flushing of reef waters, resulting in rapid dilution of any terrestrial inputs and homogenization of isotopic signatures with open-ocean values. Hence, for the subsequent results and discussion of SGD and coral samples, we consider the seawater observations as open ocean reference.

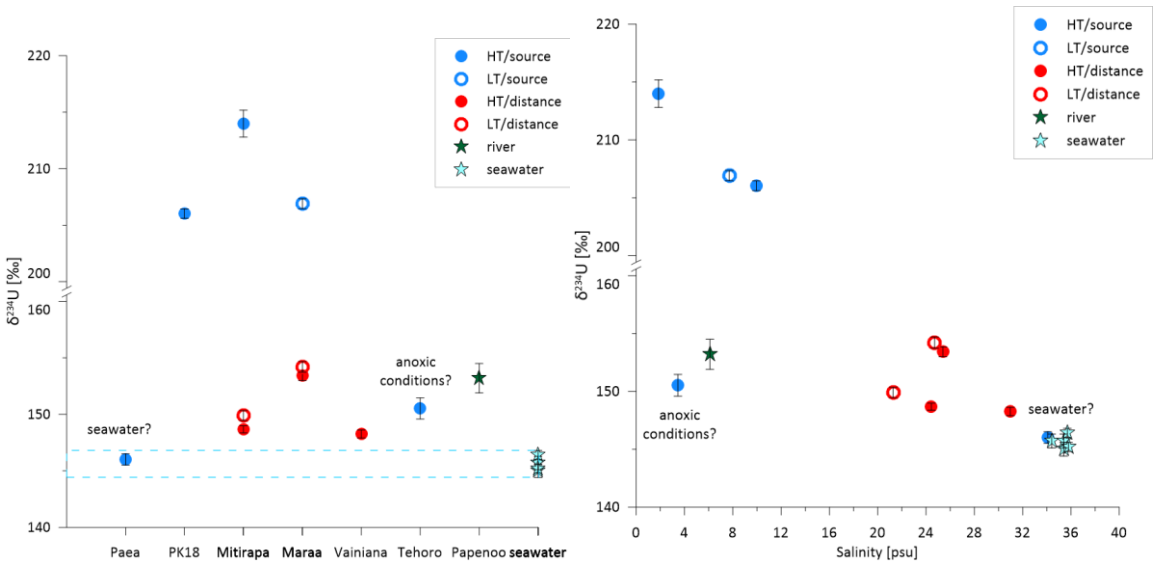

Figure 8.2 Left panel: $\delta^{234}U$ values across different sampling locations on Tahiti, distinguishing between high tide (HT) (full cycles) and low tide (LT) (open cycles) measurements at the source (blue) and approximately 1 m from the discharge point (red). Right panel: $\delta^{234}U$ values plotted against salinity, highlighting mixing trends between freshwater (river and SGD) and seawater endmembers. Elevated $\delta^{234}U$ values occur at low salinity and decrease toward marine values, with distinct clustering based on sampling position and tidal stage.

8.2 Spatial Variability in SGD $\delta^{234}U$: Endmembers and Mixing

Samples collected directly from SGD sites around Tahiti reveal clear spatial heterogeneity in both uranium concentrations and $\delta^{234}U$ values, reflecting variable hydrological and geochemical conditions across the island's coastal aquifers. When site-specific patterns are examined (Figure 8.2), significant spatial variability becomes evident. Figure 8.2 also presents $\delta^{234}U$ values from various SGD sites, differentiating high-tide (HT) and low-tide (LT) conditions, as well as sample position, directly at the discharge point or 1 meter downstream. Notably, the sites PK18, Mitirapa, and Maraa show elevated $\delta^{234}U$ values (>200‰) compared to locations such as Vainiana, where values cluster more closely to the open-ocean baseline of 148–160‰.

A complementary panel in Figure 8.2 plots $\delta^{234}U$ against salinity. At Mitirapa and Maraa, higher $\delta^{234}U$ values correspond to low-salinity waters, consistent with a terrestrial freshwaters source. A single sample collected from the Tehoro site exhibited a $\delta^{234}U$ value of approximately 151‰ and a salinity of ~4 PSU, indicative of a predominantly freshwater source (Figure 8.2). This value is notably lower than the high-$\delta^{234}U$ endmembers observed at Mitirapa and Maraa, despite the similarly low salinity and sampling directly at the source. Field observations at Tehoro revealed the presence of fine, dark sediments with a strong sulphuric odour, suggestive of reducing conditions in the discharge environment (Böttcher et al., 2024). Under anoxic conditions, uranium can be removed from solution via reduction and precipitation,

leading to lower $\delta^{234}U$ values and overall uranium depletion in the groundwater (Osmond & Cowart, 2000). This is consistent with the relatively low uranium concentration measured at Tehoro (~0.4 ppb), which supports the interpretation of U removal under reducing conditions. This may explain the muted isotopic signal observed at Tehoro, which contrasts with the more oxidizing and reactive flow paths inferred at other sites. These findings highlight the importance of local redox conditions in shaping the geochemical character of SGD, even within similarly low-salinity discharge zones.

Tahiti's complex geology contributes to this spatially variability. The island formed over four volcanic phases between 1.5 and 0.45 million years ago, resulting in diverse basaltic units (Hildenbrand et al., 2004). Carbonate platforms also underlie parts of the barrier reef (Figure 8.1) (Rougerie et al., 2004). The island's high relief topography, combined with high annual rainfall (2000 mm yr^{-1} at the sea level; 11000 mm yr^{-1} at high altitudes), drives rapid, structurally controlled erosion and efficient groundwater recharge (Ferry, 1988; Hildenbrand et al., 2008). These processes enhance uranium isotope signatures, as demonstrated in this study, despite relatively short groundwater residence times (Hildenbrand et al., 2005). While the carbonate units are characterized by reducing conditions below 30 m depth (Rougerie et al., 2004), which promote uranium precipitation and limit its mobility through the carbonate (Osmond & Cowart, 2000), the uranium isotope signal measured in coastal waters thus likely originates from interactions with the basaltic aquifer. Previous studies have shown that groundwater flowing through Tahiti's basaltic basement exhibits prolonged water-rock interaction, leading to elevated phosphate concentrations in the groundwater (Haßler et al., 2019), a finding consistent with the elevated $\delta^{234}U$ values observed in the present study. Such high $\delta^{234}U$ signals are typical of volcanic settings (Vigier et al., 2006), where uranium concentrations in the bedrock are low (~0.01ppm in Tahitian basalts (Gayer et al., 2014)), but isotopic fractionation is enhanced by the recoil effects and high erosion rates (Osmond & Cowart, 2000; Li et al., 2018).

Particularly striking is the comparison between samples taken directly at the source (blue points) and those collected approximately 1 meter downstream (red points), which show a substantial decrease in $\delta^{234}U$ values, up to -65‰, alongside a significant increase in salinity (Figure 8.2). Similar patterns have been documented on nearby Moorea, where water exchange is not driven by tidal processes but primarily by episodic offshore swell and local wind forcing (Hench et al., 2008). These wave-driven processes promote rapid circulation and short residence times of discharged groundwater. Leichter et al. (2013) further documented thin boundary layers and fast fluxes of nutrient and DOC in Moorea's back reef, supporting the potential for efficient

nearshore mixing in similar settings. This dynamic exchange likely explains the sharp decrease in $\delta^{234}U$ values observed within just 1 meter of the SGD source, as terrestrial inputs are quickly diluted and mixed with ambient seawater.

The spatial variability is best illustrated at two key locations, Maraa and Mitirapa, where coherent $\delta^{234}U$-[U] mixing trends allow for the identification of isotopically distinct terrestrial endmembers (Figure 8.3).

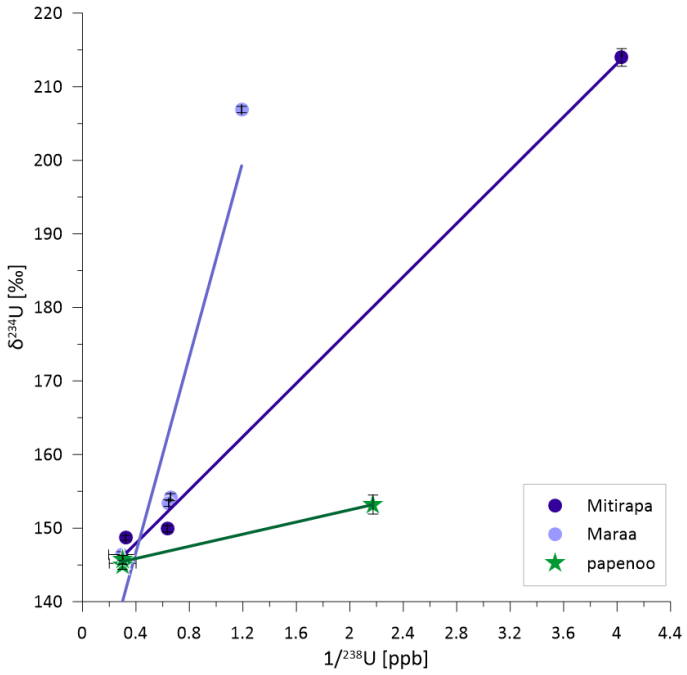

Figure 8.3 Inverse uranium concentration ($1/^{238}U$) plotted against $\delta^{234}U$ values for samples from Mitirapa (Tahiti Iti), Maraa (Tahiti Nui), and Papenoo River. Linear regressions reveal distinct mixing trends, supporting conservative mixing and the identification of isotopic endmembers for submarine groundwater discharge and freshwater inputs.

At Mitirapa, a linear relationship between $\delta^{234}U$ and 1/[U] suggests conservative mixing between a high-$\delta^{234}U$ freshwater endmember and seawater (Figure 8.3). The inferred terrestrial component from the SGD sample is characterised by a $\delta^{234}U$ value of approximately 215‰ and uranium concentrations around 0.25 ppb. This elevated $\delta^{234}U$ signature is consistent with extensive water-rock interaction, likely driven by ^{234}U recoil enrichment from basaltic aquifer minerals. Such signatures are commonly associated with long groundwater residence times, low water/rock ratios, and oxidizing conditions that promote preferential ^{234}U mobilization (Osmond & Cowart, 2000; Li et al., 2018). In contrast, the Maraa site displays a distinct mixing trend, characterized by a terrestrial endmember (SGD sample) with a lower $\delta^{234}U$ (~205‰) and higher uranium concentrations (~1 ppb). This suggests a more dynamic groundwater system, likely younger recharge with shorter residence times and reduced isotopic fractionation, consistent with shallower flow paths and less evolved hydrogeochemical conditions (Osmond & Cowart, 2000; Li et al., 2018).

The contrasting mixing slopes at Maraa and Mitirapa indicate fundamentally distinct hydrologic regimes, despite both sites being underlain by broadly similar volcanic lithologies. This may reflect spatial differences in aquifer structures on Tahiti Nui and Tahiti Iti. Surface and soil erosion rates are not significantly different between the two sites (Ye et al., 2009), and therefore cannot explain the divergent uranium isotope signatures. However, weathering and erosion intensity on Tahiti Nui is highly variable and depends on the catchment characteristic (Hildenbrand et al., 2008). For example, enhanced weathering has been linked to catchment with greater surface area and higher elevations, rather than precipitation amount alone (Hildenbrand et al., 2008; Godard & Barriot, 2022). If these relationships also apply for Tahiti Iti, a smaller and less elevated island, then one would expect lower erosion rates at Mitirapa compared to Maraa. Nevertheless, the enhanced $\delta^{234}U$ endmember at Mitirapa suggest that groundwater there undergoes longer residence times, which may enhance ^{234}U enrichment through sustained interaction with basaltic aquifers. This interpretation is consistent with geomorphological contrasts: Tahiti Nui exhibits steeper slopes and more rapid groundwater transport in areas where impermeable shield basalts contact overlying fractured flows (Hildenbrand et al., 2005; Aureau, 2014), whereas Tahiti Iti, with its lower elevation and gentler slopes likely promotes slower subsurface flow and longer residence times.

A third endmember is presented by brackish waters from the Papenoo River (Figure 8.3), which show considerably lower $\delta^{234}U$ values and uranium concentrations compared to SGD sources. As Tahiti's largest river, the Papenoo dominates surface runoff on the island. Due to the island's high rainfall, much of the river water is derived from rapid surface flow with limited bedrock interaction, resulting in a less radiogenic isotope signature and a flatter slope on the $\delta^{234}U$ vs. 1/[U] Keeling plot in Figure 8.3 relative to the SGD endmembers at Mitirapa and Maraa. This pattern is consistent with previous findings on the island, where river water exhibits lower nutrient concentrations and less isotopic enrichment than SGD-derived waters (Hildenbrand et al., 2005; Haßler et al., 2019).

Collectively, these results provide compelling evidence that multiple isotopically distinct groundwater and surface water sources contribute to the uranium isotope composition of coastal waters around Tahiti. The identification of site-specific $\delta^{234}U$ endmembers improves our ability to constrain terrestrial uranium input and underscores the complexity of uranium isotope transport in basalt-hosted aquifer systems. From a geochemical perspective, these findings highlight that the $\delta^{234}U$ variability in SGD is governed not solely by bedrock lithology, but also by hydrological parameters such as flow path length, aquifer geometry, and residence time.

8.3 Tidal Modulation of SGD $\delta^{234}U$: Short-Term Variability

Tidal fluctuations exert a strong influence on SGD in coastal systems, modulating both the volume and geochemical composition of discharging fluids (Moore, 1996; Moore, 2010; Hagedorn et al., 2020). Around Tahiti, $\delta^{234}U$ measurements collected at multiple SGD sites under both HT and LT conditions, and at varying distances from the discharge point (Figure 8.2), reveal short-term variability in isotopic signatures linked to the tidal cycle. These tidal effects are particularly evident at Mitirapa and Maraa, two sites with well-characterized endmembers. At both locations, $\delta^{234}U$ values are systematically higher during LT, by approximately 1.3‰ at Mitirapa and 6‰ at Maraa, relative to HT.

Because $\delta^{234}U$ variability is largely driven by SGD dynamics, understanding the controls of SGD magnitude is critical. Key drivers include the hydraulic gradient, which is influenced by recharge from precipitation, and tidal forcing, which modulates the pressure gradient at the land-sea interface. On short timescales, tidal cycles govern SGD flux through hydrostatic pressure changes. During low tide, reduced sea level lowers offshore pressure, enhancing groundwater outflow. In contrast, high tide increases hydrostatic pressure, suppressing SGD and potentially inducing seawater intrusion into the aquifer (Moore, 2010; Passeri et al., 2015; Hagedorn et al., 2020). This mechanism was also observed by Hagedorn et al. (2020) on the neighbouring island of Moorea, where radon concentrations in reef water fluctuated with the tidal cycle, confirming tidal forcing as the dominant control on SGD over daily timescales. In the present study, this pattern is reflected in the geochemical signatures of water samples: at HT, greater seawater intrusion leads to lower $\delta^{234}U$ values and elevated salinity, consistent with conservative mixing behaviour. Although enhanced discharge as a result of precipitation was not directly assessed in this study, it likely plays a role over longer, seasonal timescales. Given the short residence time of the groundwater inferred for Tahiti (Hildenbrand et al., 2005), a steep hydraulic gradient is likely, which would increase SGD rates during the rainy season compared to the dry season. This effect is expected to be particularly pronounced along the northern shore, where the geological profile (Figure 8.1) shows a significantly steeper slope in the impermeable basaltic basement compared to the southern part of the island. The greater hydraulic head in this region would enhance groundwater flow and discharge potential, especially following periods of intense precipitation.

In summary, the uranium isotopic composition ($\delta^{234}U$) in Tahiti's SGD is not a static signal but one that is dynamically modulated by tidal forcing and likely influenced by seasonal precipitation variability. These controls affect both the amount of freshwater reaching the coastal zone and the degree to which it mixes with ambient seawater,

ultimately shaping the uranium isotopic composition observed in nearshore environments.

8.4 Coral $\delta^{234}U$ Time Series: A Long-Term Record of SGD Influence

A coral core spanning the period from 2000 to 2008 was sampled annually for the analysis of $\delta^{234}U$ values. The core was retrieved from the barrier reef near Maraa, approximately 1.3 km from the nearest identified SGD point source (Figure 8.1). Although situated at some distance from direct terrestrial inputs, the $\delta^{234}U$ record preserved in the coral provides a unique long-term perspective on uranium isotope variability in response to regional hydroclimatic processes. As shown in Figure 8.4, $\delta^{234}U$ values in the coral increase slightly between 1999 and 2005, a period broadly associated with relatively dry conditions and negative Southern Oscillation Index (SOI) values. Around 2005, a more pronounced shift occurs: $\delta^{234}U$ values continue to rise, coinciding with a transition to wetter conditions, positive SOI values, and negative Niño 3.4 anomalies, characteristic of a transition toward La Niña-like states. As discussed earlier, uranium mixing in nearshore waters around Tahiti is rapid. Given the coral's offshore location relative to both surface runoff and SGD sources, substantial shifts in terrestrial inputs are required to measurably affect the $\delta^{234}U$ signal in coral aragonite. Supporting this, data from the Papenoo River, Tahiti's largest river system, show $\delta^{234}U$ values only slightly different from open-ocean baselines (Figure 8.2), indicating that surface runoff alone, particularly from smaller catchments, is unlikely to significantly alter the coral $\delta^{234}U$ record, even during intense rainfall events like those in 2007. Previous studies have shown that surface runoff interacts minimally with the bedrock in Tahiti (Hildenbrand et al., 2005; Haßler et al., 2019), and Godard and Barriot (2022) further demonstrated that weathering intensity is governed more by catchment size than by precipitation alone. Thus, changes in surface runoff are not the primary drivers of $\delta^{234}U$ variability in the coral. Rather, increased precipitation may enhance aquifer recharge and subsequently intensify SGD, delivering higher $\delta^{234}U$ values to the reef environment.

A comparison of tide gauge sea level data with ENSO indices reveals a strong correspondence between sea-level variability and large-scale climate oscillations (Figure 8.4). During El Niño phases, negative SOI values reflect low atmospheric pressure over Tahiti, leading to elevated sea level through oceanic response to atmospheric relaxation. Conversely, La Niña events are associated with positive SOI values and higher atmospheric pressure over Tahiti, resulting in lower local sea levels (Trenberth & Caron, 2000). This relationship is mirrored in the coral uranium isotope data. Notably, $\delta^{234}U$ values increase during the 2007/2008 La Niña event, in tandem with both the SOI and Niño 3.4 indices. This pattern is interpreted as reflecting

enhanced SGD under reduced sea-level conditions, as lower hydrostatic pressure facilitates increased groundwater discharge into the reef system. As discussed earlier, $\delta^{234}U$ values are also sensitive to short-term tidal fluctuations, which influence the hydraulic gradients and SGD intensity. The observed alignment between $\delta^{234}U$ values and ENSO-driven sea-level pressure variations suggests that both daily (tidal) and interannual (ENSO) forcings modulate SGD dynamics and, by extension, the geochemical signals preserved in coral archives.

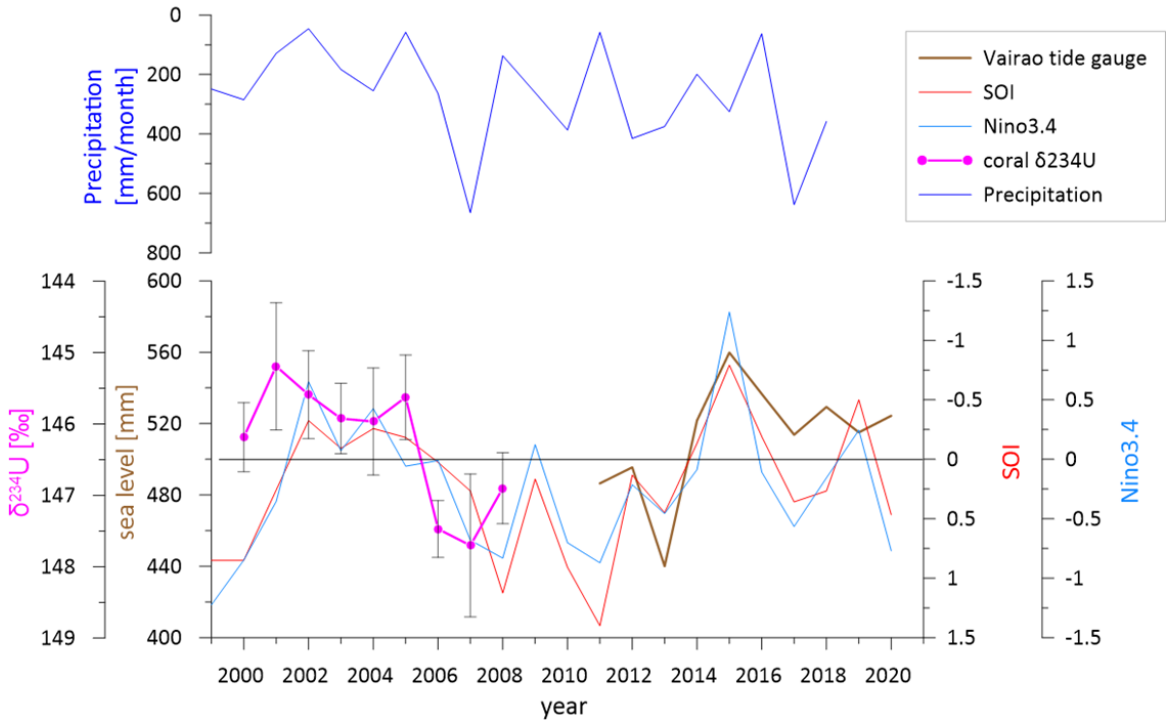

Figure 8.4 Coral $\delta^{234}U$ values (pink, inverted y-axis) compared with sea level data from the Vairao tide gauge (brown), Southern Oscillation Index (SOI, red), Niño 3.4 index (light blue), and monthly precipitation (top panel, blue, inverted y-axis) from 1999–2020. Sea level variations follow the SOI and Nino3.4 closely. Declining coral $\delta^{234}U$ values correspond to periods of reduced precipitation, with potential influence from ENSO-related variability indicated by SOI and Niño 3.4 indices.

These observations support the interpretation that coral $\delta^{234}U$ values can serve as a proxy for SGD intensity and source characteristics over interannual to decadal time scales. In the case of Tahiti, SGD appears to be modulated by both precipitation-driven aquifer recharge and sea-level-derived hydrostatic pressure gradients. As shown in this study, even relatively modest changes in sea level during ENSO cycles can leave a recognisable imprint on the uranium isotope system, which gets preserved in corals. Where SGD systems are closely coupled to climatic and oceanographic conditions, as in volcanic island settings like Tahiti, $\delta^{234}U$ values provide a valuable proxy for reconstructing groundwater-ocean interactions and associated hydroclimatic variability.

8.5 Conclusion

This study provides the first spatially resolved assessment of uranium isotopic variability in SGD within a volcanic island setting, highlighting the value of uranium isotopes for identifying local groundwater contributions. It demonstrates how $\delta^{234}U$ values can effectively trace SGD and its variability around Tahiti. Coastal seawater samples showed consistent $\delta^{234}U$ values near the open-ocean baseline, confirming rapid mixing and the conservative behaviour of uranium in reef environments.

In contrast, SGD samples revealed pronounced spatial variability in both $\delta^{234}U$ and uranium concentrations, shaped by differences in aquifer flow paths, residence times, and redox conditions. Tidal fluctuations further modulated $\delta^{234}U$ values on short timescales, with higher values at low tide reflecting enhanced groundwater discharge. The coral $\delta^{234}U$ record from Maraa adds a long-term perspective, capturing interannual changes linked to ENSO-driven sea-level variability. This supports the interpretation that $\delta^{234}U$ values reflect both hydrogeological and climatic controls on SGD.

9 Tracing Freshwater Influence in the Caribbean Basin: A Synthesis of Coral $\delta^{234}U$ Records and the Role of Basin Hydrodynamics

The Caribbean Sea plays a crucial role in global ocean circulation, acting as a major conduit for the westward transport of Atlantic surface waters into the Gulf of Mexico and ultimately toward the North Atlantic via the Gulf Stream (Centurioni & Niiler, 2003; Alexander et al., 2014). Its hydrographic characteristics are shaped not only by large-scale inflow from equatorial currents but also by evaporation and interactions with freshwater sources surrounding the basin, seasonal upwelling, and regional climate variability (Centurioni & Niiler, 2003). The water transiting the Caribbean gains salinity from evaporation and loses salinity through freshwater fluxes. Therefore, two processes compete in adjusting salinity, which is a precursor of the salinity export into the Nordic Seas. Understanding the complex nature of these processes and the influence of freshwater discharge on Caribbean surface waters is essential, particularly in light of inputs from major rivers such as the Amazon, Orinoco, Mississippi, Magdalena river, and many other, which have the potential to alter salinity, stratification, and biogeochemical cycles (Enfield et al., 2001; Chérubin & Richardson, 2007). The potential of tracing freshwater discharge by using the natural $\delta^{234}U$ ratio has been well demonstrated (Andersen et al., 2007; Wang et al., 2017; Shang et al., 2021; Li et al., 2023; Greve et al., 2025). It has also been stated that semi-closed oceanic basins are most sensitive to $\delta^{234}U$ variability (Wang et al., 2017; Border, 2020; Shang et al., 2021). Thus, the question arises to which degree the freshwater added to the Caribbean Sea alters the $\delta^{234}U$ ratio overall. This is of particular importance when using corals as archive of past sea level or as climate archive. The quality of U/Th dating is often adjusted by using criteria on the $\delta^{234}U$, which is generally presumed to be equal to sea water and within narrow isotopic ranges (Chutcharavan et al., 2018). Consequently, the degree to which these freshwater sources imprint the basin's uranium isotope composition and variability will be investigated based on the compilation of all available coral records. Moreover, it will be explored, whether the isotope signals can be traced through the Caribbean's dynamic flow path, i.e. whether a transport signal can be extracted from multiple records.

These questions are approached by evaluating the spatial and temporal variance of all coral $\delta^{234}U$ records presented in the preceding sections across the Caribbean and the past roughly hundred years. These include coral cores from Venezuela, Puerto Rico, the Yucatán Channel, and the Florida Straits, representing key points along the Caribbean Current and its outflow. A coral from Martinique, situated near the eastern boundary of the basin, completes this north-south transect and provides a crucial perspective on the region's inflow zone. Together, these records enable a basin-wide synthesis that tests whether freshwater $\delta^{234}U$ signals are preserved and advected across multiple sites, or whether isotopic variability is instead governed by localized hydrological and geomorphological conditions.

In addition to evaluating internal Caribbean dynamics, this chapter also places the findings in a broader oceanographic context through comparison with other semi-enclosed or restricted systems, including the Mediterranean and East China Seas (ECS). These settings offer contrasting examples of how basin geometry, freshwater flux, and circulation strength influence the retention and propagation of isotopically distinct freshwater inputs. By examining both the spatial coherence and the magnitude of $\delta^{234}U$ anomalies across systems, this synthesis highlights the processes that determine the relationship of uranium isotopes and freshwater transport and/or local hydroclimate variability.

9.1 Methods

Here published and new measurements of $\delta^{234}U$ from the Caribbean Sea and other semi-enclosed ocean basins covering the past ~200 to 31,000 years are compiled. For the Caribbean, 248 individual $\delta^{234}U$ measurements were obtained from long-lived corals collected at multiple sites (N = 5) in this study (see chapters above).

Data from other ocean basins were compiled from Border (2020), Wang et al. (2017) and Shang et al. (2021), while the open ocean values are taken from Kipp et al. (2022) and the $\delta^{234}U$ values for French Polynesia are described in chapter 9.

Additional coral $\delta^{234}U$ data from the Caribbean and adjacent Atlantic Ocean were taken from the global compilation of Chutcharavan et al. (2018). Data selection from that dataset followed a preliminary screening to ensure isotope precision better than 2‰ and acceptable Th/U age uncertainties. The resulting dataset includes 17 post-modern coral measurements from Bonaire, the Bahamas, Bermuda, and Tortuga (North Florida), as well as 59 Holocene coral values (11,000–1,000 years BP) from the same locations and Grand Cayman. From the work of Chutcharavan et al. (2018) a further 243 coral $\delta^{234}U$ values (11,000–31,000 years BP) were incorporated, all recalculated on the CRM 112A scale. This subset includes 56 corals from the Last

Glacial Maximum (LGM) (19,000–25,000 years BP), predominantly from Barbados, with one additional sample from Grand Cayman (Bard et al., 1990; Chen et al., 1991; Gallup et al., 1994; Ludwig et al., 1996; Toscano & Lundberg, 1998; Blanchon et al., 2002; Delanghe et al., 2002; Multer et al., 2002; Fairbanks et al., 2005; Coyne et al., 2007; Muhs et al., 2011; Giry et al., 2012; DeLong et al., 2014; Abdul et al., 2016). These values represent water masses entering the Caribbean.

The $\delta^{234}U$ and Th/U ages were originally determined using thermal ionization mass spectrometry (TIMS) or multi-collector ICP-MS (MC-ICPMS). Although different laboratories used different standards, Chutcharavan et al. (2018) recalculated all published values to the CRM-112A reference scale. In total, more than 500 $\delta^{234}U$ measurements are now available for the Caribbean and western Atlantic inflows, spanning from modern to 31,000 years BP.

9.2 Last Centuries Caribbean U-isotope and Local Influences

Comparing all new records from the Caribbean presented in this thesis, it is evident that the average $\delta^{234}U$ values remained relatively constant over the past ~200 years, consistently aligning with open ocean signatures (Figure 9.1). The only exception was observed in the Mexican coral (red in Figure 9.1), which exhibited a notable offset towards lower values (Chapter 7). This anomaly was attributed to the proximity of the sampling site to submarine groundwater discharge (SGD). However, even this signal was rapidly diluted, as an adjacent coral did not exhibit the same offset, underscoring the very local nature of such observations and efficiency of local mixing with ambient seawater.

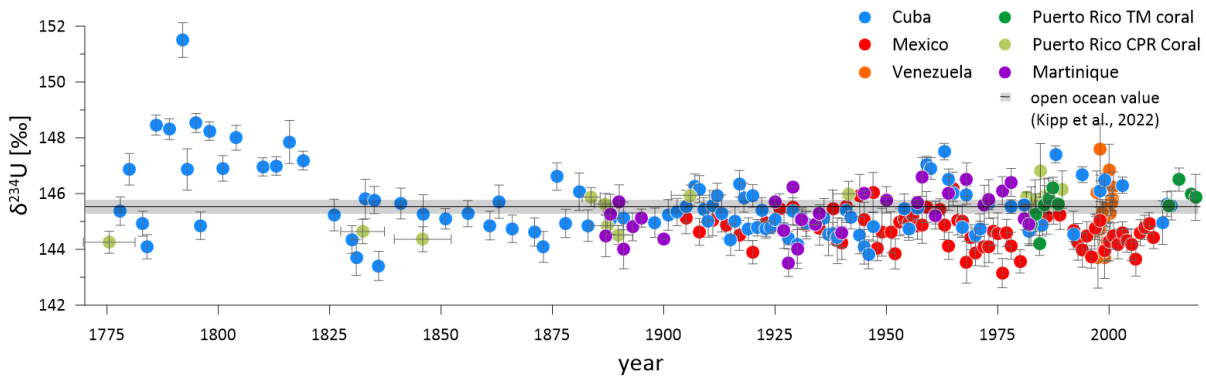

Figure 9.1 Temporal evolution of coral $\delta^{234}U$ values from multiple sites across the Caribbean. Coloured symbols represent individual coral records from Cuba (blue), Mexico (red), Venezuela (orange), Puerto Rico TM coral (green), Puerto Rico CPR coral (olive), and Martinique (purple). The grey horizontal line and shaded band denote the open ocean $\delta^{234}U$ value and associated uncertainty as reported by Kipp et al. (2022). Error bars reflect analytical uncertainty. Despite minor local excursions, most coral records remain close to the open ocean baseline, indicating rapid mixing and limited long-term influence from freshwater inputs across the basin.

Overall, the uranium isotope ratio in the Caribbean does not reflect a coherent signal that follows the flow path of the Caribbean Current through the basin and into the Gulf of Mexico. No single $\delta^{234}U$ excursion could be traced from one coral to the next (Figure 9.1), even with the added delay of about 11 months, the time needed for water to travel through the Caribbean (Murphy et al., 1999). This strongly suggests that, at each of the studied locations for the last ~150 years, $\delta^{234}U$ variability is governed by small-scale local processes rather than basin-wide hydrodynamics. The rapid return to open ocean values further implies efficient mixing and short residence times of isotopically distinct water masses. This interpretation is supported by the high flow-through rate of the Caribbean of 28 Sv, which is predominantly supplied by two major currents: the North Brazil Current and the North Equatorial Current (Johns et al., 2002).

Two of the world's largest rivers, the Amazon and the Orinoco, discharge into the western tropical Atlantic, near the entrance of the Caribbean. The Amazon River, with an average $\delta^{234}U$ value of approximately 247‰ and an annual discharge of ~209,000 $m^3\ s^{-1}$, presents a significant freshwater and isotopic source (Vorosmarty et al., 1998; Border, 2020). However, this signal is largely retained within the delta region. Previous work by Border (2020) has shown that anoxic conditions in the Amazon delta promote uranium removal via precipitation, effectively acting as a sink. The Martinique coral record, which lies downstream of the Amazon's influence, shows no persistent $\delta^{234}U$ anomalies, suggesting that this process has been consistently active over at least the last 150 years. The $\delta^{234}U$ composition of the Orinoco River is not well constrained, though it is likely similar to the Amazon due to shared geological regimes (Wesselingh & Hoorn, 2011). However, due to different weathering regimes with steep slopes and thick soils in the Amazon compared to the flatter terrain of the Orinoco (Stallard, 1985), it is plausible that the Orinoco might possess a lower $\delta^{234}U$ signature, potentially contributing to some of the more negative excursions observed in specific coral records. As shown in Chapter 6, the Cuban coral further excludes any significant influence of the Mississippi River on Caribbean $\delta^{234}U$ over the last two centuries. Only during the terminal phase of the Little Ice Age, when regional discharge and current dynamics may have differed from modern conditions, does there appear to be any influence of distant freshwater sources. Unfortunately, no corals spanning that early period were available for this study to confirm the spatial extent of such changes. And additionally, no corals have been available within the direct influence of the discharge waters of any of the larger rivers to directly test the runoff hypothesis.

Another potential factor influencing $\delta^{234}U$ is upwelling, particularly if deeper waters have distinct isotope ratios (Andersen et al., 2007; Chen et al., 2016). A prominent

seasonal upwelling system exists in the southern Caribbean near Venezuela (Muller-Karger et al., 2019). However, the coral from this region does not show isotopic variability corresponding to the seasonal upwelling cycle. Instead, it reflects variations more consistent with changes in local runoff (Chapter 4). Due to its short duration, this record cannot resolve long-term upwelling trends and warrants further investigation.

Among all sites, only the Mexican coral showed indirect evidence of a broader Caribbean hydroclimate signal. In chapter 7, $\delta^{234}U$ variations linked to local SGD were found to be modulated by sea-level fluctuations, which in turn influence the strength of the Yucatán Current (Ezer, 2022). This suggests a coupling between local groundwater discharge and regional oceanographic dynamics, although this relationship remains indirect.

After 1950, the records from Mexico and Cuba, together with the rest of the Caribbean corals, begin to diverge slightly but consistently, showing a difference of approximately 1‰, with the Cuban and Caribbean values raising. Prior to 1950, the records are indistinguishable (Figure B.16). Because this deviation is close to the detection limit for systematic seawater $\delta^{234}U$ variations (~1‰), no firm conclusions can be drawn. However, the pattern may suggest a moderate along-flow $\delta^{234}U$ gradient, potentially linked to changes in regional hydroclimate and ocean throughflow, where the Mexican coral is not influenced due to the high amount of local, low $\delta^{234}U$-SGD.

In conclusion, the coral $\delta^{234}U$ records across the Caribbean do not reveal strong, systematic and coherent regional-scale freshwater transport or mixing patterns from 1825 to present (Figure 9.1). Instead, each record acts as an archive of localized hydroclimate dynamics. On average, the $\delta^{234}U$ baseline across the basin has remained remarkably stable over the past two centuries, consistently reflecting open ocean values (Kipp et al., 2022).

9.3 Comparison to Other Semi-Enclosed Basins

In contrast to the Caribbean, water samples from the Mediterranean Sea exhibit consistently elevated $\delta^{234}U$ values, approximately +1‰ above the open ocean baseline (Figure 9.2) (Border, 2020). A similar increase is also evident in modern cold-water corals from the Alboran sea (Wienberg et al., 2022; Beisel et al., 2023). This enrichment has been attributed to intensified uranium cycling within a semi-enclosed marginal basin that experiences restricted exchange with the Atlantic Ocean. Importantly, the $\delta^{234}U$ signal in the Mediterranean can be traced coherently along the main flow path, indicating basin-wide integration of terrestrial inputs (Border, 2020).

Hydrologically, the Mediterranean is characterized by a single narrow connection to the Atlantic via the Strait of Gibraltar, with an estimated inflow of 0.86 ± 0.10 Sv (and 0.80 ± 0.08 Sv outflow) (Jordà et al., 2017). A key source of the elevated $\delta^{234}U$ is submarine SGD, particularly from the southern coast of France. Border (2020) identified this SGD as isotopically enriched and entering the basin near its western boundary, enabling its signal to be advected along the Mediterranean circulation pathway.

In total around 0.0095–0.1523 Sv of SGD (Rodellas et al., 2015) is added to the Mediterranean along with 0.0098 Sv of riverine water (Ludwig et al., 2009), resulting in a substantially higher freshwater-to-ocean inflow ratio (2.24–18.8%) compared to the Caribbean. In the Caribbean, despite significant river discharge from sources such as the Amazon and Orinoco, the inflow from open ocean currents (e.g., the North Brazil and North Equatorial Currents) dominates, yielding a freshwater contribution of only ~1% relative to total inflow volume. Furthermore, the residence time of surface waters in the Caribbean is significantly shorter than in the Mediterranean, due to the much faster and predominant surface throughflow. The Caribbean Current, fed by large-scale equatorial inflow, can reach average speeds of up to 0.8–1.2 m s^{-1}, whereas the inflow through the Strait of Gibraltar and subsequent internal circulation in the Mediterranean are markedly slower, often <0.1–0.2 m s^{-1} (Murphy et al., 1999; Menna & Poulain, 2010). This difference in advection velocity leads to more rapid mixing and shorter exposure of Caribbean surface waters to terrestrial freshwater sources, further diminishing their impact on the regional $\delta^{234}U$ signature.

The difference in water mass budget is clearly reflected in the uranium isotope composition, shown in Figure 9.2. While the Caribbean coral records remain close to the global open ocean $\delta^{234}U$ average, the Mediterranean exhibits a long-term offset that captures the cumulative influence of isotopically enriched terrestrial inputs (Border, 2020). The contrast between these two basins highlights the importance of both circulation geometry and freshwater flux in modulating regional uranium isotope budgets and their preservation in coral archives.

A similarly elevated $\delta^{234}U$ signal is observed in the ECS (Figure 9.2), making it another instructive analogue to the Caribbean. In this marginal basin, slightly elevated $\delta^{234}U$ values, up to ~+1‰ above open ocean baselines, have been documented in both seawater and coral records (Wang et al., 2017; Shang et al., 2021). This enrichment is attributed to sustained input from the Yangtze and Yellow Rivers, two of the largest fluvial systems in Asia (Shang et al., 2021). These rivers drain extensive continental areas dominated by felsic bedrock and intense chemical weathering, resulting in terrestrial freshwater enriched in $\delta^{234}U$ due to recoil mobilization and preferential ^{234}U leaching.

The broad, shallow continental shelf of the ECS plays a key role in the retention and expression of these isotopic signals. Unlike more dynamic open systems, the ECS exhibits partially restricted circulation, and the shelf geometry facilitates seasonal stratification and reduced vertical mixing (Lie & Cho, 2002). As a result, riverine inputs can persist and accumulate locally before being diluted by the inflow of Kuroshio Current waters along the shelf edge (Lie & Cho, 2002; Lin et al., 2020). This setting contrasts with the Caribbean, where faster current systems and greater throughflow quickly homogenize freshwater anomalies. In the ECS, longer residence times and lower flushing efficiency allow for more durable $\delta^{234}U$ imprints in nearshore environments (Nozaki et al., 1989).

The ECS example underscores the role of basin geometry, shelf hydrodynamics, and river discharge magnitude in modifying the uranium isotope composition of coastal and marginal seas. It highlights how $\delta^{234}U$ can serve not only as a proxy for short-term hydroclimate variability but also as a tracer of long-term terrestrial influence under specific circulation and mixing regimes.

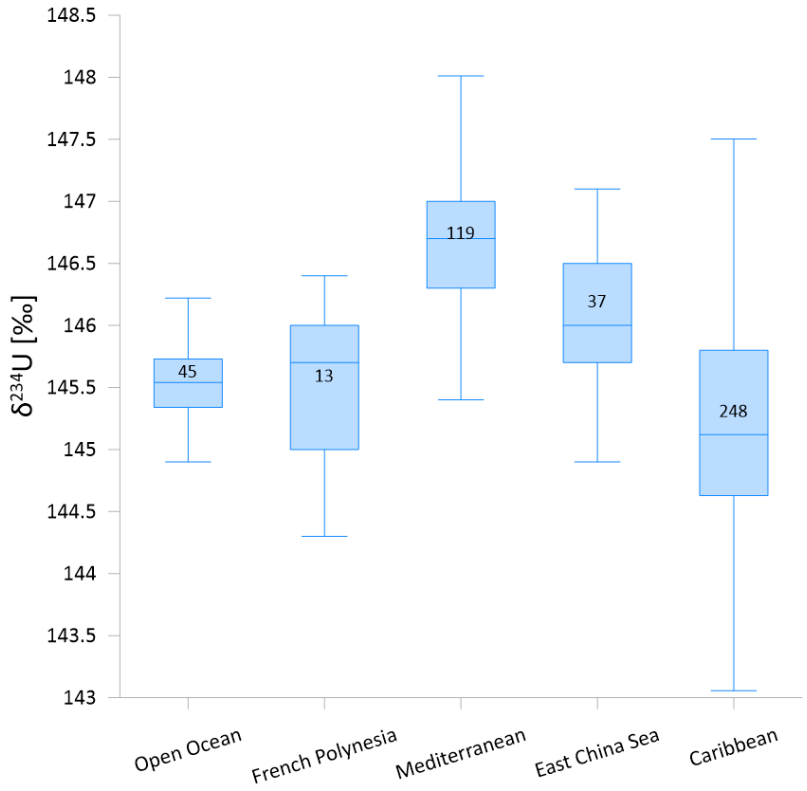

Figure 9.2 Boxplot comparison of $\delta^{234}U$ values (‰) from corals and seawater in different oceanic and marginal basin settings: Open Ocean (Kipp et al., 2022), French Polynesia (Chapter 8), Mediterranean (Border, 2020; Beisel et al., 2023), East China Sea (Yu et al., 2006; Wang et al., 2017), and Caribbean. Numbers within boxes indicate the number of samples per region. Not shown are additional positive outliers from the Mediterranean and Caribbean datasets. In the Caribbean case, these outliers correspond to elevated values from the Cuban coral spanning the terminal Little Ice Age (LIA).

In contrast to semi-enclosed basins where freshwater input can elevate regional $\delta^{234}U$ values, island settings like Tahiti and other locations in French Polynesia demonstrate how rapid mixing with ocean water can suppress isotopic signals, even in environments with potentially high terrestrial input, as discussed in Chapter 8 (Figure 9.2). Volcanic high islands such as Tahiti receive intense rainfall and have steep, reactive catchments composed of basaltic bedrock (Hildenbrand et al., 2004; Hildenbrand et al., 2008). These conditions favour the production of isotopically enriched freshwater, as prolonged water–rock interaction enhances the mobilization of ^{234}U through recoil and preferential leaching mechanisms, a process similarly observed in Martinique and other volcanic terrains. However, despite this strong theoretical potential for elevated $\delta^{234}U$ input from land, both coral and seawater measurements around Tahiti consistently reflect values near the open ocean baseline (~145‰) (Kipp et al., 2022). This isotopic homogeneity is attributed to the high flushing efficiency and open ocean exposure of the reef systems surrounding the island. The narrow shelf and direct contact with the South Pacific circulation result in very short residence times for coastal freshwater plumes. As a result, any isotopically distinct freshwater is rapidly mixed and diluted before it can significantly alter the uranium isotope composition of ambient seawater or become recorded in coral aragonite.

This behaviour highlights an important endmember in the $\delta^{234}U$ sensitivity spectrum: in high-energy, open-ocean island settings, the combination of small catchment size, steep gradients, and fast hydrodynamic exchange effectively limits the preservation of freshwater uranium signatures in coral archives. It underscores that not only the magnitude of freshwater input, but also the retention time and basin configuration, ultimately control whether a distinct $\delta^{234}U$ signal is detectable in coral records. Consequently, the comparison of different ocean basins and freshwater-influenced regions highlights a distinct characteristic of the Caribbean: a stable, open-ocean $\delta^{234}U$ mean value combined with high variability caused by numerous localized influences on the waters bathing the corals. By contrast, other regions either show a measurable deviation from the global mean (e.g., the Mediterranean Sea and East China Sea) or a suppressed freshwater influence (e.g., French Polynesia). The variance observed in the Caribbean Sea, however, clearly stands out and indicates a complex interplay of multiple localized processes.

9.4 Temporal Variability

On timescales longer than two centuries, $\delta^{234}U$ reconstructions cannot be resolved on an annual basis, and age uncertainties, coral diagenesis, and open-system behaviour may significantly alter the isotope composition on the order of the variance observed

during the past 250 years (~±2‰) (Thompson et al., 2003; Scholz et al., 2004; Frank et al., 2006; Chutcharavan et al., 2018). Fossil coral initial $\delta^{234}U$ values generally show larger uncertainties due to additional age imprecision, which does not affect the post-modern corals examined here (Hibbert et al., 2016; Chutcharavan et al., 2018). Nevertheless, a sufficient number of observations exists for comparison, and long-term global climate trends, including the ice-volume effect on global ocean $\delta^{234}U$, are well resolved. These data allow to test the sensitivity of $\delta^{234}U$ as a proxy under conditions of major environmental change, including disruptions of the Atlantic Meridional Overturning Circulation (AMOC).

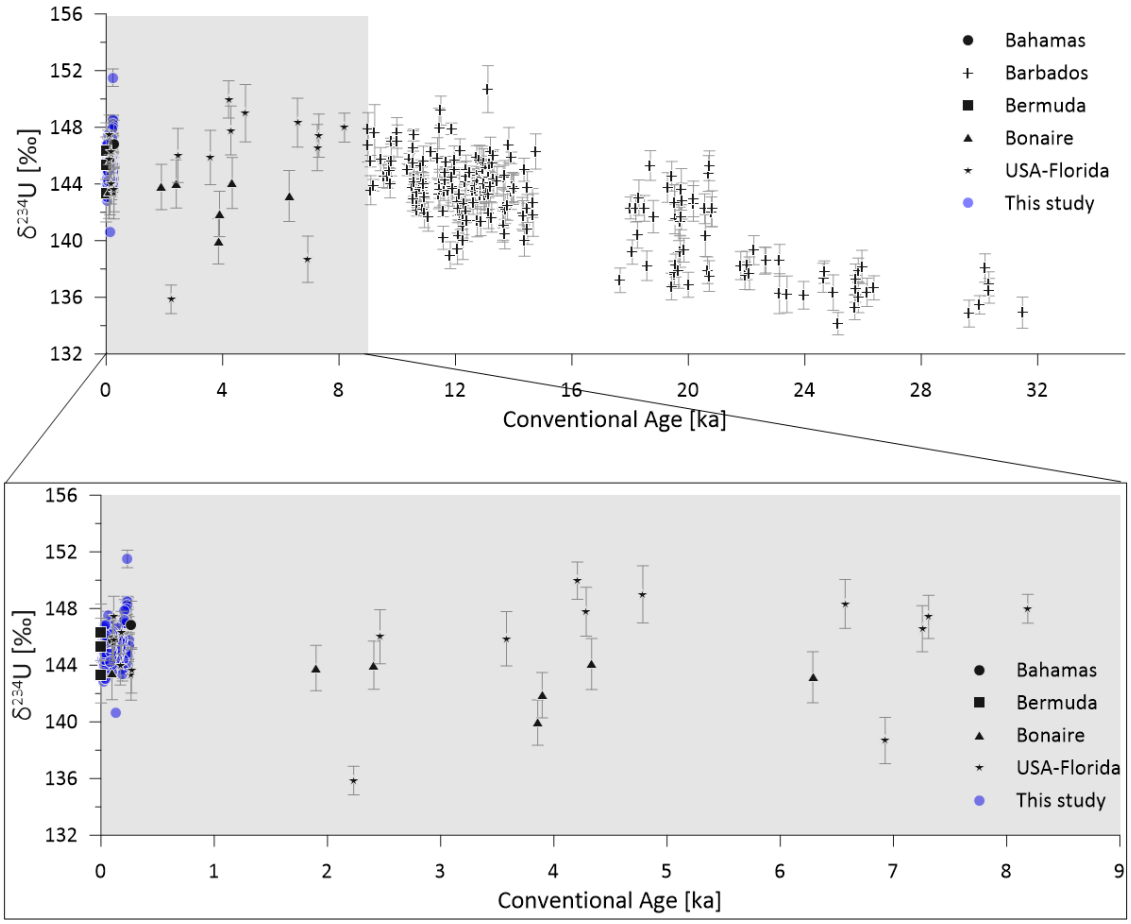

Figure 9.3 Compilation of coral $\delta^{234}U$ values from the Caribbean and western Atlantic spanning the last 30 ka. Black symbols show published fossil coral data from the Bahamas, Barbados, Bermuda, Bonaire, and Florida (Chutcharavan et al., 2018). Blue circles represent data from this study (Caribbean corals, 18th–21st century). The upper panel highlights the long-term $\delta^{234}U$ evolution, with a ~3–4‰ depletion during the Last Glacial Maximum relative to the Holocene. The lower panel zooms into the last 9 ka.

For the past two centuries (1825–2025), the mean $\delta^{234}U$ value is 145.06‰ ±0.85‰, and its variance, even when accounting for localized groundwater inputs and distant freshwater sources, does rarely exceed 1.5‰ (Figure 9.3 and Figure B.17). Thus, natural variability above this threshold is likely to reflect either substantial freshwater perturbations or diagenetic alteration in fossil corals. This reduces the

variance reported in the compilation of Chutcharavan et al. (2018) (mean = 145.7‰ ± 3.7‰, 2σ) by about a factor of two for the same interval. Over the long term, the $\delta^{234}U$ ratio has increased by ~6‰ since the Last Glacial Maximum (LGM), with temporal variability ranging from 1.5‰ to more than 5‰.

During the LGM, the variance of initial $\delta^{234}U$ in Barbados corals remained low and comparable to that observed during the past 250 years (<2–3‰, within analytical uncertainty) (Figure 9.3 and Figure B.17). Both the LGM and modern warm-climate states therefore reflect similarly small variability, consistent with rapid throughflow and only moderate continental runoff impacts. These two periods together indicate that global seawater $\delta^{234}U$ differed by ~6‰ ± 2‰ between the LGM and the present, consistent with the global mean oceanic shift. This pattern may reflect the combined effects of maximum Northern Hemisphere ice volume and minimum ice extent (Hibbert et al., 2016; Chutcharavan et al., 2018).

In contrast, the first major AMOC disruption (18–15 ka) (Clark et al., 2020) is marked by an increase in mean Atlantic $\delta^{234}U$ values and more than a doubling of variance, suggesting stronger local influences on seawater composition even at Barbados, outside the Caribbean (Figure 9.3 and Figure B.17). This variability likely reflects the southward advection of $\delta^{234}U$-enriched meltwater and/or variable mixing between northern and southern Atlantic water masses (Clark et al., 2020). Elevated variance remains a characteristic feature of the deglaciation and persists into the early Holocene, even after modern $\delta^{234}U$ mean values had been established.

For the Holocene, only a few measurements are available from both the Caribbean exit (Florida Keys) and within the basin (Bonaire) (Figure 9.3 and Figure B.17). These sites diverge significantly, with offsets of up to 4‰ and large short-term variations far exceeding those observed in other intervals. Given the consistent analytical precision and excellent coral preservation, these deviations are best explained by localized freshwater runoff at Bonaire and $\delta^{234}U$-enriched inputs to the Florida Keys, likely carried by high $\delta^{234}U$-Mississippi discharge (Grzymko et al., 2007) via the Florida Current, as local Floridian Groundwater is characterised by low $\delta^{234}U$ values (Swarzenski & Baskaran, 2007).

Taken together, these observations suggest that the small-scale processes modulating $\delta^{234}U$ in the Caribbean during the past 250 years were amplified during periods of major climate change. Both the mean $\delta^{234}U$ and its variance respond to the relative contributions of advection and freshwater input, with the mean value reflecting global oceanic freshwater balance and the variance reflecting local hydrological modulation. Finally, the Barbados record, with no high $\delta^{234}U$ outliers, implies that the reducing conditions in the Amazon delta discharge influenced the regional uranium cycle as far back as 31 ka BP.

9.5 Conclusion: Reassessment of Regional Proxy Potential

This chapter synthesizes coral-derived $\delta^{234}U$ records across the Caribbean and compares them to other ocean margin environments to assess the impact of freshwater inputs on regional uranium isotope compositions. The analysed Caribbean corals, from across the basin, reveals a remarkably stable $\delta^{234}U$ baseline (~145.5‰), consistent with open ocean values (Figure 9.1) (Kipp et al., 2022). No coherent $\delta^{234}U$ patterns could be traced along the Caribbean flow path, underscoring the dominance of local hydrological conditions over basin-scale freshwater transport. One exception is the Mexican coral, which captured $\delta^{234}U$ variability associated with SGD that was modulated by sea-level changes, indirectly reflecting fluctuations in regional current strength (Ezer, 2022). However, such coupling between $\delta^{234}U$ signals and oceanographic dynamics appears limited to specific conditions.

In contrast, semi-enclosed basins such as the Mediterranean and ECS exhibit elevated $\delta^{234}U$ values (Figure 9.2) that can be traced coherently along their respective flow paths (Border, 2020; Shang et al., 2021). In these systems, sustained terrestrial input, restricted circulation, and longer water residence times allow freshwater-derived uranium signals to persist and integrate regionally. Meanwhile, high-energy island settings like Tahiti demonstrate that even strong freshwater fluxes may not affect seawater isotopic composition if mixing is sufficiently rapid.

Over geological timescales $\delta^{234}U$ reconstructions show low variance during both the LGM and the past two centuries, but strongly elevated variability during deglaciation, likely from meltwater and shifting Atlantic circulation. Sparse Holocene data reveal local deviations, emphasizing that while long-term $\delta^{234}U$ changes reflect global ice volume, variance is driven by regional hydroclimate.

Importantly, coral $\delta^{234}U$ records remain a powerful tool for reconstructing local hydrological variability and terrestrial influence, even in dynamic, open-ocean environments where regional signals are quickly lost. Their sensitivity to short-term runoff events, precipitation patterns, and weathering intensity makes them valuable archives of past environmental change at the site scale.

Outlook

The findings of this dissertation highlight the potential of $\delta^{234}U$ in tropical corals to reconstruct freshwater influence and local hydroclimatic variability, while also revealing the complexities and limitations of the proxy. After establishing analytical precision and sampling strategies, this work demonstrated that $\delta^{234}U$ can capture signals of submarine groundwater discharge (SGD) and riverine input, but also emphasized the challenges of quantifying SGD fluxes across diverse hydrogeological settings and the limitations of short-lived tracers for extending reconstructions beyond the modern period.

Looking ahead, an important but as yet unexplored avenue lies in establishing terrestrial $\delta^{234}U$ endmembers for regions where coral archives are available. Groundwater, riverine input, and weathering regimes each impart distinct $\delta^{234}U$ signatures to coastal waters, yet systematic datasets of these terrestrial endmembers are lacking. Developing such baselines would allow for more robust attribution of coral $\delta^{234}U$ variability to specific hydrological processes, strengthening the quantitative analytical power of coral records. Similarly, investigations in other enclosed or semi-enclosed basins, for example, the Red Sea, or the South China Sea, could provide natural laboratories where terrestrial fluxes dominate over open-ocean mixing. Such settings may amplify $\delta^{234}U$ signals of runoff and groundwater discharge, offering opportunities to refine proxy-process relationships under controlled boundary conditions.

On the analytical side, advances such as $\delta^{234}U$ analyses using laser ablation or improvements in multi-collector ICP-MS precision could enable higher-resolution coral records, mitigate challenges in the sampling process and allow sub-seasonal reconstructions of freshwater variability

Future research could further advance along two complementary directions. The first involves improved quantification of contemporary SGD fluxes and their $\delta^{234}U$ signatures, particularly in tropical and storm-prone regions where hydrological forcing produces highly variable discharge. Integrating direct flux measurements with hydrological modelling and storm-event monitoring will help reduce uncertainties in SGD estimates and clarify their sensitivity to climate variability. The second direction is the development of a broader geochemical toolkit to capture long-term SGD variability. Combining coral $\delta^{234}U$ with complementary proxies such as Ba/Ca ratios and rare earth element (REE) fractionation offers a promising strategy. Unlike short-lived isotopes, these tracers are archived in coral skeletons and can extend reconstructions from seasonal to millennial scales. Such integration would

allow for a more robust distinction between SGD and riverine contributions, while also enabling identification of climatic and sea-level drivers of groundwater-seawater interactions.

In parallel, this thesis opens a second trajectory focusing on drowned coral reefs along rapidly subsiding margins, such as Hawai'i, as investigated by the IODP Expedition 389. These reefs, largely formed during glacial low stands, provide a unique yet underutilized archive of past sea-level and hydroclimatic variability. Applying the $\delta^{234}U$ framework to fossil corals from such settings could constrain precipitation, runoff, and groundwater variability under boundary conditions absent from stable margins, thereby providing new insights into ENSO, the Pacific Decadal Oscillation (PDO), and the Pacific North American (PNA) pattern during glacial states and rapid deglaciations.

By bridging modern SGD dynamics with paleo-archives, these research directions establish a framework for integrating hydrological, geochemical, and climatic perspectives. Together, they have the potential to transform our understanding of tropical water cycling and its response to sea-level fluctuations, ENSO variability, and ice-sheet instabilities over the past half-million years. In particular, the further development of $\delta^{234}U$ as a proxy holds exceptional promise. Beyond its established role in U-series dating and sea-level reconstructions, $\delta^{234}U$ emerges here as a sensitive recorder of freshwater fluxes, capable of tracking inputs from rivers, groundwater, and even glacial meltwater pulses. Continued refinement of this proxy, through modern calibration, site-specific variability assessments, and integration with complementary tracers, will enhance its reliability and resolution. Such advances could extend its use from coastal SGD reconstructions to regional hydroclimate variability across glacial-interglacial timescales, positioning $\delta^{234}U$ as a cornerstone of future research on ocean-land interactions.

Appendix

A. List of Figures

B. Supporting information

Chapter 4

U-Isotope Probenaufbereitung für Neptune: Probenmenge < 100 mg (Kleine Säulen)

--- Schritte ins Laborbuch eintragen ---

1. Proben in Probenbuch (Rene) eintragen und Becher beschriften
2. Säubern (1./2. Stock IUP)
    a. Probe mit dem Dremel in ca. 60-100 mg schwere Stücke schneiden und in beschriftete Becher geben
    b. Im 2. Stock die Probenbecher mit Milli-Q füllen, bis die Probe bedeckt ist und 10 min ins Ultraschallbad bei 100% stellen
    c. Milli-Q vorsichtig dekantieren und b. 2 Mal wiederholen
    d. Die Proben im Probenbecher für einige Stunden auf der Heizplatte trocknen
3. Wiegen (1. Stock IUP)
    a. Probe mit Wägepapier wiegen → Wägetabelle
    b. Probe in die beschrifteten Becher geben und mit Milli-Q bedecken
4. Lösen (1. Stock IUP)
    a. 7 N HNO_3 zur Probe in Milli-Q hinzugeben, bis fast keine Bläschen mehr nach oben steigen (BLANK auch „lösen“)
    b. Probe am besten einige Stunden stehen lassen
5. Spiken (1. Stock IUP)
    a. TriSpike aus dem Kühlschank nehmen, ca. eine Stunde warten, schütteln
    b. Gelöste Probe wiegen (Elektrostatik beachten) → Wägetabelle
    c. 0,1 mL Spike hinzugeben („TriSpike“ Pipette!) und direkt wieder 1x wiegen → Wägetabelle
6. Lösen (6. Stock Geos)
    a. Auf der Heizplatte bei 60°C über Nacht eindampfen
    b. 500 µL 7 N HNO_3 hinzugeben und über Nacht lösen lassen (schräg stellen)
7. 1. Säule (6. Stock Geos)
    a. Säulen beschriften und Füllstrich zeichnen, 1x mit MilliQ H_2O füllen (Abfallbecher unterstellen)
    b. Ca. 500 µL (bis zum Füllstrich) UTEVA Harz hineingeben
    c. 1x mit MilliQ H_2O füllen
    d. Laden der Säulen: 1x mit 7 N HNO_3 füllen
    e. Probe <u>langsam</u> auf Säule geben (Pipetten Spitzen in Becher lassen)
    f. Ca. 1,5 mL 7 N HNO_3 (mit Standzylinder) in Probenbecher geben, schrittweise auf die Säule geben:
        i. 500 µL
        ii. 500 µL
        iii. 500 µL

    --- Probenbecher unter die Säule stellen ---

    g. Eluierung mit 1 N HCl:
        i. 500 µL
        ii. 500 µL

iii. 500 µL

h. 1x mit MilliQ H_2O füllen und im Probenbecher auffangen
i. Probenbecher auf die Heizplatte stellen
j. Säulen verschließen und mit MilliQ H_2O füllen
k. Probe eindampfen (bei 60°C über Nacht/Wochenende)

8. 2. Säule (6. Stock Geos)
   a. Probe schräg stellen, lösen in 300 µL 7 N HNO_3
   b. Säulen öffnen, H_2O in Abfallbecher laufen lassen
   c. Laden der Säulen: 1x mit 7 N HNO_3 füllen
   d. Probe <u>langsam</u> auf Säule geben
   e. Ca. 750 µL 7N HNO_3 (mit dem Standzylinder) in Probenbecher geben, schrittweise auf die Säule geben:
      i. 250 µL
      ii. 500 µL

   --- Probenbecher unter die Säule stellen ---

   f. Eluierung mit 1N HCl:
      i. 500 µL
      ii. 500 µL
      iii. 500 µL
   i. Probenbecher auf die Heizplatte stellen und bei 60°C über Nacht/Wochenende eindampfen
9. Lösen (1. Stock IUP)
   a. Nach Eindampfen: Lösen in 1,2 mL 1% HNO_3+0,05% HF
   b. Probenbecher min. 3 Stunden schräg stehen lassen
   c. Proben zentrifugieren
   d. Für iCap Messungen 1:10 mit 0,5 N HNO_3 in Zentrifugentubes verdünnen (450 µL 0,5 N HNO_3 + 50 µL Probe)
   e. Restliche Probe in Messtubes umfüllen

Chapter 5

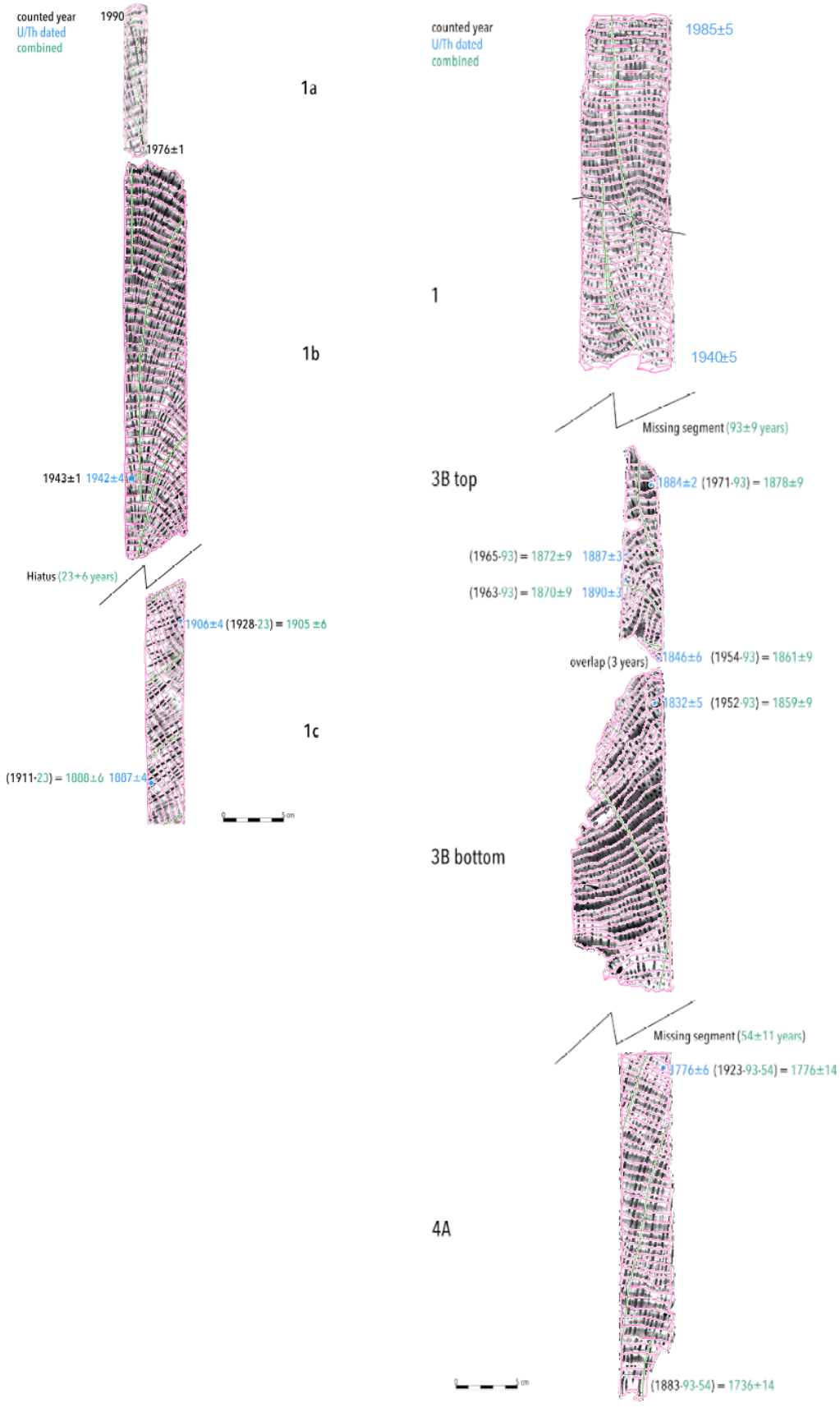

Figure B.1 left: Age model for coral core CPR1990-09-25, drilled in 1990. Right: Age model for coral core TM2020-12-04, drilled in 1985 ± 5.

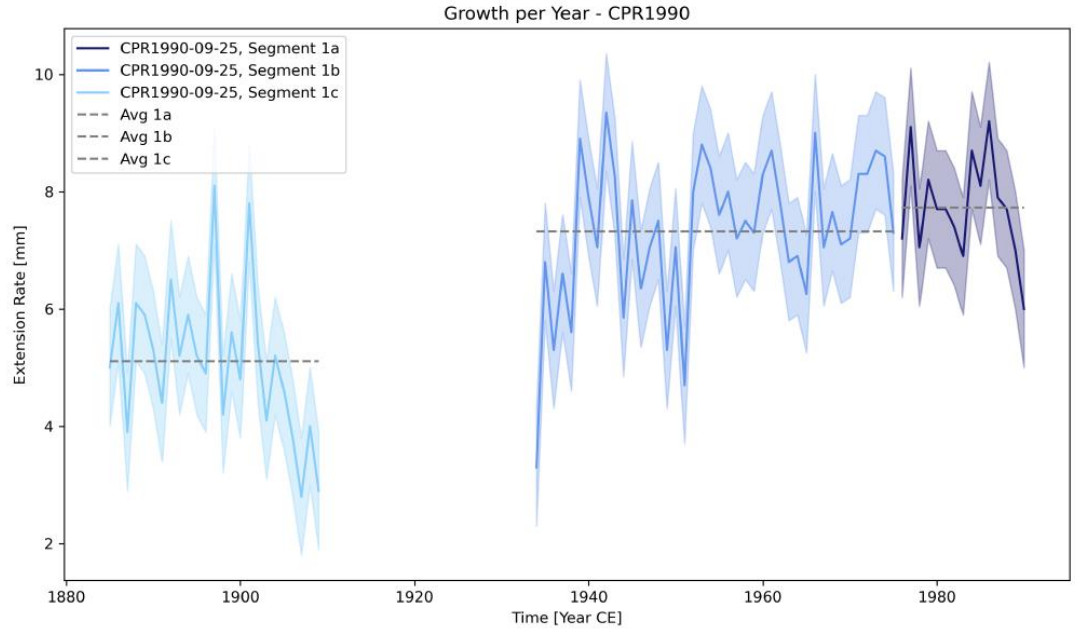

Figure B.2 Annual extension rate in CPR1990-09-25.

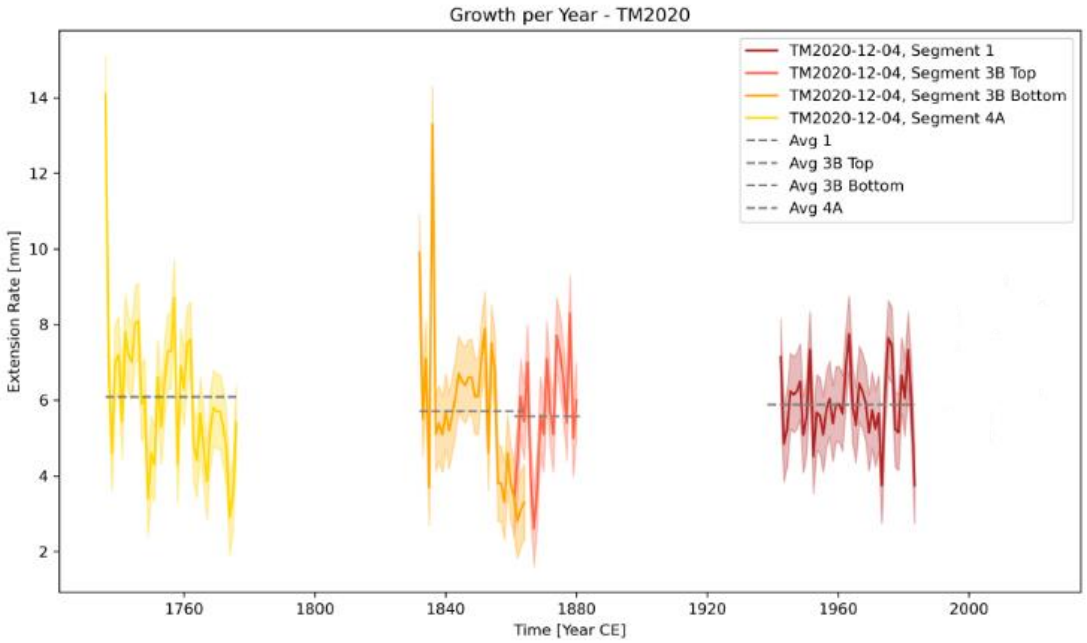

Figure B.3 Annual extension rate in TM2020-12-04.

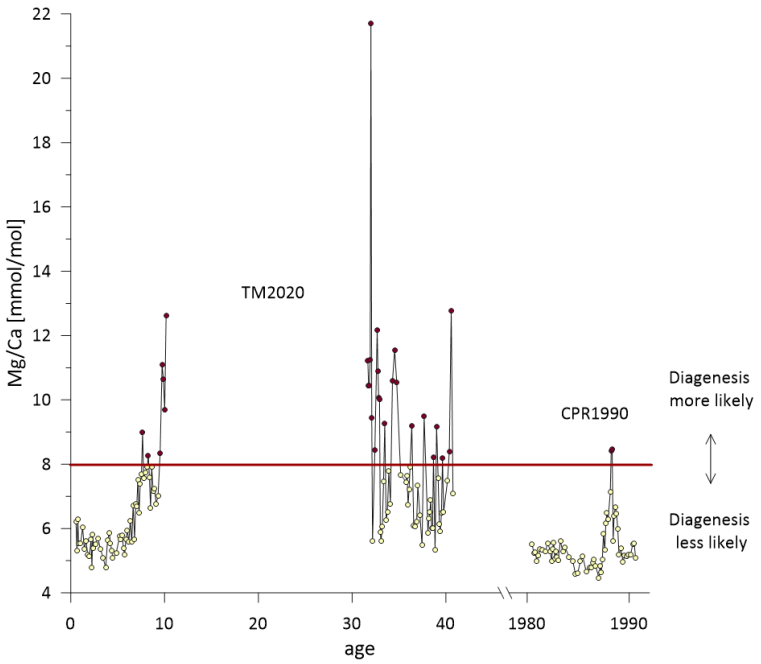

Figure B.4 Mg/Ca ratios (mmol/mol) measured in two coral cores, TM2020 and CPR1990. The TM2020 core covers an interval estimated between the 1940s and 1980s, although uncertainties in the age model preclude direct placement on an absolute timescale. The CPR1990 core is precisely dated and spans the years 1980–1990. The horizontal red line marks the diagenetic threshold (8 mmol/mol), above which secondary alteration of the coral skeleton is considered more likely. Values below this threshold indicate intervals where diagenesis is less likely to have affected the geochemical record.

SST proxies

Despite the relatively low temporal resolution of approximately six samples per year, both Sr/Ca and $\delta^{18}O$ time series display clear seasonal patterns (Figure B.5), suggesting that these proxies reliably reflect SST variability. However, such resolution may introduce sampling bias, particularly underestimating temperature extremes or rapid fluctuations, as noted in previous studies (Swart et al., 2002; Watanabe et al., 2002). Due to the higher error in the age uncertainty in the TM coral no correlation with seasonal resolved SST data was possible.

As seen in Figure B.5, Sr/Ca values range from 9.55 to 9.20 mmol/mol, while $\delta^{18}O$ varies between -4.5‰ and -3.4‰. These ranges are consistent with values reported from other tropical Atlantic corals (Winter et al., 2000; Marshall & McCulloch, 2002; Swart et al., 2002), confirming their regional application for SST proxies. The CPR coral consistently exhibited lower Sr/Ca ratios than the TM coral, which, given the established inverse relationship between Sr/Ca and SST (Smith et al., 1979), imply higher ambient temperatures at the CPR site. Interestingly, $\delta^{18}O$ values were similar across both sites, suggesting that $\delta^{18}O$ may be modulated by additional factors such as sea surface salinity (SSS) particularly in the more evaporative and enclosed lagoonal environment (Figure 3.3) (Fairbanks & Dodge, 1979; Leder et al., 1996).

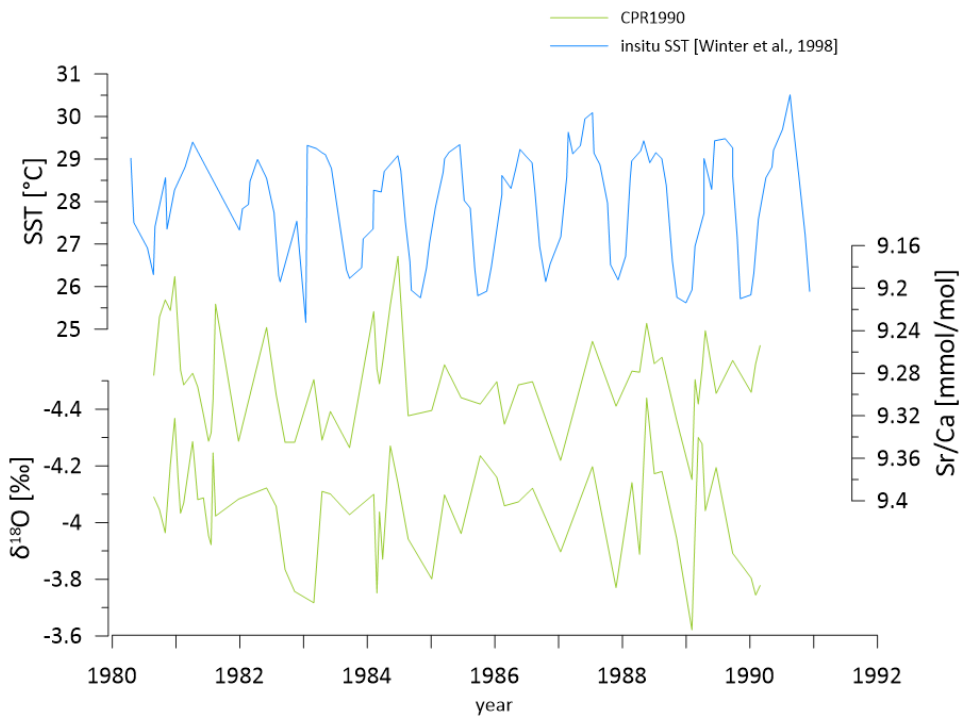

Figure B.5 Seasonal variability in sea surface temperature (SST) proxies, Sr/Ca and $\delta^{18}O$, from CPR1990 (light green) *Orbicella faveolata* coral core, compared with instrumental SST records. The top panel shows in situ SST data from La Parguera, Puerto Rico (Winter et al., 1998). Middle and lower panels show coral $\delta^{18}O$ and Sr/Ca records, respectively, which reflect SST variability with inverse relationships (higher SST corresponds to lower Sr/Ca and more negative $\delta^{18}O$).

Correlations analysis with in situ SST (Winter et al., 1998) for the 1980s are shown in Figure B.6 and further supports the interpretation of proxy performance. The CPR coral yields significant relationships of Sr/Ca and $\delta^{18}O$ with r-values of -0.39 and -0.37, respectively.

Linear regression of Sr/Ca against SST produced slopes of -0.01 mmol/mol/°C and y-intercepts between 9.66, consistent with calibration values reported for *Orbicella* (Swart et al., 2002; Smith et al., 2006; DeLong et al., 2011). The significant $\delta^{18}O$-SST correlation at CPR has a slope of -0.05‰/°C, which is shallower than commonly reported for tropical corals (typically –0.18‰/°C in *Porites*), and lower than expected even for *Orbicella* (Swart et al., 2002; DeLong et al., 2011; Sadler et al., 2014). Thus, a solely temperature driven $\delta^{18}O$ signal is unlikely in the coral core. A subset of TM coral samples from the 1980s exhibited elevated Mg/Ca ratios, potentially indicative of diagenetic alteration (Allison et al., 2007; Hendy et al., 2007; Nothdurft & Webb, 2008).

Taken together, these findings suggest that Sr/Ca is the more robust SST proxy under the studied conditions, while $\delta^{18}O$ incorporates additional environmental signals, particularly related to SSS. This highlights the need to apply $\delta^{18}O$ with caution in lagoonal or semi-enclosed reef environments, where evaporative processes may obscure its temperature sensitivity (Stevenson et al., 2018).

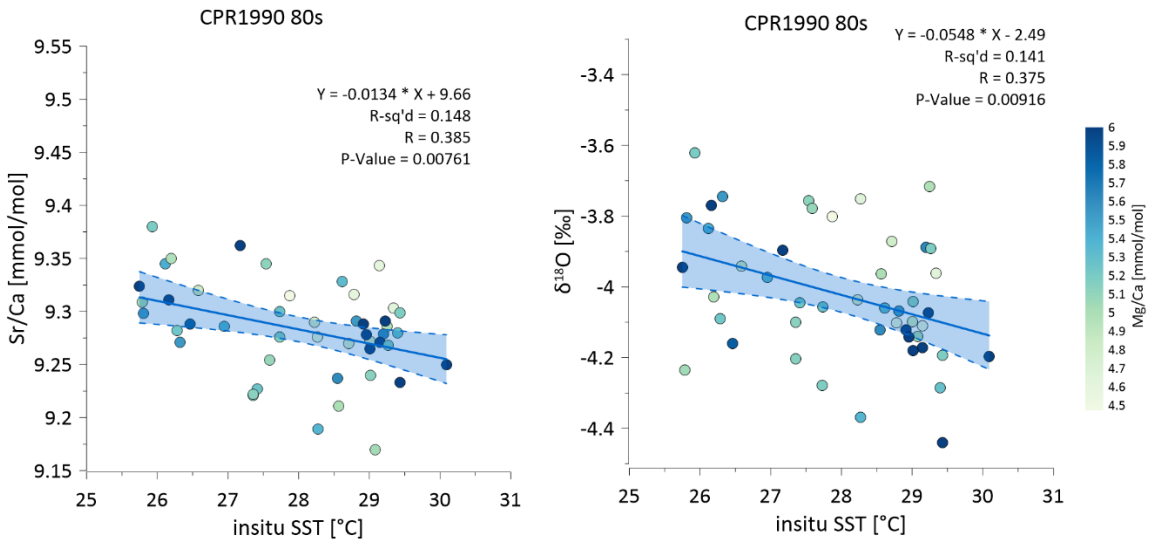

Figure B.6 Linear regression plots showing the relationships between coral Sr/Ca (left) and $\delta^{18}O$ (right) and instrumental sea surface temperature (SST) across the 1980s in the CPR coral (Winter et al., 1998). Regression lines (solid blue) with 95% confidence intervals (shaded) highlight the inverse relationship between proxies and SST. Each data point is coloured by Mg/Ca value, with darker shades indicating higher ratios, however no indications of diagenesis can be inferred. Strongest correlations are observed for Sr/Ca, affirming its robustness as an SST proxy. $\delta^{18}O$–SST correlations are generally weaker and more variable.

$\delta^{18}O_{sw}$ calculation

The $\delta^{18}O_{sw}$ was calculated by isolating the temperature-independent component of the coral $\delta^{18}O$ signal, following established dual-proxy approaches (Watanabe et al., 2002; Ren et al., 2003; Benway & Mix, 2004; Felis et al., 2009; Wu et al., 2017). This involved deriving SST from the Sr/Ca record using species-specific Sr/Ca–SST slopes calibrated for *Orbicella faveolata*. As discussed above, the applied slopes fall within reported ranges for this species and region (Swart et al., 2002; Smith et al., 2006; DeLong et al., 2011).

To isolate the salinity-related component, the theoretical temperature dependent portion of the $\delta^{18}O$ signal was removed. This was achieved by applying a linear $\delta^{18}O$-SST relationship with a slope of –0.17‰/°C, consistent with values reported in dual-proxy studies using *Porites* and corrected *Orbicella* data. Although some calibrations of *Orbicella faveolata* report shallower slopes (e.g., –0.085 to –0.10 ‰/°C; (Smith et al., 2006)), recent studies have demonstrated that the slope can vary substantially depending on local environmental conditions, skeletal growth parameters, and analytical treatment (Sadler et al., 2014). Reconstructions using annual or seasonal means, particularly when controlling for salinity, often yield steeper slopes approaching –0.17‰/°C (Watanabe et al., 2002; Ren et al., 2003; Benway & Mix, 2004; Felis et al., 2009; Wu et al., 2017).

In this study, the –0.17 ‰/°C slope was selected based on two considerations: (1) strong internal consistency between SST estimates derived from Sr/Ca and those

inferred from $\delta^{18}O$ using this slope, and (2) calculated $\delta^{18}O_{sw}$ values and seasonal seawater $\delta^{18}O$ measurements at La Parguera lagoon, reported by Watanabe et al. (2002).

The resulting $\delta^{18}O_{sw}$ values in this study ranged from –0.13‰ to 2.06‰, notably broader than the seasonal variation reported by Watanabe et al. (2002) , which ranged from 0.25‰ in November to 1.0‰ in May–July. The broader range in coral-derived $\delta^{18}O_{sw}$ in this study may reflect higher salinity variability, potentially driven by episodic freshwater input, evaporation events, or limited water exchange in the lagoonal setting. Nevertheless, the mean $\delta^{18}O_{sw}$ of 0.74‰ aligns well with in situ observations, lending support to the validity of the calculation approach and its use as a qualitative indicator of freshwater variability and salinity change in this region.

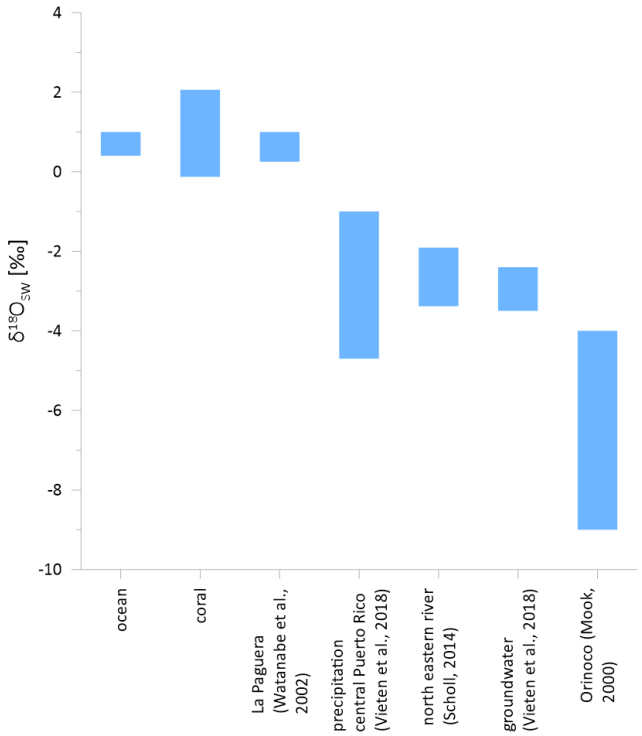

Figure B.7 $\delta^{18}O_{sw}$ values from different hydrological and environmental sources in and around Puerto Rico. Bars represent the range of $\delta^{18}O$ values compiled from the literature for open ocean water (Epstein et al., 1953), coral-derived seawater (this study), La Parguera lagoon surface water (Watanabe et al., 2002), precipitation over western Puerto Rico (Vieten et al., 2018), northeastern Puerto Rican rivers (Scholl, 2014), local groundwater (Vieten et al., 2018), and the Orinoco River water (Mook & Rozanski, 2000).

Multi-Proxy Comparison and Cross-Correlation

The seasonal-scale relationship among the freshwater-sensitive proxies Ba/Ca, $\delta^{13}C$, and $\delta^{18}O_{sw}$ was evaluated using both pairwise correlation and PCA, revealing consistent yet nuanced patterns.

At seasonal resolution, Ba/Ca and $\delta^{13}C$ showed the strongest coherence, particularly in the CPR1990 core. Their correlation ($R = 0.405$, $p = 0.002$) suggests a shared

environmental response, likely associated with terrestrial freshwater input. Ba/Ca has traditionally long been used as an indicator of riverine particulate delivery, particularly during high-discharge events (McCulloch et al., 2003; Prouty et al., 2010; Shaw et al., 2024), while $\delta^{13}C$ reflects changes in the $\delta^{13}C$ of DIC, modulated by terrestrial organic matter inputs or reduced vertical mixing (Moyer, 2008; Moyer & Grottoli, 2011). However, neither proxy is exclusively driven by freshwater. Ba/Ca can also response to upwelling of barium enriched water masses or by sediment resuspension, especially in high-energy or shallow reef environments (Ourbak et al., 2006; LaVigne et al., 2016). Similarly, $\delta^{13}C$ is influenced by coral photosynthetic rates, which are in turn controlled by light availability, cloud cover, turbidity, and shading (Fairbanks & Dodge, 1979; Verena Schoepf et al., 2014). Importantly, Ba/Ca may also be indirectly influenced by light, as light-driven photosynthesis affects calcification rates and trace element uptake via symbiont activity (Yamazaki et al., 2021). Reduced light conditions, such as those during storms or turbid runoff, can thus simultaneously influence Ba/Ca and $\delta^{13}C$, albeit through different mechanisms. These overlapping environmental controls mean that while Ba/Ca and $\delta^{13}C$ often reflect freshwater input, their signals also integrate biological and physical variability that should be carefully considered, especially during transitional or anomalous periods.

In contrast, $\delta^{18}O_{sw}$ showed consistently weakly correlations with Ba/Ca and $\delta^{13}C$ in the CPR core and loaded onto separate PCA components. This reinforces its interpretation as a salinity-sensitive proxy, more strongly governed by evaporation–precipitation balance and SST variability. In lagoonal environments like La Parguera, where water turnover is limited, such influences may be enhanced (Stevenson et al., 2018). The CPR core, located in a shallow and semi-enclosed setting, exemplifies how $\delta^{18}O_{sw}$ can be decoupled from direct runoff signals, instead tracking broader hydrological balance. Nonetheless, $\delta^{18}O_{sw}$ remains a valuable proxy when salinity trends are independently constrained.

In the TM coral core, Ba/Ca and $\delta^{13}C$ show a moderate but significant correlation ($r = 0.3$, $p = 0.03$), supporting a shared sensitivity to freshwater variability. However, PCA results reveal stronger partitioning, with $\delta^{13}C$ loading primarily on PC1 (which explains 85% of the variance), while Ba/Ca dominates PC2. This suggests that although both proxies respond to environmental variability, they may track different aspects of freshwater input or be influenced by distinct environmental controls. For instance, $\delta^{13}C$ may be more directly affected by light availability or primary production, while Ba/Ca may reflect particulate delivery or trace metal availability modulated by hydrodynamic conditions. This may reflect TM's slower extension rate (6 mm/year vs. 8 mm/year at CPR), or differing exposure to upwelling or wave action. The greater photic stress or water mass variability at TM could also explain the more

variable $\delta^{13}C$ signal, and may account for the negative loading of Ba/Ca in PC1 despite its freshwater sensitivity. These site-specific patterns underscore the importance of local hydrography, reef setting, and coral physiology in shaping proxy responses.

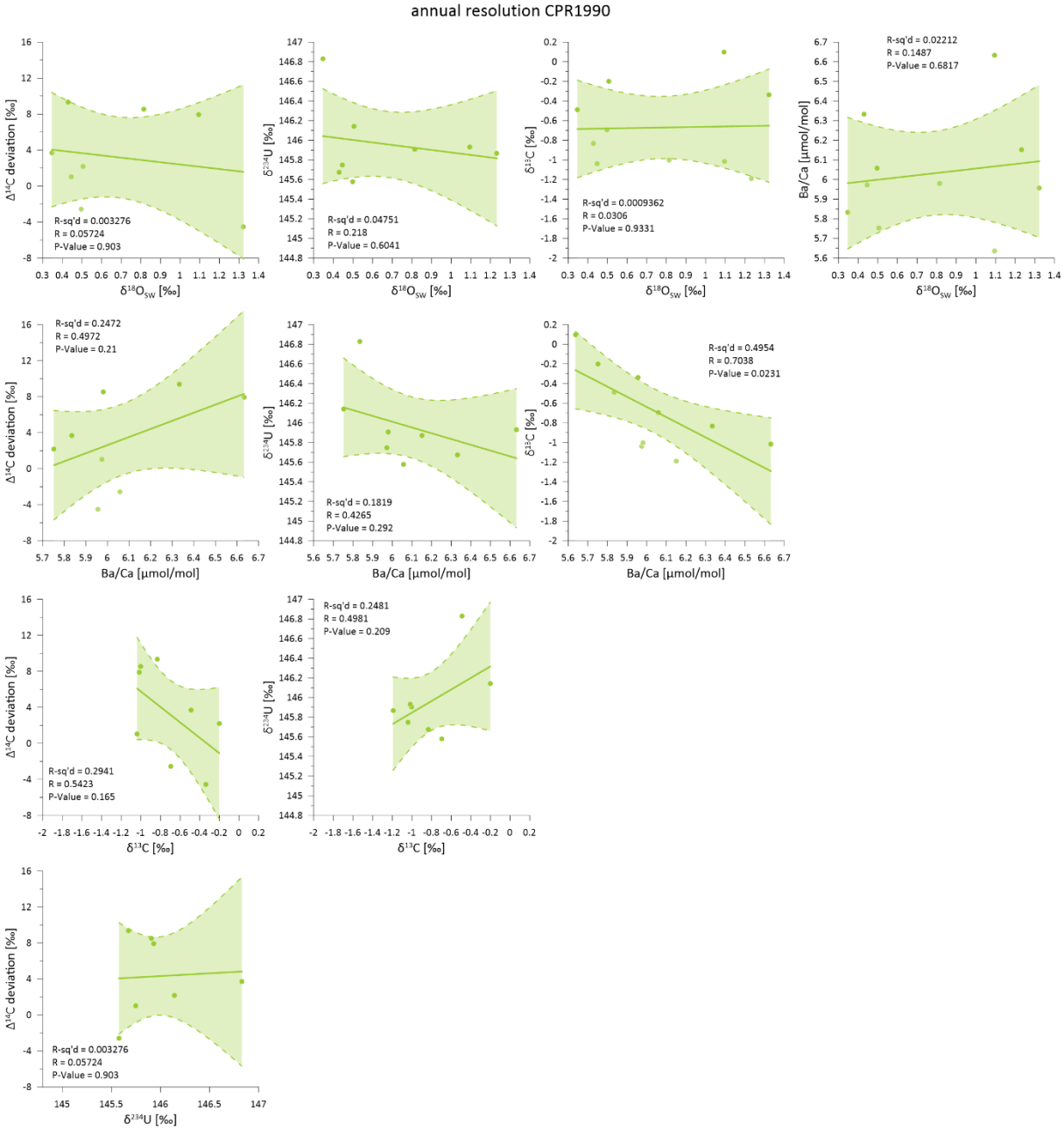

Figure B.8 Pairwise correlations between annually averaged geochemical proxies from the CPR1990 coral core. Green dots represent annual means; shaded areas show 95% confidence intervals around the linear regressions. Correlation coefficients (R), coefficients of determination (R^2), and p-values are indicated for each panel. The strongest statistically significant relationship was observed between Ba/Ca and $\delta^{13}C$ (R = 0.708, p = 0.023).

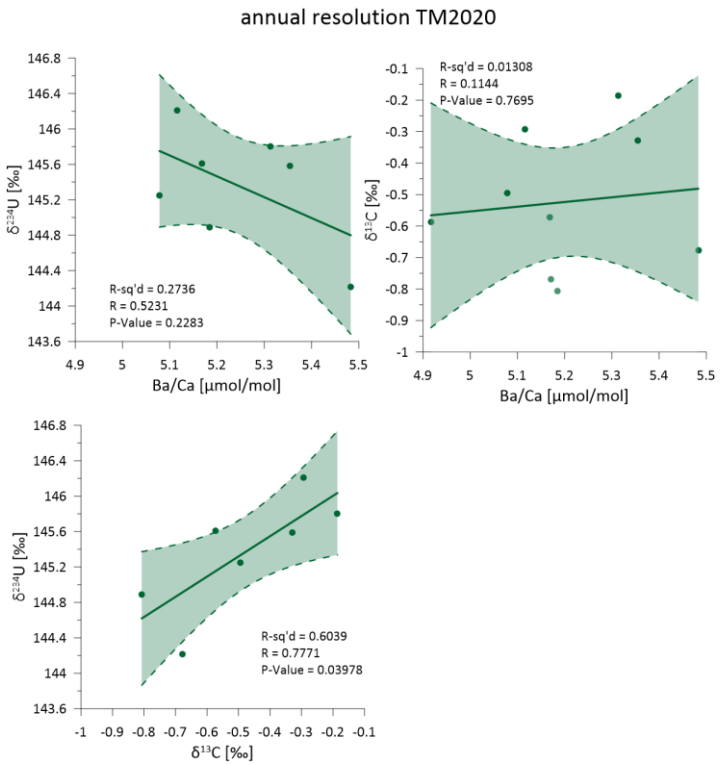

Figure B.9 Pairwise correlations between annually averaged geochemical proxies from the TM2020 coral core. Green dots represent annual means; shaded areas show 95% confidence intervals around the linear regressions. Correlation coefficients (R), coefficients of determination (R^2), and p-values are indicated for each panel.

The analysis of annual-resolution data (Figure B.**8** and Figure B.**9**) introduced two additional tracers, $\delta^{234}U$ and $\Delta^{14}C$, providing insights into water mass sourcing, residence time and potential subsurface processes. In the CPR core (Figure B.8), $\Delta^{14}C$ dominated the variance structure, accounting for 97.8% of the total variance and showing no significant correlation with any other proxy. This strongly suggests that the radiocarbon signal reflects oceanic processes, such as subsurface upwelling or changes in surface water reservoir age, rather than terrestrial freshwater input. While $\delta^{13}C$ and $\delta^{234}U$ co-loaded on PC2, their lack of significant statistical correlation indicates that any shared environmental signal is weak or inconsistent. As in the seasonal analysis, $\delta^{18}O_{sw}$ loaded separately, reinforcing its sensitivity to salinity-related variability and confirming its largely independent behaviour in the coral geochemical system.

In the TM annual dataset (Figure B.**9**), PCA revealed clear partitioning among proxies, with $\delta^{234}U$ explaining 88% of the total variance on PC1, indicating a highly consistent and dominant signal. Importantly, $\delta^{234}U$ showed a statistically significant correlation with $\delta^{13}C$ ($r = 0.7$, $p = 0.03$), suggesting a shared environmental influence, possibly related to subsurface freshwater inputs, groundwater discharge, or weathering-derived uranium. In contrast, Ba/Ca loaded predominantly on PC2 and PC3, with no

strong correlation to either $\delta^{13}C$ or $\delta^{234}U$, implying it responds to different, likely more surface-oriented or particulate-associated processes. The strong internal consistency of $\delta^{234}U$, combined with its distinct loading structure, supports its interpretation as a complementary tracer of time-integrated freshwater input, particularly valuable in settings where short-term runoff signals are weak or obscured by hydrodynamic complexity.

Across both sites and timescales, a consistent pattern emerges: no single proxy uniquely captures freshwater variability, while no single proxy uniquely captures freshwater variability, Ba/Ca and $\delta^{13}C$ together provide the most consistent surface signal. However, their partial sensitivity to biological and photic factors highlights the importance of interpreting them within an environmental context. $\delta^{18}O_{sw}$ provides useful information on salinity and hydrological balance, but its dual sensitivity to temperature and evaporation complicates its interpretation, especially in lagoonal settings.

By contrast, $\delta^{234}U$ stands out as a promising proxy for detecting geochemically distinct or time-integrated freshwater contributions, likely tied to subsurface flow paths or weathering regimes. Finally, $\Delta^{14}C$ emerges as a clear tracer of ocean circulation and water mass origin, independent of terrestrial inputs, offering complementary insights into offshore and vertical oceanographic dynamics.

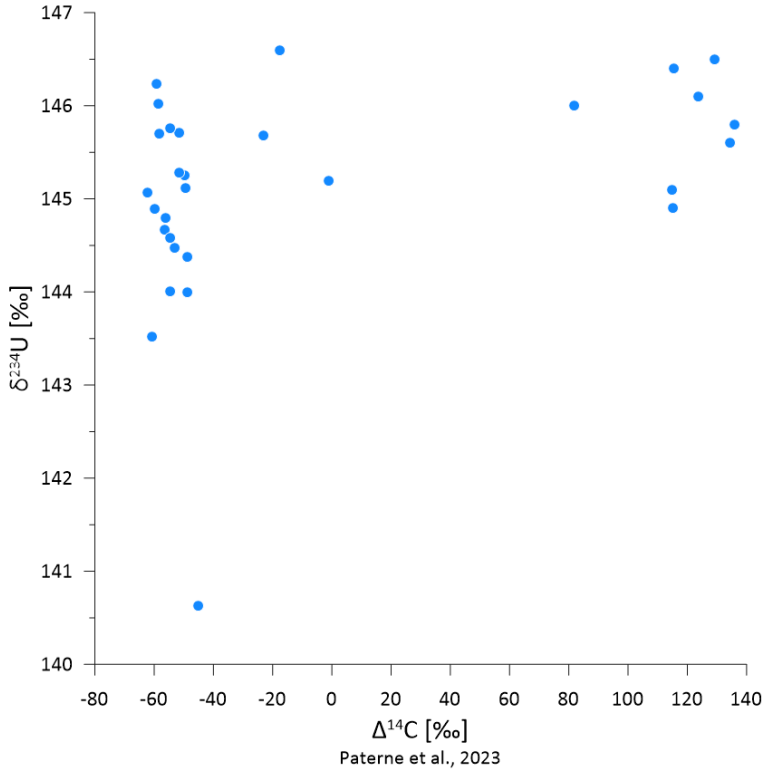

Figure B.10 Relationship between $\delta^{234}U$ (‰) and $\Delta^{14}C$ (‰) (Paterne et al., 2023) in the Martinique coral. No correlation is observed between $\delta^{234}U$ values and radiocarbon content, indicating that uranium isotopic composition in this coral is not influenced by the same processes controlling ^{14}C variability.

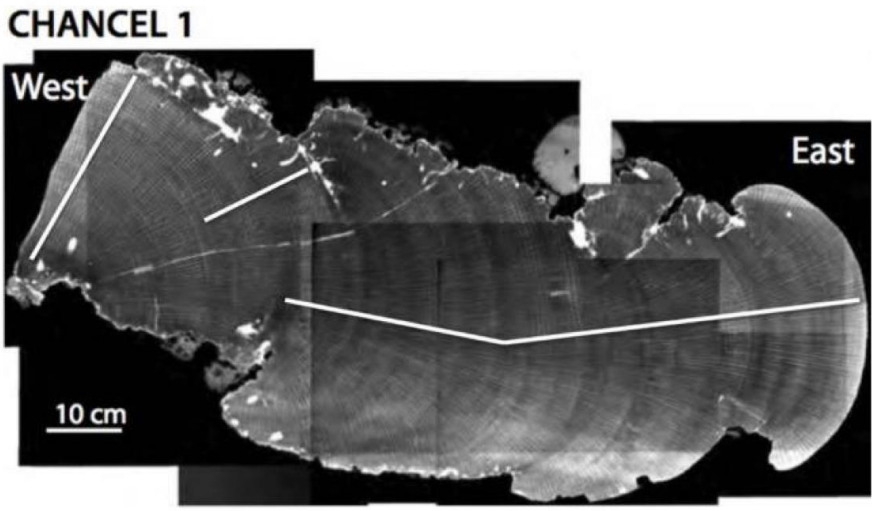

Figure B.11 X-radiograph of the Martinique microatoll (Chancel 1) of Siderastrea siderea, showing growth bands across the west–east transect. White lines indicate the sampled transects used for geochemical analyses. The clear annual density banding visible in the coral skeleton provides the chronological framework for age model development (Weil-Accardo et al., 2016).

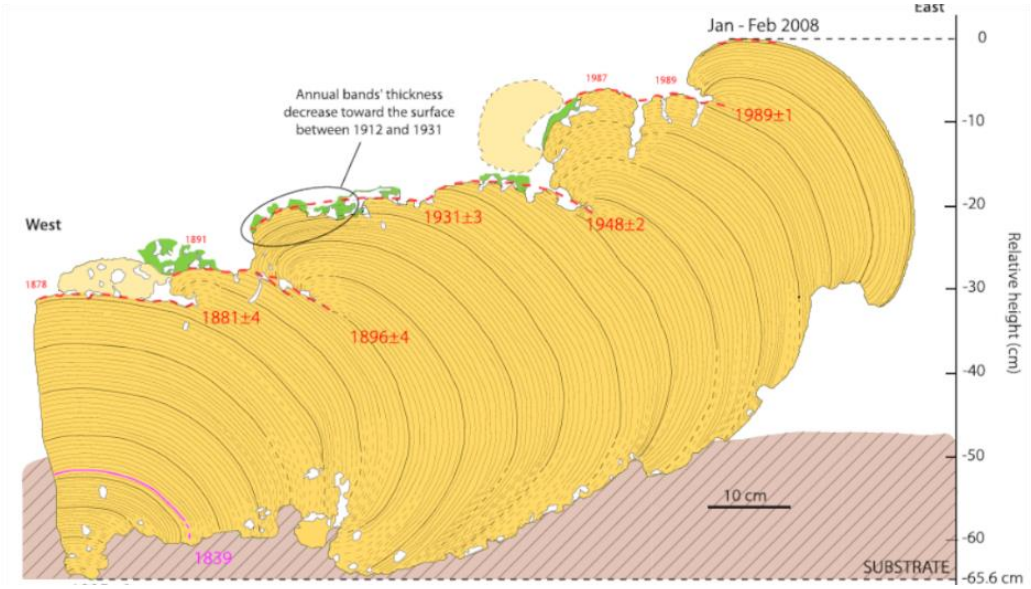

Figure B.12 Schematic representation of the Martinique microatoll (Chancel 1, Siderastrea siderea), illustrating annual growth bands and age assignments. Growth interruptions at the upper surface(red ages) indicate periods when the coral was episodically exposed above sea level and not submerged, preventing continuous vertical accretion (figure from (Weil-Accardo et al., 2016)).

Chapter 6

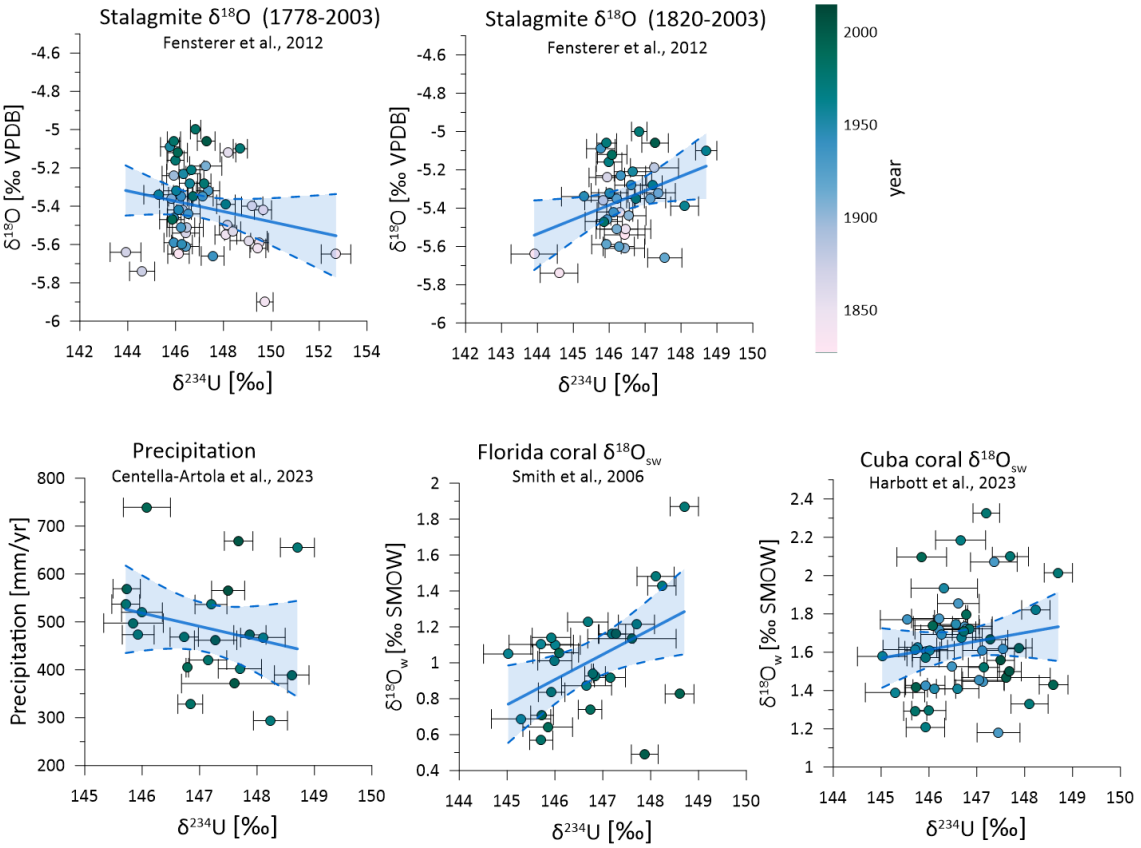

Figure B.13 Correlations between Cuban coral $\delta^{234}U$ and regional hydroclimate proxies over the past two centuries. Top panels show $\delta^{18}O$ from stalagmites (Fensterer et al., 2012) plotted against $\delta^{234}U$ for the full (1778–2003) and post-1820 intervals. Bottom panels compare $\delta^{234}U$ with annual precipitation from the Cuban coast (Centella-Artola et al., 2023), and coral $\delta^{18}O_w$ from Florida (Smith et al., 2006) and Cuba (Harbott et al., 2023) coral records. Shaded regions indicate 95% confidence intervals around linear regressions. Colour scale denotes sample year.

Supplementary Table B.1. $\delta^{18}O_w$ of a coral from the Florida Keys (Smith et al., 2006) was calculated with the SST calculated from Sr/Ca ratios by using the equation $^{Sr}/_{Ca} = -0.0282 * SST + 9.962$ (Smith et al., 2006) with this $SST_{Sr/Ca}$, the $\delta^{18}O_w$ is calculated from the measured $\delta^{18}O_C$ by $\delta^{18}O_W = ((SST_{Sr/Ca} - 5.33)/4.519) + \delta^{18}O_c$ (Leder et al., 1996; Ren et al., 2003).

year	$SST_{Sr/Ca}$ (°C)	$\delta^{18}O_w$ (‰ SMOW)
2002	29.54	1.16
2001	28.17	1.13
2000	27.76	1.04
1999	27.38	0.95
1998	24.81	0.49
1997	26.81	0.84
1996	25.89	0.71
1995	27.70	0.98
1994	27.57	0.99
1993	25.87	0.66
1992	26.33	0.83
1991	27.44	0.97

1990	28.94	1.11
1989	28.44	1.06
1988	26.64	0.81
1987	24.24	0.35
1986	26.51	0.64
1985	27.78	0.94
1984	28.28	1.06
1983	26.61	0.75
1982	26.21	0.74
1981	28.36	1.14
1980	26.02	0.68
1979	26.88	0.92
1978	25.70	0.71
1977	26.13	0.93
1976	24.54	0.57
1975	26.26	0.84
1974	25.22	0.57
1973	26.81	0.68
1972	27.02	0.92
1971	27.43	1.01
1970	27.22	0.99
1969	27.86	1.16
1968	28.03	1.21
1967	31.57	1.87
1966	29.80	1.49
1965	29.68	1.37
1964	28.91	1.48
1963	28.42	1.43
1962	28.79	1.47
1961	28.62	1.23
1960	29.20	1.40
1959	27.79	1.14
1958	26.76	0.87
1957	27.73	1.07
1956	29.22	1.42
1955	30.07	1.56
1954	30.32	1.52
1953	29.50	1.22
1952	28.52	1.21
1951	27.94	1.10
1950	27.89	1.05
1949	27.22	0.69
1948	29.25	1.10
1947	27.67	0.92

Chapter 7

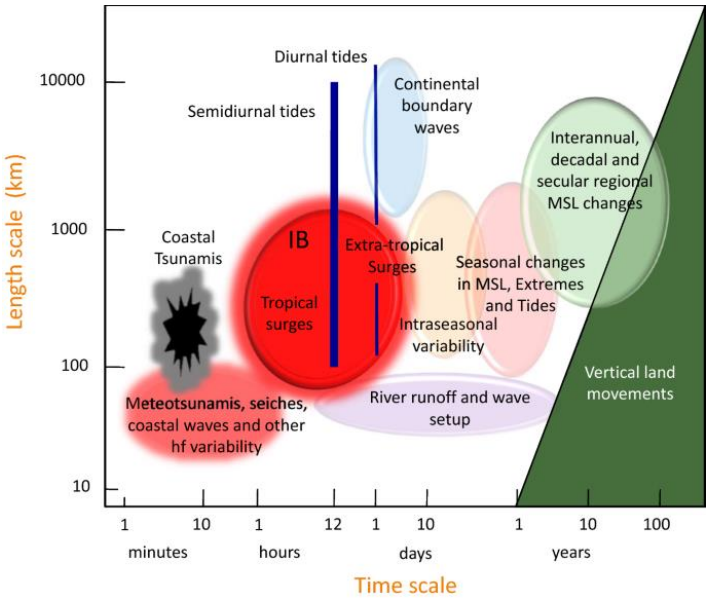

Figure B.14 Processes affecting sea level, shown as a function of their characteristic time scale (x-axis) and spatial impact (y-axis, length scale in km). Figure from (Woodworth et al., 2019).

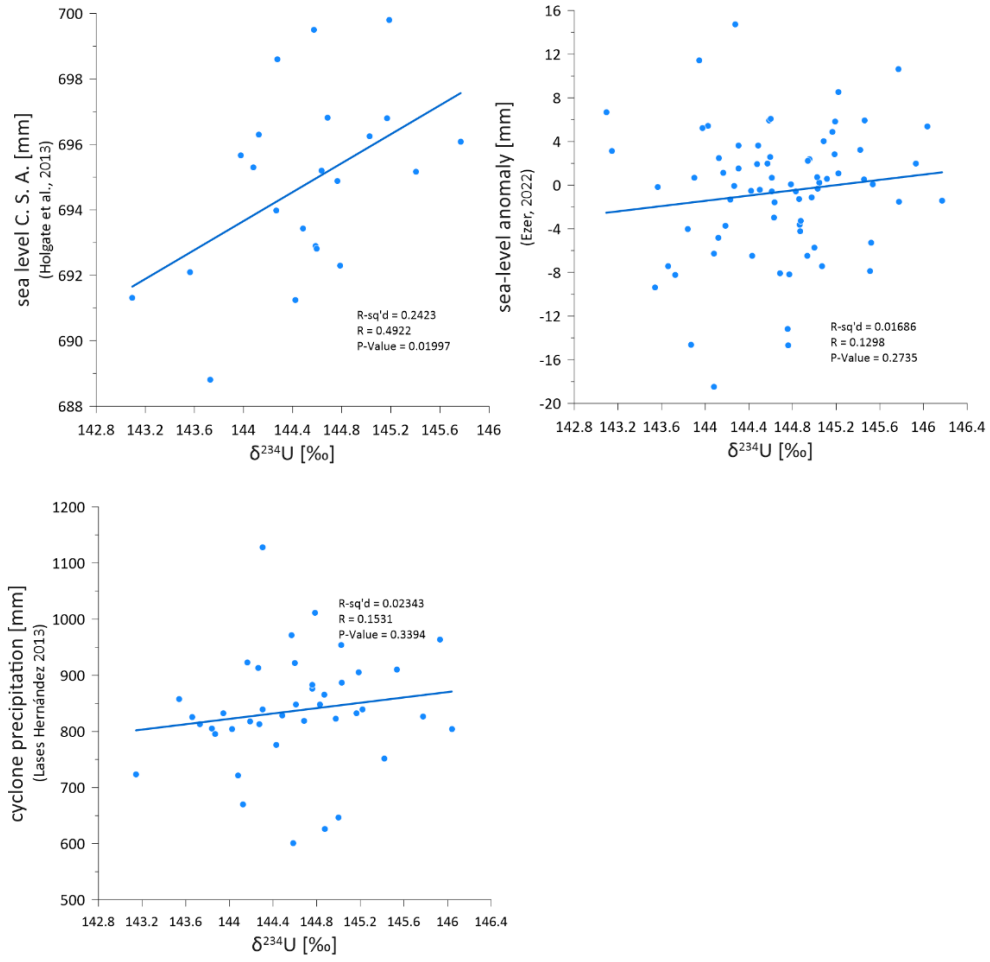

Figure B.15 Correlations between $\delta^{234}U$ (‰) in the Mexican coral and (a) tide gauge sea-level data (Holgate et al., 2013), (b) sea-level anomalies (Ezer, 2022), and (c) cyclone precipitation (Lases-Hernández, 2013).

Chapter 9

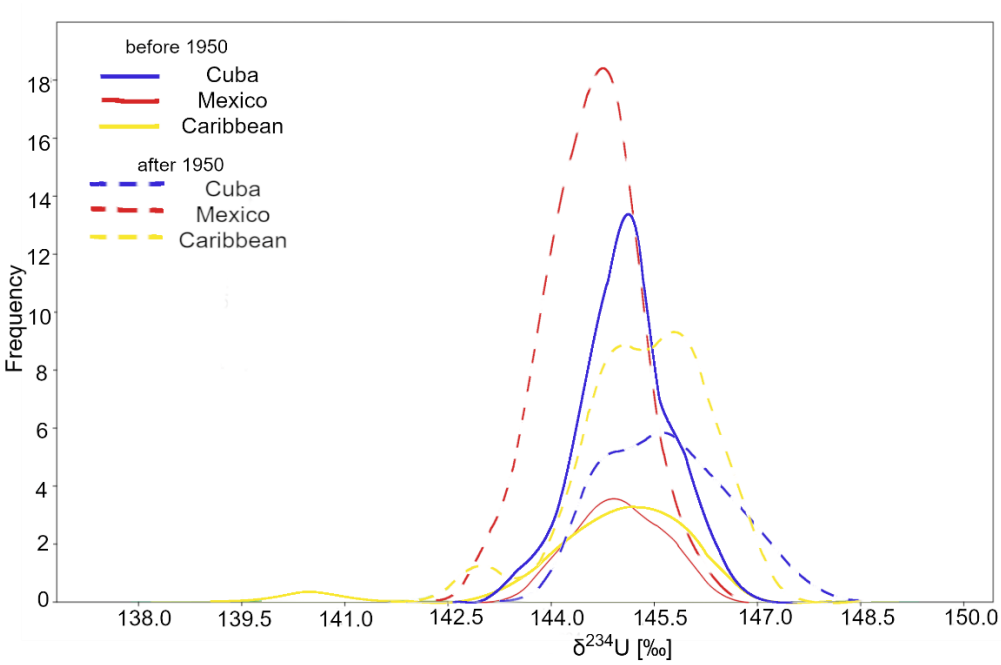

Figure B.16 KDE of coral $\delta^{234}U$ values before and after 1950 from Cuba (blue), Mexico (red) and the broader Caribbean (yellow) including Venezuela, Puerto Rico and Martinique. A slight elevation in values is seen in the Mexican and Caribbean values after 1950.

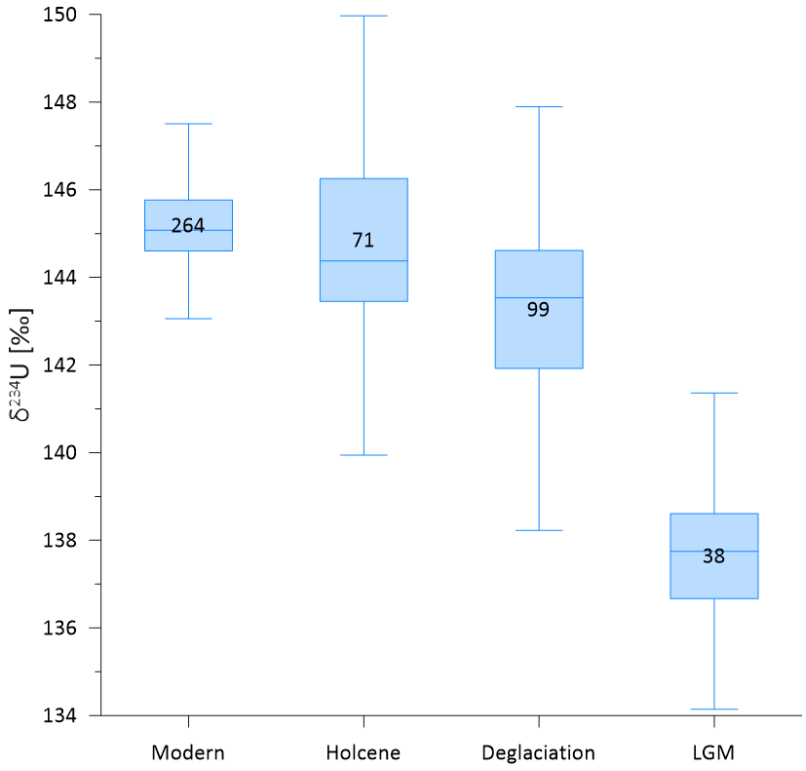

Figure B.17 Boxplot of coral $\delta^{234}U$ values grouped into four temporal intervals: modern (0–250 years), Holocene (0.25–11.7 ka), deglaciation (12–19 ka), and Last Glacial Maximum (19–26.5 ka). Each box shows the interquartile range (IQR), the horizontal line marks the median, and whiskers indicate the 5th–95th percentiles and sample count (n) written in the box.

C. Supplementary data

Table C.1 Cuban Species $\delta^{234}U$ measurements together with concentrations of ^{238}U and ^{234}U of annually integrated samples. $\delta^{234}U$ values are given normalised to HU-1 = 0 and HU-1 ≠ 0 after (Cheng et al., 2013). Measurement uncertainties are 2σ analytical errors

sample ID	sample lable	Year	$\delta^{234}U$ (‰) (HU-1 = 0)	$\delta^{234}U$ (‰) (HU-1 ≠ 0)	Error $\delta^{234}U$ (‰)	^{234}U (pg/g)	Error ^{234}U (pg/g)	^{238}U (µg/g)	Error ^{238}U (µg/g)
12477	RL_Siderastrea siderea	2015	147.21	146.01	0.59	147.20	0.31	2.37466	0.00016
12478	RL_Mycetophyllia lamarckiana	2015	146.85	145.65	0.44	139.05	0.25	2.24837	0.00010
12480	RL_Agaricia agaricites	2015	146.64	145.44	0.64	170.26	0.48	2.73821	0.00035
12481	RL_Meandrina meandites	2015	147.40	146.20	0.54	194.88	0.57	3.11970	0.00016
12482	RL_Acropora cervicornis	2015	146.82	145.62	0.50	174.16	0.53	2.79614	0.00016
12484	RL_Colpophyllia natans	2015	146.85	145.65	0.53	114.33	0.13	1.84539	0.00011
12485	RL_Diploria labyrinthifarmis	2015	146.41	145.21	0.62	142.79	0.17	2.30343	0.00017
12486	RL_Colpophyllia natans 2	2015	146.31	145.11	0.52	116.07	0.14	1.87722	0.00011
12487	RL_Montastraea cavernosa	2015	146.43	145.23	0.51	157.84	0.21	2.55018	0.00015
12490	RL_Orbicella faveolata	2015	146.67	145.47	0.58	160.94	0.44	2.58431	0.00017
12479	RL_Acropora palmata	2015	146.68	145.48	0.47	164.04	0.67	2.61844	0.00018

Table C.2 Volume test $\delta^{234}U$ measurements together with concentrations of ^{238}U and ^{234}U of annually integrated samples. $\delta^{234}U$ values are given normalised to HU-1 = 0 and HU-1 ≠ 0 after (Cheng et al., 2013). Measurement uncertainties are 2σ analytical errors

sample ID	sample lable	$\delta^{234}U$ (‰) (HU-1 = 0)	$\delta^{234}U$ (‰) (HU-1 ≠ 0)	Error $\delta^{234}U$ (‰)	^{234}U (pg/g)	Error ^{234}U (pg/g)	^{238}U (µg/g)	Error ^{238}U (µg/g)
12312	Mururoa 20mg	145.89	144.69	0.62	139.58	0.14	2.24378	0.00006
12313	Mururoa 40mg	147.52	146.32	1.16	140.36	0.61	2.22908	0.00013
12314	Mururoa 60mg	146.31	145.11	0.36	135.24	0.18	2.16803	0.00006
12315	Mururoa 70mg	147.03	145.83	0.33	137.25	0.20	2.20175	0.00006
12316	Mururoa 80mg	147.71	146.51	0.98	135.85	0.90	2.15256	0.00019
12318	Mururoa 100mg	145.12	143.92	0.38	135.85	0.44	2.17141	0.00011
12319	Mururoa 120mg	147.19	145.99	0.34	137.41	0.48	2.18193	0.00016
12320	Mururoa 150mg	147.73	146.53	0.42	136.10	0.23	2.16909	0.00007

Table C.3 ROQV $\delta^{234}U$ measurements together with concentrations of ^{238}U and ^{234}U of annually integrated samples. $\delta^{234}U$ values are given normalised to HU-1 = 0 and HU-1 ≠ 0 after (Cheng et al., 2013). Measurement uncertainties are 2σ analytical errors

sample ID	sample lable	Year	$\delta^{234}U$ (‰) (HU-1 = 0)	$\delta^{234}U$ (‰) (HU-1 ≠ 0)	Error $\delta^{234}U$ (‰)	^{234}U (pg/g)	Error ^{234}U (pg/g)	^{238}U (µg/g)	Error ^{238}U (µg/g)
12311	ROQV_1994.2	1993.5	146.11	144.91	0.33	155.65	0.31	2.50757	0.00011
12310	ROQV_1994.1	1994	146.00	144.80	0.35	155.54	0.30	2.50137	0.00011
12309	ROQV_1995.2	1994.5	145.60	144.40	0.39	160.49	0.35	2.59284	0.00010
12308	ROQV_1995.1	1995	145.85	144.65	0.33	161.45	0.33	2.60346	0.00011
12307	ROQV_1996.2	1995.5	147.08	145.88	0.54	160.79	0.48	2.58527	0.00014
12306	ROQV_1996.1	1996	146.12	144.92	0.36	156.80	0.36	2.53474	0.00009
12305	ROQV_1997.2	1996.5	146.23	145.03	0.33	158.56	0.37	2.56492	0.00011
12304	ROQV_1997.1	1997	145.90	144.70	0.33	154.98	0.34	2.50879	0.00011
12265	ROQV_1998.2	1997.5	145.19	143.99	0.55	298.41	1.15	4.87591	0.00025
12264	ROQV_1998.1	1998	147.97	146.77	0.57	154.54	0.32	2.49571	0.00015
12263	ROQV_1999.2	1998.5	145.65	144.45	0.47	96.14	0.16	1.55584	0.00009
12262	ROQV_1999.1	1999	147.53	146.33	0.55	149.29	0.36	2.40941	0.00013
12261	ROQV_2000.2	1999.5	147.86	146.66	0.57	147.11	0.41	2.36788	0.00015
12260	ROQV_2000.1	2000	146.02	144.82	0.47	128.50	0.44	2.08210	0.00011
12259	ROQV_2001.2	2000.5	144.02	142.82	1.29	147.49	1.14	2.39933	0.00152
12258	ROQV_2001.1	2001	145.43	144.23	0.48	146.22	0.53	2.36402	0.00015
12257	ROQV_2002.2	2001.5	147.38	146.18	0.58	146.95	0.61	2.37813	0.00030
12256	ROQV_2002.1	2002	147.02	145.82	0.56	138.28	0.31	2.23030	0.00044
12255	ROQV_2003.2	2002.5	146.67	145.47	0.44	146.68	0.56	2.35922	0.00054
12254	ROQV_2003.1	2003	146.42	145.22	0.58	147.75	0.40	2.38306	0.00012
12253	ROQV_2004.2	2003.5	146.02	144.82	0.60	144.22	0.50	2.32327	0.00017
12252	ROQV_2004.1	2004	146.45	145.25	0.48	146.90	0.33	2.36592	0.00014
12251	ROQV_2005.2	2004.5	146.39	145.19	0.42	147.42	0.45	2.36740	0.00016
13279	ROQV_seas_1996.75	1996.8	145.83	144.63	0.63	147.02	1.35	2.38661	0.00722
13281	ROQV_seas_1997.25	1997.3	147.22	146.02	0.79	156.56	1.62	2.49205	0.00145
13282	ROQV_seas_1997.5	1997.5	144.90	143.70	1.10	152.84	1.05	2.40777	0.00052

13283	ROQV_seas_1997.75	1997.8	145.89	144.69	0.82	153.31	0.15	2.46696	0.00018
13284	ROQV_seas_1998	1998	148.78	147.58	0.92	151.62	0.20	2.43739	0.00049
13286	ROQV_seas_1998.5	1998.5	146.52	145.32	0.47	152.61	0.22	2.44098	0.00011
13287	ROQV_seas_1998.75	1998.8	146.33	145.13	0.54	145.75	0.53	2.29657	0.00030
13288	ROQV_seas_1999	1999	144.89	143.69	0.74	148.44	1.07	2.36133	0.00169
13289	ROQV_seas_1999.25	1999.3	146.69	145.49	0.68	148.99	0.74	2.44441	0.00037
13290	ROQV_seas_1999.5	1999.5	145.47	144.27	0.66	148.19	0.88	2.41089	0.00045
13292	ROQV_seas_2000	2000	148.05	146.85	0.92	154.09	0.62	2.52346	0.00153
13293	ROQV_seas_2000.25	2000.3	146.49	145.29	0.62	153.35	1.81	2.43387	0.00109
13294	ROQV_seas_2000.5	2000.5	146.86	145.66	0.46	142.33	0.15	2.28296	0.00011
13295	ROQV_seas_2000.75	2000.8	147.01	145.81	0.43	157.09	0.43	2.43321	0.00021
13296	ROQV_seas_2001	2001	147.43	146.23	0.54	142.33	0.15	2.28296	0.00011

Table C.4 Puerto Rican $\delta^{234}U$ measurements together with concentrations of ^{238}U and ^{234}U of annually integrated samples. $\delta^{234}U$ values are given normalised to HU-1 = 0 and HU-1 ≠ O after (Cheng et al., 2013). Measurement uncertainties are 2σ analytical errors

sample ID	**sample lable**	**Year**	**$\delta^{234}U$ (‰) (HU-1 = 0)**	**$\delta^{234}U$ (‰) (HU-1 ≠ 0)**	**Error $\delta^{234}U$ (‰)**	**^{234}U (pg/g)**	**Error ^{234}U (pg/g)**	**^{238}U (µg/g)**	**Error ^{238}U (µg/g)**
13360	CPR1990_1a_1981	1981	147.07	145.87	0.18	183.74	0.34	2.94200	0.00019
13359	CPR1990_1a_1982	1982	146.78	145.58	0.66	141.63	1.18	2.83176	0.02263
13358	CPR1990_1a_1983	1983	146.95	145.75	0.74	124.08	0.56	2.90931	0.01706
13357	CPR1990_1a_1984	1984	148.03	146.83	0.96	169.46	0.50	2.71700	0.00024
13356	CPR1990_1a_1985	1985	147.11	145.91	0.62	169.30	0.04	0.27197	0.00002
13355	CPR1990_1a_1986	1986	147.13	145.93	0.62	128.36	0.58	3.01138	0.03506
13354	CPR1990_1a_1987	1987	146.88	145.68	0.78	175.84	0.80	2.85215	0.00049
13353	CPR1990_1a_1988	1988	144.26	143.06	0.62	183.95	0.79	2.88517	0.02332
13352	CPR1990_1a_1989	1989	147.34	146.14	0.67	149.92	0.61	2.70851	0.02761
13349	TM2020_1_1982	1934 ± 5	146.09	144.89	0.74	141.46	0.42	2.72213	0.03483
13348	TM2020_1_1983	1935 ± 5	146.45	145.25	0.74	173.47	0.81	2.69964	0.04600
13347	TM2020_1_1984	1936 ± 5	145.41	144.21	0.43	120.90	1.47	2.68715	0.01542
13346	TM2020_1_1985	1937 ± 5	146.79	145.59	0.70	165.56	0.41	2.64644	0.00021

13345	TM2020_1_1986	1938 ± 5	147.00	145.80	0.22	164.81	0.42	2.62963	0.00019
13344	TM2020_1_1987	1939 ± 5	147.41	146.21	0.37	149.57	1.60	2.53683	0.00828
13343	TM2020_1_1988	1940 ± 5	146.81	145.61	0.06	161.44	0.48	2.56460	0.00026
13342	TM2020_1_1989	1941 ± 5	147.70	146.50	0.82	148.90	0.83	2.76074	0.02477
13341	TM2020_1_1990	1942 ± 5	148.49	147.29	0.69	148.47	0.63	2.79512	0.08090
13338	TM2020_1_2013	1977.5 ± 3.5	146.76	145.56	0.11	153.00	0.41	2.64169	0.04124
13337	TM2020_1_2014	1978.5 ± 3.5	146.26	145.06	0.38	165.24	0.54	2.62953	0.00028
13336	TM2020_1_2015	1979.5 ± 3.5	147.70	146.50	0.42	156.33	4.58	2.53171	0.07792
13334	TM2020_1_2017	1980.5 ± 3.5	147.95	146.75	0.80	186.49	1.38	2.69745	0.02599
13333	TM2020_1_2018	1981.5 ± 3.5	147.18	145.98	0.16	153.80	5.15	2.67785	0.00247
13332	TM2020_1_2019	1982.5 ± 3.5	147.06	145.86	0.82	164.27	3.22	2.84013	0.08805
13331	TM2020_1_2020	1983.5 ± 3.5	146.88	145.68	0.60	164.48	0.86	2.68518	0.00040

Table C.5 Chancel_1 $\delta^{234}U$ measurements together with concentrations of ^{238}U and ^{234}U of annually integrated samples. $\delta^{234}U$ values are given normalised to HU-1 = 0 and HU-1 ≠ 0 after (Cheng et al., 2013). Measurement uncertainties are 2σ analytical errors

sample ID	**sample lable**	**Year**	**$\delta^{234}U$ (‰) (HU-1 = 0)**	**$\delta^{234}U$ (‰) (HU-1 ≠ 0)**	**Error $\delta^{234}U$ (‰)**	**^{234}U (pg/g)**	**Error ^{234}U (pg/g)**	**^{238}U (µg/g)**	**Error ^{238}U (µg/g)**
12781	Chancel_1_1887	1887	145.68	144.48	0.75	149.40	0.63	2.41084	0.00015
12782	Chancel_1_1888	1888	146.46	145.26	0.71	169.55	1.08	2.73752	0.00032
12783	Chancel_1_1890	1890	146.90	145.70	0.61	152.91	0.92	2.49200	0.00330
12784	Chancel_1_1891	1891	145.20	144.00	0.70	180.31	2.55	3.01859	0.00300
12785	Chancel_1_1893	1893	146.00	144.80	0.50	192.71	2.29	3.09978	0.00043
12786	Chancel_1_1894	1894	141.83	140.63	0.18	166.91	1.24	2.71868	0.00494
12787	Chancel_1_1895	1895	146.32	145.12	0.32	159.55	0.79	2.58196	0.00022
12788	Chancel_1_1900	1900	145.57	144.37	0.75	211.68	3.06	3.33359	0.00067
12791	Chancel_1_1925	1925	146.91	145.71	0.15	157.85	1.47	2.59821	0.00041
12793	Chancel_1_1927	1927	145.87	144.67	0.64	159.73	1.26	2.60614	0.00041
12794	Chancel_1_1928	1928	144.72	143.52	0.49	165.16	1.61	2.71916	0.00133
12795	Chancel_1_1929	1929	147.43	146.23	0.00	161.59	1.28	2.66918	0.00094
12796	Chancel_1_1930	1930	145.21	144.01	0.70	163.97	1.82	2.70942	0.00203

12797	Chancel_1_1931	1931	146.27	145.07	0.35	160.38	0.88	2.59537	0.00025
12798	Chancel_1_1934	1934	146.09	144.89	0.01	156.82	1.18	2.55899	0.00042
12799	Chancel_1_1935	1935	146.48	145.28	0.31	163.87	0.71	2.64864	0.00026
12800	Chancel_1_1940	1940	145.78	144.58	0.53	168.69	1.58	2.74518	0.00070
12801	Chancel_1_1945	1945	147.22	146.02	0.08	157.24	2.15	2.58842	0.00082
12802	Chancel_1_1950	1950	146.96	145.76	0.14	154.67	2.23	2.58264	0.00054
12804	Chancel_1_1957	1957	146.88	145.68	0.08	154.07	1.51	2.50038	0.00073
12805	Chancel_1_1958	1958	147.80	146.60	0.70	165.05	1.32	2.67027	0.00042
12806	Chancel_1_1961	1961	146.40	145.20	0.29	160.57	1.03	2.60172	0.00026
12807	Chancel_1_1964	1964	147.21	146.01	0.60	160.85	0.74	2.60662	0.00020
12810	Chancel_1_1968	1968	147.70	146.50	0.60	192.96	2.57	3.10219	0.00047
12812	Chancel_1_1972	1972	146.80	145.60	0.70	155.75	1.34	2.50156	0.00056
12813	Chancel_1_1973	1973	147.00	145.80	0.70	175.86	1.26	2.65972	0.00048
12815	Chancel_1_1976	1976	147.30	146.10	0.50	167.42	1.17	2.57861	0.00059
12816	Chancel_1_1978	1978	147.60	146.40	0.50	167.62	2.67	2.67842	0.00034
12817	Chancel_1_1981	1981	146.30	145.10	0.40	158.54	1.15	2.59454	0.00028
12818	Chancel_1_1982	1982	146.10	144.90	0.70	163.49	1.57	2.78924	0.00045

Table C.6 CSM_1 $\delta^{234}U$ measurements together with concentrations of ^{238}U and ^{234}U of annually integrated samples. $\delta^{234}U$ values are given normalised to HU-1 = 0 and HU-1 ≠ 0 after (Cheng et al., 2013). Measurement uncertainties are 2σ analytical errors

sample ID	**sample lable**	**Year**	**$\delta^{234}U$ (‰) (HU-1 = 0)**	**$\delta^{234}U$ (‰) (HU-1 ≠ 0)**	**Error $\delta^{234}U$ (‰)**	**^{234}U (pg/g)**	**Error ^{234}U (pg/g)**	**^{238}U (µg/g)**	**Error ^{238}U (µg/g)**
12021	CSM_1_1777	1777	147.00	145.80	0.39	152.59	0.44	2.42213	0.00010
12037	CSM_1_1778	1778	146.57	145.37	0.51	144.06	0.70	2.27359	0.00035
12022	CSM_1_1780	1780	148.07	146.87	0.57	143.30	0.61	2.26880	0.00012
12023	CSM_1_1783	1783	146.12	144.92	0.45	151.19	0.35	2.37845	0.00012
12039	CSM_1_1784	1784	145.15	143.95	0.43	153.88	0.56	2.44541	0.00014
12039	CSM_1_1784	1784	145.93	144.73	0.48	151.61	0.55	2.44541	0.00014
12024	CSM_1_1786	1786	149.65	148.45	0.36	151.17	0.40	2.38237	0.00009
12025	CSM_1_1789	1789	149.51	148.31	0.37	145.86	0.35	2.28090	0.00008

12026	CSM_1_1792	1792	152.70	151.50	0.62	152.70	0.53	2.40982	0.00014
12042	CSM_1_1793	1793	148.06	146.86	0.74	147.37	1.37	2.32583	0.00053
12027	CSM_1_1795	1795	149.73	148.53	0.34	154.70	0.40	2.44896	0.00011
12043	CSM_1_1796	1796	146.05	144.85	0.50	155.12	0.75	2.44817	0.00032
12028	CSM_1_1798	1798	149.44	148.24	0.33	162.69	0.48	2.57655	0.00011
12029	CSM_1_1801	1801	148.10	146.90	0.46	158.76	0.74	2.47612	0.00014
12030	CSM_1_1804	1804	149.20	148.00	0.44	154.93	0.47	2.46215	0.00012
12032	CSM_1_1810	1810	148.16	146.96	0.33	159.03	0.37	2.54664	0.00010
12033	CSM_1_1813	1813	148.19	146.99	0.33	161.74	0.56	2.60148	0.00012
12034	CSM_1_1816	1816	149.05	147.85	0.78	109.21	0.58	1.75896	0.00011
12035	CSM_1_1819	1819	148.38	147.18	0.34	156.45	0.46	2.49199	0.00010
12085	CSM_1_1826	1826	146.43	145.23	0.57	162.14	0.39	2.61460	0.00011
12742	CSM_1_1830	1830	145.55	144.35	0.50	162.89	0.74	2.65195	0.00019
12086	CSM_1_1831	1831	144.91	143.71	0.64	154.86	0.83	2.46227	0.00019
12237	CSM_1_1833	1833	147.00	145.80	0.71	174.42	0.21	2.76123	0.00007
12743	CSM_1_1835	1835	146.97	145.77	0.49	172.83	0.69	2.80582	0.00017
12087	CSM_1_1836	1836	144.60	143.40	0.52	160.43	0.66	2.59963	0.00018
12088	CSM_1_1841	1841	146.84	145.64	0.56	152.50	0.88	2.43149	0.00017
12089	CSM_1_1846	1846	146.45	145.25	0.71	153.65	1.00	2.48071	0.00022
12090	CSM_1_1851	1851	146.29	145.09	0.36	156.02	0.36	2.51152	0.00010
12091	CSM_1_1856	1856	146.48	145.28	0.47	156.50	0.59	2.49942	0.00014
12092	CSM_1_1861	1861	146.05	144.85	0.51	157.41	0.63	2.54989	0.00015
12243	CSM_1_1863	1863	146.91	145.71	0.60	178.40	0.34	2.80513	0.00011
12093	CSM_1_1866	1866	145.93	144.73	0.50	155.21	0.50	2.51000	0.00012
12094	CSM_1_1871	1871	145.82	144.62	0.50	158.06	0.68	2.55106	0.00015
12245	CSM_1_1873	1873	145.29	144.09	0.56	172.51	1.01	2.71382	0.00024
12095	CSM_1_1876	1876	147.81	146.61	0.49	164.82	0.62	2.65627	0.00014
12246	CSM_1_1878	1878	146.52	145.32	0.62	180.49	0.80	2.90753	0.00019
12246	CSM_1_1878	1878	145.74	144.54	0.40	180.28	0.60	2.90794	0.00016
12096	CSM_1_1881	1881	147.26	146.06	0.67	161.91	0.71	2.63037	0.00020

12247	CSM_1_1883	1883	145.86	144.66	0.70	180.41	0.55	2.91539	0.00015
12247	CSM_1_1883	1883	146.23	145.03	0.43	180.81	0.42	2.91486	0.00012
12248	CSM_1_1888	1888	146.26	145.06	0.41	180.79	0.55	2.91405	0.00015
12248	CSM_1_1888	1888	146.27	145.07	0.45	181.79	0.73	2.91448	0.00017
12098	CSM_1_1891	1891	146.31	145.11	0.58	165.23	0.37	2.66403	0.00012
12250	CSM_1_1898	1898	146.40	145.20	0.47	108.60	0.22	1.75415	0.00021
12250	CSM_1_1898	1898	146.15	144.95	0.52	108.21	0.27	1.30571	0.00009
12009	CSM_1_1901	1901	146.43	145.23	0.55	156.06	0.64	2.49575	0.00014
12008	CSM_1_1903	1903	146.54	145.34	0.49	154.28	0.59	2.48686	0.00012
12007	CSM_1_1905	1905	146.75	145.55	0.58	154.00	0.52	2.48983	0.00013
12006	CSM_1_1907	1907	147.45	146.25	0.45	151.55	0.53	2.43363	0.00011
12005	CSM_1_1908	1908	147.36	146.16	0.49	142.45	0.54	2.31126	0.00013
12004	CSM_1_1909	1909	146.61	145.41	0.44	153.61	0.63	2.45685	0.00015
12003	CSM_1_1910	1910	146.22	145.02	0.58	159.71	0.89	2.49557	0.00019
12002	CSM_1_1911	1911	146.77	145.57	0.53	147.50	0.61	2.32692	0.00014
11850	CSM_1_1912	1912	147.14	145.94	0.43	148.99	0.60	2.36703	0.00012
12001	CSM_1_1913	1913	146.49	145.29	0.67	148.97	1.10	2.34173	0.00020
12000	CSM_1_1915	1915	145.55	144.35	0.57	150.67	0.58	2.38999	0.00014
11999	CSM_1_1916	1916	146.22	145.02	0.51	147.05	0.56	2.32909	0.00012
11851	CSM_1_1917	1917	147.55	146.35	0.48	148.37	0.50	2.35604	0.00013
11998	CSM_1_1918	1918	147.05	145.85	0.52	143.79	0.58	2.26205	0.00013
11997	CSM_1_1919	1919	145.92	144.72	0.41	140.69	0.64	2.22103	0.00013
11996	CSM_1_1920	1920	147.11	145.91	0.41	134.46	0.47	2.13877	0.00011
11993	CSM_1_1921	1921	145.97	144.77	0.30	154.46	0.15	2.50315	0.00005
11852	CSM_1_1922	1922	147.07	145.87	0.51	151.02	0.59	2.43088	0.00019
11852	CSM_1_1922	1922	146.61	145.41	0.44	146.90	0.33	2.36592	0.00014
11992	CSM_1_1923	1923	145.94	144.74	0.29	160.20	0.27	2.57318	0.00008
11991	CSM_1_1924	1924	145.98	144.78	0.22	155.20	0.15	2.51104	0.00005
11990	CSM_1_1925	1925	146.26	145.06	0.43	151.19	0.28	2.44404	0.00008
11853	CSM_1_1927	1927	145.94	144.74	0.21	149.59	0.11	2.41882	0.00004

11988	CSM_1_1928	1928	145.60	144.40	0.24	147.59	0.18	2.38818	0.00005
11987	CSM_1_1929	1929	146.57	145.37	0.48	157.73	0.64	2.55735	0.00015
11986	CSM_1_1930	1930	145.38	144.18	0.68	138.11	0.75	2.20027	0.00018
11985	CSM_1_1931	1931	146.32	145.12	0.36	137.84	0.40	2.24588	0.00010
11854	CSM_1_1932	1932	146.11	144.91	0.45	152.45	0.55	2.46002	0.00012
11983	CSM_1_1935	1935	146.27	145.07	0.32	153.59	0.36	2.49154	0.00009
11982	CSM_1_1936	1936	146.32	145.12	0.69	148.15	1.05	2.42380	0.00026
11855	CSM_1_1937	1937	145.73	144.53	0.75	154.36	1.27	2.46899	0.00024
11981	CSM_1_1938	1938	145.76	144.56	0.40	154.39	0.53	2.51621	0.00012
11980	CSM_1_1939	1939	145.62	144.42	0.29	145.61	0.26	2.36179	0.00007
11979	CSM_1_1941	1941	146.60	145.40	0.44	154.11	0.57	2.48011	0.00013
11856	CSM_1_1942	1942	146.34	145.14	0.41	147.62	0.45	2.40337	0.00011
11978	CSM_1_1944	1944	145.71	144.51	0.67	134.27	0.53	2.17744	0.00012
11977	CSM_1_1945	1945	145.29	144.09	0.62	150.82	0.80	2.38667	0.00015
11976	CSM_1_1946	1946	145.02	143.82	0.52	135.07	0.60	2.15260	0.00013
11857	CSM_1_1947	1947	146.01	144.81	0.52	145.84	0.71	2.33466	0.00013
11970	CSM_1_1954	1954	146.66	145.46	0.52	146.68	0.50	2.35754	0.00011
11969	CSM_1_1955	1955	145.93	144.73	0.40	155.47	0.43	2.50060	0.00011
11859	CSM_1_1957	1957	146.69	145.49	0.42	147.23	0.29	2.37460	0.00009
11933	CSM_1_1959	1959	148.23	147.03	0.30	152.74	0.31	2.39127	0.00008
11932	CSM_1_1960	1960	148.10	146.90	0.39	143.46	0.32	2.23839	0.00008
11931	CSM_1_1963	1963	148.70	147.50	0.30	168.75	0.36	2.43135	0.00008
11930	CSM_1_1964	1964	147.70	146.50	0.38	158.54	0.53	2.48707	0.00013
11929	CSM_1_1965	1965	147.20	146.00	0.28	151.70	0.25	2.40619	0.00007
11861	CSM_1_1967	1967	146.00	144.80	0.36	150.38	0.23	2.43263	0.00007
11928	CSM_1_1968	1968	147.15	145.95	0.32	133.64	0.23	2.10927	0.00007
11926	CSM_1_1970	1970	145.71	144.51	0.24	152.46	0.20	2.41220	0.00006
11925	CSM_1_1971	1971	145.93	144.73	0.28	159.25	0.22	2.50958	0.00007
11924	CSM_1_1973	1973	146.84	145.64	0.22	153.26	0.15	2.42868	0.00005
11923	CSM_1_1978	1978	146.73	145.53	0.25	150.17	0.22	2.41358	0.00006

11862	CSM_1_1981	1981	146.79	145.59	0.02	147.22	0.63	2.39343	0.00014
11864	CSM_1_1982	1982	145.85	144.65	0.52	140.01	0.57	2.24503	0.00014
11894	CSM_1_1985	1985	146.08	144.88	0.41	146.10	0.35	2.36433	0.00010
11866	CSM_1_1992	1992	145.73	144.53	0.24	142.36	0.18	2.29424	0.00006
11892	CSM_1_1994	1994	147.88	146.68	0.28	145.25	0.38	2.32208	0.00011
11876	CSM_1_1998	1998	147.28	146.08	0.37	79.18	0.12	1.27193	0.00004
11875	CSM_1_1999	1999	147.68	146.48	0.25	130.65	0.19	2.09186	0.00006
11874	CSM_1_2003	2003	147.50	146.30	0.29	143.38	0.41	2.29588	0.00011
11870	CSM_1_2012	2012	146.16	144.96	0.78	129.87	0.77	2.05394	0.00017
11872	CSM_1_2013	2013	146.82	145.62	0.44	138.60	0.47	2.21898	0.00010
11871	CSM_1_2014	2014	146.77	145.57	0.52	130.13	0.52	2.07838	0.00011

Table C.7 BOC_1 and BOC_2 $\delta^{234}U$ measurements together with concentrations of ^{238}U and ^{234}U of annually integrated samples. $\delta^{234}U$ values are given normalised to HU-1 = 0 and HU-1 ≠ 0 after (Cheng et al., 2013). Measurement uncertainties are 2σ analytical errors

sample ID	**sample lable**	**Year**	**$\delta^{234}U$ (‰) (HU-1 = 0)**	**$\delta^{234}U$ (‰) (HU-1 ≠ 0)**	**Error $\delta^{234}U$ (‰)**	**^{234}U (pg/g)**	**Error ^{234}U (pg/g)**	**^{238}U (µg/g)**	**Error ^{238}U (µg/g)**
12662	BOC_2_piece_1994	1994	146.56	145.36	0.41	176.39	0.57	2.84157	0.00016
12663	BOC_2_piece_1995	1995	146.90	145.70	0.46	173.85	0.40	2.79826	0.00012
12664	BOC_2_piece_1996	1996	146.40	145.20	0.46	170.72	0.45	2.76238	0.00013
12665	BOC_2_piece_1997	1997	146.55	145.35	0.40	176.94	0.58	2.85947	0.00020
12666	BOC_2_piece_1998	1998	146.58	145.38	0.43	179.63	0.67	2.91201	0.00017
12667	BOC_2_piece_1999	1999	146.18	144.98	0.45	180.57	0.48	2.91889	0.00018
12668	BOC_2_piece_2001	2001	145.34	144.14	0.40	171.35	0.51	2.78035	0.00014
12669	BOC_2_piece_2002	2002	146.24	145.04	0.42	173.65	0.54	2.82173	0.00016
12670	BOC_2_piece_2003	2003	146.23	145.03	0.20	181.23	0.23	2.92659	0.00007
12671	BOC_2_piece_2004	2004	146.15	144.95	0.52	174.24	0.43	2.82595	0.00014
12672	BOC_2_piece_2005	2005	145.90	144.70	0.49	176.21	0.70	2.86372	0.00013
12673	BOC_2_piece_2006	2006	146.38	145.18	0.54	180.24	0.70	2.94112	0.00022
12674	BOC_2_piece_2007	2007	146.39	145.19	0.49	173.31	0.51	2.81876	0.00015
12675	BOC_2_piece_2008	2008	146.20	145.00	0.42	168.10	0.50	2.73091	0.00015

12676	BOC_2_piece_2009	2009	145.85	144.65	0.49	174.77	0.53	2.83265	0.00017
12677	BOC_2_piece_2010	2010	145.54	144.34	0.47	170.15	0.55	2.75220	0.00016
12678	BOC_2_piece_2011	2011	147.11	145.91	0.44	165.29	0.52	2.68210	0.00011
12679	BOC_2_piece_2012	2012	147.02	145.82	0.44	163.26	0.44	2.64808	0.00019
12680	BOC_2_piece_2013	2013	146.46	145.26	0.45	164.58	0.44	2.66412	0.00016
12682	BOC_2_piece_2015	2015	145.82	144.62	0.46	159.45	0.47	2.58012	0.00019
12581	BOC_2_pulver_2005	2005	146.88	145.68	0.55	175.27	0.41	2.82260	0.00013
12582	BOC_2_pulver_2006	2006	146.37	145.17	0.60	182.29	0.79	2.93549	0.00025
12583	BOC_2_pulver_2007	2007	147.05	145.85	0.56	175.27	0.41	2.82260	0.00013
12584	BOC_2_pulver_2008	2008	146.54	145.34	0.56	167.96	0.60	2.71213	0.00019
12585	BOC_2_pulver_2009	2009	145.78	144.58	0.56	173.59	0.60	2.82018	0.00017
12586	BOC_2_pulver_2010	2010	145.25	144.05	0.54	160.24	0.58	2.57853	0.00017
12587	BOC_2_pulver_2011	2011	145.22	144.02	0.59	162.26	0.68	2.60320	0.00019
12588	BOC_2_pulver_2012	2012	146.73	145.53	0.60	159.20	0.67	2.56244	0.00018
12589	BOC_2_pulver_2013	2013	145.47	144.27	0.64	167.09	0.83	2.67359	0.00024
12590	BOC_2_pulver_2014	2014	145.98	144.78	0.46	167.60	0.52	2.68783	0.00015
12558	BOC_1_pulver_2007	2007	145.81	144.61	0.69	168.35	0.89	2.70404	0.00097
12559	BOC_1_pulver_2008	2008	146.10	144.90	0.53	181.16	0.68	2.91181	0.00020
12560	BOC_1_pulver_2009	2009	146.33	145.13	0.46	168.46	0.51	2.71257	0.00013
12561	BOC_1_pulver_2010	2010	145.92	144.72	0.51	175.53	0.68	2.81771	0.00018
12562	BOC_1_pulver_2011	2011	145.38	144.18	0.58	186.13	0.68	2.98531	0.00020
12563	BOC_1_pulver_2012	2012	147.32	146.12	0.61	169.52	0.46	2.72677	0.00013
12564	BOC_1_pulver_2013	2013	145.94	144.74	0.46	164.82	0.60	2.66585	0.00012
12565	BOC_1_pulver_2014	2014	146.20	145.00	0.57	158.26	0.70	2.53675	0.00016
12566	BOC_1_pulver_2015	2015	145.95	144.75	0.53	164.21	0.63	2.64247	0.00023
12567	BOC_1_pulver_2016	2016	146.58	145.38	0.49	159.24	0.50	2.55828	0.00012
12896	BOC_1_piece_1905	1905	146.32	145.12	0.56	175.57	0.86	2.82859	0.00022
12895	BOC_1_piece_1908	1908	145.83	144.63	0.48	172.38	0.27	2.77651	0.00017
12894	BOC_1_piece_1911	1911	146.25	145.05	0.56	166.43	0.67	2.69292	0.00017
12893	BOC_1_piece_1914	1914	146.06	144.86	0.48	172.54	0.81	2.79386	0.00014

12892	BOC_1_piece_1917	1917	145.70	144.50	0.54	167.16	0.66	2.71631	0.00021
12891	BOC_1_piece_1920	1920	145.10	143.90	0.42	168.93	0.74	2.72796	0.00018
12890	BOC_1_piece_1923	1923	146.15	144.95	0.56	170.35	0.71	2.75870	0.00021
12889	BOC_1_piece_1926	1926	146.66	145.46	0.53	166.71	0.49	2.70935	0.00016
12888	BOC_1_piece_1929	1929	146.72	145.52	0.65	159.82	0.76	2.59817	0.00021
12887	BOC_1_piece_1932	1932	146.06	144.86	0.49	162.99	0.55	2.64675	0.00015
12886	BOC_1_piece_1935	1935	145.97	144.77	0.62	166.48	0.57	2.68536	0.00017
12885	BOC_1_piece_1938	1938	146.66	145.46	0.66	160.93	0.51	2.60452	0.00016
13128	BOC_1_piece_1939	1939	145.51	144.31	0.82	164.26	0.21	2.66651	0.00018
13127	BOC_1_piece_1940	1940	145.43	144.23	0.59	166.42	0.23	2.68896	0.00014
12884	BOC_1_piece_1941	1941	146.74	145.54	0.50	165.62	0.50	2.70337	0.00014
12844	BOC_1_piece_1944	1944	147.13	145.93	0.75	157.45	1.10	2.56024	0.00062
13124	BOC_1_piece_1945	1945	146.27	145.07	0.61	165.26	0.23	2.66908	0.00017
12843	BOC_1_piece_1947	1947	147.24	146.04	0.71	166.30	1.13	2.71917	0.00043
13122	BOC_1_piece_1948	1948	145.22	144.02	0.43	166.98	0.16	2.69903	0.00013
13121	BOC_1_piece_1949	1949	145.81	144.61	0.86	167.06	0.33	2.70532	0.00021
12842	BOC_1_piece_1950	1950	146.98	145.78	0.47	171.15	0.42	2.78390	0.00016
13120	BOC_1_piece_1951	1951	145.81	144.61	0.74	170.87	0.29	2.75804	0.00027
13119	BOC_1_piece_1952	1952	145.04	143.84	0.54	168.53	0.18	2.72402	0.00015
12841	BOC_1_piece_1953	1953	146.17	144.97	0.49	164.83	0.68	2.68489	0.00016
13117	BOC_1_piece_1955	1955	146.14	144.94	0.51	163.94	0.14	2.65255	0.00013
12840	BOC_1_piece_1956	1956	146.39	145.19	0.44	172.83	0.52	2.80083	0.00018
13089	BOC_1_piece_1957	1957	146.03	144.83	0.47	177.41	0.25	2.86773	0.00019
13088	BOC_1_piece_1958	1958	146.07	144.87	0.66	175.90	0.33	2.84130	0.00021
12839	BOC_1_piece_1959	1959	146.71	145.51	0.55	173.20	0.53	2.81679	0.00014
13086	BOC_1_piece_1961	1961	146.42	145.22	0.50	173.26	0.16	2.79881	0.00013
12838	BOC_1_piece_1962	1962	146.62	145.42	0.39	169.15	0.40	2.74160	0.00015
13085	BOC_1_piece_1963	1963	146.08	144.88	0.53	174.79	0.25	2.82115	0.00019
13084	BOC_1_piece_1964	1964	145.32	144.12	0.48	180.37	0.19	2.91179	0.00014
12837	BOC_1_piece_1965	1965	147.37	146.17	0.60	177.60	0.58	2.88761	0.00018

13083	BOC_1_piece_1966	1966	146.23	145.03	0.51	173.19	0.18	2.79637	0.00016
13082	BOC_1_piece_1967	1967	146.20	145.00	0.57	171.06	0.27	2.76565	0.00018
12836	BOC_1_piece_1968	1968	144.74	143.54	0.75	176.03	0.74	2.85864	0.00040
13081	BOC_1_piece_1969	1969	145.63	144.43	0.45	171.91	0.21	2.77662	0.00016
13080	BOC_1_piece_1970	1970	145.07	143.87	0.45	174.35	0.17	2.82028	0.00014
12835	BOC_1_piece_1971	1971	145.96	144.76	0.51	176.68	0.17	2.85150	0.00014
13079	BOC_1_piece_1972	1972	145.28	144.08	0.70	174.75	0.27	2.82104	0.00016
13078	BOC_1_piece_1973	1973	145.28	144.08	0.56	166.34	0.16	2.68831	0.00015
12834	BOC_1_piece_1974	1974	145.83	144.63	0.49	162.46	0.50	2.63802	0.00015
13077	BOC_1_piece_1975	1975	145.77	144.57	0.73	172.77	0.23	2.79232	0.00021
13076	BOC_1_piece_1976	1976	144.34	143.14	0.53	175.61	0.16	2.83984	0.00014
12833	BOC_1_piece_1977	1977	145.79	144.59	0.49	167.42	0.69	2.72553	0.00018
13075	BOC_1_piece_1978	1978	145.32	144.12	0.48	270.55	0.28	4.38209	0.00026
12832	BOC_1_piece_1980	1980	144.76	143.56	0.42	157.69	0.19	2.54379	0.00011
12831	BOC_1_piece_1983	1983	146.39	145.19	0.52	170.53	0.78	2.77040	0.00017
12753	BOC_1_piece_1986	1986	146.37	145.17	0.62	168.00	0.56	2.72671	0.00015
12752	BOC_1_piece_1989	1989	146.42	145.22	0.51	163.87	0.47	2.66847	0.00012
12751	BOC_1_piece_1992	1992	145.89	144.69	0.69	175.97	0.57	2.85574	0.00017
12370	BOC_1_piece_1993	1993	145.47	144.27	0.66	164.35	0.38	2.65053	0.00012
12371	BOC_1_piece_1994	1994	145.18	143.98	0.62	159.80	0.40	2.57821	0.00011
12372	BOC_1_piece_1995	1995	145.81	144.61	0.50	169.01	0.54	2.72030	0.00013
12373	BOC_1_piece_1996	1996	144.93	143.73	0.40	148.60	0.38	2.40412	0.00010
12374	BOC_1_piece_1997	1997	145.96	144.76	0.41	168.31	0.32	2.69140	0.00011
12375	BOC_1_piece_1998	1998	146.09	144.89	0.43	168.37	0.49	2.72195	0.00013
12376	BOC_1_piece_1999	1999	145.14	143.94	0.38	146.78	2.67	2.58595	0.00077
12377	BOC_1_piece_2000	2000	145.48	144.28	0.70	158.83	0.72	2.57350	0.00020
12378	BOC_1_piece_2001	2001	145.25	144.05	0.52	168.47	0.33	2.72502	0.00013
12379	BOC_1_piece_2002	2002	145.39	144.19	0.53	174.09	0.36	2.81713	0.00013
12380	BOC_1_piece_2003	2003	145.80	144.60	0.38	171.94	1.39	2.75097	0.00028
12381	BOC_1_piece_2004	2004	144.76	143.56	0.48	164.71	0.59	2.65459	0.00015

12382	BOC_1_piece_2005	2005	145.37	144.17	0.57	166.32	0.33	2.68830	0.00011
12383	BOC_1_piece_2006	2006	144.86	143.66	0.62	120.66	0.25	1.94520	0.00008
12267	BOC_1_piece_2008	2008	145.99	144.79	0.44	165.45	0.21	2.65794	0.00006
12268	BOC_1_piece_2009	2009	146.14	144.94	0.37	165.95	0.18	2.65956	0.00006
12269	BOC_1_piece_2010	2010	144.80	143.60	0.31	171.61	0.21	2.75950	0.00006
12270	BOC_1_piece_2011	2011	144.29	143.09	0.28	173.96	0.17	2.79949	0.00006
12271	BOC_1_piece_2012	2012	146.97	145.77	0.45	173.31	0.31	2.77193	0.00022
12272	BOC_1_piece_2013	2013	146.98	145.78	0.38	174.60	0.44	2.79230	0.00013

Table C.8 Tahitian Maraa#7 $\delta^{234}U$ measurements together with concentrations of ^{238}U and ^{234}U of annually integrated samples. $\delta^{234}U$ values are given normalised to HU-1 = 0 and HU-1 ≠ 0 after (Cheng et al., 2013). Measurement uncertainties are 2σ analytical errors

sample ID	sample lable	Year	$\delta^{234}U$ (‰) (HU-1 = 0)	$\delta^{234}U$ (‰) (HU-1 ≠ 0)	Error $\delta^{234}U$ (‰)	^{234}U (pg/g)	Error ^{234}U (pg/g)	^{238}U (µg/g)	Error ^{238}U (µg/g)
13474	Maraa#7_2000	2000	147.39	146.19	0.48	146.84	0.16	2.39317	0.00013
13473	Maraa#7_2001	2001	146.39	145.19	0.89	167.47	0.21	2.69144	0.00015
13472	Maraa#7_2002	2002	146.79	145.59	0.62	166.60	0.23	2.66885	0.00014
13471	Maraa#7_2003	2003	147.12	145.92	0.49	151.62	0.16	2.43926	0.00009
13470	Maraa#7_2004	2004	147.17	145.97	0.75	162.93	1.46	2.66469	0.00081
13469	Maraa#7_2005	2005	146.83	145.63	0.59	149.32	0.16	2.39661	0.00011
13468	Maraa#7_2006	2006	148.67	147.47	0.40	144.79	0.22	2.36252	0.00015
13467	Maraa#7_2007	2007	148.90	147.70	1.00	144.54	1.39	2.35371	0.00070
13466	Maraa#7_2008	2008	148.10	146.90	0.50	138.43	0.16	2.25461	0.00012

Table C.9 Tahitian $\delta^{234}U$ measurements of water samples together with concentrations of ^{238}U, ^{234}U and Salinity. $\delta^{234}U$ values are given normalised to HU-1 = 0 and HU-1 ≠ 0 after (Cheng et al., 2013). Measurement uncertainties are 2σ analytical errors

sample ID	sample lable	latitude	longitude	$\delta^{234}U$ (‰) (HU-1 = 0)	$\delta^{234}U$ (‰) (HU-1 ≠ 0)	Error $\delta^{234}U$ (‰)	^{234}U (pg/g)	Error ^{234}U (pg/g)	^{238}U (µg/g)	Error ^{238}U (µg/g)	Salinity (psu)
12354	501	-17.5240	-149.5220	146.90	145.70	0.60	164.85	0.26	3.29000	0.13000	34.40
12356	506	-17.5130	-149.4190	154.40	153.20	1.30	51.78	0.17	0.46000	0.02000	6.10

12360	577	-17.5171	-149.7472	146.20	145.00	0.60	149.56	0.05	3.35000	0.13000	35.40
12361	578	-17.6266	-149.5610	146.90	145.70	0.60	158.34	0.09	3.36000	0.10000	35.40
12367	705	-17.7472	-149.5764	147.60	146.40	0.40	163.86	0.12	3.28000	0.10000	35.70
12368	706	-17.7533	-149.5817	146.40	145.20	0.40	148.37	0.24	3.33000	0.10000	35.80
13218	PF_TAH24_TDL_11m	-17.7670	-149.3230	144.73	143.53	0.77	182.72	0.22	2.95440	0.00039	32.45
13219	PF_TAH24_Baie#1	-17.7430	-149.3340	145.50	144.30	0.39	182.18	0.09	2.94085	0.00009	32.38
13220	PF_TAH24_Paea_LT_source	-17.7050	-149.5850	146.01	144.81	0.50	194.51	0.22	3.14199	0.00018	34.08
13221	PF_TAH24_PK18_LT_source	-17.6546	-149.6002	206.03	204.83	0.42	71.03	0.04	1.09107	0.00004	9.95
13222	PF_TAH24_Mitirapa_LT_source	-17.7327	-149.2807	213.99	212.79	1.19	16.21	0.01	0.24785	0.00001	1.85
13223	PF_TAH24_Mitirapa_LT_dis	-17.7327	-149.2807	148.67	147.47	0.31	192.16	0.12	3.09623	0.00024	24.44
13224	PF_TAH24_Mitirapa_HT_dis	-17.7327	-149.2807	149.89	148.69	0.44	97.76	0.06	1.57483	0.00019	21.28
13225	PF_TAH24_Baie#3	-17.7301	-149.3226	146.77	145.57	0.34	128.16	0.06	2.06348	0.00005	35.50
13226	PF_TAH24_Maraa_LT_source	-17.7417	-149.5725	206.90	205.70	0.44	54.69	0.03	0.84014	0.00007	7.71
13227	PF_TAH24_Maraa_LT_dis	-17.7417	-149.5725	154.20	153.00	0.48	94.76	0.06	1.51939	0.00021	24.71
13228	PF_TAH24_Vainiana_HT_dis	-17.7514	-149.5469	148.26	147.06	0.36	158.62	0.12	2.55252	0.00010	30.98
13229	PF_TAH24_Maraa_HT_dis	-17.7417	-149.5725	153.41	152.21	0.43	96.71	0.06	1.55109	0.00007	25.39
13230	PF_TAH24_Tehoro_HT_source	-17.7711	-149.4368	150.52	149.32	0.94	24.99	0.02	0.40280	0.00003	3.45

Table C.10 Puerto Rican trace element and stable isotope measurements of coral samples. Trace element values are given normalised to JCP (Hathorne et al., 2013). Stable isotope values are normalised to the VPDB. Measurement uncertainties are 2σ analytical errors

Sample ID	**Sample lable**	**year**	**Ba/Ca (µmol/ mol)**	**Error Ba/Ca (µmol/ mol)**	**Sr/Ca (mmol/ mol)**	**Error Sr/Ca (mmol/ mol)**	**Mg/Ca (mmol/ mol)**	**Error Mg/Ca (mmol/ mol)**	**$\delta^{13}C_{VPDB}$ (‰)**	**Error $\delta^{13}C_{VP\ DB}$ (‰)**	**$\delta^{18}O_{VP\ DB}$ (‰)**	**Error $\delta^{18}O_{VP\ DB}$ (‰)**
1981_6	CPR1990_1a_1981_6	1980.5	5.70	0.06	9.230	0.013	5.511	0.008	-1.30	0.22	-4.00	0.36
1981_5	CPR1990_1a_1981_5	1980.7	5.50	0.03	9.282	0.010	5.245	0.005	-0.26	0.23	-4.09	0.36
1981_4	CPR1990_1a_1981_4	1980.8	5.83	0.04	9.227	0.008	5.262	0.007	-0.24	0.22	-4.05	0.36
1981_3	CPR1990_1a_1981_3	1981	6.79	0.05	9.211	0.014	4.992	0.003	0.46	0.22	-3.96	0.37
1981_2	CPR1990_1a_1981_2	1981.1	6.24	0.06	9.221	0.008	5.151	0.003	-0.32	0.23	-4.20	0.36
1981_1	CPR1990_1a_1981_1	1981.3	6.32	0.06	9.189	0.002	5.372	0.005	-1.41	0.22	-4.37	0.35
1982_6	CPR1990_1a_1982_6	1981.5	6.13	0.04	9.238	0.008	5.342	0.004	-1.89	0.23	-4.16	0.36

1982_5	CPR1990_1a_1982_5	1981.8	5.92	0.03	9.277	0.016	5.295	0.004	-1.16	0.23	-4.03	0.36
1982_4	CPR1990_1a_1982_4	1982	5.74	0.04	9.291	0.010	5.542	0.001	-0.42	0.22	-4.07	0.36
1982_3	CPR1990_1a_1982_3	1982.3	5.91	0.04	9.280	0.005	5.294	0.005	-0.96	0.24	-4.29	0.36
1982_2	CPR1990_1a_1982_2	1982.4	6.36	0.03	9.293	0.004	4.993	0.011	0.06	0.23	-4.08	0.37
1982_1	CPR1990_1a_1982_1	1982.5	6.54	0.06	9.319	0.005	5.371	0.004	-0.65	0.23	-4.09	0.36
1983_6	CPR1990_1a_1983_6	1982.6	6.16	0.04	9.344	0.017	5.569	0.003	-1.30	0.23	-3.95	0.36
1983_5	CPR1990_1a_1983_5	1982.7	6.00	0.05	9.336	0.004	5.059	0.001	-0.87	0.22	-3.92	0.36
1983_4	CPR1990_1a_1983_4	1982.8	5.85	0.02	9.305	0.009	5.280	0.005	-1.42	0.22	-4.25	0.36
1983_3	CPR1990_1a_1983_3	1982.9	5.91	0.07	9.215	0.008	5.115	0.005	0.00	0.25	-4.02	0.36
1983_2	CPR1990_1a_1983_2	1983	5.78	0.06	9.344	0.009	5.001	0.011	-0.18	0.23	-4.08	0.36
1983_1	CPR1990_1a_1983_1	1983.3	6.10	0.02	9.237	0.009	5.612	0.005	-0.85	0.22	-4.12	0.36
1984_6	CPR1990_1a_1984_6	1983.5	5.99	0.06	9.300	0.009	5.276	0.003	-1.52	0.22	-4.06	0.33
1984_5	CPR1990_1a_1984_5	1983.7	6.03	0.06	9.345	0.015	5.420	0.006	-1.60	0.22	-3.83	0.33
1984_4	CPR1990_1a_1984_4	1984.1	5.82	0.03	9.345	0.011	5.123	0.001	-0.77	0.22	-3.76	0.36
1984_3	CPR1990_1a_1984_3	1984.5	5.41	0.01	9.286	0.022	4.984	0.006	0.38	0.23	-3.72	0.36
1984_2	CPR1990_1a_1984_2	1984.7	5.66	0.03	9.343	0.016	4.599	0.007	-0.39	0.22	-4.11	0.37
1984_1	CPR1990_1a_1984_1	1985	6.45	0.07	9.316	0.007	4.618	0.008	-1.17	0.23	-4.10	0.36
1985l_6	CPR1990_1a_1985l_6	1985.2	6.37	0.09	9.350	0.003	4.977	0.006	-0.88	0.24	-4.03	0.35
1985l_5	CPR1990_1a_1985l_5	1985.5	5.87	0.09	9.222	0.015	5.137	0.010	-1.94	0.23	-4.10	0.33
1985l_4	CPR1990_1a_1985l_4	1985.8	5.70	0.09	9.276	0.015	4.666	0.002	-0.20	0.22	-3.75	0.33
1985l_3	CPR1990_1a_1985l_3	1986.1	5.70	0.05	9.290	0.009	4.787	0.011	-0.45	0.22	-4.04	0.33
1985l_2	CPR1990_1a_1985l_2	1986.3	5.94	0.08	9.270	0.020	4.798	0.001	0.46	0.22	-3.87	0.33
1985l_1	CPR1990_1a_1985l_1	1986.4	7.62	0.13	9.216	0.017	4.935	0.006	-1.56	0.22	-4.27	0.33
1986r_6	CPR1990_1a_1986r_6	1986.6	7.38	0.07	9.170	0.009	5.036	0.002	-1.98	0.23	-4.14	0.33
1986r_5	CPR1990_1a_1986r_5	1986.7	6.52	0.05	9.320	0.004	4.847	0.007	-1.55	0.22	-3.94	0.32
1986r_4	CPR1990_1a_1986r_4	1987	6.17	0.04	9.315	0.015	4.474	0.011	-0.28	0.23	-3.80	0.33
1986r_3	CPR1990_1a_1986r_3	1987.2	5.96	0.06	9.272	0.016	4.841	0.003	-0.49	0.22	-4.10	0.33
1986r_2	CPR1990_1a_1986r_2	1987.3	6.17	0.04	9.303	0.022	4.649	0.003	0.06	0.23	-3.96	0.33
1986r_1	CPR1990_1a_1986r_1	1987.4	6.56	0.05	9.309	0.007	5.042	0.008	-1.86	0.23	-4.24	0.33
1987r_6	CPR1990_1a_1987r_6	1987.5	6.66	0.03	9.288	0.008	5.842	0.009	-1.49	0.25	-4.16	0.36

1987r_5	CPR1990_1a_1987r_5	1987.6	6.85	0.04	9.328	0.004	5.328	0.009	-1.43	0.23	-4.06	0.33
1987r_4	CPR1990_1a_1987r_4	1987.7	6.33	0.04	9.291	0.013	6.155	0.009	-1.20	0.22	-4.07	0.33
1987r_3	CPR1990_1a_1987r_3	1987.8	6.11	0.06	9.288	0.016	6.487	0.004	-0.31	0.26	-4.12	0.37
1987r_2	CPR1990_1a_1987r_2	1987.9	6.19	0.04	9.362	0.017	6.277	0.010	-0.49	0.22	-3.90	0.33
1987r_1	CPR1990_1a_1987r_1	1988.2	6.93	0.06	9.250	0.023	7.146	0.011	-1.33	0.22	-4.20	0.33
1988_4	CPR1990_1a_1988_4	1988.4	5.22	0.10	9.279	0.011	5.625	0.007	0.02	0.22	-3.89	0.33
1988_3	CPR1990_1a_1988_3	1988.5	5.44	0.08	9.233	0.011	6.392	0.005	-1.72	0.24	-4.44	0.36
1988_2	CPR1990_1a_1988_2	1988.6	5.76	0.09	9.271	0.005	6.676	0.010	-0.83	0.22	-4.17	0.33
1988_1	CPR1990_1a_1988_1	1988.8	5.69	0.07	9.265	0.008	6.457	0.011	-1.82	0.23	-4.18	0.34
1989_6	CPR1990_1a_1989_6	1988.9	5.49	0.08	9.324	0.009	6.000	0.001	-0.98	0.25	-3.95	0.36
1989_5	CPR1990_1a_1989_5	1989	5.32	0.07	9.380	0.004	5.197	0.006	0.04	0.22	-3.62	0.33
1989_4	CPR1990_1a_1989_4	1989.2	5.54	0.13	9.286	0.011	5.378	0.004	0.27	0.22	-3.97	0.33
1989_3	CPR1990_1a_1989_3	1989.4	5.73	0.04	9.309	0.017	4.955	0.008	0.32	0.22	-4.30	0.32
1989_2	CPR1990_1a_1989_2	1989.6	6.09	0.12	9.276	0.014	5.174	0.007	-0.66	0.25	-4.28	0.37
1989_1	CPR1990_1a_1989_1	1989.7	6.09	0.04	9.240	0.001	5.136	0.005	-0.27	0.24	-4.04	0.36
1990_5	CPR1990_1a_1990_5	1989.9	5.75	0.12	9.299	0.007	5.180	0.004	-0.91	0.21	-4.19	0.32
1990_4	CPR1990_1a_1990_4	1990.1	5.73	0.10	9.268	0.006	5.190	0.005	-1.59	0.22	-3.89	0.32
1990_3	CPR1990_1a_1990_3	1990.4	5.59	0.08	9.298	0.017	5.525	0.006	-0.22	0.22	-3.80	0.33
1990_2	CPR1990_1a_1990_2	1990.5	5.76	0.10	9.271	0.008	5.541	0.005	0.91	0.25	-3.74	0.37
1990_1	CPR1990_1a_1990_1	1990.6	5.48	0.09	9.254	0.013	5.086	0.002	1.29	0.24	-3.78	0.36
1988_6	CPR1990_1a_1988_6	1988.2	6.13	0.09	9.311	0.011	8.424	0.009	-0.68	0.22	-3.77	0.32
1988_5	CPR1990_1a_1988_5	1988.3	5.25	0.09	9.278	0.014	8.460	0.011	-0.34	0.26	-4.14	0.36
TM1981_6	TM2020_1_TM1981_6		4.98	0.06	9.353	0.014	6.221	0.009	-1.18	0.21	-3.96	0.33
TM1981_5	TM2020_1_TM1981_5		4.92	0.10	9.386	0.008	5.303	0.003	-0.17	0.21	-3.84	0.32
TM1981_4	TM2020_1_TM1981_4		4.79	0.07	9.318	0.006	6.287	0.009	-0.65	0.21	-4.19	0.32
TM1981_3	TM2020_1_TM1981_3		4.98	0.06	9.282	0.017	5.535	0.013	-0.35	0.21	-3.98	0.33
TM1981_2	TM2020_1_TM1981_2		5.22	0.07	9.321	0.012	5.548	0.001	-0.48	0.21	-4.23	0.32
TM1981_1	TM2020_1_TM1981_1		5.21	0.09	9.271	0.016	6.037	0.001	-0.56	0.21	-3.88	0.32
TM1982_6	TM2020_1_TM1982_6		5.25	0.13	9.306	0.012	5.355	0.006	-1.55	0.21	-4.31	0.32
TM1982_5	TM2020_1_TM1982_5		5.27	0.16	9.283	0.018	5.626	0.003	-1.43	0.21	-4.15	0.33

TM1982_4	TM2020_1_TM1982_4		5.15	0.07	9.390	0.016	5.197	0.007	-0.61	0.21	-4.16	0.32
TM1982_3	TM2020_1_TM1982_3		5.01	0.15	9.452	0.008	5.140	0.009	-0.22	0.22	-3.71	0.32
TM1982_2	TM2020_1_TM1982_2		4.97	0.10	9.330	0.007	5.666	0.003	-0.24	0.22	-3.83	0.32
TM1982_1	TM2020_1_TM1982_1		4.98	0.15	9.357	0.006	4.789	0.004	-0.51	0.21	-4.01	0.32
TM1983_6	TM2020_1_TM1983_6		4.96	0.08	9.329	0.022	5.813	0.007	-0.90	0.21	-4.17	0.32
TM1983_5	TM2020_1_TM1983_5		5.35	0.09	9.329	0.007	5.385	0.004	-0.71	0.22	-3.90	0.34
TM1983_4	TM2020_1_TM1983_4		5.27	0.14	9.433	0.014	5.504	0.003	0.16	0.21	-3.56	0.33
TM1983_3	TM2020_1_TM1983_3		4.94	0.11	9.401	0.005	5.695	0.000	-0.77	0.22	-3.82	0.33
TM1983_2	TM2020_1_TM1983_2		5.16	0.14	9.320	0.015	5.362	0.004	-0.16	0.21	-3.64	0.33
TM1983_1	TM2020_1_TM1983_1		5.33	0.16	9.311	0.021	5.094	0.005	-1.07	0.21	-4.16	0.33
TM1984_6	TM2020_1_TM1984_6		5.60	0.11	9.338	0.006	4.779	0.004	-0.54	0.22	-4.20	0.32
TM1984_5	TM2020_1_TM1984_5		5.85	0.13	9.326	0.015	5.629	0.015	-0.95	0.22	-4.05	0.32
TM1984_4	TM2020_1_TM1984_4		5.59	0.09	9.291	0.019	5.866	0.002	-1.66	0.21	-4.12	0.32
TM1984_3	TM2020_1_TM1984_3		5.28	0.09	9.341	0.010	5.548	0.006	0.02	0.21	-3.70	0.33
TM1984_2	TM2020_1_TM1984_2		5.11	0.04	9.346	0.011	5.308	0.008	0.10	0.22	-3.59	0.33
TM1984_1	TM2020_1_TM1984_1		5.16	0.07	9.269	0.002	5.090	0.005	-0.29	0.21	-3.94	0.32
TM1985_6	TM2020_1_TM1985_6		5.64	0.08	9.369	0.009	5.248	0.005	0.19	0.21	-3.90	0.33
TM1985_5	TM2020_1_TM1985_5		5.64	0.03	9.260	0.014	5.760	0.010	-0.89	0.21	-4.18	0.32
TM1985_4	TM2020_1_TM1985_4		5.34	0.08	9.307	0.015	5.657	0.010	-0.25	0.21	-3.75	0.33
TM1985_3	TM2020_1_TM1985_3		5.07	0.08	9.323	0.016	5.790	0.007	-0.21	0.22	-3.75	0.32
TM1985_2	TM2020_1_TM1985_2		5.28	0.04	9.359	0.011	5.378	0.004	-0.09	0.22	-4.02	0.33
TM1985_1	TM2020_1_TM1985_1		5.22	0.08	9.386	0.017	5.176	0.002	0.18	0.21	-4.00	0.32
TM1986_6	TM2020_1_TM1986_6		5.33	0.06	9.382	0.019	5.675	0.003	0.15	0.21	-3.94	0.32
TM1986_5	TM2020_1_TM1986_5		5.20	0.08	9.334	0.013	5.943	0.003	-0.53	0.22	-3.91	0.33
TM1986_4	TM2020_1_TM1986_4		4.86	0.06	9.380	0.011	5.583	0.008	-0.02	0.21	-3.67	0.32
TM1986_3	TM2020_1_TM1986_3		4.84	0.11	9.341	0.007	6.242	0.002	-0.10	0.21	-3.89	0.32
TM1986_2	TM2020_1_TM1986_2		5.12	0.12	9.309	0.015	5.593	0.001	0.01	0.21	-4.05	0.32
TM1986_1	TM2020_1_TM1986_1		5.29	0.12	9.347	0.010	6.715	0.011	-0.51	0.22	-4.16	0.33
TM1987_6	TM2020_1_TM1987_6		5.26	0.08	9.392	0.006	5.672	0.009	-0.12	0.21	-3.91	0.33
TM1987_5	TM2020_1_TM1987_5		5.23	0.05	9.366	0.009	6.776	0.006	-0.79	0.24	-4.00	0.36

TM1987_4	TM2020_1_TM1987_4		5.12	0.06	9.398	0.004	6.694	0.004	-0.57	0.25	-3.91	0.35
TM1987_3	TM2020_1_TM1987_3		5.32	0.07	9.321	0.006	7.527	0.014	-0.19	0.24	-3.86	0.36
TM1987_2	TM2020_1_TM1987_2		4.86	0.09	9.323	0.013	6.484	0.001	-0.09	0.25	-3.87	0.36
TM1987_1	TM2020_1_TM1987_1		4.90	0.05	9.313	0.025	7.401	0.010	0.45	0.24	-3.73	0.35
TM1988_6	TM2020_1_TM1988_6		5.37	0.08	9.205	0.011	7.678	0.012	-1.00	0.25	-4.17	0.36
TM2020_2	TM2020_1_TM2020_2		5.41	0.09	9.372	0.007	7.096	0.008	-1.05	0.20	-4.06	0.38
TM1988_4	TM2020_1_TM1988_4		5.37	0.07	9.286	0.006	7.575	0.011	-1.24	0.26	-4.12	0.36
TM1988_3	TM2020_1_TM1988_3		5.25	0.06	9.311	0.006	7.734	0.007	-1.37	0.24	-4.13	0.36
TM1988_2	TM2020_1_TM1988_2		5.21	0.06	9.274	0.013	7.925	0.021	-1.32	0.25	-4.07	0.37
TM1988_5	TM2020_1_TM1988_5		5.64	0.10	9.224	0.014	8.987	0.015	-1.77	0.24	-4.14	0.36
TM1989_6	TM2020_1_TM1989_6		5.30	0.07	9.275	0.023	7.602	0.016	-0.82	0.25	-4.14	0.36
TM1989_5	TM2020_1_TM1989_5		5.32	0.08	9.323	0.016	6.635	0.006	-0.67	0.25	-4.15	0.36
TM1989_4	TM2020_1_TM1989_4		5.14	0.11	9.284	0.015	7.919	0.009	-1.10	0.25	-4.11	0.36
TM1989_3	TM2020_1_TM1989_3		5.04	0.10	9.330	0.005	7.157	0.005	-0.33	0.24	-4.04	0.36
TM1989_2	TM2020_1_TM1989_2		5.02	0.05	9.345	0.007	7.250	0.007	-0.37	0.25	-3.92	0.36
TM1989_1	TM2020_1_TM1989_1		4.94	0.06	9.369	0.007	6.760	0.008	0.02	0.24	-3.89	0.35
TM1990_6	TM2020_1_TM1990_6		4.99	0.05	9.305	0.008	7.027	0.003	-0.59	0.25	-4.22	0.36
TM1988_1	TM2020_1_TM1988_1		5.45	0.06	9.310	0.014	8.269	0.009	-0.53	0.25	-4.23	0.35
TM1990_5	TM2020_1_TM1990_5		5.09	0.04	9.371	0.013	8.336	0.010	-0.67	0.25	-4.28	0.35
TM1990_4	TM2020_1_TM1990_4		5.44	0.05	9.288	0.020	11.093	0.024	-1.33	0.25	-4.18	0.35
TM1990_3	TM2020_1_TM1990_3		5.41	0.12	9.342	0.003	10.637	0.006	-1.41	0.26	-4.04	0.36
TM1990_2	TM2020_1_TM1990_2		5.27	0.11	9.383	0.024	9.685	0.006	-0.53	0.24	-3.83	0.35
TM1990_1	TM2020_1_TM1990_1		5.08	0.09	9.258	0.006	12.627	0.014	-0.49	0.24	-4.01	0.36
TM2011_6	TM2020_1_TM2011_6		5.12	0.02	9.273	0.010	11.224	0.011	-0.84	0.24	-4.05	0.36
TM2011_5	TM2020_1_TM2011_5		5.70	0.03	9.255	0.012	10.434	0.002	-1.44	0.23	-4.32	0.37
TM2011_4	TM2020_1_TM2011_4		5.66	0.02	9.284	0.017	10.446	0.009	-1.06	0.23	-4.16	0.36
TM2011_3	TM2020_1_TM2011_3		5.13	0.06	9.319	0.005	11.247	0.016	-1.57	0.23	-4.01	0.36
TM2011_2	TM2020_1_TM2011_2		5.05	0.02	9.354	0.023	21.706	0.018	-0.30	0.25	-3.71	0.36
TM2012_6	TM2020_1_TM2012_6		5.14	0.04	9.547	0.009	5.610	0.002	-0.69	0.23	-4.12	0.36
TM2011_1	TM2020_1_TM2011_1		4.86	0.03	9.423	0.007	9.432	0.019	0.12	0.23	-3.59	0.36

TM2012_5	TM2020_1_TM2012_5		5.38	0.03	9.317	0.012	8.439	0.003	-0.67	0.22	-4.00	0.36
TM2012_4	TM2020_1_TM2012_4		5.50	0.04	9.273	0.018	12.160	0.013	-0.29	0.23	-3.92	0.36
TM2012_3	TM2020_1_TM2012_3		5.37	0.03	9.306	0.014	10.905	0.006	-1.66	0.23	-3.96	0.36
TM2012_2	TM2020_1_TM2012_2		5.12	0.03	9.368	0.016	10.059	0.008	-1.23	0.23	-3.83	0.36
TM2013_6	TM2020_1_TM2013_6		5.09	0.02	9.405	0.024	5.882	0.002	-0.32	0.23	-4.16	0.37
TM2013_5	TM2020_1_TM2013_5		5.35	0.05	9.430	0.012	5.615	0.005	-0.50	0.23	-4.01	0.36
TM2013_4	TM2020_1_TM2013_4		5.35	0.03	9.377	0.007	6.071	0.003	-1.08	0.23	-3.90	0.36
TM2013_3	TM2020_1_TM2013_3		5.20	0.02	9.327	0.002	7.473	0.013	-1.79	0.22	-3.89	0.36
TM2012_1	TM2020_1_TM2012_1		5.60	0.02	9.396	0.017	10.020	0.012	-0.84	0.23	-3.93	0.36
TM2013_1	TM2020_1_TM2013_1		5.04	0.03	9.335	0.010	6.253	0.004	0.05	0.22	-3.76	0.36
TM2014_6	TM2020_1_TM2014_6		5.09	0.02	9.278	0.013	6.512	0.004	-0.69	0.20	-3.81	0.38
TM2014_5	TM2020_1_TM2014_5		6.03	0.02	9.311	0.016	7.793	0.006	-0.24	0.20	-3.87	0.39
TM2014_4	TM2020_1_TM2014_4		5.52	0.02	9.392	0.006	6.771	0.005	-0.84	0.20	-3.60	0.38
TM2013_2	TM2020_1_TM2013_2		5.23	0.01	9.321	0.008	9.279	0.012	-0.67	0.23	-3.90	0.36
TM2014_3	TM2020_1_TM2014_3		5.49	0.03	9.366	0.003	10.587	0.005	-1.42	0.21	-3.77	0.39
TM2014_2	TM2020_1_TM2014_2		5.55	0.04	9.352	0.015	11.553	0.016	0.29	0.21	-3.33	0.38
TM2015_6	TM2020_1_TM2015_6		5.14	0.02	9.477	0.021	7.676	0.003	-0.07	0.20	-3.75	0.39
TM2015_5	TM2020_1_TM2015_5		5.37	0.01	9.368	0.019	7.446	0.003	0.40	0.21	-3.61	0.38
TM2015_4	TM2020_1_TM2015_4		6.46	0.03	9.408	0.011	7.639	0.006	-1.39	0.21	-4.07	0.39
TM2015_3	TM2020_1_TM2015_3		5.71	0.03	9.403	0.007	6.740	0.011	0.46	0.20	-3.44	0.38
TM2015_2	TM2020_1_TM2015_2		6.09	0.03	9.406	0.003	7.220	0.004	-0.78	0.20	-3.69	0.38
TM2015_1	TM2020_1_TM2015_1		5.51	0.04	9.417	0.001	7.909	0.002	0.60	0.20	-3.43	0.38
TM2014_1	TM2020_1_TM2014_1		5.54	0.02	9.320	0.021	10.556	0.003	-0.72	0.20	-3.59	0.38
TM2016_5	TM2020_1_TM2016_5		5.41	0.03	9.390	0.016	6.078	0.008	-0.21	0.24	-3.77	0.36
TM2016_4	TM2020_1_TM2016_4		6.35	0.03	9.359	0.006	6.061	0.003	-0.55	0.20	-3.82	0.39
TM2016_3	TM2020_1_TM2016_3		6.74	0.02	9.395	0.003	6.208	0.015	-1.91	0.20	-3.89	0.38
TM2016_2	TM2020_1_TM2016_2		5.72	0.02	9.420	0.021	7.327	0.007	-0.89	0.20	-3.52	0.39
TM2016_1	TM2020_1_TM2016_1		5.48	0.02	9.419	0.020	6.425	0.007	-0.46	0.21	-3.62	0.38
TM2017_6	TM2020_1_TM2017_6		5.46	0.02	9.369	0.017	5.485	0.011	0.05	0.22	-3.90	0.38
TM2016_6	TM2020_1_TM2016_6		5.39	0.02	9.392	0.001	9.193	0.013	0.11	0.21	-3.71	0.39

TM2017_4	TM2020_1_TM2017_4		5.53	0.02	9.450	0.006	5.873	0.006	0.55	0.21	-3.57	0.38
TM2017_3	TM2020_1_TM2017_3		5.46	0.02	9.428	0.012	6.308	0.011	-0.73	0.21	-3.86	0.38
TM2017_2	TM2020_1_TM2017_2		5.96	0.02	9.395	0.008	6.502	0.004	-0.58	0.21	-3.65	0.38
TM2017_1	TM2020_1_TM2017_1		4.97	0.03	9.403	0.017	6.886	0.009	-0.32	0.21	-3.62	0.38
TM2018_6	TM2020_1_TM2018_6		5.05	0.03	9.390	0.006	6.013	0.003	0.47	0.20	-3.71	0.39
TM2018_5	TM2020_1_TM2018_5		5.22	0.02	9.348	0.004	6.025	0.006	0.64	0.20	-3.65	0.40
TM2017_5	TM2020_1_TM2017_5		5.58	0.02	9.322	0.013	9.499	0.007	0.72	0.20	-3.58	0.38
TM2018_4	TM2020_1_TM2018_4		5.76	0.02	9.285	0.017	8.225	0.002	-1.40	0.21	-4.12	0.39
TM2018_3	TM2020_1_TM2018_3		5.74	0.03	9.396	0.011	5.332	0.004	-1.20	0.21	-4.02	0.38
TM2018_1	TM2020_1_TM2018_1		5.41	0.03	9.407	0.013	7.568	0.008	-0.01	0.21	-3.88	0.38
TM2019_6	TM2020_1_TM2019_6		4.36	0.15	9.381	0.020	6.139	0.001	-0.40	0.20	-3.96	0.38
TM2019_5	TM2020_1_TM2019_5		4.04	0.17	9.361	0.012	5.922	0.007	-0.05	0.21	-4.06	0.39
TM2018_2	TM2020_1_TM2018_2		5.55	0.02	9.370	0.007	9.166	0.006	-0.61	0.21	-3.96	0.38
TM2019_4	TM2020_1_TM2019_4		4.00	0.12	9.350	0.018	6.485	0.006	-0.09	0.21	-3.90	0.39
TM2019_2	TM2020_1_TM2019_2		5.69	0.02	9.355	0.022	6.520	0.003	-0.94	0.20	-3.85	0.39
TM2019_3	TM2020_1_TM2019_3		5.57	0.07	9.359	0.020	8.181	0.004	-1.73	0.20	-4.08	0.38
TM2020_4	TM2020_1_TM2020_4		4.96	0.09	9.436	0.011	8.403	0.005	0.04	0.20	-3.69	0.38
TM2019_1	TM2020_1_TM2019_1		5.39	0.02	9.467	0.013	7.492	0.008	-0.10	0.20	-3.51	0.38
TM2020_3	TM2020_1_TM2020_3		5.70	0.16	9.239	0.011	12.765	0.012	-0.64	0.20	-3.83	0.38
TM2020_1	TM2020_1_TM2020_1		4.85	0.13	9.268	0.003	8.248	0.006	-0.31	0.21	-3.85	0.38

Bibliography

Abdul, N. A., Mortlock, R. A., Wright, J. D., & Fairbanks, R. G. (2016). Younger Dryas sea level and meltwater pulse 1B recorded in Barbados reef crest coral Acropora palmata. *Paleoceanography*, *31*(2), 330-344. https://doi.org/https://doi.org/10.1002/2015PA002847

Aguiar, A. L., Marta-Almeida, M., Cruz, L. O., Pereira, J., & Cirano, M. (2022). Forcing mechanisms of the circulation on the Brazilian Equatorial Shelf. *Continental Shelf Research*, *247*, 104811. https://doi.org/https://doi.org/10.1016/j.csr.2022.104811

Alexander, M. A., Bladé, I., Newman, M., Lanzante, J. R., Lau, N.-C., & Scott, J. D. (2002). The Atmospheric Bridge: The Influence of ENSO Teleconnections on Air–Sea Interaction over the Global Oceans. *Journal of Climate*, *15*(16), 2205-2231. https://doi.org/10.1175/1520-0442(2002)015<2205:Tabtio>2.0.Co;2

Alexander, M. A., Halimeda Kilbourne, K., & Nye, J. A. (2014). Climate variability during warm and cold phases of the Atlantic Multidecadal Oscillation (AMO) 1871–2008. *Journal of Marine Systems*, *133*, 14-26. https://doi.org/10.1016/j.jmarsys.2013.07.017

Allison, N., Finch, A. A., Webster, J. M., & Clague, D. A. (2007). Palaeoenvironmental records from fossil corals: The effects of submarine diagenesis on temperature and climate estimates. *Geochimica et Cosmochimica Acta*, *71*(19), 4693-4703. https://doi.org/10.1016/j.gca.2007.07.026

Alonso-Hernández, C. M., Fanelli, E., Diaz-Asencio, M., Santamaría, J. M., & Morera-Gómez, Y. (2020). Carbon and nitrogen isotopes to distinguish sources of sedimentary organic matter in a Caribbean estuary. *Isotopes in Environmental and Health Studies*, *56*(5-6), 654-672. https://doi.org/10.1080/10256016.2020.1819263

Alonso-Hernández, C. M., Gómez-Batista, M., Helguera Pedraza, Y., Hernández-Albernas, J., Rico-Esenaro, S. D., Ruiz-Fernández, A. C., Sánchez-Cabeza, J. A., Douville, E., & Montagna, P. (2022). Registro de temperatura superficial del mar (1778-2015) en Orbicella faveolata (Cnidaria: Scleractinia) del arrecife Cayo Santa María, Cuba. In (Vol. 42, pp. 37-53): Revista de Investigaciones Marinas.

Alpert, A. E., Cohen, A. L., Oppo, D. W., DeCarlo, T. M., Gove, J. M., & Young, C. W. (2016). Comparison of equatorial Pacific sea surface temperature variability and trends with Sr/Ca records from multiple corals. *Paleoceanography*, *31*(2), 252-265. https://doi.org/https://doi.org/10.1002/2015PA002897

Álvera-Azcárate, A., Barth, A., & Weisberg, R. H. (2009). The Surface Circulation of the Caribbean Sea and the Gulf of Mexico as Inferred from Satellite Altimetry. *Journal of Physical Oceanography*, *39*, 640-657.

Andersen, M. B., Elliott, T., Freymuth, H., Sims, K. W., Niu, Y., & Kelley, K. A. (2015). The terrestrial uranium isotope cycle. *Nature*, *517*(7534), 356-359. https://doi.org/10.1038/nature14062

Andersen, M. B., Stirling, C. H., Porcelli, D., Halliday, A. N., Andersson, P. S., & Baskaran, M. (2007). The tracing of riverine U in Arctic seawater with very precise 234U/238U measurements. *Earth and Planetary Science Letters*, *259*(1-2), 171-185. https://doi.org/10.1016/j.epsl.2007.04.051

Andersen, M. B., Stirling, C. H., Potter, E.-K., & Halliday, A. N. (2004a). Toward epsilon levels of measurement precision on 234U/238U by using MC-ICPMS. *International Journal of Mass Spectrometry*, *237*, 107–118.

Andersen, M. B., Stirling, C. H., Potter, E. K., & Halliday, A. N. (2004b). Toward epsilon levels of measurement precision on 234U/238U by using MC-ICPMS. *International Journal of Mass Spectrometry*, *237*(2), 107-118. https://doi.org/https://doi.org/10.1016/j.ijms.2004.07.004

Andersen, M. B., Stirling, C. H., Zimmermann, B., & Halliday, A. N. (2010). Precise determination of the open ocean 234U/238U composition. *Geochemistry, Geophysics, Geosystems*, *11*(12). https://doi.org/10.1029/2010gc003318

Androulidakis, Y., Kourafalou, V., Le Hénaff, M., Kang, H., Ntaganou, N., & Hu, C. (2020). Gulf Stream evolution through the Straits of Florida: the role of eddies and upwelling near Cuba. *Ocean Dynamics*, *70*(8), 1005-1032. https://doi.org/10.1007/s10236-020-01381-5

Antuña-Marrero, J. C., Otterå, O. H., Robock, A., & Mesquita, M. d. S. (2016). Modelled and observed sea surface temperature trends for the Caribbean and Antilles. *International Journal of Climatology*, *36*(4), 1873-1886. https://doi.org/https://doi.org/10.1002/joc.4466

Appeldoorn, R. S., & Bejarano, I. (2013). Seawater turbidity and fish communities on coral reefs of Puerto Rico. *Marine Ecology Progress Series*, *474*, 217-226. https://www.int-res.com/abstracts/meps/v474/meps10051

Arendt, C. A., Aciego, S. M., Sims, K. W. W., Das, S. B., Sheik, C., & Stevenson, E. I. (2018). Influence of glacial meltwater on global seawater δ234U. *Geochimica et Cosmochimica Acta*, *225*, 102-115. https://doi.org/10.1016/j.gca.2018.01.007

Asikainen, M. (1981). State of disequilibrium between 238U, 234U, 226Ra and 222Rn in groundwater from bedrock. *Geochimica et Cosmochimica Acta*, *45*(2), 201-206. https://doi.org/https://doi.org/10.1016/0016-7037(81)90163-0

Aubaud, C., Athanase, J.-E., Clouard, V., Barras, A.-V., & Sedan, O. (2013). A review of historical landslides, floods, and lahars in the Prêcheur river catchment, Montagne Pelée Volcano (Martinique, Lesser Antilles). *Bulletin de la Societe Geologique de France*, *184*, 137-154. https://doi.org/10.2113/gssgfbull.184.1-2.137

Aureau, M. (2014). *Modelling Flows Surface and Underground : Valley Punaruu - Tahiti, Modélisation des Écoulements en Surface et Souterrains : vallée de la Punaru'u – Tahiti* (Publication Number 2014POLF0006) Université de la Polynésie Française]. https://theses.hal.science/tel-01482856

Back, W. (1985). Part III: Hydrogeology of the Yucatan. In W. C. Ward, A. E. Weidie, & W. Back (Eds.), *Geology and hydrogeology of the Yucatan and quaternary geology of northeastern Yucatan Peninsula* (pp. 99–124). New Orleans Geological Society.

Bard, E., Hamelin, B., Fairbanks, R. G., & Zindler, A. (1990). Calibration of the 14C timescale over the past 30,000 years using mass spectrometric U–Th ages from Barbados corals. *Nature*, *345*(6274), 405-410. https://doi.org/10.1038/345405a0

Barnes, D. J., & Devereux, M. J. (1988). Variations in skeletal architecture associated with density banding in the hard coral Porites. *Journal of Experimental Marine Biology and Ecology*, *121*(1), 37-54. https://doi.org/https://doi.org/10.1016/0022-0981(88)90022-6

Bauer-Gottwein, P., Gondwe, B. R. N., Charvet, G., Marín, L. E., Rebolledo-Vieyra, M., & Merediz-Alonso, G. (2011). Review: The Yucatán Peninsula karst aquifer, Mexico. *Hydrogeology Journal*, *19*(3), 507-524. https://doi.org/10.1007/s10040-010-0699-5

Beck, J. W., Edwards, R. L., Ito, E., Taylor, F. W., Recy, J., Rougerie, F., Joannot, P., & Henin, C. (1992). Sea-Surface Temperature from Coral Skeletal Strontium/Calcium Ratios. *Science*, *257*(5070), 644-647. https://doi.org/doi:10.1126/science.257.5070.644

Beddows, P. A. (2004). Groundwater Hydrology of a Coastal Conduit Carbonate Aquifer: Caribbean Coast of the Yucatán Peninsula, México, PhD Thesis.

Beier, E., Bernal, G., Ruiz-Ochoa, M., & Barton, E. D. (2017). Freshwater exchanges and surface salinity in the Colombian basin, Caribbean Sea. *PLoS One*, *12*(8), e0182116. https://doi.org/10.1371/journal.pone.0182116

Beisel, E., Frank, N., Wienberg, C., Titschack, J., Hebbeln, D., Robinson, L. F., Lausecker, M., Friedrich, R., Therre, S., Schröder-Ritzrau, A., & Butzin, M. (2023). *Uranium-thorium dating of Atlantic cold-water corals from the last 32,000 years* (PANGAEA. https://doi.org/10.1594/PANGAEA.959510

Beisel, E., Therre, S., Wienberg, C., Friedrich, R., & Frank, N. (2025). Status report of the Heidelberg Radiocarbon Laboratory: Precision and application in Mauritanian cold-water corals over the last 30,000 years. *Radiocarbon*, *67*(3), 450-460. https://doi.org/10.1017/RDC.2025.7

Bender, M. A., Knutson, T. R., Tuleya, R. E., Sirutis, J. J., Vecchi, G. A., Garner, S. T., & Held, I. M. (2010). Modeled Impact of Anthropogenic Warming on the Frequency of Intense Atlantic Hurricanes. *Science*, *327*(5964), 454-458. https://doi.org/10.1126/science.1180568

Benoit, L., & Sichoix, L. (2023). Sub-daily rainfall patterns in the mountainous regions of the Island of Tahiti: Insights from a one-year rain gauge network expansion. *Journal of Hydrology: Regional Studies*, *50*, 101559. https://doi.org/https://doi.org/10.1016/j.ejrh.2023.101559

Benway, H. M., & Mix, A. C. (2004). Oxygen isotopes, upper-ocean salinity, and precipitation sources in the eastern tropical Pacific. *Earth and Planetary Science Letters*, *224*(3-4), 493-507. https://doi.org/10.1016/j.epsl.2004.05.014

Blaha, J. P. (1984). Fluctuations of monthly sea level as related to the intensity of the Gulf Stream from Key West to Norfolk. *Journal of Geophysical Research: Oceans*, *89*(C5), 8033-8042. https://doi.org/https://doi.org/10.1029/JC089iC05p08033

Blanchon, P., Jones, B., & Ford, D. C. (2002). Discovery of a submerged relic reef and shoreline off Grand Cayman: further support for an early Holocene jump in sea level. *Sedimentary Geology*, *147*(3), 253-270. https://doi.org/https://doi.org/10.1016/S0037-0738(01)00143-9

Bonotto, D. M., & Andrews, J. N. (1993). The mechanism of 234U238U activity ratio enhancement in karstic limestone groundwater. *Chemical Geology*, *103*(1), 193-206. https://doi.org/https://doi.org/10.1016/0009-2541(93)90301-X

Border, E. C. (2020). *Variability of δ234U in the Mediterranean Sea, Amazon Estuary, and Atlantic Ocean* (Publication Number Available from INIS: http://inis.iaea.org/search/search.aspx?orig_q=RN:52022202; Available from INIS in electronic form. Also available from: https://d-nb.info/1215758243/34; Available from: https://fiz.tind.io/record/335900/files/335900.pdf)

Böttcher, M. E., Mallast, U., Massmann, G., Moosdorf, N., Müller-Petke, M., & Waska, H. (2024). Coastal–Groundwater Interfaces (Submarine Groundwater Discharge). In *Ecohydrological Interfaces* (pp. 123-147). https://doi.org/https://doi.org/10.1002/9781119489702.ch6

Bourdon, B., Turner, S., Henderson, G. M., & Lundstrom, C. C. (2003). *Uranium-series Geochemistry*. De Gruyter. https://doi.org/doi:10.1515/9781501509308-006

Buddemeier, R. W., Maragos, J. E., & Knutson, D. W. (1974). Radiographic studies of reef coral exoskeletons: Rates and patterns of coral growth. *Journal of Experimental Marine Biology and Ecology*, *14*(2), 179-199. https://doi.org/https://doi.org/10.1016/0022-0981(74)90024-0

Burn, M. J., Holmes, J., Kennedy, L. M., Bain, A., Marshall, J. D., & Perdikaris, S. (2016). A sediment-based reconstruction of Caribbean effective precipitation during the 'Little Ice Age' from Freshwater Pond, Barbuda. *The Holocene*, *26*(8), 1237-1247. https://doi.org/10.1177/0959683616638418

Burnett, W. C., Bokuniewicz, H., Huettel, M., Moore, W. S., & Taniguchi, M. (2003). Groundwater and pore water inputs to the coastal zone. *Biogeochemistry*, *66*(1), 3-33. https://doi.org/10.1023/B:BIOG.0000006066.21240.53

Cai, W., Wu, L., Lengaigne, M., Li, T., McGregor, S., Kug, J. S., Yu, J. Y., Stuecker, M. F., Santoso, A., Li, X., Ham, Y. G., Chikamoto, Y., Ng, B., McPhaden, M. J., Du, Y., Dommenget, D., Jia, F., Kajtar, J. B., Keenlyside, N., . . . Chang, P. (2019). Pantropical climate interactions. *Science*, *363*(6430). https://doi.org/10.1126/science.aav4236

Caldwell, P. C., Merrifield, M. A., & Thompson, P. R. (2015). *Sea level measured by tide gauges from global oceans — the Joint Archive for Sea Level holdings (NCEI Accession 0019568), Version 5.5* (https://doi.org/doi: 10.7289/V5V40S7W

Canul-Macario, C., Salles, P., Hernández-Espriú, A., & Pacheco-Castro, R. (2020). Empirical relationships of groundwater head–salinity response to variations of sea level and vertical recharge in coastal confined karst aquifers. *Hydrogeology Journal*, *28*(5), 1679-1694. https://doi.org/10.1007/s10040-020-02151-9

Carroll, J. L. (1990). Dams and Damages: The Ojibway, the United States, and the Mississippi Headwaters Reservoirs. *Minnesota History*, *52*(1), 2-15.

Centella-Artola, A., Bezanilla-Morlot, A., Serrano-Notivoli, R., Vazquez-Montenegro, R., Sierra-Lorenzo, M., & Chang-Dominguez, D. (2023). A new long term gridded daily precipitation dataset at high-resolution for Cuba (CubaPrec1). *Data Brief*, *48*, 109294. https://doi.org/10.1016/j.dib.2023.109294

Centurioni, L. R., & Niiler, P. P. (2003). On the surface currents of the Caribbean Sea. *Geophysical Research Letters*, *30*(6). https://doi.org/https://doi.org/10.1029/2002GL016231

Chabaux, F., Bourdon, B., & Riotte, J. (2008). Chapter 3 U-Series Geochemistry in Weathering Profiles, River Waters and Lakes. In S. Krishnaswami & J. K. Cochran (Eds.), *Radioactivity in the Environment* (Vol. 13, pp. 49-104). Elsevier. https://doi.org/https://doi.org/10.1016/S1569-4860(07)00003-4

Chen, J. H., Curran, H. A., White, B., & Wasserburg, G. J. (1991). Precise chronology of the last interglacial period: 234U-230Th data from fossil coral reefs in the Bahamas. *GSA Bulletin*, *103*(1), 82-97. https://doi.org/10.1130/0016-7606(1991)103<0082:Pcotli>2.3.Co;2

Chen, J. H., Lawrence Edwards, R., & Wasserburg, G. J. (1986). 238U,234U and232Th in seawater. *Earth and Planetary Science Letters*, *80*(3), 241-251. https://doi.org/https://doi.org/10.1016/0012-821X(86)90108-1

Chen, T., Robinson, L. F., Beasley, M. P., Claxton, L. M., Andersen, M. B., Gregoire, L. J., Wadham, J., Fornari, D. J., & Harpp, K. S. (2016). Ocean mixing and ice-sheet control of seawater ²³⁴U/²³⁸U during the last deglaciation. *Science*, *354*(6312), 626-629. https://doi.org/doi:10.1126/science.aag1015

Cheng, H., Edwards, R. L., Hoff, J., Gallup, C. D., Richards, D. A., & Asmerom, Y. (2000). The half-lives of uranium-234 and thorium-230. *Chemical Geology*, *169*(1), 17-33. https://doi.org/https://doi.org/10.1016/S0009-2541(99)00157-6

Cheng, H., Lawrence Edwards, R., Shen, C.-C., Polyak, V. J., Asmerom, Y., Woodhead, J., Hellstrom, J., Wang, Y., Kong, X., Spötl, C., Wang, X., & Calvin Alexander, E. (2013). Improvements in 230Th dating, 230Th and 234U half-life values, and U–Th isotopic measurements by multi-collector

inductively coupled plasma mass spectrometry. *Earth and Planetary Science Letters*, *371-372*, 82-91. https://doi.org/10.1016/j.epsl.2013.04.006

Chérubin, L. M., & Richardson, P. L. (2007). Caribbean current variability and the influence of the Amazon and Orinoco freshwater plumes. *Deep Sea Research Part I: Oceanographic Research Papers*, *54*(9), 1451-1473. https://doi.org/https://doi.org/10.1016/j.dsr.2007.04.021

Choppin, G., Liljenzin, J. O., Rydberg, J., & Ekberg, C. (2013). Radiochemistry and Nuclear Chemistry: Fourth Edition. *Radiochemistry and Nuclear Chemistry: Fourth Edition*, 1-858.

Church, T. M. (1996). An underground route for the water cycle. *Nature*, *380*(6575), 579. https://doi.org/10.1038/380579a0

Chutcharavan, P. M., Dutton, A., & Ellwood, M. J. (2018). Seawater 234U/238U recorded by modern and fossil corals. *Geochimica et Cosmochimica Acta*, *224*, 1-17. https://doi.org/10.1016/j.gca.2017.12.017

Clark, P. U., He, F., Golledge, N. R., Mitrovica, J. X., Dutton, A., Hoffman, J. S., & Dendy, S. (2020). Oceanic forcing of penultimate deglacial and last interglacial sea-level rise. *Nature*, *577*(7792), 660-664. https://doi.org/10.1038/s41586-020-1931-7

Coronado, C., Candela, J., Iglesias-Prieto, R., Sheinbaum, J., López, M., & Ocampo-Torres, F. J. (2007). On the circulation in the Puerto Morelos fringing reef lagoon. *Coral Reefs*, *26*(1), 149-163. https://doi.org/10.1007/s00338-006-0175-9

Coutino, A., Stastna, M., Kovacs, S., & Reinhardt, E. (2017). Hurricanes Ingrid and Manuel (2013) and their impact on the salinity of the Meteoric Water Mass, Quintana Roo, Mexico. *Journal of Hydrology*, *551*, 715-729. https://doi.org/https://doi.org/10.1016/j.jhydrol.2017.04.022

Coyne, M. K., Jones, B., & Ford, D. (2007). Highstands during Marine Isotope Stage 5: evidence from the Ironshore Formation of Grand Cayman, British West Indies. *Quaternary Science Reviews*, *26*(3), 536-559. https://doi.org/https://doi.org/10.1016/j.quascirev.2006.06.013

Cummings, J. A., & Smedstad, O. M. (2013). Variational Data Assimilation for the Global Ocean. In S. K. Park & L. Xu (Eds.), *Data Assimilation for Atmospheric, Oceanic and Hydrologic Applications (Vol. II)* (pp. 303-343). Springer Berlin Heidelberg. https://doi.org/10.1007/978-3-642-35088-7_13

Dai, A., & Trenberth, K. E. (2002). Estimates of Freshwater Discharge from Continents: Latitudinal and Seasonal Variations. *Journal of Hydrometeorology*, *3*(6), 660-687. https://doi.org/https://doi.org/10.1175/1525-7541(2002)003<0660:EOFDFC>2.0.CO;2

de Villiers, S., Nelson, B. K., & Chivas, A. R. (1995). Biological Controls on Coral Sr/Ca and δ¹⁸O Reconstructions of Sea Surface Temperatures. *Science*, *269*(5228), 1247-1249. https://doi.org/doi:10.1126/science.269.5228.1247

DeCarlo, T. M., Gaetani, G. A., Cohen, A. L., Foster, G. L., Alpert, A. E., & Stewart, J. A. (2016). Coral Sr-U thermometry. *Paleoceanography*, *31*(6), 626-638. https://doi.org/10.1002/2015pa002908

DeCarlo, T. M., Gaetani, G. A., Holcomb, M., & Cohen, A. L. (2015). Experimental determination of factors controlling U/Ca of aragonite precipitated from seawater: Implications for interpreting coral skeleton. *Geochimica et Cosmochimica Acta*, *162*, 151-165. https://doi.org/10.1016/j.gca.2015.04.016

Delanghe, D., Bard, E., & Hamelin, B. (2002). New TIMS constraints on the uranium-238 and uranium-234 in seawaters from the main ocean basins and the Mediterranean Sea. *Marine Chemistry*, *80*(1), 79-93. https://doi.org/https://doi.org/10.1016/S0304-4203(02)00100-7

DeLong, K. L., Flannery, J. A., Maupin, C. R., Poore, R. Z., & Quinn, T. M. (2011). A coral Sr/Ca calibration and replication study of two massive corals from the Gulf of Mexico. *Palaeogeography, Palaeoclimatology, Palaeoecology*, *307*(1-4), 117-128. https://doi.org/10.1016/j.palaeo.2011.05.005

DeLong, K. L., Flannery, J. A., Poore, R. Z., Quinn, T. M., Maupin, C. R., Lin, K., & Shen, C.-C. (2014). A reconstruction of sea surface temperature variability in the southeastern Gulf of Mexico from 1734 to 2008 C.E. using cross-dated Sr/Ca records from the coral Siderastrea siderea. *Paleoceanography*, *29*(5), 403-422. https://doi.org/https://doi.org/10.1002/2013PA002524

DeLong, K. L., Maupin, C. R., Flannery, J. A., Quinn, T. M., & Shen, C.-C. (2016). Refining temperature reconstructions with the Atlantic coral Siderastrea siderea. *Palaeogeography, Palaeoclimatology, Palaeoecology*, *462*, 1-15. https://doi.org/10.1016/j.palaeo.2016.08.028

Deschamps, P., Doucelance, R., Ghaleb, B., & Michelot, J.-L. (2003). Further investigations on optimized tail correction and high-precision measurement of uranium isotopic ratios using multi-collector ICP-MS. *Chemical Geology*, *201*, 141–160.

Dişa, D., Münnich, M., Vogt, M., & Gruber, N. (2022). A space-time mosaic of seawater carbonate chemistry conditions in the north-shore Moorea coral reef system. *Frontiers in Marine Science*, *9*. https://doi.org/10.3389/fmars.2022.1004107

Dorel, J. (1981). Seismicity and seismic gap in the Lesser Antilles arc and earthquake hazard in Guadeloupe. *Geophysical Journal of the Royal Astronomical Society*, *67*(3), 679-695. https://doi.org/https://doi.org/10.1111/j.1365-246X.1981.tb06947.x

Douville, E., Sallé, E., Frank, N., Eisele, M., Pons-Branchu, E., & Ayrault, S. (2010). Rapid and accurate U–Th dating of ancient carbonates using inductively coupled plasma-quadrupole mass spectrometry. *Chemical Geology*, *272*(1-4), 1-11. https://doi.org/10.1016/j.chemgeo.2010.01.007

Drinkwater, K. F. (1986). On the Role of Freshwater Outflow on Coastal Marine Ecosystems—A Workshop Summary. In S. Skreslet, *The Role of Freshwater Outflow in Coastal Marine Ecosystems* Berlin, Heidelberg.

Dunk, R. M., Mills, R. A., & Jenkins, W. J. (2002). A reevaluation of the oceanic uranium budget for the Holocene. *Chemical Geology*, *190*(1), 45-67. https://doi.org/https://doi.org/10.1016/S0009-2541(02)00110-9

Eggins, S. M., Grün, R., McCulloch, M. T., Pike, A. W. G., Chappell, J., Kinsley, L., Mortimer, G., Shelley, M., Murray-Wallace, C. V., Spötl, C., & Taylor, L. (2005). In situ U-series dating by laser-ablation multi-collector ICPMS: new prospects for Quaternary geochronology. *Quaternary Science Reviews*, *24*(23), 2523-2538. https://doi.org/https://doi.org/10.1016/j.quascirev.2005.07.006

Enfield, D. B., & Mayer, D. A. (1997). Tropical Atlantic sea surface temperature variability and its relation to El Niño-Southern Oscillation. *Journal of Geophysical Research: Oceans*, *102*(C1), 929-945. https://doi.org/10.1029/96jc03296

Enfield, D. B., Mestas-Nuñez, A. M., & Trimble, P. J. (2001). The Atlantic Multidecadal Oscillation and its relation to rainfall and river flows in the continental U.S. *Geophysical Research Letters*, *28*(10), 2077-2080. https://doi.org/https://doi.org/10.1029/2000GL012745

Epstein, S., Buchsbaum, R., Lowenstam, H. A., & Urey, H. C. (1953). Revised Carbonate-Water Isotopic Temperature Scale. *GSA Bulletin*, *64*(11), 1315-1326. https://doi.org/10.1130/0016-7606(1953)64[1315:Rcits]2.0.Co;2

Esat, T. M., & Yokoyama, Y. (2006). Variability in the uranium isotopic composition of the oceans over glacial–interglacial timescales. *Geochimica et Cosmochimica Acta*, *70*(16), 4140-4150. https://doi.org/https://doi.org/10.1016/j.gca.2006.06.013

Esat, T. M., & Yokoyama, Y. (2010). Coupled uranium isotope and sea-level variations in the oceans. *Geochimica et Cosmochimica Acta*, *74*(24), 7008-7020. https://doi.org/https://doi.org/10.1016/j.gca.2010.09.007

Ezer, T. (2022). Sea level variability in the Gulf of Mexico since 1900 and its link to the Yucatan Channel and the Florida Strait flows. *Ocean Dynamics*, *72*(11), 741-759. https://doi.org/10.1007/s10236-022-01530-y

Fairbanks, R., G., & Dodge, R., E. . (1979). Annual periodicity of the 18O16O and 13C12C ratios in the coral Montastrea annularis. *Geochimica et Cosmochimica Acta*, *43*(7), 1009-1020. https://doi.org/https://doi.org/10.1016/0016-7037(79)90090-5

Fairbanks, R. G., Mortlock, R. A., Chiu, T.-C., Cao, L., Kaplan, A., Guilderson, T. P., Fairbanks, T. W., Bloom, A. L., Grootes, P. M., & Nadeau, M.-J. (2005). Radiocarbon calibration curve spanning 0 to 50,000 years BP based on paired 230Th/234U/238U and 14C dates on pristine corals. *Quaternary Science Reviews*, *24*(16), 1781-1796. https://doi.org/https://doi.org/10.1016/j.quascirev.2005.04.007

Felis, T., Pätzold, J., & Loya, Y. (2003). Mean oxygen-isotope signatures in Porites spp. corals: inter-colony variability and correction for extension-rate effects. *Coral Reefs*, *22*(4), 328-336. https://doi.org/10.1007/s00338-003-0324-3

Felis, T., Suzuki, A., Kuhnert, H., Dima, M., Lohmann, G., & Kawahata, H. (2009). Subtropical coral reveals abrupt early-twentieth-century freshening in the western North Pacific Ocean. *Geology*, *37*(6), 527-530. https://doi.org/10.1130/g25581a.1

Fensterer, C., Scholz, D., Hoffmann, D., Spötl, C., Pajón, J. M., & Mangini, A. (2012). Cuban stalagmite suggests relationship between Caribbean precipitation and the Atlantic Multidecadal Oscillation during the past 1.3 ka. *The Holocene*, *22*(12), 1405-1412. https://doi.org/10.1177/0959683612449759

Fensterer, C., Scholz, D., Hoffmann, D. L., Spötl, C., Schröder-Ritzrau, A., Horn, C., Pajón, J. M., & Mangini, A. (2013). Millennial-scale climate variability during the last 12.5ka recorded in a Caribbean

speleothem. *Earth and Planetary Science Letters*, *361*, 143-151. https://doi.org/https://doi.org/10.1016/j.epsl.2012.11.019

Ferry, L. (1988). *Contribution à l'étude des régimes hydrologiques de l'île de Tahiti* [THE : Thèses, Université Paris 11 (FRA) ; ORSTOM]. Orsay (FRA) ; Paris. https://www.documentation.ird.fr/hor/fdi:010020461

Feuillet, N., Beauducel, F., & Tapponnier, P. (2011). Tectonic context of moderate to large historical earthquakes in the Lesser Antilles and mechanical coupling with volcanoes. *Journal of Geophysical Research: Solid Earth*, *116*(B10). https://doi.org/https://doi.org/10.1029/2011JB008443

Fietzke, J., Liebetrau, V., Eisenhauer, A., & Dullo, C. (2005). Determination of uranium isotope ratios by multi-static MIC-ICP-MS: method and implementation for precise U- and Th-series isotope measurements. *J. Anal. At. Spectrom.*, *20*(5), 395-401.

Folwell, W. W. (1921). *A History of Minnesota*. Minnesota Historical Society. https://books.google.de/books?id=2SYUAAAAYAAJ

Forman, E. C. G., Baldini, J. U. L., Jamieson, R. A., Lechleitner, F. A., Walczak, I. W., Nita, D. C., Smith, S. R., Richards, D. A., Baldini, L. M., McIntyre, C., Müller, W., & Peters, A. J. (2025). The Gulf Stream moved northward at the end of the Little Ice Age. *Communications Earth & Environment*, *6*(1), 552. https://doi.org/10.1038/s43247-025-02446-3

Fowell, S. E., Sandford, K., Stewart, J. A., Castillo, K. D., Ries, J. B., & Foster, G. L. (2016). Intrareef variations in Li/Mg and Sr/Ca sea surface temperature proxies in the Caribbean reef-building coral Siderastrea siderea. *Paleoceanography*, *31*(10), 1315-1329. https://doi.org/10.1002/2016pa002968

Fox, P. J., & Heezen, B. C. (1975). Geology of the Caribbean Crust. In A. E. M. Nairn & F. G. Stehli (Eds.), *The Gulf of Mexico and the Caribbean* (pp. 421-466). Springer US. https://doi.org/10.1007/978-1-4684-8535-6_10

Frank, N., & Hemsing, F. (2021). Dating of corals and other geological samples via the radioactive disequilibrium of uranium and thorium isotopes. *Paleoclimatology*, 89-100.

Frank, N., Turpin, L., Cabioch, G., Blamart, D., Tressens-Fedou, M., Colin, C., & Jean-Baptiste, P. (2006). Open system U-series ages of corals from a subsiding reef in New Caledonia: Implications for sea level changes, and subsidence rate. *Earth and Planetary Science Letters*, *249*(3), 274-289. https://doi.org/https://doi.org/10.1016/j.epsl.2006.07.029

Gagan, M. K., Ayliffe, L. K., Beck, J. W., Cole, J. E., Druffel, E. R. M., Dunbar, R. B., & Schrag, D. P. (2000). New views of tropical paleoclimates from corals. *Quaternary Science Reviews*, *19*(1), 45-64. https://doi.org/https://doi.org/10.1016/S0277-3791(99)00054-2

Gagan, M. K., Ayliffe, L. K., Hopley, D., Cali, J. A., Mortimer, G. E., Chappell, J., McCulloch, M. T., & Head, M. J. (1998). Temperature and Surface-Ocean Water Balance of the Mid-Holocene Tropical Western Pacific. *Science*, *279*(5353), 1014-1018. https://doi.org/doi:10.1126/science.279.5353.1014

Gallup, C. D., Edwards, R. L., & Johnson, R. G. (1994). The timing of high sea levels over the past 200,000 years. *Science*, *263*(5148), 796-800. https://doi.org/10.1126/science.263.5148.796

Gayer, E., Ye, F., Barriot, J. P., & Moreir, M. (2014). Cosmogenic Erosion Rate Estimation from Detrital Olivine without Soil Characterization: The Case of the Matatia Basin (Tahiti Island). *Procedia Earth and Planetary Science*, *10*, 254-259. https://doi.org/https://doi.org/10.1016/j.proeps.2014.08.035

Giry, C., Felis, T., Kölling, M., & Scheffers, S. (2010). Geochemistry and skeletal structure of Diploria strigosa, implications for coral-based climate reconstruction. *Palaeogeography, Palaeoclimatology, Palaeoecology*, *298*(3), 378-387. https://doi.org/https://doi.org/10.1016/j.palaeo.2010.10.022

Giry, C., Felis, T., Kölling, M., Scholz, D., Wei, W., Lohmann, G., & Scheffers, S. (2012). Mid-to late Holocene changes in tropical Atlantic temperature seasonality and interannual to multidecadal variability documented in southern Caribbean corals. *Earth and Planetary Science Letters*, *331*, 187-200.

Glenn, E., Comarazamy, D., González, J. E., & Smith, T. (2015). Detection of recent regional sea surface temperature warming in the Caribbean and surrounding region. *Geophysical Research Letters*, *42*(16), 6785-6792. https://doi.org/https://doi.org/10.1002/2015GL065002

Godard, J., & Barriot, J.-P. (2022). Relationships between erosion rates and physiographic factors of drainage basins through a regression analysis: The case of Tahiti Nui Island. *Geomorphology*, *404*, 108176. https://doi.org/https://doi.org/10.1016/j.geomorph.2022.108176

Gondwe, B. R. N., Lerer, S., Stisen, S., Marín, L., Rebolledo-Vieyra, M., Merediz-Alonso, G., & Bauer-Gottwein, P. (2010). Hydrogeology of the south-eastern Yucatan Peninsula: New insights from water level measurements, geochemistry, geophysics and remote sensing. *Journal of Hydrology*, *389*(1), 1-17. https://doi.org/https://doi.org/10.1016/j.jhydrol.2010.04.044

Gonzalez-De Zayas, R., Merino-Ibarra, M., Soto-Jimenez, M. F., & Castillo-Sandoval, F. S. (2013). Biogeochemical responses to nutrient inputs in a Cuban coastal lagoon: runoff, anthropogenic, and groundwater sources. *Environ Monit Assess*, *185*(12), 10101-10114. https://doi.org/10.1007/s10661-013-3316-y

González-Herrera, R., Cortazar-Cepeda, M., Sánchez-Pinto, I., & Canto-Rios, J. (2022). A homogeneous approach in modeling a coastal karst aquifer. *Earth Science Informatics*, *15*(3), 1825-1840. https://doi.org/10.1007/s12145-022-00841-4

Greve, S., Frank, N., Montagna, P., Alonso-Hernández, C. M., Gomez-Batista, M., Douville, E., & Warken, S. F. (2025). Cuban coral traces annual hydrologically driven variability in δ234U values since the end of the Little Ice Age. https://doi.org/10.22541/au.173990739.96182414/v1

Grzymko, T. J., Marcantonio, F., McKee, B. A., & Mike Stewart, C. (2007). Temporal variability of uranium concentrations and 234U/238U activity ratios in the Mississippi river and its tributaries. *Chemical Geology*, *243*(3-4), 344-356. https://doi.org/10.1016/j.chemgeo.2007.05.024

Gu, S., Liu, Z., & Wu, L. (2020). Time Scale Dependence of the Meridional Coherence of the Atlantic Meridional Overturning Circulation. *Journal of Geophysical Research*, *125*.

Haase-Schramm, A., Böhm, F., Eisenhauer, A., Dullo, W.-C., Joachimski, M. M., Hansen, B., & Reitner, J. (2003). Sr/Ca ratios and oxygen isotopes from sclerosponges: Temperature history of the Caribbean mixed layer and thermocline during the Little Ice Age. *Paleoceanography*, *18*(3). https://doi.org/https://doi.org/10.1029/2002PA000830

Hagedorn, B., Becker, M. W., & Silbiger, N. J. (2020). Evidence of freshened groundwater below a tropical fringing reef. *Hydrogeology Journal*, *28*(7), 2501-2517. https://doi.org/10.1007/s10040-020-02191-1

Harbott, M., Wu, H. C., Kuhnert, H., Jimenez, C., González-Díaz, P., & Rixen, T. (2023). A Warming Southern Gulf of Mexico: Reconstruction of Anthropogenic Environmental Changes From a Siderastrea siderea Coral on the Northern Coast of Cuba. *Paleoceanography and Paleoclimatology*, *38*(12), e2023PA004717. https://doi.org/https://doi.org/10.1029/2023PA004717

Haßler, K., Dähnke, K., Kölling, M., Sichoix, L., Nickl, A.-L., & Moosdorf, N. (2019). Provenance of nutrients in submarine fresh groundwater discharge on Tahiti and Moorea, French Polynesia. *Applied Geochemistry*, *100*, 181-189. https://doi.org/10.1016/j.apgeochem.2018.11.020

Hathorne, E. C., Felis, T., James, R. H., & Thomas, A. (2011). Laser ablation ICP-MS screening of corals for diagenetically affected areas applied to Tahiti corals from the last deglaciation. *Geochimica et Cosmochimica Acta*, *75*(6), 1490-1506. https://doi.org/https://doi.org/10.1016/j.gca.2010.12.011

Hathorne, E. C., Gagnon, A., Felis, T., Adkins, J., Asami, R., Boer, W., Caillon, N., Case, D., Cobb, K. M., Douville, E., deMenocal, P., Eisenhauer, A., Garbe-Schönberg, D., Geibert, W., Goldstein, S., Hughen, K., Inoue, M., Kawahata, H., Kölling, M., . . . You, C. F. (2013). Interlaboratory study for coral Sr/Ca and other element/Ca ratio measurements. *Geochemistry, Geophysics, Geosystems*, *14*(9), 3730-3750. https://doi.org/10.1002/ggge.20230

Haug, H. G., Konrad, A. H., Daniel, M. S., Larry, C. P., & Ursula, R. (2001). Southward Migration of the Intertropical Convergence Zone Through the Holocene. *Science*, *293*(5533), 1304-1308. https://doi.org/10.1126/science.1059725

Hench, J. L., Leichter, J. J., & Monismith, S. G. (2008). Episodic circulation and exchange in a wave-driven coral reef and lagoon system. *Limnology and Oceanography*, *53*(6), 2681-2694. https://doi.org/https://doi.org/10.4319/lo.2008.53.6.2681

Henderson, G. M. (2002). Seawater (234U/238U) during the last 800 thousand years. *Earth and Planetary Science Letters*, *199*(1), 97-110. https://doi.org/https://doi.org/10.1016/S0012-821X(02)00556-3

Henderson, G. M., Cohen, A. S., & O'Nions, R. K. (1993). 234U/238U ratios and230Th ages for Hateruma Atoll corals: implications for coral diagenesis and seawater234U/238U ratios. *Earth and Planetary Science Letters*, *115*(1), 65-73. https://doi.org/https://doi.org/10.1016/0012-821X(93)90213-S

Hendy, E. J., Gagan, M. K., Lough, J. M., McCulloch, M., & deMenocal, P. B. (2007). Impact of skeletal dissolution and secondary aragonite on trace element and isotopic climate proxies in Porites corals. *Paleoceanography*, *22*(4). https://doi.org/10.1029/2007pa001462

Hernández-Terrones, L. M., Street, J., Null, K., & Paytan, A. (2021). Groundwater chemistry and Sr isotope ratios shed light on connectivity and water-rock interactions in the coastal aquifer of the Caribbean coast, Mexico. *Continental Shelf Research*, *212*, 104293. https://doi.org/https://doi.org/10.1016/j.csr.2020.104293

Hetzinger, S., Pfeiffer, M., Dullo, W.-C., Keenlyside, N., Latif, M., & Zinke, J. (2008). Caribbean coral tracks Atlantic Multidecadal Oscillation and past hurricane activity. *Geology*, *36*(1), 11-14. https://doi.org/10.1130/g24321a.1

Hibbert, F. D., Rohling, E. J., Dutton, A., Williams, F. H., Chutcharavan, P. M., Zhao, C., & Tamisiea, M. E. (2016). Coral indicators of past sea-level change: A global repository of U-series dated benchmarks. *Quaternary Science Reviews*, *145*, 1-56. https://doi.org/10.1016/j.quascirev.2016.04.019

Hildenbrand, A., Gillot, P.-Y., & Le Roy, I. (2004). Volcano-tectonic and geochemical evolution of an oceanic intra-plate volcano: Tahiti-Nui (French Polynesia). *Earth and Planetary Science Letters*, *217*(3), 349-365. https://doi.org/https://doi.org/10.1016/S0012-821X(03)00599-5

Hildenbrand, A., Gillot, P.-Y., & Marlin, C. (2008). Geomorphological study of long-term erosion on a tropical volcanic ocean island: Tahiti-Nui (French Polynesia). *Geomorphology*, *93*(3), 460-481. https://doi.org/https://doi.org/10.1016/j.geomorph.2007.03.012

Hildenbrand, A., Marlin, C., Conroy, A., Gillot, P.-Y., Filly, A., & Massault, M. (2005). Isotopic approach of rainfall and groundwater circulation in the volcanic structure of Tahiti-Nui (French Polynesia). *Journal of Hydrology*, *302*(1-4), 187-208. https://doi.org/10.1016/j.jhydrol.2004.07.006

Hitchcock, G. L., Wiseman, W. J., Boicourt, W. C., Mariano, A. J., Walker, N., Nelsen, T. A., & Ryan, E. (1997). Property fields in an effluent plume of the Mississippi river. *Journal of Marine Systems*, *12*(1), 109-126. https://doi.org/https://doi.org/10.1016/S0924-7963(96)00092-9

Hodell, D. A., Brenner, M., Curtis, J. H., Medina-González, R., Ildefonso-Chan Can, E., Albornaz-Pat, A., & Guilderson, T. P. (2005). Climate change on the Yucatan Peninsula during the Little Ice Age. *Quaternary Research*, *63*(2), 109-121. https://doi.org/10.1016/j.yqres.2004.11.004

Holgate, S. J., Matthews, A., Woodworth, P. L., Rickards, L. J., Tamisiea, M. E., Bradshaw, E., Foden, P. R., Gordon, K. M., Jevrejeva, S., & Pugh, J. (2013). New data systems and products at the permanent service for mean sea level. *Journal of Coastal Research*, *29*(3), 493-504.

Horwitz, E. P., Dietz, M. L., Chlanzla, R., & Diamond, H. (1992). Separation and preconcentration of uranium from acidic media by extraction chromatography. *Anatytica Chemica Acta*, *226*, 25-37.

Huyghues-Belrose, V. (2006). Variations et cycles climatiques à la Martinique. *Études caribéennes*(5). https://doi.org/https://doi.org/10.4000/etudescaribeennes.273

Inoue, M., Suwa, R., Suzuki, A., Sakai, K., & Kawahata, H. (2011). Effects of seawater pH on growth and skeletal U/Ca ratios ofAcropora digitiferacoral polyps. *Geophysical Research Letters*, *38*(12), n/a-n/a. https://doi.org/10.1029/2011gl047786

Instituto Nacional de Ecología, M., D.F. (2006). *Programa de Manejo del Parque Nacional Arrecife de Puerto Morelos (Management Program of the Puerto Morelos Reef National Park)* (

Iturralde-Vinent, M. A., Díaz, O. C., Antonio, G.-C., & and van Hinsbergen, D. J. J. (2008). Paleogene Foredeep Basin Deposits of North-Central Cuba: A Record of Arc-Continent Collision between the Caribbean and North American Plates. *International Geology Review*, *50*(10), 863-884. https://doi.org/10.2747/0020-6814.50.10.863

Iturralde-Vinent, M. A., García-Casco, A., Rojas-Agramonte, Y., Proenza, J. A., Murphy, J. B., & Stern, R. J. (2016). The geology of Cuba: A brief overview and synthesis. *GSA Today*, 4-10. https://doi.org/10.1130/gsatg296a.1

Ivanovich, M., & Harmon, R. S. (1992). *Uranium-series disequilibrium: applications to earth, marine, and environmental sciences. 2. ed*. Oxford (United Kingdom); Clarendon Press;. https://doi.org/https://doi.org/ Other: ISBN: 0 19 854278 X GBN

Jaffey, A. H., Flynn, K. F., Glendenin, L. E., Bentley, W. C., & Essling, A. M. (1971). Precision Measurement of Half-Lives and Specific Activities ofU235andU238. *Physical Review C*, *4*(5), 1889-1906. https://doi.org/10.1103/PhysRevC.4.1889

Johns, W. E., Townsend, T. L., Fratantoni, D. M., & Wilson, W. D. (2002). On the Atlantic inflow to the Caribbean Sea. *Deep Sea Research Part I: Oceanographic Research Papers*, *49*(2), 211-243. https://doi.org/https://doi.org/10.1016/S0967-0637(01)00041-3

Johnson, S. (2011). *Climate and Catastrophe in Cuba and the Atlantic World in the Age of Revolution*. University of North Carolina Press. https://doi.org/10.5149/9780807869345_johnson

Jones, P. D., Harpham, C., Harris, I., Goodess, C. M., Burton, A., Centella-Artola, A., Taylor, M. A., Bezanilla-Morlot, A., Campbell, J. D., Stephenson, T. S., Joslyn, O., Nicholls, K., & Baur, T. (2016). Long-term

trends in precipitation and temperature across the Caribbean. *International Journal of Climatology*, *36*(9), 3314-3333. https://doi.org/https://doi.org/10.1002/joc.4557

Jordà, G., Von Schuckmann, K., Josey, S. A., Caniaux, G., García-Lafuente, J., Sammartino, S., Özsoy, E., Polcher, J., Notarstefano, G., Poulain, P. M., Adloff, F., Salat, J., Naranjo, C., Schroeder, K., Chiggiato, J., Sannino, G., & Macías, D. (2017). The Mediterranean Sea heat and mass budgets: Estimates, uncertainties and perspectives. *Progress in Oceanography*, *156*, 174-208. https://doi.org/https://doi.org/10.1016/j.pocean.2017.07.001

Kennett, D. J., Breitenbach, S. F. M., Aquino, V. V., Asmerom, Y., Awe, J., Baldini, J. U. L., Bartlein, P., Culleton, B. J., Ebert, C., Jazwa, C., Macri, M. J., Marwan, N., Polyak, V., Prufer, K. M., Ridley, H. E., Sodemann, H., Winterhalder, B., & Haug, G. H. (2012). Development and Disintegration of Maya Political Systems in Response to Climate Change. *Science*, *338*(6108), 788-791. https://doi.org/doi:10.1126/science.1226299

Kerber, I. K., Arps, J., Eichstädter, R., Kontor, F., Dornick, C., Schröder-Ritzrau, A., Babu, A., Warken, S., & Frank, N. (2023). Simultaneous U and Th isotope measurements for U-series dating using MCICPMS. *Nuclear Instruments & Methods in Physics Research Section B-Beam Interactions with Materials and Atoms*, *539*, 169-178. https://doi.org/10.1016/j.nimb.2023.04.003

Kerber, I. K., Kontor, F., Mielke, A., Warken, S., & Frank, N. (2025). Technical note: „U-Th Analysis" – an open-source software dedicated to MCICPMS U-series-data treatment and evaluation. *Geochronology*, *7*, 1–13. https://doi.org/https://doi.org/10.5194/gchron-7-1-2025

Kigoshi, K. (1971). Alpha-Recoil Thorium-234: Dissolution into Water and the Uranium-234/Uranium-238 Disequilibrium in Nature. *Science*, *173*, 47-48.

Kilbourne, K. H., Quinn, T. M., Guilderson, T. P., Webb, R. S., & Taylor, F. W. (2007). Decadal- to interannual-scale source water variations in the Caribbean Sea recorded by Puerto Rican coral radiocarbon. *Climate Dynamics*, *29*(1), 51-62. https://doi.org/10.1007/s00382-007-0224-2

Kilbourne, K. H., Quinn, T. M., Webb, R., Guilderson, T., Nyberg, J., & Winter, A. (2008). Paleoclimate proxy perspective on Caribbean climate since the year 1751: Evidence of cooler temperatures and multidecadal variability. *Paleoceanography*, *23*(3). https://doi.org/10.1029/2008pa001598

Kipp, M. A., Li, H., Ellwood, M. J., John, S. G., Middag, R., Adkins, J. F., & Tissot, F. L. H. (2022). 238U, 235U and 234U in seawater and deep-sea corals: A high-precision reappraisal. *Geochimica et Cosmochimica Acta*, *336*, 231-248. https://doi.org/10.1016/j.gca.2022.09.018

Knebel, O., Felis, T., Asami, R., Deschamps, P., Kölling, M., & Scholz, D. (2024). Last Deglacial Environmental Change in the Tropical South Pacific From Tahiti Corals. *Paleoceanography and Paleoclimatology*, *39*(2), e2022PA004585. https://doi.org/https://doi.org/10.1029/2022PA004585

Ku, T.-L., Knauss, K. G., & Mathieu, G. G. (1977). Uranium in open ocean: concentration and isotopic composition. *Deep-Sea Research*, *24*, 1005-1017.

Kuang, X., Liu, J., Scanlon, B. R., Jiao, J. J., Jasechko, S., Lancia, M., Biskaborn, B. K., Wada, Y., Li, H., Zeng, Z., Guo, Z., Yao, Y., Gleeson, T., Nicot, J.-P., Luo, X., Zou, Y., & Zheng, C. (2024). The changing nature of groundwater in the global water cycle. *Science*, *383*(6686), eadf0630. https://doi.org/doi:10.1126/science.adf0630

Kwon, E. Y., Kim, G., Primeau, F., Moore, W. S., Cho, H.-M., DeVries, T., Sarmiento, J. L., Charette, M. A., & Cho, Y.-K. (2014). Global estimate of submarine groundwater discharge based on an observationally constrained radium isotope model. *Geophysical Research Letters*, *41*(23), 8438-8444. https://doi.org/https://doi.org/10.1002/2014GL061574

Kwon, Y. O., & Frankignoul, C. (2014). Mechanisms of Multidecadal Atlantic Meridional Overturning Circulation Variability Diagnosed in Depth versus Density Space. *Journal of Climate*, *27*, 9359-9376.

Ladd, M., Viau, A., Way, R., Gajewski, K., & Sawada, M. (2018). Variations in precipitation in North America during the past 2000 years. *The Holocene*, *28*(4), 667-675. https://doi.org/10.1177/0959683617735583

Landerer, F. W., Flechtner, F. M., Save, H., Webb, F. H., Bandikova, T., Bertiger, W. I., Bettadpur, S. V., Byun, S. H., Dahle, C., Dobslaw, H., Fahnestock, E., Harvey, N., Kang, Z., Kruizinga, G. L. H., Loomis, B. D., McCullough, C., Murböck, M., Nagel, P., Paik, M., . . . Yuan, D.-N. (2020). Extending the Global Mass Change Data Record: GRACE Follow-On Instrument and Science Data Performance. *Geophysical Research Letters*, *47*(12), e2020GL088306. https://doi.org/https://doi.org/10.1029/2020GL088306

Landsea, C. W., & Franklin, J. L. (2013). Atlantic Hurricane Database Uncertainty and Presentation of a New Database Format. *Monthly Weather Review*, *141*(10), 3576-3592. https://doi.org/https://doi.org/10.1175/MWR-D-12-00254.1

Lases-Hernández, M. F. (2013). *ANÁLISIS TEMPORAL Y ESPACIAL DE LA INFLUENCIA DE LOS CICLONES TROPICALES EN LA PRECIPITACIÓN DE LA PENÍNSULA DE YUCATÁN.* Cancún, Quintana Roo

LaVigne, M., Grottoli, A. G., Palardy, J. E., & Sherrell, R. M. (2016). Multi-colony calibrations of coral Ba/Ca with a contemporaneous in situ seawater barium record. *Geochimica et Cosmochimica Acta*, *179*, 203-216. https://doi.org/https://doi.org/10.1016/j.gca.2015.12.038

Lawrence, M. B., & Clark, G. B. (1985). Atlantic hurricane season of 1984. *Monthly Weather Review*, *113*(7), 1228-1237.

Lea, D. W., Shen, G. T., & Boyle, E. A. (1989). Coralline barium records temporal variability in equatorial Pacific upwelling. *Nature*, *340*(6232), 373-376. https://doi.org/10.1038/340373a0

Leaman, K. D., Vertes, P. S., Atkinson, L. P., Lee, T. N., Hamilton, P., & Waddell, E. (1995). Transport, potential vorticity, and current/temperature structure across Northwest Providence and Santaren Channels and the Florida Current off Cay Sal Bank. *Journal of Geophysical Research: Oceans*, *100*(C5), 8561-8569. https://doi.org/https://doi.org/10.1029/94JC01436

Leclerc, F., Feuillet, N., Perret, M., Cabioch, G., Bazin, S., Jean-Frédéric, L., & Saurel, J. m. (2015). The reef platform of Martinique: Interplay between eustasy, tectonic subsidence and volcanism since Late Pleistocene. *Marine Geology*, *369*, 34-51. https://doi.org/10.1016/j.margeo.2015.08.001

Leder, J. J., Swart, P. K., Szmant, A. M., & Dodge, R. E. (1996). The origin of variations in the isotopic record of scleractinian corals: I. Oxygen. *Geochimica et Cosmochimica Acta*, *60*(15), 2857-2870. https://doi.org/https://doi.org/10.1016/0016-7037(96)00118-4

Leichter, J., Aildredge, A., Bernardi, G., Brooks, A., Carlson, C., Carpenter, R., Edmunds, P., Fewing, M., Hanson, K., & Hench, J. (2013). Biological and Physical Interactions on a Tropical Island Coral Reef: Transport and Retention Processes on Moorea, French Polynesia. *OCEANOGRAPHY*, *26*, 52-63. https://doi.org/10.5670/oceanog.2013.45

Lesser, J. (1976). Resumen del estudio hidrogeológico e hidrogeoquímico de la Peninsula de Yucatán [Summary of the hydrogeological and hydrochemical study of the Yucatan Peninsula], Secretaria de Recursos Hidraulicos (SARH), DF, Mexico. In.

Li, L., Chen, J., Chen, T., Chen, Y., Hedding, D. W., Li, G., Li, L., Li, T., Robinson, L. F., West, A. J., Wu, W., You, C.-F., Zhao, L., & Li, G. (2018). Weathering dynamics reflected by the response of riverine uranium isotope disequilibrium to changes in denudation rate. *Earth and Planetary Science Letters*, *500*, 136-144. https://doi.org/10.1016/j.epsl.2018.08.008

Li, T., Robinson, L. F., MacGilchrist, G. A., Chen, T., Stewart, J. A., Burke, A., Wang, M., Li, G., Chen, J., & Rae, J. W. B. (2023). Enhanced subglacial discharge from Antarctica during meltwater pulse 1A. *Nature Communications*, *14*(1), 7327. https://doi.org/10.1038/s41467-023-42974-0

Lie, H.-J., & Cho, C.-H. (2002). Recent advances in understanding the circulation and hydrography of the East China Sea. *Fisheries Oceanography*, *11*(6), 318-328. https://doi.org/https://doi.org/10.1046/j.1365-2419.2002.00215.x

Limia, M., Vega, R., & Pérez, R. (2003). Climatología de los ciclones tropicales que han afectado a Cuba y sus provincias. Memorias del X Congreso Latinoamericano e Ibérico de Meteorología "La meteorología y el desarrollo sostenible". La Habana, Cuba,

Lin, L., Liu, D., Guo, X., Luo, C., & Cheng, Y. (2020). Tidal Effect on Water Export Rate in the Eastern Shelf Seas of China. *Journal of Geophysical Research: Oceans*, *125*(5), e2019JC015863. https://doi.org/https://doi.org/10.1029/2019JC015863

Liu, F., Lu, J., Kwon, Y. O., Frankignoul, C., & Luo, Y. (2022). Freshwater Flux Variability Lengthens the Period of the Low-Frequency AMOC Variability. *Geophysical Research Letters*, *49*.

Ludwig, K., Muhs, D., Simmons, K., Halley, R., & Shinn, E. (1996). Sea-level records at~ 80 ka from tectonically stable platforms: Florida and Bermuda. *Geology*, *24*(3), 211-214.

Ludwig, W., Dumont, E., Meybeck, M., & Heussner, S. (2009). River discharges of water and nutrients to the Mediterranean and Black Sea: Major drivers for ecosystem changes during past and future decades? *Progress in Oceanography*, *80*(3), 199-217. https://doi.org/https://doi.org/10.1016/j.pocean.2009.02.001

Lund, D. C., & Curry, W. (2006). Florida Current surface temperature and salinity variability during the last millennium. *Paleoceanography*, *21*(2). https://doi.org/https://doi.org/10.1029/2005PA001218

Lund, D. C., Lynch-Stieglitz, J., & Curry, W. B. (2006). Gulf Stream density structure and transport during the past millennium. *Nature*, *444*(7119), 601-604. https://doi.org/10.1038/nature05277

Lyon, B. (2003). Enhanced Seasonal Rainfall in Northern Venezuela and the Extreme Events of December 1999. *Journal of Climate*, *16*(13), 2302-2306. https://doi.org/https://doi.org/10.1175/2772.1

Ma, Q., & Zhang, Y. (2020). Global Research Trends and Hotspots on Submarine Groundwater Discharge (SGD): A Bibliometric Analysis. *International Journal of Environmental Research and Public Health*, *17*(3), 830. https://www.mdpi.com/1660-4601/17/3/830

Marshall, J. F., & McCulloch, M. T. (2002). An assessment of the Sr/Ca ratio in shallow water hermatypic corals as a proxy for sea surface temperature. *Geochimica et Cosmochimica Acta*, *66*(18), 3263-3280. https://doi.org/https://doi.org/10.1016/S0016-7037(02)00926-2

Martin, J. B., Kastner, M., Henry, P., Le Pichon, X., & Lallement, S. (1996). Chemical and isotopic evidence for sources of fluids in a mud volcano field seaward of the Barbados accretionary wedge. *Journal of Geophysical Research: Solid Earth*, *101*(B9), 20325-20345. https://doi.org/https://doi.org/10.1029/96JB00140

Martinez, C., Goddard, L., Kushnir, Y., & Ting, M. (2019). Seasonal climatology and dynamical mechanisms of rainfall in the Caribbean. *Climate Dynamics*, *53*(1), 825-846. https://doi.org/10.1007/s00382-019-04616-4

Maul, G. A. (1993). Climatic change in the Intra-Americas Sea. In G. A. Maul (Ed.). London ;: E. Arnold.

Mayfield, K. K., Eisenhauer, A., Santiago Ramos, D. P., Higgins, J. A., Horner, T. J., Auro, M., Magna, T., Moosdorf, N., Charette, M. A., Gonneea, M. E., Brady, C. E., Komar, N., Peucker-Ehrenbrink, B., & Paytan, A. (2021). Groundwater discharge impacts marine isotope budgets of Li, Mg, Ca, Sr, and Ba. *Nature Communications*, *12*(1), 148. https://doi.org/10.1038/s41467-020-20248-3

McCulloch, M., Fallon, S., Wyndham, T., Hendy, E., Lough, J., & Barnes, D. (2003). Coral record of increased sediment flux to the inner Great Barrier Reef since European settlement. *Nature*, *421*(6924), 727-730. https://doi.org/10.1038/nature01361

McCulloch, M. T., Gagan, M. K., Mortimer, G. E., Chivas, A. R., & Isdale, P. J. (1994). A high-resolution Sr/Ca and δ18O coral record from the Great Barrier Reef, Australia, and the 1982–1983 El Niño. *Geochimica et Cosmochimica Acta*, *58*(12), 2747-2754. https://doi.org/https://doi.org/10.1016/0016-7037(94)90142-2

Menna, M., & Poulain, P. M. (2010). Mediterranean intermediate circulation estimated from Argo data in 2003–2010. *Ocean Sci.*, *6*(1), 331-343. https://doi.org/10.5194/os-6-331-2010

Milne, G. A., Gehrels, W. R., Hughes, C. W., & Tamisiea, M. E. (2009). Identifying the causes of sea-level change. *Nature Geoscience*, *2*(7), 471-478. https://doi.org/10.1038/ngeo544

Molinari, R. L., Festa, J. F., & Behringer, D. W. (1978). The Circulation in the Gulf of Mexico Derived from Estimated Dynamic Height Fields. *Journal of Physical Oceanography*, *8*(6), 987-996. https://doi.org/https://doi.org/10.1175/1520-0485(1978)008<0987:TCITGO>2.0.CO;2

Monismith, S. G. (2007). Hydrodynamics of Coral Reefs. *Annual Review of Fluid Mechanics*, *39*(Volume 39, 2007), 37-55. https://doi.org/https://doi.org/10.1146/annurev.fluid.38.050304.092125

Monzote, R. F. (2024). Land Use in the Caribbean from the Mid-Nineteenth Century to 1950. *The Anthropocene as Multiple Crisis: Perspectives from Latin America*, 281.

Mook, W., & Rozanski, K. (2000). Environmental isotopes in the hydrological cycle. *IAEA Publish*, *39*(1), 2.

Moore, W. S. (1996). Large groundwater inputs to coastal waters revealed by 226Ra enrichments. *Nature*, *380*(6575), 612-614. https://doi.org/10.1038/380612a0

Moore, W. S. (2010). The effect of submarine groundwater discharge on the ocean. *Ann Rev Mar Sci*, *2*, 59-88. https://doi.org/10.1146/annurev-marine-120308-081019

Moyer, R. P. (2008). *Carbon Isotopes (δ¹³C & Δ¹⁴C) and Trace Elements (Ba, Mn, Y) in Small Mountainous Rivers and Coastal Coral Skeletons in Puerto Rico* The Ohio State University]. http://rave.ohiolink.edu/etdc/view?acc_num=osu1227292285

Moyer, R. P., & Grottoli, A. G. (2011). Coral skeletal carbon isotopes (δ13C and Δ14C) record the delivery of terrestrial carbon to the coastal waters of Puerto Rico. *Coral Reefs*, *30*(3). https://doi.org/10.1007/s00338-011-0758-y

Muhs, D. R., Simmons, K. R., Schumann, R. R., & Halley, R. B. (2011). Sea-level history of the past two interglacial periods: new evidence from U-series dating of reef corals from south Florida. *Quaternary Science Reviews*, *30*(5-6), 570-590.

Muller-Karger, F. E., Astor, Y. M., Benitez-Nelson, C. R., Buck, K. N., Fanning, K. A., Lorenzoni, L., Montes, E., Rueda-Roa, D. T., Scranton, M. I., Tappa, E., Taylor, G. T., Thunell, R. C., Troccoli, L., & Varela, R. (2019). The Scientific Legacy of the CARIACO Ocean Time-Series Program. *Annual Review of*

Marine Science, *11*(Volume 11, 2019), 413-437. https://doi.org/https://doi.org/10.1146/annurev-marine-010318-095150

Multer, H. G., Gischler, E., Lundberg, J., Simmons, K. R., & Shinn, E. A. (2002). Key Largo Limestone revisited: Pleistocene shelf-edge facies, Florida Keys, USA. *Facies*, *46*(1), 229-271. https://doi.org/10.1007/BF02668083

Murphy, S. J., Hurlburt, H. E., & O'Brien, J. J. (1999). The connectivity of eddy variability in the Caribbean Sea, the Gulf of Mexico, and the Atlantic Ocean. *Journal of Geophysical Research: Oceans*, *104*(C1), 1431-1453. https://doi.org/https://doi.org/10.1029/1998JC900010

Nothdurft, L. D., & Webb, G. E. (2008). Earliest diagenesis in scleractinian coral skeletons: implications for palaeoclimate-sensitive geochemical archives. *Facies*, *55*(2), 161-201. https://doi.org/10.1007/s10347-008-0167-z

Nozaki, Y., Kasemsupaya, V., & Tsubota, H. (1989). Mean residence time of the shelf water in the East China and the Yellow Seas determined by 228Ra/226Ra measurements. *Geophysical Research Letters*, *16*(11), 1297-1300. https://doi.org/https://doi.org/10.1029/GL016i011p01297

Null, K. A., Knee, K. L., Crook, E. D., de Sieyes, N. R., Rebolledo-Vieyra, M., Hernández-Terrones, L., & Paytan, A. (2014). Composition and fluxes of submarine groundwater along the Caribbean coast of the Yucatan Peninsula. *Continental Shelf Research*, *77*, 38-50. https://doi.org/https://doi.org/10.1016/j.csr.2014.01.011

Osmond, J., & Cowart, J. (1976). The theory and uses of natural uranium isotopic variations in hydrology. *Atomic Energy Review*, *14*(4), 621-679.

Osmond, J. K., & Cowart, J. B. (2000). U-Series Nuclides as Tracers in Groundwater Hydrology. In P. G. Cook & A. L. Herczeg (Eds.), *Environmental Tracers in Subsurface Hydrology* (pp. 145-173). Springer US. https://doi.org/10.1007/978-1-4615-4557-6_5

Ourbak, T., Corrège, T., Malaizé, B., Le Cornec, F., Charlier, K., & Peypouquet, J. P. (2006). A high-resolution investigation of temperature, salinity, and upwelling activity proxies in corals. *Geochemistry, Geophysics, Geosystems*, *7*(3). https://doi.org/10.1029/2005gc001064

Paces, J. B., Ludwig, K. R., Peterman, Z. E., & Neymark, L. A. (2002). 234U/238U evidence for local recharge and patterns of ground-water flow in the vicinity of Yucca Mountain, Nevada, USA. *Applied Geochemistry*, *17*(6), 751-779. https://doi.org/https://doi.org/10.1016/S0883-2927(02)00037-9

Palmer, M. R., & Edmond, J. M. (1993). Uranium in river water. *Geochimica et Cosmochimica Acta*, *57*(20), 4947-4955. https://doi.org/https://doi.org/10.1016/0016-7037(93)90131-F

Park, J., & Sweet, W. (2015). Accelerated sea level rise and Florida Current transport. *Ocean Science*, *11*, 607-615.

Parra, S. M., Valle-Levinson, A., Mariño-Tapia, I., & Enriquez, C. (2015). Salt intrusion at a submarine spring in a fringing reef lagoon. *Journal of Geophysical Research: Oceans*, *120*(4), 2736-2750. https://doi.org/https://doi.org/10.1002/2014JC010459

Parra, S. M., Valle-Levinson, A., Mariño-Tapia, I., Enriquez, C., Candela, J., & Sheinbaum, J. (2016). Seasonal variability of saltwater intrusion at a point-source submarine groundwater discharge. *Limnology and Oceanography*, *61*(4), 1245-1258. https://doi.org/https://doi.org/10.1002/lno.10286

Passeri, D. L., Hagen, S. C., Medeiros, S. C., Bilskie, M. V., Alizad, K., & Wang, D. (2015). The dynamic effects of sea level rise on low-gradient coastal landscapes: A review. *Earth's Future*, *3*(6), 159-181. https://doi.org/https://doi.org/10.1002/2015EF000298

Paterne, M., Druffel, E. R. M., Guilderson, T. P., Blamart, D., Moreau, C., Weil-Accardo, J., & Feuillet, N. (2023). Pulses of South Atlantic water into the tropical North Atlantic since 1825 from coral isotopes. *Science Advances*, *9*(50), eadi1687. https://doi.org/doi:10.1126/sciadv.adi1687

Paterne, M., Feuillet, N., Cabioch, G., Cortijo, E., Blamart, D., Weill-Accardo, J., Bonneau, L., Colin, C., Douville, E., & Pons-Branchu, E. (2018). Reservoir Ages in the Western Tropical North Atlantic from One Coral off Martinique Island (Lesser Antilles). *Radiocarbon*, *60*(2), 639-652. https://doi.org/10.1017/rdc.2017.118

Patricola, C. M., & Wehner, M. F. (2018). Anthropogenic influences on major tropical cyclone events. *Nature*, *563*(7731), 339-346. https://doi.org/10.1038/s41586-018-0673-2

Patterson, E., Eanes, S., Lancrete, P., Gothman, A., & Roback, P. (2021). Factors Controlling Coral Skeletal U/Ca Ratios with Implications for their Use as a Proxy for Past Ocean Conditions. *American Journal of Undergraduate Research*, *17*(4), 3-17. https://doi.org/10.33697/ajur.2020.031

Paul, D., Skrzypek, G., & Fórizs, I. (2007). Normalization of measured stable isotopic compositions to isotope reference scales – a review. *Rapid Communications in Mass Spectrometry*, *21*(18), 3006-3014. https://doi.org/https://doi.org/10.1002/rcm.3185

Perrin, C. (2003). Compositional heterogeneity and microstructural diversity of coral skeletons: implications for taxonomy and control on early diagenesis. *Coral Reefs*, *22*(2), 109-120. https://doi.org/10.1007/s00338-003-0291-8

Perry, E., Velazquez-Oliman, G., & Marin, L. (2002). The Hydrogeochemistry of the Karst Aquifer System of the Northern Yucatan Peninsula, Mexico. *International Geology Review*, *44*(3), 191-221. https://doi.org/10.2747/0020-6814.44.3.191

Pomeroy, A. W. M., Ghisalberti, M., Peterson, M., & Farooji, V. E. (2023). A framework to quantify flow through coral reefs of varying coral cover and morphology. *PLoS One*, *18*(1), e0279623. https://doi.org/10.1371/journal.pone.0279623

Pourmand, A., Tissot, F. L. H., Arienzo, M., & Sharifi, A. (2014). Introducing a Comprehensive Data Reduction and Uncertainty Propagation Algorithm for U-Th Geochronometry with Extraction Chromatography and Isotope Dilution MC-ICP-MS. *Geostandards and Geoanalytical Research*, *38*(2), 129-148. https://doi.org/https://doi.org/10.1111/j.1751-908X.2013.00266.x

Prouty, N. G., Field, M. E., Stock, J. D., Jupiter, S. D., & McCulloch, M. (2010). Coral Ba/Ca records of sediment input to the fringing reef of the southshore of Moloka'i, Hawai'i over the last several decades. *Marine Pollution Bulletin*, *60*(10), 1822-1835. https://doi.org/https://doi.org/10.1016/j.marpolbul.2010.05.024

Pugh, D., & Woodworth, P. (2014). *Sea-Level Science: Understanding Tides, Surges, Tsunamis and Mean Sea-Level Changes*. Cambridge University Press. https://doi.org/DOI: 10.1017/CBO9781139235778

Rad, S., Rivé, K., Vittecoq, B., Cerdan, O., & Allègre, C. J. (2013). Chemical weathering and erosion rates in the Lesser Antilles: An overview in Guadeloupe, Martinique and Dominica. *Journal of South American Earth Sciences*, *45*, 331-344. https://doi.org/https://doi.org/10.1016/j.jsames.2013.03.004

Reed, E. V., Thompson, D. M., Cole, J. E., Lough, J. M., Cantin, N. E., Cheung, A. H., Tudhope, A., Vetter, L., Jimenez, G., & Edwards, R. L. (2021). Impacts of Coral Growth on Geochemistry: Lessons From the Galápagos Islands. *Paleoceanography and Paleoclimatology*, *36*(4). https://doi.org/10.1029/2020pa004051

Ren, L., Braddock, K. L., Gerard, M. W., Daniel, P. S., & Ove, H.-g. (2003). Deconvolving the δ18O seawater component from subseasonal coral δ18O and Sr/Ca at Rarotonga in the southwestern subtropical Pacific for the period 1726 to 1997. *Geochimica et Cosmochimica Acta*, *67*(9), 1609-1621. https://doi.org/https://doi.org/10.1016/S0016-7037(02)00917-1

Richey, J. N., Poore, R. Z., Flower, B. P., Quinn, T. M., & Hollander, D. J. (2009). Regionally coherent Little Ice Age cooling in the Atlantic Warm Pool. *Geophysical Research Letters*, *36*(21). https://doi.org/https://doi.org/10.1029/2009GL040445

Rico-Esenaro, S., Sanchez-Cabeza, J.-A., Ruiz-Fernández, A., Montagna, P., & Carricart-Ganivet, J. P. (2022). Comparison of 100 Years of Growth in Two Nearby Coral Colonies of Orbicella Faveolata and Their Relationship with Climatic Oscillations in the Mexican Caribbean. *SSRN Electronic Journal*. https://doi.org/10.2139/ssrn.4264477

Rico-Esenaro, S. D., Sanchez-Cabeza, J. A., Carricart-Ganivet, J. P., Montagna, P., & Ruiz-Fernandez, A. C. (2019). Uncertainty and variability of extension rate, density and calcification rate of a hermatypic coral (Orbicella faveolata). *Sci Total Environ*, *650*(Pt 1), 1576-1581. https://doi.org/10.1016/j.scitotenv.2018.08.397

Ritter, S. M., Isenbeck-Schröter, M., Scholz, C., Keppler, F., Gescher, J., Klose, L., Schorndorf, N., Avilés Olguín, J., González-González, A., & Stinnesbeck, W. (2019). Subaqueous speleothems (Hells Bells) formed by the interplay of pelagic redoxcline biogeochemistry and specific hydraulic conditions in the El Zapote sinkhole, Yucatán Peninsula, Mexico. *Biogeosciences*, *16*(11), 2285-2305. https://doi.org/10.5194/bg-16-2285-2019

Robinson, L. F., Adkins, J. F., Fernandez, D. P., Burnett, D. S., Wang, S. L., Gagnon, A. C., & Krakauer, N. (2006). Primary U distribution in scleractinian corals and its implications for U series dating. *Geochemistry, Geophysics, Geosystems*, *7*(5). https://doi.org/10.1029/2005gc001138

Robinson, L. F., Belshaw, N. S., & Henderson, G. M. (2004b). U and Th concentrations and isotope ratios in modern carbonates and waters from the Bahamas. *Geochimica et Cosmochimica Acta*, *68*(8), 1777-1789. https://doi.org/10.1016/j.gca.2003.10.005

Robinson, L. F., Henderson, G. M., Hall, L., & Matthews, I. (2004a). Climatic Control of Riverine and Seawater Uranium-Isotope Ratios. *Science*, *305*, 851-854.

Robinson, L. F., Henderson, G. M., & Slowey, N. C. (2002). U-Th dating of marine isotope stage 7 in Bahamas slope sediments. *Earth and Planetary Science Letters*, *196*, 175–187.

Rodellas, V., Garcia-Orellana, J., Masque, P., Feldman, M., & Weinstein, Y. (2015). Submarine groundwater discharge as a major source of nutrients to the Mediterranean Sea. *Proc Natl Acad Sci U S A*, *112*(13), 3926-3930. https://doi.org/10.1073/pnas.1419049112

Romero-Sierra, P., Rivas, D., Almazán-Becerril, A., & Hernández-Terrones, L. (2018). Hydrochemistry and hydrodynamics of a Mexican Caribbean Lagoon: Nichupté Lagoon System. *Estuarine, Coastal and Shelf Science*, *215*, 185-198. https://doi.org/https://doi.org/10.1016/j.ecss.2018.10.012

Ross, C. L., DeCarlo, T. M., & McCulloch, M. T. (2019). Calibration of Sr/Ca, Li/Mg and Sr-U Paleothermometry in Branching and Foliose Corals. *Paleoceanography and Paleoclimatology*, *34*(8), 1271-1291. https://doi.org/10.1029/2018pa003426

Rougerie, F., Fichez, R., & Déjardin, P. (2004). Chapter 15 - Geomorphology and Hydrogeology of Selected Islands of French Polynesia: Tikehau (Atoll) and Tahiti (Barrier Reef). In H. L. Vacher & T. M. Quinn (Eds.), *Developments in Sedimentology* (Vol. 54, pp. 475-502). Elsevier. https://doi.org/https://doi.org/10.1016/S0070-4571(04)80037-2

Roy-Barman, M., Jeandel, C., Roy-Barman, M., & Jeandel, C. (2016). 129Radioactive and Radiogenic Isotopes. In *Marine Geochemistry: Ocean Circulation, Carbon Cycle and Climate Change* (pp. 0). Oxford University Press. https://doi.org/10.1093/acprof:oso/9780198787495.003.0004

Rueda-Roa, D. T., & Muller-Karger, F. E. (2013). The southern Caribbean upwelling system: Sea surface temperature, wind forcing and chlorophyll concentration patterns. *Deep Sea Research Part I: Oceanographic Research Papers*, *78*, 102-114. https://doi.org/https://doi.org/10.1016/j.dsr.2013.04.008

Sadler, J., Gregory, E. W., Luke, D. N., & Belinda, D. (2014). Geochemistry-based coral palaeoclimate studies and the potential of 'non-traditional' (non-massive Porites) corals: Recent developments and future progression. *Earth-Science Reviews*, *139*, 291-316. https://doi.org/https://doi.org/10.1016/j.earscirev.2014.10.002

Saha, S., Nadiga, S., Thiaw, C., Wang, J., Wang, W., Zhang, Q., Van den Dool, H. M., Pan, H. L., Moorthi, S., Behringer, D., Stokes, D., Peña, M., Lord, S., White, G., Ebisuzaki, W., Peng, P., & Xie, P. (2006). The NCEP Climate Forecast System. *Journal of Climate*, *19*(15), 3483-3517. https://doi.org/https://doi.org/10.1175/JCLI3812.1

Sayani, H. R., Cobb, K. M., DeLong, K., Hitt, N. T., & Druffel, E. R. M. (2019). Intercolony δ18O and Sr/Ca variability among Porites spp. corals at Palmyra Atoll: Toward more robust coral-based estimates of climate. *Geochemistry, Geophysics, Geosystems*, *20*(11), 5270-5284. https://doi.org/https://doi.org/10.1029/2019GC008420

Schmidt, M. W., Spero, H. J., & Lea, D. W. (2004). Links between salinity variation in the Caribbean and North Atlantic thermohaline circulation. *Nature*, *428*(6979), 160-163. https://doi.org/10.1038/nature02346

Schoepf, V., Levas, S. J., Rodrigues, L. J., McBride, M. O., Aschaffenburg, M. D., Matsui, Y., Warner, M. E., Hughes, A. D., & Grottoli, A. G. (2014). Kinetic and metabolic isotope effects in coral skeletal carbon isotopes: A re-evaluation using experimental coral bleaching as a case study. *Geochimica et Cosmochimica Acta*, *146*, 164-178. https://doi.org/10.1016/j.gca.2014.09.033

Schoepf, V., McCulloch, M. T., Warner, M. E., Levas, S. J., Matsui, Y., Aschaffenburg, M. D., & Grottoli, A. G. (2014). Short-term coral bleaching is not recorded by skeletal boron isotopes. *PLoS One*, *9*(11), e112011. https://doi.org/10.1371/journal.pone.0112011

Scholl, M. (2014). *Stable Isotope (δ18O and δ2H) Data for Precipitation, Stream Water, and Groundwater in Puerto Rico*. https://doi.org/10.3133/ofr20141101

Scholz, D., Mangini, A., & Felis, T. (2004). U-series dating of diagenetically altered fossil reef corals. *Earth and Planetary Science Letters*, *218*(1), 163-178. https://doi.org/https://doi.org/10.1016/S0012-821X(03)00647-2

Schorndorf, N., Frank, N., Ritter, S. M., Warken, S. F., Scholz, C., Keppler, F., Scholz, D., Weber, M., Aviles Olguin, J., & Stinnesbeck, W. (2023). Mid- to late Holocene sea-level rise recorded in Hells Bells (234)U/(238)U ratio and geochemical composition. *Sci Rep*, *13*(1), 10011. https://doi.org/10.1038/s41598-023-36777-y

Shackleton, N. J. (1987). Oxygen isotopes, ice volume and sea level. *Quaternary Science Reviews*, *6*(3), 183-190. https://doi.org/https://doi.org/10.1016/0277-3791(87)90003-5

Shang, T., Jiang, X., & Yu, C. (2021). 234U/238U as a potential tracer for tracking water masses mixing in the northern East China Sea. *Acta Oceanologica Sinica*, *40*(4), 23-31. https://doi.org/10.1007/s13131-021-1773-7

Shaw, K. M. M., Standish, C. D., Fowell, S. E., Stewart, J. A., Castillo, K. D., Ries, J. B., & Foster, G. L. (2024). Century-Long Records of Sedimentary Input on a Caribbean Reef From Coral Ba/Ca Ratios.

Paleoceanography and Paleoclimatology, *39*(5), e2023PA004746. https://doi.org/https://doi.org/10.1029/2023PA004746

Shen, C.-C., Lawrence Edwards, R., Cheng, H., Dorale, J. A., Thomas, R. B., Bradley Moran, S., Weinstein, S. E., & Edmonds, H. N. (2002). Uranium and thorium isotopic and concentration measurements by magnetic sector inductively coupled plasma mass spectrometry. *Chemical Geology*, *185*, 165–178.

Shen, C.-C., Li, K.-S., Sieh, K., Natawidjaja, D., Cheng, H., Wang, X., Edwards, R. L., Lam, D. D., Hsieh, Y.-T., Fan, T.-Y., Meltzner, A. J., Taylor, F. W., Quinn, T. M., Chiang, H.-W., & Kilbourne, K. H. (2008). Variation of initial 230Th/232Th and limits of high precision U–Th dating of shallow-water corals. *Geochimica et Cosmochimica Acta*, *72*(17), 4201-4223. https://doi.org/10.1016/j.gca.2008.06.011

Shen, G. T., Cole, J. E., Lea, D. W., Linn, L. J., McConnaughey, T. A., & Fairbanks, R. G. (1992). Surface ocean variability at Galapagos from 1936–1982: Calibration of geochemical tracers in corals. *Paleoceanography*, *7*(5), 563-588. https://doi.org/https://doi.org/10.1029/92PA01825

Shen, G. T., & Dunbar, R. B. (1995). Environmental controls on uranium in reef corals. *Geochimica et Cosmochimica Acta*, *59*(10), 2009-2024. https://doi.org/https://doi.org/10.1016/0016-7037(95)00123-9

Siddall, M., Rohling, E. J., Almogi-Labin, A., Hemleben, C., Meischner, D., Schmelzer, I., & Smeed, D. A. (2003). Sea-level fluctuations during the last glacial cycle. *Nature*, *423*(6942), 853-858. https://doi.org/10.1038/nature01690

Smith, J. M., Quinn, T. M., Helmle, K. P., & Halley, R. B. (2006). Reproducibility of geochemical and climatic signals in the Atlantic coral Montastraea faveolata. *Paleoceanography*, *21*(1). https://doi.org/https://doi.org/10.1029/2005PA001187

Smith, S. V., Buddemeier, R. W., Redalje, R. C., & Houck, J. E. (1979). Strontium-Calcium Thermometry in Coral Skeletons. *Science*, *204*(4391), 404-407. https://doi.org/doi:10.1126/science.204.4391.404

Stallard, R. F. (1985). River Chemistry, Geology, Geomorphology, and Soils in the Amazon and Orinoco Basins. In J. I. Drever (Ed.), *The Chemistry of Weathering* (pp. 293-316). Springer Netherlands. https://doi.org/10.1007/978-94-009-5333-8_17

Stammer, D., Cazenave, A., Ponte, R. M., & Tamisiea, M. E. (2013). Causes for Contemporary Regional Sea Level Changes. *Annual Review of Marine Science*, *5*(Volume 5, 2013), 21-46. https://doi.org/https://doi.org/10.1146/annurev-marine-121211-172406

Starke, C., Ekau, W., & Moosdorf, N. (2020). Enhanced Productivity and Fish Abundance at a Submarine Spring in a Coastal Lagoon on Tahiti, French Polynesia [Original Research]. *Frontiers in Marine Science*, *6*. https://doi.org/10.3389/fmars.2019.00809

Stevenson, S., Powell, B., Cobb, K. M., Nusbaumer, J., Merrifield, M., & Noone, D. (2018). Twentieth Century Seawater δ18O Dynamics and Implications for Coral-Based Climate Reconstruction. *Paleoceanography and Paleoclimatology*, *33*(6), 606-625. https://doi.org/https://doi.org/10.1029/2017PA003304

Suksi, J., Rasilainen, K., & Pitkänen, P. (2006). Variations in 234U/238U activity ratios in groundwater—A key to flow system characterisation? *Physics and Chemistry of the Earth, Parts A/B/C*, *31*(10), 556-571. https://doi.org/https://doi.org/10.1016/j.pce.2006.04.007

Survey, U. S. G. (2012). *Option 7 -- Display algorithm in reverse polish notation (RPN), in User's Manual for the National Water Information System of the U.S. Geological Survey--Water-Quality System: U.S. Geological Survey* (https://doi.org/http://nwis.usgs.gov/currentdocs/index.html

Swart, P. K., Elderfield, H., & Greaves, M. J. (2002). A high-resolution calibration of Sr/Ca thermometry using the Caribbean coral Montastraea annularis. *Geochemistry, Geophysics, Geosystems*, *3*(11), 1-11. https://doi.org/https://doi.org/10.1029/2002GC000306

Swart, P. K., & Grottoli, A. (2003). Proxy indicators of climate in coral skeletons: a perspective. *Coral Reefs*, *22*(4), 313-315. https://doi.org/10.1007/s00338-003-0332-3

Swarzenski, P., Campbell, P., Porcelli, D., & McKee, B. (2004). The estuarine chemistry and isotope systematics of 234,238U in the Amazon and Fly Rivers. *Continental Shelf Research*, *24*(19), 2357-2372. https://doi.org/https://doi.org/10.1016/j.csr.2004.07.025

Swarzenski, P. W., & Baskaran, M. (2007). Uranium distribution in the coastal waters and pore waters of Tampa Bay, Florida. *Marine Chemistry*, *104*(1), 43-57. https://doi.org/https://doi.org/10.1016/j.marchem.2006.05.002

Taïlamé, A.-L. L., S. (2020). *Définition des volumes d'eau prélevables en Martinique*. BRGM. https://www.martinique.developpement-durable.gouv.fr/IMG/pdf/volume_d_eau_prelevable.pdf

Taylor, M. A., Clarke, L. A., Centella, A., Bezanilla, A., Stephenson, T. S., Jones, J. J., Campbell, J. D., Vichot, A., & Charlery, J. (2018). Future Caribbean Climates in a World of Rising Temperatures: The 1.5 vs 2.0 Dilemma. *Journal of Climate*, *31*(7), 2907-2926. https://doi.org/https://doi.org/10.1175/JCLI-D-17-0074.1

Terry, J. P., & Kim, I.-H. (2015). Morphometric analysis of tropical storm and hurricane tracks in the North Atlantic basin using a sinuosity-based approach. *International Journal of Climatology*, *35*(6), 923-934. https://doi.org/https://doi.org/10.1002/joc.4027

Thompson, D. M. (2021). Environmental records from coral skeletons: A decade of novel insights and innovation. *WIREs Climate Change*, *13*(1). https://doi.org/10.1002/wcc.745

Thompson, W. G., & Goldstein, S. L. (2005). Open-system coral ages reveal persistent suborbital sea-level cycles. *Science*, *308*(5720), 401–404. https://doi.org/doi:10.1126/science.1104035

Thompson, W. G., Spiegelman, M. W., Goldstein, S. L., & Speed, R. C. (2003). An open-system model for U-series age determinations of fossil corals. *Earth and Planetary Science Letters*, *210*(1), 365-381. https://doi.org/https://doi.org/10.1016/S0012-821X(03)00121-3

Toggweiler, J. R., Druffel, E. R. M., Key, R. M., & Galbraith, E. D. (2019). Upwelling in the Ocean Basins North of the ACC: 2. How Cool Subantarctic Water Reaches the Surface in the Tropics. *Journal of Geophysical Research: Oceans*, *124*(4), 2609-2625. https://doi.org/10.1029/2018jc014795

Tomer, A. S., McKenzie, T., Majtényi-Hill, C., Cabral, A., Yau, Y. Y. Y., Call, M., Chen, X., Correa, R. E., Davis, K., Jeffrey, L., Sadat-Noori, M., Tait, D., Webb, J., Maher, D. T., Henriksson, L., Bonaglia, S., Zhao, S., Cardenas, M. B., & Santos, I. R. (2025). Groundwater releases CO₂ to diverse global coastal ecosystems. *Science Advances*, *11*(2), eadr3240. https://doi.org/doi:10.1126/sciadv.adr3240

Torres, R. R., & Tsimplis, M. N. (2013). Sea-level trends and interannual variability in the Caribbean Sea. *Journal of Geophysical Research: Oceans*, *118*(6), 2934-2947. https://doi.org/https://doi.org/10.1002/jgrc.20229

Toscano, M. A., & Lundberg, J. (1998). Early Holocene sea-level record from submerged fossil reefs on the southeast Florida margin. *Geology*, *26*(3), 255-258.

Trenberth, K. E., & Caron, J. M. (2000). The Southern Oscillation Revisited: Sea Level Pressures, Surface Temperatures, and Precipitation. *Journal of Climate*, *13*(24), 4358-4365. https://doi.org/https://doi.org/10.1175/1520-0442(2000)013<4358:TSORSL>2.0.CO;2

Uchupi, E. (1975). Physiography of the Gulf of Mexico and Caribbean Sea. In A. E. M. Nairn & F. G. Stehli (Eds.), *The Gulf of Mexico and the Caribbean* (pp. 1-64). Springer US. https://doi.org/10.1007/978-1-4684-8535-6_1

Veron, J. E. N. (1995). *Corals in space and time: the biogeography and evolution of the Scleractinia*. Cornell University Press.

Viau, A. E., Gajewski, K., Sawada, M. C., & Fines, P. (2006). Millennial-scale temperature variations in North America during the Holocene. *Journal of Geophysical Research: Atmospheres*, *111*(D9). https://doi.org/https://doi.org/10.1029/2005JD006031

Vieten, R., Warken, S., Winter, A., Schröder-Ritzrau, A., Scholz, D., & Spötl, C. (2018). Hurricane Impact on Seepage Water in Larga Cave, Puerto Rico. *Journal of Geophysical Research: Biogeosciences*, *123*(3), 879-888. https://doi.org/https://doi.org/10.1002/2017JG004218

Vieten, R., Warken, S. F., Zanchettin, D., Winter, A., Scholz, D., Black, D., Koltai, G., & Spötl, C. (2024). Northeastern Caribbean Rainfall Variability Linked to Solar and Volcanic Forcing. *Paleoceanography and Paleoclimatology*, *39*(4), e2023PA004720. https://doi.org/https://doi.org/10.1029/2023PA004720

Vigier, N., Burton, K. W., Gislason, S. R., Rogers, N. W., Duchene, S., Thomas, L., Hodge, E., & Schaefer, B. (2006). The relationship between riverine U-series disequilibria and erosion rates in a basaltic terrain. *Earth and Planetary Science Letters*, *249*(3), 258-273. https://doi.org/https://doi.org/10.1016/j.epsl.2006.07.001

Villemant, B., & Feuillet, N. (2003). Dating open systems by the 238U–234U–230Th method: application to Quaternary reef terraces. *Earth and Planetary Science Letters*, *210*(1), 105-118. https://doi.org/https://doi.org/10.1016/S0012-821X(03)00100-6

Vorosmarty, C. J., Fekete, B. M., & Tucker, B. A. (1998). Global River Discharge, 1807-1991, V[ersion]. 1.1 (RivDIS). In: ORNL Distributed Active Archive Center.

Vose, R. S., Schmoyer, R. L., Steurer, P., Peterson, T. C., Heim, R., Karl, T. R., & Eischeid, J. K. (1992). The Global Historical Climatology Network: Long-term monthly temperature, precipitation, sea level pressure, and station pressure data.

Wang, C. (2002). Atlantic Climate Variability and Its Associated Atmospheric Circulation Cells. *Journal of Climate*, *15*(13), 1516-1536. https://doi.org/10.1175/1520-0442(2002)015<1516:Acvaia>2.0.Co;2

Wang, C. (2019). Three-ocean interactions and climate variability: a review and perspective. *Climate Dynamics*, *53*(7-8), 5119-5136. https://doi.org/10.1007/s00382-019-04930-x

Wang, C., & Enfield, D. B. (2001). The Tropical Western Hemisphere Warm Pool. *Geophysical Research Letters*, *28*(8), 1635-1638. https://doi.org/https://doi.org/10.1029/2000GL011763

Wang, C., Lee, S.-K., & Enfield, D. B. (2008). Climate Response to Anomalously Large and Small Atlantic Warm Pools during the Summer. *Journal of Climate*, *21*(11), 2437-2450. https://doi.org/https://doi.org/10.1175/2007JCLI2029.1

Wang, C., Lee, S.-K., & Mechoso, C. R. (2010). Interhemispheric Influence of the Atlantic Warm Pool on the Southeastern Pacific. *Journal of Climate*, *23*(2), 404-418. https://doi.org/10.1175/2009jcli3127.1

Wang, L., Ma, Z., Sun, Z., Wang, Y., Wang, X., Cheng, H., & Xiao, J. (2017). U concentration and 234 U/ 238 U of seawater from the Okinawa Trough and Indian Ocean using MC-ICPMS with SEM protocols. *Marine Chemistry*, *196*, 71-80. https://doi.org/10.1016/j.marchem.2017.08.001

Wanner, H., Solomina, O., Grosjean, M., Ritz, S. P., & Jetel, M. (2011). Structure and origin of Holocene cold events. *Quaternary Science Reviews*, *30*(21), 3109-3123. https://doi.org/https://doi.org/10.1016/j.quascirev.2011.07.010

Watanabe, T., Gagan, M. K., Corrége, T., Scott-Gagan, H., Cowley, J., & Hantoro, W. S. (2003). Oxygen isotope systematics in Diploastrea heliopora: new coral archive of tropical paleoclimate. *Geochimica et Cosmochimica Acta*, *67*(7), 1349-1358. https://doi.org/https://doi.org/10.1016/S0016-7037(02)01221-8

Watanabe, T., Winter, A., Oba, T., Anzai, R., & Ishioroshi, H. (2002). Evaluation of the fidelity of isotope records as an environmental proxy in the coral Montastraea. *Coral Reefs*, *21*(2), 169-178. https://doi.org/10.1007/s00338-002-0218-9

Wefing, A.-M., Arps, J., Blaser, P., Wienberg, C., Hebbeln, D., & Frank, N. (2017). High precision U-series dating of scleractinian cold-water corals using an automated chromatographic U and Th extraction. *Chemical Geology*, *475*, 140-148. https://doi.org/10.1016/j.chemgeo.2017.10.036

Weil-Accardo, J., Feuillet, N., Jacques, E., Deschamps, P., Beauducel, F., Cabioch, G., Tapponnier, P., Saurel, J.-M., & Galetzka, J. (2016). Two hundred thirty years of relative sea level changes due to climate and megathrust tectonics recorded in coral microatolls of Martinique (French West Indies). *Journal of Geophysical Research: Solid Earth*, *121*(4), 2873-2903. https://doi.org/https://doi.org/10.1002/2015JB012406

Wesselingh, F. P., & Hoorn, C. (2011). Three. Geological Development of Amazon and Orinoco Basins. In S. A. James & R. Roberto (Eds.), *Historical Biogeography of Neotropical Freshwater Fishes* (pp. 59-68). University of California Press. https://doi.org/doi:10.1525/9780520948501-005

Wienberg, C., Krengel, T., Frank, N., Wang, H., Van Rooij, D., & Hebbeln, D. (2022). Cold-water coral mounds in the western Mediterranean Sea: New insights into their initiation and development since the Mid-Pleistocene in response to changes of African hydroclimate. *Quaternary Science Reviews*, *293*. https://doi.org/10.1016/j.quascirev.2022.107723

Winter, A., Appeldoorn, R., Bruckner, A., Williams Jr, E., & Goenaga, C. (1998). Sea surface temperatures and coral reef bleaching off La Parguera, Puerto Rico (northeastern Caribbean Sea). *Coral Reefs*, *17*, 377-382.

Winter, A., Ishioroshi, H., Watanabe, T., Oba, T., & Christy, J. (2000). Caribbean sea surface temperatures: Two-to-three degrees cooler than present during the Little Ice Age. *Geophysical Research Letters*, *27*(20), 3365-3368. https://doi.org/https://doi.org/10.1029/2000GL011426

Woodworth, P. L., Melet, A., Marcos, M., Ray, R. D., Wöppelmann, G., Sasaki, Y. N., Cirano, M., Hibbert, A., Huthnance, J. M., Monserrat, S., & Merrifield, M. A. (2019). Forcing Factors Affecting Sea Level Changes at the Coast. *Surveys in Geophysics*, *40*(6), 1351-1397. https://doi.org/10.1007/s10712-019-09531-1

Wu, H. C., Felis, T., Scholz, D., Giry, C., Kolling, M., Jochum, K. P., & Scheffers, S. R. (2017). Changes to Yucatan Peninsula precipitation associated with salinity and temperature extremes of the Caribbean Sea during the Maya civilization collapse. *Sci Rep*, *7*(1), 15825. https://doi.org/10.1038/s41598-017-15942-0

Xu, C., Wang, X., Zhang, F., Lao, Y., Liu, J., & Du, J. (2024). Potential Linkages Between Submarine Groundwater (Fresh and Saline) Nutrient Inputs and Eutrophication in a Coastal Aquaculture

Bay. *Journal of Geophysical Research: Oceans*, *129*(10), e2024JC021501. https://doi.org/https://doi.org/10.1029/2024JC021501

Yamazaki, A., Yano, M., Harii, S., & Watanabe, T. (2021). Effects of light on the Ba/Ca ratios in coral skeletons. *Chemical Geology*, *559*. https://doi.org/10.1016/j.chemgeo.2020.119911

Ye, F., Sichoix, L., Barriot, J.-P., & Dumas, P. (2009). Modeling the erosion of tropical volcanic ocean islands : The Tahiti island case (French Polynesia). *AGU Fall Meeting Abstracts*.

Young, C., Martin, J. B., Branyon, J., Pain, A., Valle-Levinson, A., Mariño-Tapia, I., & Vieyra, M. R. (2018). Effects of short-term variations in sea level on dissolved oxygen in a coastal karst aquifer, Quintana Roo, Mexico. *Limnology and Oceanography*, *63*(1), 352-362. https://doi.org/https://doi.org/10.1002/lno.10635

Yu, J.-Y., & Kim, S. T. (2011). Relationships between Extratropical Sea Level Pressure Variations and the Central Pacific and Eastern Pacific Types of ENSO. *Journal of Climate*, *24*(3), 708-720. https://doi.org/https://doi.org/10.1175/2010JCLI3688.1

Yu, K.-F., Zhao, J.-X., Shi, Q., Chen, T.-G., Wang, P.-X., Collerson, K. D., & Liu, T.-S. (2006). U-series dating of dead Porites corals in the South China sea: Evidence for episodic coral mortality over the past two centuries. *Quaternary Geochronology*, *1*(2), 129-141. https://doi.org/https://doi.org/10.1016/j.quageo.2006.06.005

Zhou, J., Du, J., Moore, W. S., Qu, J., & Zhang, G. (2015). Concentrations and fluxes of uranium in two major Chinese rivers: The Changjiang River and the Huanghe River. *Estuarine, Coastal and Shelf Science*, *152*, 56-64. https://doi.org/10.1016/j.ecss.2014.11.004

Zhou, Y., Sawyer, A. H., David, C. H., & Famiglietti, J. S. (2019). Fresh Submarine Groundwater Discharge to the Near-Global Coast. *Geophysical Research Letters*, *46*(11), 5855-5863. https://doi.org/https://doi.org/10.1029/2019GL082749

Danksagung

An erster Stelle möchte ich meinem Betreuer, Prof. Dr. Norbert Frank, meinen herzlichsten Dank aussprechen. Seine wissenschaftliche Unterstützung, seine stete Bereitschaft zur Diskussion und seine wertvollen Anregungen haben dieses Projekt entscheidend geprägt. Meiner Co-Betreuerin Dr. Sophie Warken danke ich herzlich für ihre kontinuierliche Unterstützung, ihre Zeit und ihre wertvollen fachlichen wie auch persönlichen Ratschläge. Ebenso danke ich meinem Zweitgutachter, Prof. Dr. Oliver Friedrich, für seine konstruktiven Rückmeldungen und die Begleitung meiner Arbeit.

Ein besonderer Dank gilt auch meinen Kooperationspartnern, die dieses Projekt durch ihre Expertise und Unterstützung maßgeblich bereichert haben. Hervorheben möchte ich insbesondere Dr. Paolo Montagna und Dr. Eric Douville, die mir den Zugang zu wichtigen Korallenproben ermöglicht bzw. die Durchführung von Messungen unterstützt haben.

Ebenso danke ich den gesamten PUA‘s, mit der ich nicht nur wissenschaftlich viel gelernt, sondern auch immer großen Spaß gehabt habe. Besonders danken möchte ich Nils, Aaron und Pauline, nicht nur für ihre Unterstützung im wissenschaftlichen Alltag, sondern auch für die vielen gemeinsamen Darts-Abende, die mir Motivation und Ausgleich gegeben haben. Auch allen Kolleginnen und Kollegen am Institut für Umweltphysik gilt mein Dank für das inspirierende Arbeitsumfeld, hilfreiches Feedback und die freundschaftliche Atmosphäre, insbesondere Julia, Eva und Pauline, die mir beim BBP einen wichtigen Ausgleich zum Arbeitsalltag gegeben haben.

Ein herzlicher Dank geht zudem an die Bachelor- und Masterstudierenden, die ich während ihrer Arbeiten mitbetreuen durfte. Beiträge von Ida Schatz, Katrin Pretranovic, Emma Gerlach, Hannah Janecke und Marika Hiemisch haben diese Dissertation direkt bereichert und neue Impulse gesetzt. Mein besonderer Dank gilt auch dem René Eichstädter der mir die Einführung in die Labor- und Messtechnik ermöglicht hat und mir stets bei technischen Problemen kompetent zur Seite stand. Darüber hinaus möchte ich mich bei den Hiwis bedanken, die mich tatkräftig bei den oft aufwendigen Laborarbeiten unterstützt haben, insbesondere Marius Feuerle.

Mein Dank geht auch an die anderen Early Career Researcher des SPP2299, deren kollegiale Zusammenarbeit und Engagement meine wissenschaftliche und persönliche Entwicklung gefördert haben. Dem SPP2299 danke ich zudem ausdrücklich für das Mobility Scholarship, das mir die Durchführung der Studie auf Tahiti ermöglicht hat.

Ein Dank geht außerdem an die künstliche Intelligenz, die mich beim sprachlichen Überarbeiten und Verfeinern der Texte unterstützt hat. Alle wissenschaftlichen Ergebnisse und Diskussionen beruhen jedoch vollständig auf meinen eigenen Gedanken und Arbeiten.

Für die Unterstützung jenseits des wissenschaftlichen Alltags möchte ich meiner Familie und meinen Freunden danken. Ihre Ermutigung, Geduld und ihr Vertrauen, sowie das ein oder andere Care-Paket, haben mir die nötige Kraft und Motivation gegeben, auch in herausfordernden Phasen weiterzumachen.

Zum Schluss gilt mein tiefster Dank an Nils, der in all den Jahren immer für mich da war. Er hat mich mit Geduld, Verständnis und Humor begleitet, mich aufgemuntert, wenn es mal nicht so gut lief, und mir so die Kraft gegeben, weiterzumachen, das bedeutet mir unendlich viel. Auch danke, dass er mich sogar bis nach Tahiti unterstützt und motiviert hat. Ohne seine Begleitung, im Alltag wie auf der Arbeit, wäre diese Dissertation nicht in dieser Form entstanden.

NATURWISSENSCHAFTLICH-MATHEMATISCHE GESAMTFAKULTÄT

COMBINED FACULTY OF NATURAL SCIENCES AND MATHEMATICS

RUPRECHT-KARLS-
UNIVERSITÄT
HEIDELBERG

Eidesstattliche Versicherung gemäß § 8 der Promotionsordnung für die Naturwissenschaftlich-Mathematische Gesamtfakultät der Universität Heidelberg / Sworn Affidavit according to § 8 of the doctoral degree regulations of the Combined Faculty of Natural Sciences and Mathematics

1. Bei der eingereichten Dissertation zu dem Thema / The thesis I have submitted entitled

   From River to Reef: Developing Coral δ234U as a Proxy for Freshwater Influence in the Caribbean and Beyond

   handelt es sich um meine eigenständig erbrachte Leistung / is my own work.

2. Ich habe nur die angegebenen Quellen und Hilfsmittel (inkl. KI-basierter Hilfsmittel) benutzt und mich keiner unzulässigen Hilfe Dritter bedient. Insbesondere habe ich wörtlich oder sinngemäß aus anderen Werken übernommene Inhalte als solche kenntlich gemacht. / I have only used the sources indicated (incl. AI-based tools) and have not made unauthorised use of services of a third party. Where the work of others has been quoted or reproduced, the source is always given.

3. Die Arbeit oder Teile davon habe ich ~~wie folgt/~~bislang nicht[1)] an einer Hochschule des In- oder Auslands als Bestandteil einer Prüfungs- oder Qualifikationsleistung vorgelegt. / I have not yet/have already[1)] presented this thesis or parts thereof to a university as part of an examination or degree.

   Titel der Arbeit / Title of the thesis:

   Hochschule und Jahr / University and year:

   Art der Prüfungs- oder Qualifikationsleistung / Type of examination or degree:

4. Die Richtigkeit der vorstehenden Erklärungen bestätige ich. / I confirm that the declarations made above are correct.

5. Die Bedeutung der eidesstattlichen Versicherung und die strafrechtlichen Folgen einer unrichtigen oder unvollständigen eidesstattlichen Versicherung sind mir bekannt. / I am aware of the importance of a sworn affidavit and the criminal prosecution in case of a false or incomplete affidavit

Ich versichere an Eides statt, dass ich nach bestem Wissen die reine Wahrheit erklärt und nichts verschwiegen habe. / I affirm that the above is the absolute truth to the best of my knowledge and that I have not concealed anything.

Ort und Datum / Place and date

……..……
Unterschrift / Signature

[1)] Nicht Zutreffendes streichen. Bei Bejahung sind anzugeben: der Titel der andernorts vorgelegten Arbeit, die Hochschule, das Jahr der Vorlage und die Art der Prüfungs- oder Qualifikationsleistung. / Please cross out what is not applicable. If applicable, please provide: the title of the thesis that was presented elsewhere, the name of the university, the year of presentation and the type of examination or degree.

The German text is legally binding.